## QUANTUM LIQUIDS AND QUANTUM CRYSTALS

# Collisionless mechanism of zero-point sound attenuation in a normal Fermi liquid

Yu. V. Slyusarenko

*National Science Center ''Kharkov Institute of Physics and Technology,'' 310108 Kharkov, Ukraine**

(Submitted October 8, 1997; revised November 18, 1997)
Fiz. Nizk. Temp. **24**, 291–298 (April 1998)

The possibility of collisionless (Landau) mechanism of attenuation of long-lived zero-point oscillations in a normal Fermi liquid is studied. Expressions are obtained for the coefficients of zero-point sound attenuation in a simple model. Limiting cases of large and small amplitudes of particle interaction are considered. © *1998 American Institute of Physics.* [S1063-777X(98)00104-2]

### INTRODUCTION

The possibility of the existence of specific collective modes in normal Fermi liquids was reported in the pioneering works of Landau and Silin.[1–4] The symmetric longitudinal mode, which is the only one associated with density fluctuations of a normal Fermi liquid, is the high-frequency analog of normal sound, and was therefore termed ''zero-point sound'' by Landau. The attenuation of zero-point sound is associated with ''blurring'' of the equilibrium quasiparticle distribution function, say, as a result of collisions. If such a ''blurring'' is taken into account, the zero-point sound attenuation coefficient $\gamma$ is found to be proportional to the square of the ratio of the temperature $T$ to the Fermi energy $\varepsilon_F$ (see, for example, Refs. 5 and 6), i.e., $\gamma \propto (T/\varepsilon_F)^2$. It follows hence and in accordance with one of the basic concepts of the theory of normal Fermi liquids ($(T/\varepsilon_F) \ll 1$) that zero-point vibrations have a long life in dissipation processes due to collisions of quasiparticles. The possibility of collisionless mechanism of zero-point sound attenuation (of the type of Landau damping) was mentioned in very few works, and even in these works the authors confined the analysis to the conditions under which the attenuation is so large that the very concept of zero-point vibrations becomes meaningless (see, for example, Refs. 7 and 8 in this connection).

In the present work, which is devoted to a more detailed analysis of the collisionless mechanism of zero-point sound attenuation, we shall show that such a mechanism can be realized without imposing any restrictions in addition to the conventional constraints (see below) associated with the existence of long-lived zero-point vibrations in a normal Fermi liquid.

In order to simplify the subsequent analysis, let us recall certain basic concepts of the kinetic theory of a normal Fermi liquid.

### 1. BASIC EQUATIONS OF THE KINETICS OF A NORMAL FERMI LIQUID

By a normal Fermi liquid, we usually mean a degenerate Fermi liquid in which the essential properties of noninteracting fermion systems are preserved. Examples of normal Fermi liquids are $^3$He above $4\times10^{-3}$ K and conduction electrons in nonsuperconducting metals at temperatures below $5\times10^4$ K.[7,8] In view of the large value of the range of Coulomb interaction between fermions, a charged Fermi liquid differs considerably from a neutral Fermi liquid. Extensive literature is available on various properties of charged and neutral Fermi liquids, and hence we shall not dwell on the same in this work. The aim of our research is to single out the characteristic features that are common to charged and neutral Fermi liquids. The most significant among these characteristics is the dependence of the excitation Hamiltonian $\varepsilon$ on the quasiparticle distribution function $n(\mathbf{x},\mathbf{p},t)$, viz., $\varepsilon(\mathbf{x},\mathbf{p},t)=\varepsilon(\mathbf{x},\mathbf{p},n)$.[1–10] We shall also disregard the spin of the particles, which can be done while solving a wide range of problems. In other words, we shall assume that the state of a system is described by a one-particle distribution function $n(x,t)$ [$x\equiv(\mathbf{x},\mathbf{p})$], which is a function of the coordinate $\mathbf{x}$ and momentum $\mathbf{p}$ at the instant $t$, and is independent of spin variables. It will be shown in the following analysis that we could have done without many simplifying assumptions in the approach used by us, but this would have considerably complicated the calculations and the results would not appear in such a clear form.

Note that the use of a coordinate- and momentum-dependent distribution function to describe a system is equivalent to the semiclassical Wigner approximation in statistical mechanics and is in accord with the uncertainty principle in an analysis of macroscopic phenomena for which the characteristic scales of space and time are much larger than the corresponding atomic parameters. In the case of Coulomb interaction between conduction electrons in metals, the characteristic small spatial scale is the Thomas-Fermi screening radius $r_0$

$$r_0=\left(\frac{\varepsilon_F}{6\pi\eta e^2}\right)^{1/2}, \tag{1}$$

where $\varepsilon_F$ is the Fermi energy, $\eta$ the number density of elec-

 

trons, and $e$ the elementary charge. Such a screening is associated with the existence of an inert positively charged component, i.e., the system is quasineutral.

Naturally, it is assumed that the main condition of applicability of the normal Fermi liquid theory is satisfied everywhere in the following analysis:

$$\varepsilon_F \gg T, \tag{2}$$

where $T$ is the temperature measured in energy units.

Taking the above assumptions into consideration, we can present the kinetic equation describing the nonequilibrium state of a normal Fermi liquid in the form

$$\frac{\partial}{\partial t} n(x,t) = \frac{\partial \varepsilon(x;n)}{\partial \mathbf{p}} \frac{\partial n(x,t)}{\partial \mathbf{x}} - \frac{\partial \varepsilon(x;n)}{\partial \mathbf{x}} \frac{\partial n(x,t)}{\partial \mathbf{p}} = L(x;n), \tag{3}$$

where $L(x;n)=L[\mathbf{x},\mathbf{p};n(\mathbf{x}',\mathbf{p}')]$ is the collision integral whose explicit form will not be required in the present work (see, in this connection, Refs. 1–4). The specific form of the energy of a quasiparticle as a functional of the distribution function is not known in the phenomenological theory of a normal Fermi liquid. In the Landau-Silin theory[1–4] devoted to low-lying longwave excitations against the background of equilibrium distribution

$$n_0(\mathbf{p}) = \left\{ \exp\left( \frac{\varepsilon_0(\mathbf{p}) - \mu}{T} \right) + 1 \right\}^{-1} \tag{4}$$

[where $\varepsilon_0(\mathbf{p})$ is the energy corresponding to the equilibrium state and $\mu$ is the chemical potential], it is sufficient to introduce the quasiparticle interaction function $f(x,x')=f\times(\mathbf{x}-\mathbf{x}',\mathbf{p},\mathbf{p}')$ (Landau amplitude) as a linear reaction of the quasiparticle energy to a small variation $\delta n(x,t)$ of the distribution function $n(x,t)$, i.e.,

$$n(x,t) = n_0(\mathbf{p}) + \delta n(x,t), \tag{5}$$

$$\varepsilon(x,t) = \varepsilon_0(\mathbf{p}) + \sum_{\mathbf{p}'} \int d\mathbf{x}' f(\mathbf{x}-\mathbf{x}';\mathbf{p},\mathbf{p}') \delta n(x,t).$$

The function $f(x,x')$, which is the second variational derivative of the system energy with respect to the distribution function, is a parameter of the theory whose characteristics can be determined experimentally (see, for example, Refs. 1–4 in this connection).

It is also worth noting that, according to formula (2), the equilibrium distribution $n_0(\mathbf{p})$ differs insignificantly from the ''step'' distribution

$$\mathbf{n}_0(\varepsilon) = \theta(\varepsilon_F - \varepsilon) \tag{6}$$

or

$$n_0(p) = \theta(p_F - p), \tag{6a}$$

where $\theta(x)$ is the Heaviside unit function, $\varepsilon_F=\varepsilon_0(p_F)$, and the Fermi momentum $p_F$ is determined, as usual, from the relation

$$\varepsilon_0(p_F) = \mu. \tag{7}$$

For simplicity, we assume that the Fermi surface is spherical, and the quasi-particle energy $\varepsilon_0(\mathbf{p})$ corresponding to the equilibrium distribution (4) depends only on the magnitude of momentum: $\varepsilon_0(\mathbf{p})=\varepsilon_0(p)$.

Let us now go over directly to an analysis of the Landau damping of zero-point sound in a normal Fermi liquid.

## 2. COLLISIONLESS MECHANISM OF ATTENUATION OF LONG-LIVED ZERO-POINT VIBRATIONS

The emergence of zero-point sound is possible in the frequency range $\omega\tau_\tau \gg 1$, where $\tau_\tau$ is the relaxation time, so that we can disregard collisions between quasiparticles and hence neglect the collision integral in the kinetic equation (3). We shall consider the simplest model of zero-point sound.[5] We assume that the forces of interaction between quasiparticles are short-range forces and that the interaction function $f(\mathbf{x}-\mathbf{x}',\mathbf{p},\mathbf{p}')$ is independent of momenta:

$$f(\mathbf{x}-\mathbf{x}';\mathbf{p},\mathbf{p}') = f\delta(\mathbf{x}-\mathbf{x}'), \tag{8}$$

where $f=\text{const}$.

Disregarding collisions, we can present the kinetic equation (3) linearized by using formulas (5) and (8) in the form

$$\frac{\partial}{\partial t} \delta n(x,t) + \frac{\partial \varepsilon_0(p)}{\partial \mathbf{p}} \frac{\partial}{\partial \mathbf{x}} \delta n(x,t) - f \frac{\partial n_0(p)}{\partial \mathbf{p}} \frac{\partial}{\partial \mathbf{x}} \sum_{\mathbf{p}'} \delta n(\mathbf{x},\mathbf{p}',t) = 0. \tag{9}$$

Going over to the Fourier transform of the deviation $\delta n(x,t)$ from the equilibrium distribution function (4)

$$\delta n(\mathbf{x},\mathbf{p},t) = \int d\mathbf{k} \int_{-\infty}^{\infty} d\omega \, \exp(i\mathbf{k}\cdot\mathbf{x} - i\omega t) \delta n_{\mathbf{k}}(\mathbf{p},\omega), \tag{10}$$

we obtain

$$\delta n_{\mathbf{k}}(\mathbf{p},\omega)(-\omega + \mathbf{v}\cdot\mathbf{k}) - f\mathbf{k} \frac{\partial n_0(p)}{\partial \mathbf{p}} \sum_{\mathbf{p}'} \delta n_{\mathbf{k}}(\mathbf{p}',\omega) = 0. \tag{11}$$

The solution of this equation can be presented in the form

$$\delta n_{\mathbf{k}}(\mathbf{p},\omega) = -f\{\omega - \mathbf{v}\cdot\mathbf{k} + i0\}^{-1}\mathbf{k} \frac{\partial n_0(p)}{\partial \mathbf{p}} \delta\varphi_{\mathbf{k}}(\omega) + \delta A(\mathbf{p},\mathbf{k})\delta(\omega - \mathbf{v}\cdot\mathbf{k}), \tag{12}$$

where we have introduced the notation

$$\mathbf{v} \equiv \frac{\partial \varepsilon_0(p)}{\partial \mathbf{p}} = \frac{\partial \varepsilon_0(p)}{\partial p} \frac{\mathbf{p}}{p}. \tag{13}$$

The function $\delta\varphi_{\mathbf{k}}(\omega)$ is defined by the expression

$$\delta\varphi_{\mathbf{k}}(\omega) = \sum_{\mathbf{p}} \delta n_{\mathbf{k}}(\mathbf{p},\omega), \tag{14}$$

while the quantities $\delta A(\mathbf{p},\mathbf{k})$ are arbitrary functions subjected to constraints in view of the fact that the function $\delta n(\mathbf{x},\mathbf{p},t)$ calculated by using formula (10) must be small in

comparison with the equilibrium distribution function $n_0(p)$ [see formula (4)]. It also follows from formula (10) that the functions $\delta A(\mathbf{p},\mathbf{k})$ must satisfy the relation

$$\delta A^*(\mathbf{p},\mathbf{k}) = \delta A(\mathbf{p},-\mathbf{k}). \tag{15}$$

We shall use the notation $\delta A_\nu(\mathbf{p},\mathbf{k})$ to describe the entire admissible set of such functions, where $\nu$ is a symbolic discrete or continuous parameter on which the functions $\delta A(\mathbf{p},\mathbf{k}) \equiv \delta A_\nu(\mathbf{p},\mathbf{k})$ may depend.

Formula (12) obtained above can be used to determine the value of $\delta\varphi_{\mathbf{k}}(\omega)$ in terms of the functions $\delta A_\nu(\mathbf{p},\mathbf{k})$:

$$\delta\varphi_{\nu\mathbf{k}}(\omega) = \overline{\delta A_\nu}(\mathbf{k},\omega)\tilde{\varepsilon}^{-1}(\mathbf{k},\omega), \tag{16}$$

where

$$\delta\tilde{A}_\nu(\mathbf{k},\omega) \equiv \sum_{\mathbf{p}} \delta A(\mathbf{p},\mathbf{k})\,\delta(\omega-\mathbf{v}\cdot\mathbf{k}), \tag{17}$$

$$\delta\tilde{A}^*_\nu(\mathbf{k},\omega) = \delta\tilde{A}_\nu(-\mathbf{k},-\omega).$$

Substituting (16) into (12), we arrive at the following expression for the quantity $\delta n_{\mathbf{k}}(\mathbf{p},\omega)$:

$$\delta n_{\mathbf{k}}(\mathbf{p},\omega) = \delta A(\mathbf{p},\mathbf{k})\,\delta(\omega-\mathbf{v}\cdot\mathbf{k}) - f\{\omega-\mathbf{v}\cdot\mathbf{k} + i0\}^{-1}\tilde{\varepsilon}^{-1}(\mathbf{k},\omega)\,\delta\tilde{A}_\nu(\mathbf{k},\omega)\mathbf{k}\,\frac{\partial n_0(p)}{\partial\mathbf{p}}. \tag{18}$$

Note that the quantity $\tilde{\varepsilon}(\mathbf{k},\omega)$ in (16) and (18), which is defined as

$$\tilde{\varepsilon}(\mathbf{k},\omega) = \tilde{\varepsilon}^*(-\mathbf{k},-\omega) = \tilde{\varepsilon}_1(\mathbf{k},\omega) + i\tilde{\varepsilon}_2(\mathbf{k},\omega) = 1 + f\mathbf{k}\sum_{\mathbf{p}} \frac{\partial n_0(p)}{\partial\mathbf{p}}\{\omega-\mathbf{v}\cdot\mathbf{k}+i0\}^{-1}, \tag{19}$$

is the complex permittivity of the system in the case of a charged Fermi-liquid (see, for example, Ref. 11). The presence of an imaginary correction to $\tilde{\varepsilon}(\mathbf{k},\omega)$ indicates dissipation of energy of waves whose energy-momentum relation $\omega_0(\mathbf{k})$ can be derived from the equation

$$\tilde{\varepsilon}[\mathbf{k},\omega_0(\mathbf{k}) - i\gamma_{\mathbf{k}}] = 0. \tag{20}$$

The damping decrement $\gamma_{\mathbf{k}}$ of the wave is defined by the imaginary component $\tilde{\varepsilon}_2(\mathbf{k},\omega)$ of the quantity $\tilde{\varepsilon}(\mathbf{k},\omega)$. Hence weakly attenuating vibrations can exist in the system

$$|\omega_0(\mathbf{k})| \gg \gamma_{\mathbf{k}} \tag{21}$$

only under the condition

$$|\tilde{\varepsilon}_1(\mathbf{k},\omega)| \gg |\tilde{\varepsilon}_2(\mathbf{k},\omega)|. \tag{22}$$

Going over in formula (19) from summation over $p$ to integration and using the relation

$$(z+i0)^{-1} = P\,\frac{1}{z} - i\pi\delta(z) \tag{23}$$

where the symbol $P$ indicates that the principal value is taken for the subsequent integration, we can present the quantities $\tilde{\varepsilon}_1(\mathbf{k},\omega)$ and $\tilde{\varepsilon}_2(\mathbf{k},\omega)$ in the form

$$\tilde{\varepsilon}_1(\mathbf{k},\omega) = \tilde{\varepsilon}_1(k,\omega) = 1 + \frac{f}{2\pi^2\hbar^3}\int_0^\infty dpp^2\,\frac{\partial n_0(\varepsilon)}{\partial\varepsilon} \times\left\{-1+\frac{\omega}{2kv}\ln\left|\frac{\omega+kv}{\omega-kv}\right|\right\}, \tag{24}$$

$$\tilde{\varepsilon}_2(\mathbf{k},\omega) = -\frac{f}{4\pi\hbar^3}\int_0^\infty dpp^2\,\frac{\omega}{kv}\,\frac{\partial n_0(\varepsilon)}{\partial\varepsilon}\,\theta(kv-|\omega|). \tag{25}$$

Assuming that the sound attenuation is small, the dispersion relation for determining $\omega_0(k)$ assumes the following form in accordance with formulas (20)–(22), (24) and (25):

$$\tilde{\varepsilon}_1(k,\omega(k)) = 0 \tag{26}$$

or

$$1 + \frac{f}{2\pi^2\hbar^3}\int_0^\infty dpp^2\,\frac{\partial n_0(\varepsilon)}{\partial\varepsilon}\left\{-1+\frac{\omega}{2kv}\ln\left|\frac{\omega+kv}{\omega-kv}\right|\right\} = 0, \tag{26a}$$

while the damping decrement of the wave is defined by the expression

$$\gamma_k = \left\{\frac{\partial\tilde{\varepsilon}_1(k,\omega)}{\partial\omega}\right\}^{-1}_{\omega=\omega_0}\tilde{\varepsilon}_2(\mathbf{k},\omega_0). \tag{27}$$

It is well known that specific vibrations (zero-point sound) in which we are interested in the present work exist even at zero temperature in the system under consideration. Proceeding from Eq. (26) and taking into account formula (4), we can easily obtain the dispersion equation for zero-point sound

$$1 + F\left[1-\frac{s}{2}\ln\frac{s+1}{s-1}\right] - \frac{f}{2\pi^2\hbar^3}\int_0^\infty dz \times(e^z+1)^{-1}\,\frac{\partial}{\partial z}\,[\chi(\varepsilon_F+Tz)+\chi(\varepsilon_F-Tz)] = 0, \tag{28}$$

where we have used the notation

$$F \equiv \frac{fp_F^2}{2\pi^2\hbar^3 v_F}, \quad s \equiv \frac{\omega_0}{kv_F} > 1, \tag{29}$$

and, in accordance with formula (13),

$$v_F = \left.\frac{\partial\varepsilon_0(p)}{\partial p}\right|_{p=p_F}. \tag{30}$$

In formula (28), the function

$$\chi(\varepsilon) = \frac{p^2(\varepsilon)}{v(\varepsilon)}\left\{-1+\frac{sv_F}{2v(\varepsilon)}\ln\left|\frac{s+1+(v(\varepsilon)-v_F)/v_F}{s-1-(v(\varepsilon)-v_F)/v_F}\right|\right\} \tag{31}$$

defines the effect of thermal blurring of the equilibrium distribution function on the energy-momentum relation of the zero-point sound. It can be seen from the above expression for the function $\chi(\varepsilon)$ that it is important to take into account this effect only for $s\to 1$. We shall consider this situation below.

Let us now derive an expression for the coefficient $\gamma_k$ of zero-point sound attenuation. For this purpose, we must de-

termine the quantity $\tilde{\varepsilon}_2(\mathbf{k},\omega)$ which can be presented, in accordance with formulas (25) and (29), in the form

$$\tilde{\varepsilon}_2(\mathbf{k},\omega_0)=-\frac{fsv_F}{4\pi\hbar^3}\int_0^\infty d\varepsilon\,\frac{p^2(\varepsilon)}{v^2(\varepsilon)}\,\frac{\partial n_0(\varepsilon)}{\partial\varepsilon}\,\theta[v(\varepsilon)-sv_F], \tag{32}$$

where the dependence of $v$ on $\varepsilon$ must be determined from (13). It can be seen easily that on account of the presence of a Heaviside unit function in the integrand, the attenuation of sound is defined by the region of temperature ''blurring'' of equilibrium distribution with a quasiparticle energy $\varepsilon\geqslant\overline{\varepsilon}>\varepsilon_F$, where $\overline{\varepsilon}=\varepsilon_0(p)$, while the limiting momentum $p$ is determined from the condition

$$\left.\frac{\partial\varepsilon_0(p)}{\partial p}\right|_{p=\overline{p}}=sv_F=s\left.\frac{\partial\varepsilon_0(p)}{\partial p}\right|_{p=p_F}. \tag{33}$$

Let us evaluate integrals of the type

$$\int_{\overline{\varepsilon}}^\infty d\varepsilon g(\varepsilon)\,\frac{\partial}{\partial\varepsilon}\{\exp[(\varepsilon-\mu)/T]+1\}^{-1},\overline{\varepsilon}>\mu. \tag{34}$$

Using the change of variables $z=(\varepsilon-\mu)/T$, we arrive at the expression

$$\int_{(\overline{\varepsilon}-\mu)/T}^\infty dz g(\mu+zT)\,\frac{d}{dz}\{e^z+1\}^{-1}. \tag{35}$$

It can be seen easily that for $(\overline{\varepsilon}-\mu)/T\geqslant 1$ or $0<(\overline{\varepsilon}-\mu)/T\leqslant 1$, the function $g(\mu+zT)$ appearing in the above expression can be expanded into a power series in $(zT)$ in view of a rapid decrease in the function $1/(\exp z+1)$ for $z\to\infty$ and the validity of the inequality $\mu\gg T$ (see Eqs. (2) and (7)) (naturally, for the case when the function $g(\mu)$ is differentiable at the point $\mu$). In the main approximation in temperature, we can write, in accordance with (7), (33) and (34),

$$\int_{\overline{\varepsilon}}^\infty d\varepsilon g(\varepsilon)\,\frac{\partial}{\partial\varepsilon}\{\exp[(\varepsilon-\mu)/T]+1\}^{-1}\approx -g(\varepsilon_F)\times\left\{\exp\left(\frac{\overline{\varepsilon}-\varepsilon_F}{T}\right)+1\right\}^{-1},$$

and hence the following expression is valid for the quantity $\tilde{\varepsilon}_2(\mathbf{k},\omega_0)$ in the same approximation:

$$\tilde{\varepsilon}_2(\mathbf{k},\omega_0)\approx\frac{\pi}{2}\,sF\left\{\exp\left(\frac{\overline{\varepsilon}-\varepsilon_F}{T}\right)+1\right\}^{-1}. \tag{36}$$

It can also be verified easily that for $(\tilde{\varepsilon}-\mu)/T\gg 1$, the integral (34) is evaluated by using the formula

$$\int_{\overline{\varepsilon}}^\infty d\varepsilon g(\varepsilon)\,\frac{\partial}{\partial\varepsilon}\{\exp[(\varepsilon-\mu)/T]+1\}^{-1}\approx -g(\overline{\varepsilon})\exp\left(-\frac{\overline{\varepsilon}-\varepsilon_F}{T}\right),$$

Consequently, we obtain

$$\overline{\varepsilon}_2(\mathbf{k},\omega_0)\approx\frac{\pi}{2}\,sF\left(\frac{p(\varepsilon)}{p_F}\right)^2\left(\frac{v_F}{v(\varepsilon)}\right)^2\exp\left(-\frac{\overline{\varepsilon}-\varepsilon_F}{T}\right),$$

$$(\overline{\varepsilon}-\varepsilon_F)/T\gg 1. \tag{36a}$$

Further, we take into consideration the fact that the following formula is valid in view of the relations (24) and (26):

$$\left.\frac{\partial\overline{\varepsilon}_1(k,\omega)}{\partial\omega}\right|_{\omega=\omega_0}=\frac{(F+1-s^2)}{(s^2-1)\omega_0}. \tag{37}$$

In accordance with formulas (27) and (36), the damping decrement $\gamma_k$ can be presented in the form

$$\gamma_k=\omega_0\,\frac{\pi}{2}\,\frac{s(s^2-1)F}{(F+1-s^2)}\left\{\exp\left(\frac{\varepsilon-\varepsilon_F}{T}\right)+1\right\}^{-1} \tag{38}$$

for $(\overline{\varepsilon}-\varepsilon_F)/T\geqslant 1$ or $0<(\overline{\varepsilon}-\varepsilon_F)/T\leqslant 1$ and in accordance with formula (36a), the damping decrement assumes the form

$$\gamma_k=\omega_0\,\frac{\pi}{2}\,\frac{s(s^2-1)F}{(F+1-s^2)}\left(\frac{p(\overline{\varepsilon})}{p_F}\right)^2\left(\frac{v_F}{v(\overline{\varepsilon})}\right)^2\times\exp\left(-\frac{\overline{\varepsilon}-\varepsilon_F}{T}\right) \tag{38a}$$

for $(\overline{\varepsilon}-\varepsilon_F)/T\gg 1$. It should be recalled that formulas (38) and (38a) are obtained under the assumption $\gamma_k\ll|\omega_0(k)|$ and are therefore valid only if the following conditions are observed:

$$\frac{\pi}{2}\,\frac{s(s^2-1)F}{(F+1-s^2)}\left\{\exp\left(\frac{\overline{\varepsilon}-\varepsilon_F}{T}\right)+1\right\}^{-1}\ll 1 \tag{39}$$

for $(\overline{\varepsilon}-\varepsilon_F)/T\geqslant 1$ or $0<(\overline{\varepsilon}-\varepsilon_F)/T\ll 1$ and

$$\frac{\pi}{2}\,\frac{s(s^2-1)F}{(F+1-s^2)}\left(\frac{p(\overline{\varepsilon})}{p_F}\right)^2\left(\frac{v_F}{v(\overline{\varepsilon})}\right)^2\exp\left(-\frac{\overline{\varepsilon}-\varepsilon_F}{T}\right)\ll 1 \tag{39a}$$

for $(\overline{\varepsilon}-\varepsilon_F)/T\gg 1$.

It is also worthwhile to note that the invariance of the expression (28) relative to the substitution $s\to -s$ indicates the presence of two waves propagating in opposite directions with the same damping coefficient $\gamma_k$ defined by formulas (38) and (39). Analyzing the behavior of the function $\partial\tilde{\varepsilon}_1(\omega)/\partial\omega|_{\omega=skv_F}$ [see Eq. (37)] and considering that $\tilde{\varepsilon}_2(\mathbf{k},\omega_0)$ is positive, we can easily prove that the damping coefficient $\gamma_k$ is also positive. It can be shown that as $s$ changes from 1 to infinity, this function decreases monotonically but always remains positive, and hence the damping coefficient $\gamma_k$ is also positive.

Let us now derive expressions for the damping coefficient of zero-point vibrations in two limiting cases $s\approx 1$ $(s>1)$ and $s\gg 1$ [see (29)]. It was mentioned above that for the case $s\gtrsim 1$, which is realized for interaction amplitudes lying in the interval $0<F\leqslant 2$, we must take into consideration the effect of thermal ''blurring'' of the equilibrium distribution function on the energy-momentum relation for the zero-point sound. For $s\gtrsim 1$, the dispersion equation (28) assumes the form

$$1+\frac{1}{F}-\frac{1}{2}\ln\frac{2}{s-1}-2\left[\frac{T}{2\varepsilon_F(s-1)}\right]^2\int_0^\infty dz \times z(e^z+1)^{-1}\left\{1-z^2\left[\frac{T}{2\varepsilon_F(s-1)}\right]^2\right\}^{-1}, \tag{40}$$

where the integral has the meaning of the principal value. This equation is quite complex and cannot be solved analytically in the general form. However, from the point of view of the problem being considered in the present work, the most interesting case corresponds to $T[\varepsilon_F(s-1)]^{-1}\lesssim 1$, when the damping coefficient for the zero-point sound is the most significant. In this case, the integral in Eq. (30) can be replaced by the asymptotic series

$$1+\frac{1}{F}-\frac{1}{2}\ln\frac{2}{s-1}-\sum_{n=1}^{\infty}\left[\frac{\pi T}{\varepsilon_F(s-1)}\right]^{2n}\frac{1-2^{1-2n}}{2n}B_n=0, \tag{41}$$

where $B_n$ are the Bernoulli numbers. It can be seen easily that in the main approximation in the parameter

$$\frac{\pi T}{\varepsilon_F(s-1)}\lesssim 1 \tag{42}$$

the deviation of $s$ from unity is determined by the interaction of quasiparticles [see Eq. (29)] and can therefore be presented in the form

$$s-1\approx\delta s_{\rm int}+\delta s_T,\quad \delta s_T<\delta s_{\rm int}, \tag{43}$$

where $\delta s_{\rm int}$ is obtained from the dispersion equation (41) without taking into account the thermal corrections:

$$\delta s_{\rm int}\approx 2\exp\{-2(1+1/F)\}\ll 1, \tag{44}$$

while the deviation $\delta s_T$, which determines the contribution of thermal effects to the energy-momentum relation for the zero-point sound, can be derived as a correction to $\delta s_{\rm int}$ in the theory of perturbations in the parameter $\pi T(\varepsilon_F\delta s_{\rm int})^{-1}\lesssim 1$:

$$\delta s_T\approx\frac{1}{12F}\left(\frac{\pi T}{\varepsilon_F\delta s_{\rm int}}\right)^2\delta s_{\rm int}. \tag{45}$$

Note that formulas (43)–(45) are valid for $0<F\lesssim 2$, when $0<\delta s_{\rm int}\lesssim 0.1$. Hence we need not take into consideration the thermal corrections to the zero-point sound frequency if the conditions (42), (43) and (45) are satisfied, and the expression for the zero-point sound damping coefficient can be presented in accordance with (38) in the form

$$\gamma_k\approx\pi\delta s_{\rm int}\left\{\exp\left[2\pi\frac{\tilde m}{m^*}\left(\frac{\partial s_{\rm int}\varepsilon_F}{\pi T}\right)\right]+1\right\}^{-1}\omega_0, \tag{46}$$

$$\omega_0=kv_F,$$

where we have taken into account the fact that, in view of formula (44), the limiting energy $\bar\varepsilon$ (see (38)) is of the order of the energy $\varepsilon_F$:

$$\bar\varepsilon-\varepsilon_F\approx 2\frac{\tilde m}{m^*}\varepsilon_F\delta s_{\rm int}, \tag{47}$$

where

$$\tilde m^{-1}\equiv\left(\frac{\partial^2\varepsilon_0(p)}{(\partial p)^2}\right)_{p=p_F} \tag{48}$$

and the effective mass $m^*$ is defined, as usual, by the formula

$$p_F=m^*v_F. \tag{49}$$

Note that, in spite of the relation $\varepsilon_F\gg T$ in this approximation, the expression in the exponent of formula (46) is not necessarily large because of the validity of relations (42) and (44). Proceeding from formula (46), taking into account relation (42) and putting $m^*\sim\bar m$, we can estimate the maximum value of the damping coefficient of zero-point sound having a frequency $\omega_0=kv_F$:

$$\gamma_k^{\max}\approx\pi\delta s_{\rm int}\exp(-2\pi)\omega_0. \tag{50}$$

In the opposite limiting case $s\gg 1$ corresponding to the interaction amplitudes $F\gg 1$, the influence of thermal effects on the energy-momentum relation for zero-point sound can also be taken into consideration in the perturbation theory in temperature. In this case, however, it follows from formula (28) that it is not essential to take thermal corrections into consideration, and hence we shall disregard them in this work. Thus we obtain from (28) the relation

$$s\approx\sqrt{F/3}\gg 1. \tag{51}$$

Assuming for simplicity a quadratic energy-momentum relation for quasiparticles

$$\varepsilon_0(p)=\frac{p^2}{2m^*},$$

we obtain after simple calculations from formula (38a)

$$\gamma_k\approx\frac{\pi}{12}kv_FF^2\exp\left(-\frac{F}{3}\frac{\varepsilon_F}{T}\right). \tag{52}$$

A comparison of formulas (38) and (46) with (38a) and (52) shows that the dependence of the zero-point sound damping coefficient on reciprocal temperature may be exponential [see (38a) and (52)], and hence the zero-point sound attenuation is exponentially small in the present case. However, such a dependence of the damping coefficient on reciprocal temperature may be suppressed in a number of cases in view of the validity of relations (42) and (46). Hence it can be expected that conditions ensuring a predominance of collisionless mechanism of zeroth sound attenuation (over the hydrodynamic mechanism) may prevail in physical systems displaying the properties of normal Fermi-liquids in spite of the fact that in the case of damping due to collisions, the damping factor has a power dependence on temperature, viz., $\gamma\sim(T/\varepsilon_F)^2$.

## CONCLUSION

We shall illustrate the last statement with the help of rough estimates. In other words, we shall find the conditions under which the collisionless zero-point sound damping coefficient may be of the same order as the coefficient of absorption due to collisions:

$$\gamma_k - 1/\tau_r, \tag{53}$$

where $\tau_r$ is the relaxation time. Note that, according to relations (38) and (38a), this condition is equivalent to the requirement that the parameter $(\gamma_k/\omega_0(k)) \ll 1$, which determines the conditions for the existence of long-lived zero-point vibrations in a normal Fermi liquid, must be of the order of the parameter $[\omega_0(k)\tau_r]^{-1} \ll 1$ which defines the condition of applicability of the collisionless approximation. It follows from formulas (38) and (38a) that the collisionless absorption of zero-point sound is maximum when condition (42) is satisfied, which occurs (see above) in the region of relatively small values of the Landau amplitudes ($0 < F \lesssim 2$). The relaxation time $\tau_r$ associated with the collisions of quasiparticles in $^3$He can be estimated by formula

$$\tau_r \sim 10^2 \frac{\hbar}{\varepsilon_F}\left(\frac{\varepsilon_F}{T}\right)^2.$$

and is found to be in good agreement with the experimental results.[7,8,12–15] In this case, we obtain from (53) by taking formula (46) into consideration

$$\pi^3 \exp\left\{-2\pi\left(\frac{\delta s_{\rm int}\varepsilon_F}{\pi T}\right)\right\} \approx 10^{-2}\delta s_{\rm int}\left(\frac{\pi T}{\delta s_{\rm int}\varepsilon_F}\right)\frac{\varepsilon_F}{\hbar\omega_0}, \tag{54}$$

$$\frac{\hbar\omega_0}{\varepsilon_F} \ll 1.$$

The expression for the maximum value of the zero-point sound damping coefficient has the form [see (50)]

$$\frac{\hbar\omega_0}{\varepsilon_F} \sim 10^{-2}\frac{\delta s_{\rm int}}{\pi^3}\exp(2\pi), \quad \frac{\hbar\omega_0}{\varepsilon_F} \ll 1. \tag{55}$$

It should be recalled that the relation

$$\frac{\hbar\omega_0}{\varepsilon_F} \ll 1,$$

which points towards the smallness of the zero-point sound in comparison with the characteristic atomic frequencies is a necessary condition for the applicability of the kinetic theory of a normal Fermi-liquid.

Formulas (54) and (55) determine the zero-point sound frequencies for which the collisionless damping is comparable with the hydrodynamic damping of zero-point vibrations.

It should be observed that it is not appropriate to use the existing experimental data on the zero-point sound in $^3$He (see, for examples, Refs. 7, 12–16) for verifying the validity of formulas (53)–(55), if only because of the fact that the most simplified model of zero-point sound considered in this work is mainly intended for proving in principle the possibility of realizing collisionless damping mechanism for $s > 1$. However, it is clear from all that has been stated above that the collisionless mechanism of zero-point sound absorption will be realized in the best way when the system is closest to a weakly nonideal Fermi gas.

It was mentioned earlier by us that in the literature devoted to the investigation of a normal Fermi liquid, the zero-point sound attenuation occurs either according to hydrodynamic mechanisms which cannot be considered in the framework of the collisionless approximation, or under the assumption of collisionless damping (Landau mechanism), but only for $s < 1$ when this damping is so strong that it is hardly appropriate to speak of the existence of zero-point sound. Apparently, the latter circumstance is associated with the fact that according to formulas (46) and (52) there is no attenuation of zero-point sound strictly at $T = 0$, but the decrement $\gamma_k$ cannot be obtained for $T \neq 0$ and $\varepsilon_F \gg T$ by a traditional expansion in small values of temperature (as is done in the case of hydrodynamic mechanism of zero-point sound attenuation) due to a nonanalytic dependence of the damping factor on temperature.

In conclusion, the author would like to express his gratitude to Academician S. V. Peletminskii of the Ukrainian National Academy of Sciences for fruitful discussions of the obtained results.

This research was carried out under financial support from the Ukrainian State Foundation of Fundamental Research (Grant No. 24/378).

*E-mail: slusarenko@kipt.kharkov.ua

[1] L. D. Landau, Zh. Éksp. Teor. Fiz. **30**, 1058 (1957) [Sov. Phys. JETP **3**, 920 (1957)].
[2] V. P. Silin, Zh. Éksp. Teor. Fiz. **33**, 495 (1958) [Sov. Phys. JETP **6**, 387 (1958)].
[3] L. D. Landau, Zh. Éksp. Teor. Fiz. **32**, 59 (1957) [Sov. Phys. JETP **5**, 101 (1957)].
[4] V. P. Silin, Zh. Éksp. Teor. Fiz. **35**, 1243 (1959) [Sov. Phys. JETP **8**, 870 (1959)].
[5] E. M. Lifshitz and L. P. Pitaevskii, *Statistical Physics*, Pergamon Press, Oxford (1981).
[6] E. M. Lifshitz and L. P. Pitaevskii, *Physical Kinetics* [in Russian], Nauka, Moscow (1979).
[7] D. Pines and Ph. H. Nozière, *The Theory of Quantum Liquids*, New York (1966).
[8] P. Platzman and P. Wolff, *Waves and Interactions in Solid State Plasmas*, Academic Press, New York (1973).
[9] A. I. Akhiezer, V. V. Krasil'nikov, S. V. Peletminskii, and A. A. Yatsenko, Usp. Fiz. Nauk **163**, 1 (1993) [Phys. Usp. **36**, 35 (1993)].
[10] M. Luft and S. V. Peletminsky, Physica A **162**, 542 (1990).
[11] A. I. Akhiezer and S. V. Peletminskii, *Methods of Statistical Physics*, Pergamon Press, Oxford (1981).
[12] J. Gavoret, Phys. Rev. A **137**, 731 (1965).
[13] A. C. Anderson, J. I. Connoly, and J. C. Wheatley, Phys. Rev. A **135**, 910 (1964).
[14] B. E. Keen, P. W. Matthews, and J. Wilks, Phys. Lett. **5**, 5 (1963).
[15] W. P. Halperin and L. P. Pitaevskii (Eds.) *Helium Three*, North-Holland, Amsterdam (1990).
[16] E. V. Bezuglyi *et al.*, J. Phys.: Condens. Matter **3**, 7867 (1991).

Translated by R. S. Wadhwa

# Stability of a bounded charged He film on a metal substrate

V. B. Shikin and E. V. Lebedeva

*Institute of Solid State Physics, Russian Academy of Sciences, 142432 Chernogolovka, Russia**

(Submitted September 30, 1997)
Fiz. Nizk. Temp. **24**, 299–304 (April 1998)

Peculiarities in the problem of surface stability of a charged bounded helium film on a metal substrate are considered. The dependence of critical instability parameters on the in-plane film size is determined. A method is proposed for observing metastable states of a charged liquid film. © *1998 American Institute of Physics.* [S1063-777X(98)00204-7]

A charged liquid surface is known to lose its stability upon a gradual increase in the surface charge density on it.[1] This phenomenon was studied most completely for a liquid helium surface charged with electrons or ions,[2,3] on which the loss of stability by the helium surface can be tracked in detail, and basic predictions of the theory can be verified. In the case of semi-infinite helium, stability is lost for finite wave numbers (at the so-called capillary wavelength). In the supercritical region, the helium surface undergoes a reconstruction, i.e., a transition from a plane to a periodically deformed boundary with a period close to the capillary wavelength with a modulation amplitude which is a complex function of the extent of supercriticality (see theoretical[4,5] and experimental[6–8] papers).

The observation of the effect of boundedness of the free charged surface of a semi-infinite liquid also plays an important role along with other results on the stability of bulk helium with a charged surface. The expected result is qualitatively predictable although it has not been analyzed consistently. Since the instability of a bulk liquid is developed primarily over a capillary wavelength, a decrease in the size of the free liquid surface to values smaller than the capillary wavelength must increase its stability. This was proved experimentally by Volodin and Edelman.[9]

In the case of an infinitely large charged liquid film, the mode with zero wave vector turns out to be most ''vulnerable.'' This theoretical prediction (see Ref. 10) yet has not been confirmed by direct experiments. The correctness of theoretical predictions follows only from indirect and mainly qualitative indications,[11] e.g., the observed decrease (as compared to the bulk value) in the critical charge density leading to a loss in stability. A quantitative comparison of the results obtained in Refs. 10 and 11 is not quite justified since the experiments were made in a finite-size cell, while the calculations[10] give zero critical wave number, i.e., are applicable in actual practice only to the case of an infinite charged film. In order to remove the prevailing discrepancy, it is expedient to solve the problem of instability of a charged liquid film of finite dimensions. Such an analysis should be conducted to find out which film can be regarded as infinitely large and whether the qualitative discrepancy between the results obtained in Refs. 10 and 11 can be eliminated in this way. Naturally, the solution of this problem will clarify the role of geometrical factors in the behavior of critical parameters of a liquid film (in other words, we solve a film problem similar to that for bulk helium[9]).

The present publication is devoted to analysis of the behavior of a charged liquid film under the conditions facilitating the maintaining a constant value of electric potential along a charged bounded liquid film. Apart from critical parameters, we are also interested in determining the local deformation of the liquid film. The possibility of such measurements was demonstrated in recent experiments[12] with charged liquid hydrogen films. The optical methods used in Ref. 12 make it possible to study experimentally the effect of geometrical factors not only on the stability of a charged liquid film, but also on its local strain $\xi(r)$.

The first part of this paper is devoted to the structure of equilibrium equations for a charged finite liquid film in its plane and to the properties of one-dimensional version of deformation of such a film. The second part deals with the details of cylindrically symmetric case of deformation.

## ONE-DIMENSIONAL DEFORMATION OF A FINITE CHARGED LIQUID FILM

1. Let us consider a charged He film on a metallic substrate under complete compensation of the electric field above the film. The position of the upper electrode relative to the film, which is always present in the problem of a charged helium surface, is immaterial (the separation between the upper electrode and the surface must be larger than the film thickness). The geometry of the electrodes satisfies the requirements that allow us to assume that the deformation of the film thickness $\xi$ under the action of electric forces is one-dimensional (a function of the coordinate $x$ alone).

The initial equilibrium equation describing this deformation has the structure

$$\rho g\xi-\alpha\frac{\xi''}{[1+(\xi')^2]^{3/2}}+\frac{V^2}{8\pi(d+\xi)^2}=0,\quad -l\leqslant x\leqslant +l, \tag{1}$$

$$\xi(\pm l)=0, \tag{2}$$

$$V=\text{const},\quad -l\leqslant x\leqslant +l, \tag{3}$$

$$\xi''=d^2\xi/dx^2,\quad \xi'=d\xi/dx.$$

Here $\xi(x)$ is the deformation of the helium surface under the action of the aggregate of forces acting on the film surface:

 

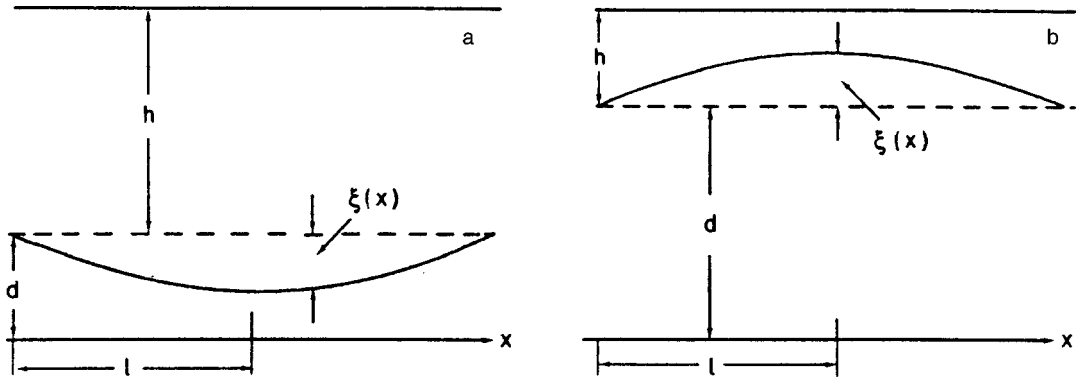


FIG. 1. Schematic diagram of the cell intended for studying the deformation of a charged He film (a) and antifilm (b).

gravity, surface tension, as well as forces of electric origin proportional to the potential difference $V$ between the charged He surface and the metallic substrate [$\xi(x)\to 0$] as $V\to 0$), $\rho$ and $g$ are the helium density and acceleration due to gravity, $\alpha$ is the surface tension, $d$ the equilibrium thickness of He film for $V\to 0$, and $2l$ the film thickness in the $x$-direction. According to (2) the deformation at the ends of this interval is maintained at zero level. The electric component of Eq. (1) is written under the assumption that the solid substrate possesses ideal metallic properties; moreover, it is assumed that the total number of electrons at the He film is not fixed (the potential difference $V$ is preset; care must be taken while deriving the equilibrium equation (1) from the total energy functional, see Ref. 1). Charges arrive at the film from a radioactive source at the upper electrode. The ''generation'' of these charges is terminated after the neutralization of the given external field $E=V/h$ by the field of charges deposited on the free surface of the film. The origin is at the metallic substrate. The $z$-axis is directed vertically upwards. The geometry of the problem is shown in Fig. 1 for a liquid film (a) and antifilm (b) (both cases are realized in Ref. 12).

2. It is appropriate to make some general remarks that explain the behavior of $\xi(x)$. If the interval $2l$ is large enough, the quantity $\xi(x)$ attains its asymptotic form $\xi_0$ away of the ends of this interval:

$$\rho g\xi_0+\frac{V^2}{8\pi(d+\xi_0)^2}=0. \tag{4}$$

In this case, only the gravitational term competes with the electric component of the problem.

A stable solution of Eq. (4) in $\xi_0$, which satisfies the requirement $\xi_0\to 0$ for $V\to 0$. exists only in the region

$$V<V_{\rm cr},\quad V_{\rm cr}^2=(2/3)^3V_*^2,\quad V_*^2=4\pi\rho g d^3. \tag{5}$$

In this case,

$$\xi_0^{\rm cr}=-d/3. \tag{5a}$$

One more characteristic value of $\xi_p$ corresponding to inflection points on the $\xi(x)$ profile also exists. The position of such points is defined by the requirement $d^2\xi/dx^2=0$ or, which is the same, by

$$\rho g\xi_p+\frac{V^2}{8\pi(d+\xi_p)^2}=0. \tag{6}$$

Obviously, the definition (4) coincides with (6). For this reason, the points of inflection on the one-dimensional profile of $\xi(x)$ are absent for large values of $l$.

Thus, the theory aims at refining the concept of ''quite large'' interval $l$, defining the dependence $\xi(l)$ near the ends of the $2D$ system, and determining the effect of finiteness of $l$ on the structure of $\xi(x)$.

3. Returning to problem (1) and (2), let us first consider the linear solution under the conditions

$$\xi(x)=\ll d. \tag{7}$$

In this case, we have

$$\begin{aligned} &d^2\xi/dx^2-p^2\xi=v^2/d^2,\quad v^2=\frac{V_2}{8\pi\alpha},\quad \xi(\pm l)=0,\\ &p^2=\kappa^2\left[1-\frac{V^2}{4\pi(d+\xi_0)^3\rho g}\right],\quad \kappa^2=\rho g/\alpha. \end{aligned} \tag{8}$$

The solution of Eq. (8) has the form

$$\xi(x)=\delta\left(1-\frac{\cosh(px)}{\cosh(pl)}\right),\quad \delta=-v^2/p^2d^2. \tag{9}$$

We shall also write the derivative $d\xi(+l)/dx$ at the end of the interval, where it assumes its maximum value:

$$\begin{aligned} &\left.\frac{d\xi(x)}{dx}\right|_{x=l}=v^2\,\tanh(pl)/pd,\\ &\left.\frac{\tanh(pl)}{p}\right|_{V\to 0}\to\kappa^{-1}. \end{aligned} \tag{10}$$

According to (9) and (10), the size effects associated with the finiteness of $l$ are determined by the parameter $pl$. In the region of small $v$, we are speaking of the combination $\kappa l$. If, however, the quantity $v$ tends to its critical value, the requirement

$$pl\gg 1, \tag{11}$$

corresponding to the limit of large values of $l$ can apply to a size much larger than the capillary constant for the given

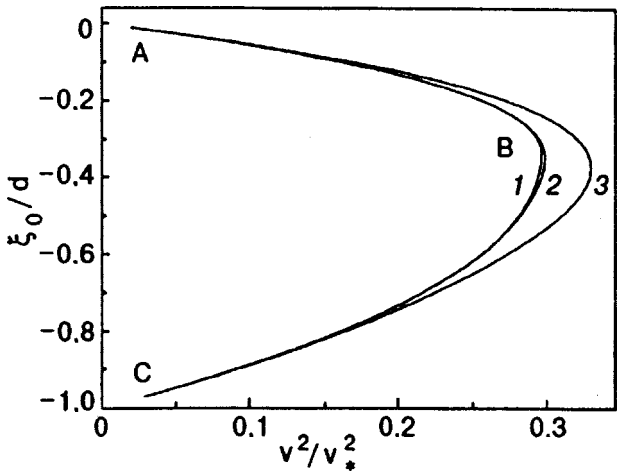


FIG. 2. Maximum deformation $\xi(0)/d$ of the film thickness as a function of the dimensionless electric potential $V/V_*$ following from (12) for different values of the parameter $l/d$. Curves *1*, *2*, and *3* correspond to $l/d=10$, 5, and 2 respectively. The points *A*, *B*, and *C* mark stable ($AB$) and metastable ($BC$) regions on the curves.

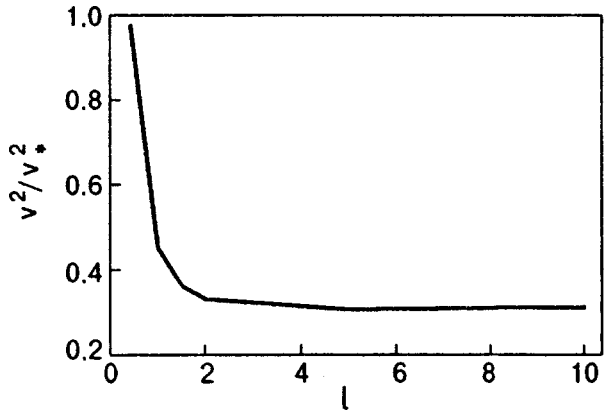


FIG. 3. Dependence of the critical field $V_c^2/V_*^2$ on the film size along the substrate.

liquid. This forms a specific feature of the problem on deformation of a helium film in comparison with the version of the same problem for a semi-infinite liquid.

4. With increasing supercritically, the position of points with the maximum derivative $\xi'_{\max}$ (points of inflection) can be shifted from the boundaries $\pm l$ to the bulk of the $2D$ system. The amplitude $\xi_p$ corresponding to these points can be found, as before, from relation (6). As regards the critical value $V_{\rm cr}$, it must be determined in the general case from an analysis of the dependence of $\xi(0)$ on the parameters of the problem. Solving Eqs. (1) and (2), we can find the required dependence in the form

$$\int_{\xi_0}^{0} \frac{d\xi}{\{0.5\kappa^2(\xi^2-\xi_0^2)+v^2[1/(d+\xi_0)-1/(d+\xi)]\}^{1/2}}=\sqrt{2}l, \tag{12}$$

where $v$ can be determined from (8).

It can easily be proved that as $l\to\infty$, the quantity $\xi(0)$ assumes the value following from (4). If, however, $l$ is finite, $\xi(0)$ becomes a function of $l$ which can be determined only numerically.

Knowing $\xi(0)$, we can easily calculate $\xi(x)$:

$$\int_{\xi(x)}^{0} \frac{d\xi}{\{0.5\kappa^2(\xi^2-\xi_0^2)+v^2[1/(d+\xi_0)-1/(d+\xi)]\}^{1/2}} =\sqrt{2}(l-x), \quad x>0. \tag{13}$$

The behavior of $\xi(0)$ (12) as a function of $v$ for various values of $l$ is illustrated in Fig. 2. An analysis of these dependences allows us to determine the behavior of $V_{\rm cr}(l)$ (Fig. 3). Figure 4 also contains information on $\xi(x)$ in (13). It should be noted that, according to Fig. 4, the statement about the absence of inflection points (6) on the coordinate dependence of film deformation in the stability region $0<V<V_{\rm cr}$ (segment $AB$ on the curve in Fig. 2) becomes universal.

5. The segment $BC$ in Fig. 2 requires special consideration. This region is not physical since, starting from small values of $V$, we cannot ''reach'' the $BC$ curve continuously. If, however, we track the evolution of the film after its loss of stability, we can expect the following scenario. The breakdown indicates the escape of charged particles from the surface of the liquid film to the metallic substrate. If the charge mobility in the liquid is quite small, the vacuum gap above the liquid film immediately after a breakdown becomes unscreened (new charges have no time to reach the film). The potential difference $V$ concentrated completely on the liquid film prior to the breakdown is redistributed over the entire interval $h$ (see Fig. 1a). Only its fraction $\delta V\ll V$ (associated with the residual surface charge) continues to exert electrostatic pressure on the liquid film. In other words, the stability breakdown under the conditions depicted in Fig. 1a with a source at the upper metallic plate automatically brings the system to a state on the $BC$ curve (see Fig. 2). If we also reduce slightly the initial voltage $V$, we can hope that the problem will be stabilized on the $BC$ curve in Fig. 2.

Considering what has been said above (in addition to the data presented in Fig. 4), we obtain the solution of the problem on the deformation on the liquid film on the $BC$ curve (Fig. 5). A typical feature of this deformation is the reverse variation of deformation as a function of voltage $V$ and the emergence of points of inflection on the $\xi(x)$ curves.

6. The case of the antifilm investigated in Ref. 12 does not require special calculations. We should only place the origin at the upper electrode and direct the $x$-axis vertically downwards (see Fig. 1b). After this, the problem of the antifilm is reduced to the film problem.

## DEFORMATION OF A CYLINDRICALLY SYMMETRIC FILM

Let us now suppose that the deformation of the film surface is cylindrically symmetric. Will formal changes in the structure of the equilibrium equation (1) lead to new physical consequences like the emergence of points of inflection on the stable segment $AB$ in Fig. 2? The answer to this question is not obvious since in this case definitions (5) and (6) are not equivalent.

Thus, instead of (1) we have

$$\rho g\xi-\alpha\frac{\xi''+\xi'/r}{[1+(\xi')^2]^{3/2}}+\frac{V^2}{8\pi(d+\xi)^2}=0, \tag{14}$$

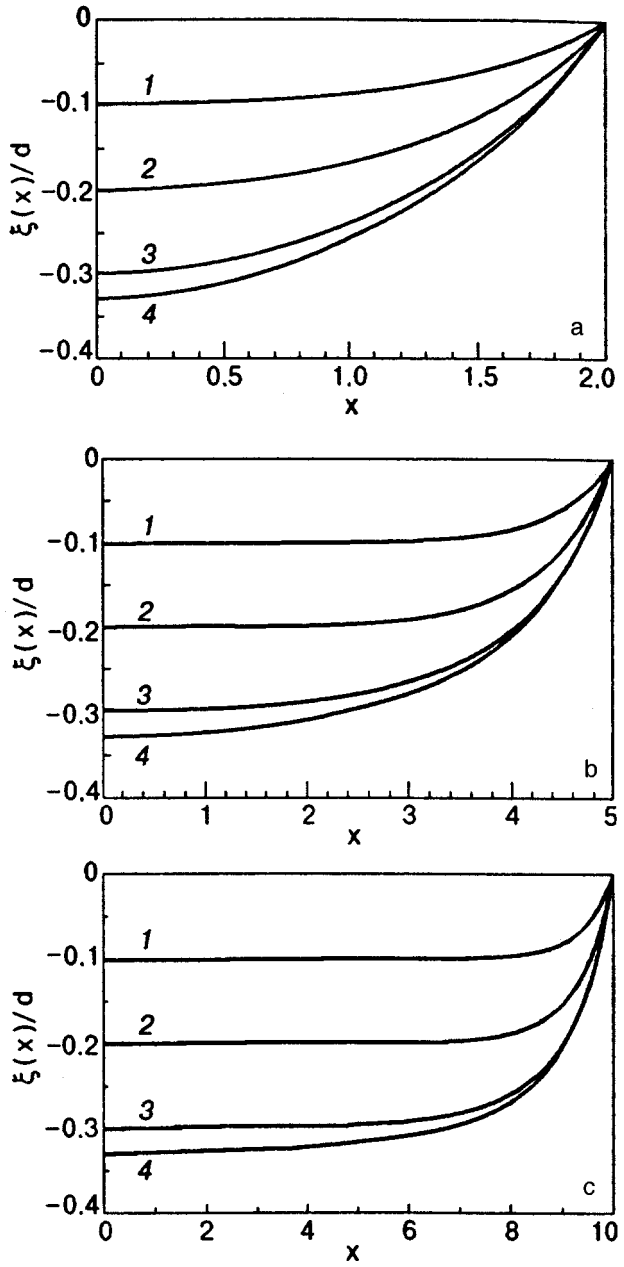


FIG. 4. Deformation $\xi(x)/d$ calculated on the basis of (13) for different values of $V/V_*$ and $l/d$ on the stable segment $AB$ of the curve in Fig. 2. Versions a, b, and c were obtained for $l/d=10$, 5, and 2 respectively. Curves 1–4 in each figure correspond to different values of the parameter $V/V_*$ and are obtained upon its monotonic increase.

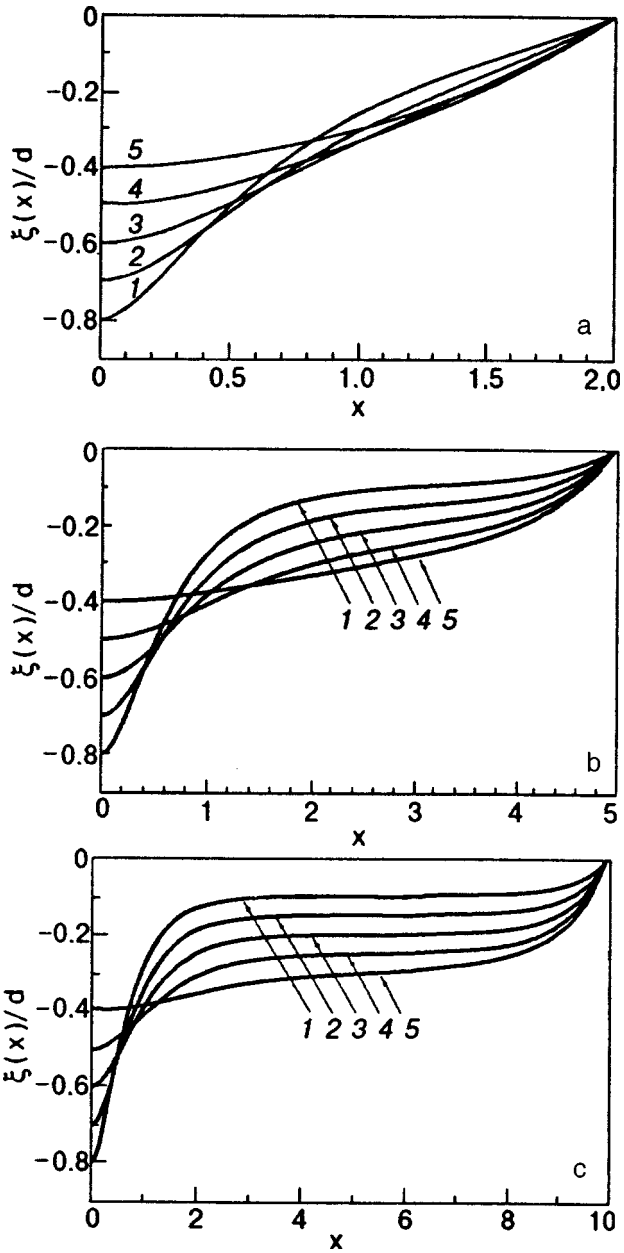


FIG. 5. Deformation $\xi(x)/d$ calculated on the basis of (13) for different values of $V/V_*$ and $l/d$ on the metastable segment $BC$ of the curve in Fig. 2. Versions a, b, and c were obtained for $l/d=2$, 5, and 10, respectively. Curves *1–5* in each figure correspond to different values of the parameter $V/V_*$ and are obtained upon its monotonic decrease.

$$0 \leqslant r \leqslant R,$$

$$\xi(r=R)=0, \tag{15}$$

$$\xi''=d^2\xi/dr^2, \quad \xi'=d\xi/dr.$$

Here, as before, $\xi(r)$ is the film deformation under the action of the aggregate of forces acting on its surface: gravity, surface tension, and forces of electric origin, which are proportional to the potential difference $V$ between the charge helium surface and the metallic substrate [$\xi(r)\to 0$ as $V\to 0$]; $\rho$ and $g$ are the liquid density and acceleration due to gravity, $\alpha$ is the surface tension, $d$ the equilibrium film thickness for $V\to 0$, and $R$ is the size of the film in the direction $r$. According to (15), the deformation is maintained at zero level on the perimeter of the film.

Going over to an analysis of the solution of Eq. (14), we write this equation for the central part of the film:

$$\rho g\xi(o)-2\alpha\xi''(o)+\frac{V^2}{8\pi[d+\xi(o)]^2}=0. \tag{16}$$

Here we have used the assumption concerning the behavior of $\xi(r)$ in the vicinity of the origin:

$$\xi(r)\cong\xi(o)+\xi''(o)r^2/2. \tag{17}$$

As regards the point of inflection $r_p$ on the $\xi(r)$ profile, it is defined, as before, by the requirement

$$\xi''(r_p)=0, \tag{18}$$

Consequently, taking into account (14), we can write

$$\rho g\xi(r_p)-\alpha\frac{\xi'(r_p)/r_p}{[1+\xi')^2(r_p)]^{3/2}}+\frac{V^2}{8\pi(d+\xi(r_p))^2}=0. \tag{19}$$

Besides, the following condition must be satisfied by hypothesis:

$$|\xi(r_p)|<|\xi(o)|. \tag{20}$$

For the subsequent analysis, it is important to know the signs of $\xi''(o)$ and $\xi'(r_p)$. By hypothesis, we have

$$\xi'(r_p)>0, \quad \xi''(o)>0 \tag{21}$$

and

$$\xi'(r_p)\cong\xi''(o)r_p. \tag{22}$$

Combining now (16) and (19), we obtain

$$\alpha\xi''(o)\left[2-\frac{1}{[1+\{\xi'(r_p)\}^2]^{3/2}}\right]=\frac{V^2}{8\pi}\left[\frac{1}{[d+\xi(o)]^2}-\frac{1}{[d+\xi(r_p)]^2}\right]-\rho g[\xi(o)-\xi(r_p)]. \tag{23}$$

The left-hand side of this relation is positive. The sign of the right-hand side is determined by contributions of the expressions in the two brackets. Taking into (20) account, we can easily see that the quantity in the first brackets is positive and in the second brackets negative. In other words, both contributions to the right-hand side of (23) are positive. Consequently, a point of inflection might appear on the $\xi(r)$ curve in the cylindrically symmetric case even on the segment $AB$ in Fig. 4.

## CONCLUSION

The problem on deformation and loss of stability of a charged film on a metallic substrate has been analyzed in detail in the one-dimensional approximation. Here we present a complete pattern of deformation of a He film, including the determination of critical parameters and their dependence on the film thickness and size along the substrate. It is noted that there are no points of inflection on the static deformation profile of the film on the entire segment $AB$ (see Fig. 2). Moreover, it is noted that the states of the film which are regarded as commonly unfeasible can be stabilized on the segment $BC$ in Fig. 2.

The nonlinear radially-symmetric equation (14) cannot be solved analytically. Nevertheless, some exact statements make the experimental verification possible. Indeed, the following quantities can be determined: $\xi(o);\xi(r_p);$ $r_p;d\xi(r_p)/dr$.

These parameters are not independent. For example, substituting these parameters into (22) and (23), we can verify whether they satisfy these relations. Naturally, the presence of a point of inflection on the $\xi(r)$ profile in the case of a cylindrically symmetric stable solution of Eq. (14) is naturally of primary importance.

This research was supported under the project TM 17 of the NASA RSA Program.

*E-mail: shikin@issp.as.ru

[1] L. D. Landau and E. M. Lifshitz, *Electrodynamics of Continuous Media* [in Russian], Gostekhizdat, Moscow (1957).
[2] L. P. Gor'kov and D. M. Chernikova, Pis'ma Zh. Éksp. Teor. Fiz. [JETP Lett.] (in press).
[3] V. B. Shikin and Yu. P. Monarkha, *Two-dimensional Charged Systems in Helium* [in Russian], Nauka, Moscow (1989).
[4] L. P. Gor'kov and D. M. Chernikova, Dokl. Akad. Nauk SSSR **228**, 829 (1976) [Sov. Phys. Dokl. **21**, 328 (1976)].
[5] V. I. Mel'nikov and S. V. Meshkov, Pis'ma Zh. Éksp. Teor. Fiz. **33**, 222 (1981) [JETP Lett. **33**, 211 (1981)].
[6] M. Wanner and P. Leiderer, Phys. Rev. Lett. **42**, 315 (1979).
[7] P. Leiderer and M. Wanner, Phys. Lett. **A73**, 1869 (1979).
[8] R. W. Giannetta and H. Ikezi, Surf. Sci. **113**, 412 (1982).
[9] A. P. Volodin and V. S. Edelman, Pis'ma Zh. Éksp. Teor. Fiz. **37**, 8 (1983) [JETP Lett. **37**, 7 (1983)].
[10] D. M. Chernikova, Fiz. Nizk. Temp. **2**, 1374 (1976) [Sov. J. Low Temp. Phys. **2**, 669 (1976)].
[11] A. P. Volodin and V. S. Edelman, Pis'ma Zh. Eksp. Teor. Fiz. **26**, 707 (1977) [JETP Lett. **26**, 543 (1977)].
[12] A. Levchenko, E. Teske, G. Kolmakov, *et al.*, Pis'ma Zh. Éksp. Teor. Fiz. **65**, 547 (1997) [JETP Lett. **65**, 572 (1997)].

Translated by R. S. Wadhwa

## SUPERCONDUCTIVITY, HIGH TEMPERATURE SUPERCONDUCTIVITY

# Superconductivity above 250K in $Tl_{1.8}Ba_{2.0}Ca_{2.6}Cu_{3.0}O_{10+\delta}$ at high pressure

C. Y. Han,[1] W. Lin,[2] Y. S. Wu,[2] B. Yin,[1] and D. S. Tang[1]

[1]*State Key Laboratory of Magnetism, Institute of Physics, Chinese Academy of Sciences, Beijing 100080, China*
[2]*Changsha Research Institute of Mining and Metallurgy, Changsha, Hunan 410012, China*
(Submitted November 3, 1997)
Fiz. Nizk. Temp. **24**, 305–308 (April 1998)

The pressure dependence of the superconducting transition temperature $T_c$ (onset) of $Tl_{1.8}Ba_{2.0}Ca_{2.6}Cu_{3.0}O_{10+\delta}$ (Tl-2223) has been measured under quasi-hydrostatic pressure (QHP) up to 5.0 GPa. The $T_c$ increases with increasing pressure at a relatively high rate and reaches a maximum at 255.4 K and pressure of about 4.3 GPa. This is the highest $T_c$ yet observed for any high-$T_c$ superconductor. The total change in $T_c$ from ambient condition ($T_c = 129$ K) to the high pressure applied can be greater than 126 K. The $T_c$ above 200 K was replicated several times in our experiments. The site of the maximum of $T_c$ and the value of $dT_c/dP = 1.7$ K/GPa (at $P = 0$) agree with previous results obtained by D. Tristan Jover *et al.* (Physica C **218**, 24 (1993)) and J. G. Lin *et al.* (Physica C **175**, 627 (1991)), respectively.
 [S1063-777X(98)00304-1]

### 1. INTRODUCTION

High pressure has played an important role in identification of new materials and mechanisms in high-temperature superconductivity.[1–3] The pressure dependence of the critical temperature of high-temperature superconductors has been studied extensively. For example, L. Gao *et al.*[3] obtained a much higher value of $T_c$ (164 K) at a pressure of up to 31 GPa in the high-$T_c$ superconductor Hg-Ba-Ca-Cu-O (1223). D. D. Berkeley *et al.*[4] observed a maximum $T_c$ of 131.8 K at 7.4 GPa in single crystals of $Tl_2Ba_2Ca_2Cu_3O_{10-\delta}$. Tristan Jover *et al.*[1] obtained the superconducting transition temperature in $Tl_2Ba_2Ca_2Cu_3O_{10+\delta}$, which increased from 128.5 K to 133 K with increasing pressure from 0 to 13 GPa. The maximum value of $T_c$ (onset) in this compound was found at pressure of about 4.0 GPa. A systematic study of the pressure effects on the superconducting transition temperatures of Tl-based family has been made by J. G. Lin *et al.*,[2] who obtained $dT_c/dP = 2.5$ K/GPa for Tl-2223 samples at a pressure of only up to 2 GPa.

From their plot of $T_c$ vs $P$ for a Tl-based compound system, it seems that for Tl-2223 and Tl-2122 compounds the $T_c$ may be further enhanced. In view of these circumstances and based upon our previous experience in high-pressure experiments, we have carried out some experiments on Tl-2223 compounds.

Here we report our investigation on the superconductivity of $Tl_{1.8}Ba_{2.0}Ca_{2.6}Cu_{3.0}O_{10+\delta}$ compound under high pressures up to 5.0 GPa. We found that $T_c$ changes rapidly with applied high pressures, especially in the range of pressures from 3.0 to 4.0 GPa. The $T_c(P)$ is observed to increase from 129 K at atmospheric pressure to 255.4 K at 4.3 GPa.

### 2. EXPERIMENTAL TECHNIQUE

The samples were prepared by using the ordinary solid reaction technique. After the powders of $Tl_2O_3$, CaO, BaO, and CuO had been thoroughly mixed and ground, they were pressed into pellets with a diameter of $\sim 12$ mm and thickness of $\sim 2$ mm, and then sintered at 890 °C for 5 h in flowing oxygen gas. The samples prepared in this way were then put into quartz cells, which were evacuated to $10^{-4}$ Torr, sealed, heat treated at 750 °C for 250 h, and finally air-quenched to room temperature.[5] Samples ($30 \times 50 \times 300\ \mu m^3$) used for measurements under quasihydrostatic pressure (QHP) up to 5.0 GPa were cut from the above pellet.

The QHP was generated in a high-pressure chamber by a special system to compress the planes of Bridgman anvil made of tungsten carbide, which was fitted into a cylinder made of fully hardened beryllium copper alloy, with the diameter of the plane 1.2 mm. A thin disk made by pressing the $Fe_2O_3$ powder was used as the pressure transmitting medium, which had a diameter equal to that of the anvil plane. The gasket was made of $Fe_2O_3$ and talc powder mixture compressed into a thin ring ($\sim 10-15\ \mu$m thick). Pressures in the cells were calibrated against the various phase transitions of bismuth at room temperature and by using the superconducting Pb manometer at low temperature in separate calibration runs; however, the pressure was not directly measured *in situ* during the experimental cycles. The overall uncertainty in QHP was estimated to be $\pm(10-15\%)$ at different temperatures.

Superconducting transition of the $Tl_{1.8}Ba_{2.0}Ca_{2.6}Cu_{3.0}O_{10+\delta}$ sample under pressure was determined electrically by the four-probe technique, with thin

 

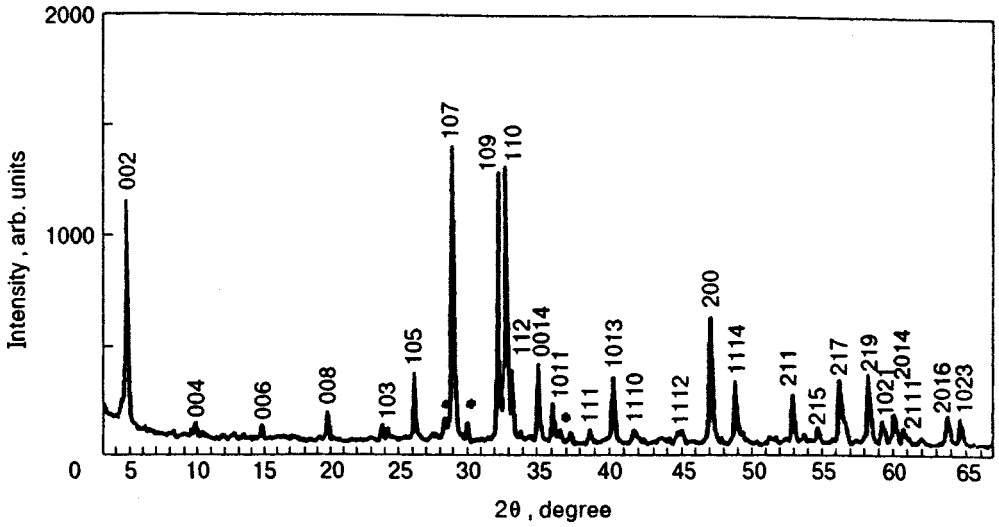


FIG. 1. Powder X-ray diffraction pattern of the as-prepared $Tl_{1.8}Ba_{2.0}Ca_{2.6}Cu_{3.0}O_{10+\delta}$ sample.

platinum strips ($\sim 20$ $\mu$m thick) used as electrical leads. The measuring direct current of $(100 \pm 0.2)$ $\mu$A was held constant in the whole range of pressures and temperatures. Sample temperature was measured using a rhodium-iron thermometer (Calibrated by Cryogenic Laboratory, CAS, China), which was inserted into the high-pressure cell and placed 10 mm from the sample. All of the $T_c(P)$ curves were measured during dropping and rising of temperature and recorded by a X-Y recorder.

### 3. RESULTS AND DISCUSSION

The X-ray powder diffraction patterns for an as-prepared sample $Tl_{1.8}Ba_{2.0}Ca_{2.6}Cu_{3.0}O_{10+\delta}$ measured with a RAX-10 X-ray diffractometer (Fig. 1) show a nearly perfect single phase of Tl-2223 with a tetragonal unit cell with parameters $a = 3.85$ Å and $c = 35.70$ Å.

The dc magnetization was measured using a SQUID magnetometer (quantum design). The ZFC magnetization as a function of temperature for the $Tl_{1.8}Ba_{2.0}Ca_{2.6}Cu_{3.0}O_{10+\delta}$ sample in a field of $H = 5$ Oe and at ambient pressure shows a sharp single-phase superconducting transition at 129 K and antimagnetic factor of 19% (Fig. 2).

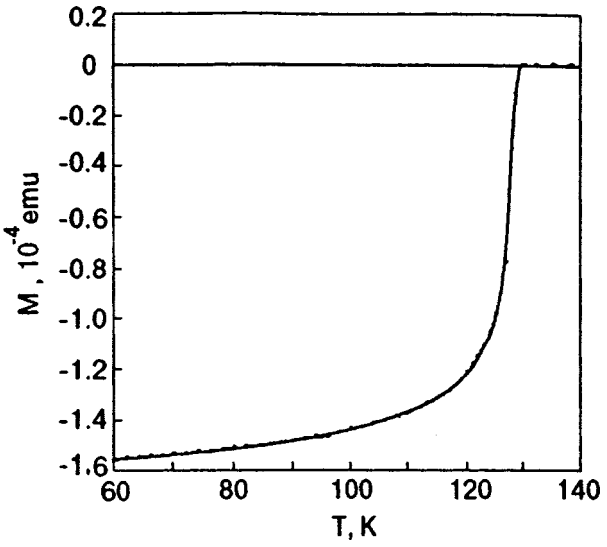


FIG. 2. Temperature dependence of magnetization of the pellet sample at ambient pressure in zero-field cooling (ZFC) at $H = 5$ Oe.

In order to determine the uncertainty of the temperature measurements, the system was put into a liquid LN2 of 77.4 K and the ice water of 273.15 K, respectively. Under this condition the temperature uncertainties are shown in Table I.

We have measured the $R(T,P)$ curves for the cooling and warming processes. In this paper we gave all the curves of the superconducting transition during the warming processes, because the warming rate could be made as small as $\sim 0.2$ K/min, and steady state can easily be achieved, even though we found that the superconducting transition occurs at considerable higher temperatures in both processes.

The temperature dependence of normalized resistance with respect to the resistance values measured at $T_c$ under different pressures up to 4.3 GPa for one sample $Tl_{1.8}Ba_{2.0}Ca_{2.6}Cu_{3.0}O_{10+\delta}$ is shown in Fig. 3. The pressures were applied slowly and continuously from zero to 5 GPa. It can be seen that the $T_c$ (onset) is clearly shifted upward with the increase of the applied pressure. When the pressure increases continuously, the $T_c$ rises rapidly and reaches 255.4 K at pressure of 4.3 GPa. The total change in $T_c$ from ambient condition to the high pressure applied can be greater than 126 K. As the pressure is further increased to 4.8 GPa, the $R(T,P)$ curve changes, the behavior of the temperature dependence becomes semiconducting, and there is a marked drop of transition temperature ($T_c \sim 206$ K).

TABLE I. $\Delta T(K)$-temperature difference between the sample and the thermometer which is located 10 mm from the sample.

| Sample temperature | Temperatures were measured by rhodium-iron thermometer 5# | | | |
|---|---|---|---|---|
| | $P = 0$ GPa | $\Delta T(K)$ | $P = 3.5$ GPa | $\Delta T(K)$ |
| 77.4 K | 77.44 K | 0.04 | 77.43 K | 0.03 |
| 273.15 K | 273.65 K | 0.5 | 272.55 K | 0.6 |

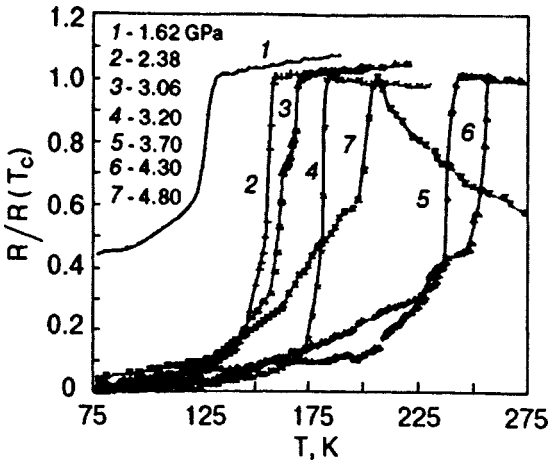


FIG. 3. Temperature dependence of normalized resistance of the $Tl_{1.8}Ba_{2.0}Ca_{2.6}Cu_{3.0}O_{10+\delta}$ (Tl-2p4) sample under different pressures.

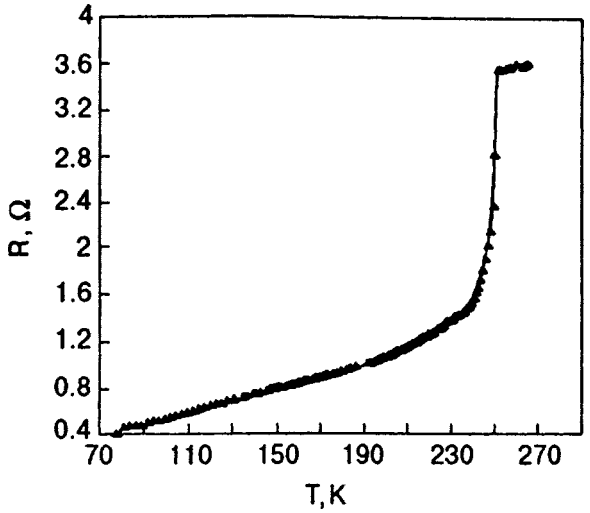


FIG. 5. Temperature dependence of the resistance of $Tl_{1.8}Ba_{2.0}Ca_{2.6}Cu_{3.0}O_{10+\delta}$ (Tl-2p7) at a pressure of 3.2 GPa.

From Fig. 3 we can also see that the resistance ($R$) of the sample decreases with the increase of pressure, which, however, does not reach zero in the range of pressures applied, by analogy with the previous study of superconducting cuprates at high pressure.[6,7] The reason for the nonzero behavior of $R(T,P)$ may be attributed to possible defects and microcracks generated in the sample, as reported by C. W. Chu *et al.*,[6] but we think it may also come from the possible pressure gradient generated in the anvils, especially at low and very high pressures for the QHP system. The maximum value of the resistances of the sample are about $\sim 3\,\Omega$ at the normal state and under high pressures.

To verify the reproducibility of the effect of high pressure, we have also carried out experiments with decreasing pressure. The results are summarized in Fig. 4, where the transition temperatures $T_c$ are plotted versus pressure for both increasing and decreasing pressures. We found that $T_c(P)$ is a reversible nonlinear function of pressure. The location of the maximum of $T_c$ and the value of $dT_c/dP = 1.7$ K/GPa (at $P = 0$) agree with the previous studies of Tristan Jover *et al.*[1] and J. G. Lin *et al.*,[2] respectively.

To test the reliability of the above results, we have repeated our experiments several times with other samples cut from the same pellet which was described above. We obtained similar results, one of which is shown in Fig. 5. It can be seen that at a pressure of 3.2 GPa $T_c$ rises to 250 K, while the resistance drops sharply to 13.5% (at 80 K) in comparison with its maximum value. For yet another sample we have obtained $T_c(\text{onset}) = 153.7$ and 235 K at pressures 1.9 and 3.4 GPa, respectively, which are not shown in the figure.

In summary, the pressure dependence of the superconducting transition temperature in the compound of $Tl_{1.8}Ba_{2.0}Ca_{2.6}Cu_{3.0}O_{10+\delta}$ has been determined: the $T_c$ (onset) increases with increasing pressure at a relatively high rate and reaches a maximum value of 255.4 K at a pressure of about 4.3 GPa. External pressure greatly enhances the critical temperature of the oxide superconductor sample. The basic physical reason for this phenomenon is the stronger coupling between the $CuO_2$ planes and the change in free charge concentrations in the superconducting $CuO_2$ layers caused by external pressure. Our experimental investigation on the effect of high pressure on $T_c$ of another pellet of Tl-2223 superconductor is continuing.

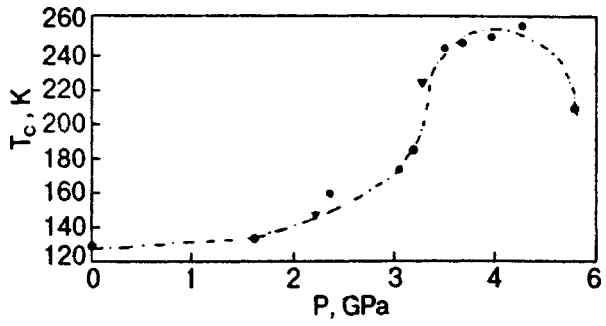


FIG. 4. Superconducting transition temperature $T_c$ (onset) of $Tl_{1.8}Ba_{2.0}Ca_{2.6}Cu_{3.0}O_{10+\delta}$ (Tl-2p4) as a function of pressures: ●—as pressure is increased; ▼—as pressure is decreased.

This work was supported by the National Center for R&D on Superconductivity of China and by The State Commission for Education of China.

The authors would like to gratefully acknowledge help and discussions with Profs. G. Z. Yang, L. Lin, and Q. S. Yang. We would also like to thank Prof. N. B. Brandt (Moscow National University) for guidance in technology for superconductivity at high pressure.

[1] D. Tristan, R. J. Wijngaarden, R. S. Liu, L. Tallon, and R. Griessen, Physica C **218**, 24 (1993).
[2] J. G. Lin, K. Matsuishi, Y. Q. Wang, Y. Y. Xue, P. H. Hor, and C. W. Chu, Physica C **175**, 627 (1991).
[3] L. Gao, Y. Y. Xue, F. Chen, O. Xiong, R. L. Meng, D. Ramirez, and C. W. Chu, Phys. Rev. B **50**, 4260 (1994).
[4] D. D. Berkley, E. F. Skelton, N. E. Moulton, M. S. Osofsky, W. T. Lechter, and V. M. Browning, Phys. Rev. B **47**, 5524 (1993).
[5] Y. S. Wu, Z. W. Oi, Q. Y. Peng, X. Y. Lon, H. T. Peng, J. P. Chen, J. S.

Huang, and B. X. Cui, *Proceedings of the Beijing International Conference on ''High-Temperature Superconductivity''* (BHTSC'92), World Scientific (1992), p. 256.
[6] C. W. Chu, L. Gao, F. Chan, Z. L. Huang, R. L. Meng, and Y. Y. Xue, Nature (London) **365**, 323 (1993).
[7] H. Ihara, M. Hirabayashi, H. Tanino, K. Tokiwa, H. Ozawa, Y. Akahama, and H. J. Kawamura, J. Appl. Phys. **32L**, 1732 (1993).

This article was translated in English in the original Russian journal. It was edited by S. J. Amoretty.

# Magnetic-field suppression of superconductivity in layered high-$T_c$ materials

V. N. Varyukhin, G. G. Levchenko, Yu. V. Medvedev, and A. V. Pashchenko

*A. Galkin Physicotechnical Institute, National Academy of Sciences of the Ukraine, 340114 Donetsk, Ukraine**

S. J. Lewandowski

*Institut Fizyki, Polish Academy of Sciences, PL02-668 Warszawa, Poland***

(Submitted May 13, 1997; revised November 17, 1997)
Fiz. Nizk. Temp. **24**, 309–315 (April 1998)

The dependence of the superconducting transition temperature in $GdBa_2Cu_3O_{6+\delta}$ single crystals on the magnetic field $H$ applied parallel to the intercrystalline layers is studied experimentally. A nontrivial dependence of the superconducting transition temperature on the field $H$ is explained by magnetic field penetration into high-$T_c$ single crystals. The presence of a layered structure leads to the formation of a spatially periodic magnetic structure with a period varying discretely in fields $H \gg H_{c1}$ ($H_{c1}$ is the lower critical field). Any change in the magnetic structure results in a nonmonotonic (jumpwise) dependence of the superconducting transition temperature on the field $H$. The effect is estimated numerically by using the results of calculation of the critical temperature of small samples in strong magnetic fields.  [S1063-777X(98)00404-6]

New layered HTS materials with a relatively weak Josephson coupling between layers possess specific properties similar to those observed in the study of two-dimensional or nearly $2D$ superconductivity. The effect of the layered crystal structure on the thermodynamics and electrodynamics of HTS materials is being studied intensely both theoretically and experimentally (e.g., the crossover from the two- to three-dimensional behavior in phase transitions, the same for fluctuational diamagnetism, heat capacity, paraconductivity effect, and observation of the Berezinskii–Kosterlitz–Thouless phase transition).

The studies of layered superconductors in a strong magnetic field applied parallel to the layer are of considerable interest. In this case, the properties of the vortex lattice differ from those analyzed in the $3D$ approximation. For example, Bulaevskii and Clem[1] proved that strong magnetic fields induce a new effect, i.e., a first-order transition between vortex lattices with different periods $L=2ks$ in a direction perpendicular to the layers (here $k=1,2,\ldots$ and $s$ is the separation between the planes). Such jumps in the lattice structure are associated with the discrete layered structure of the crystal and the Josephson nature of the coupling between the layers.

The results of investigations of superconducting properties of oxygen-deficient $GdBa_2Cu_3O_{6+\delta}$ single crystals[2,3] revealed that single crystals with a low oxygen concentration ($\delta=0.4$) acquire quasi-two-dimensional superconductivity. No phase coherence was observed between layers in systems with $\delta=0.4$. As the oxygen concentration in single crystals increases to $\delta=0.56$, a weak Josephson coupling is established between the planes, and a further increase in the oxygen content (to $\delta=0.75$) leads to clearly manifested three-dimensional superconductivity. For this reason, the study of superconductivity suppression in $GdBa_2Cu_3O_{6+\delta}$ single crystals by a magnetic field is undoubtedly of physical importance.

In this research, we carry out an exterimental investigation of the effect of an external magnetic field on the emergence of superconductivity in $GdBa_2Cu_3O_{6+\delta}$ single crystals with oxygen concentration of 6.2, 6.56, and 6.75, i.e., in samples with a Josephson coupling between the layers, as well as theoretical analysis of this effect on the basis of the model concepts of the layered $2D$ structure of HTS materials. We discovered peculiarities in the behavior of the superconducting transition temperature $T_c$ in the above sincle crystals depending on the direction of the applied magnetic field. Instead of a monotonic decrease in $T_c$ that can be expected due to antisymmetric properties of perturbations excited by strong magnetic fields (see Ref. 4), we observed a nontrivial (jumpwise) dependence $T_c(H)$ for single crystals with the $C$-axis directed at right angles to the field. Using the results obtained by Bulaevskii and Clem (see above),[1] as well as the results of calculations of the superconducting transition temperature for small samples in strong magnetic fields,[4] we can prove that such a behavior of $T_c(H)$ is due to transitions between vortex lattices with different periods.

## EXPERIMENTAL TECHNIQUE

We investigated $GdBa_2Cu_3O_{6+\delta}$ single crystals with oxygen content 6.75 (sample 1), 6.56 (sample 2), and 6.2 (sample 3). The samples were grown in an Alundum crucible. The oxygen concentration after synthesis was 6.4. In order to increase the oxygen index, we subjected the samples to a special thermal treatment in oxygen atmosphere. The oxygen content and uniformity of its distribution over the sample were analyzed on a Syntex P2 diffractometer. Single crystals had a tetragonal structure and were homogeneous in

 

oxygen. It was found that the samples contain 1% aluminum impurity acquired during the sample growth. The sizes of the samples were $1.2\times1.2\times0.4$ mm (sample 1), $1.2\times2\times0.6$ mm (sample 2), and $2.1\times2.2\times1.6$ mm (sample 3). More detailed characteristics of the samples can be found in Ref. 5.

We measured the temperature dependences of differential susceptibility (ac-susceptibility) in constant magnetic fields applied along two directions (perpendicular and parallel to the $C$-axis) for all the samples as well as the temperature and field dependences of magnetization in sample 3 and the temperature dependence of the electrical resistance of the same sample in external magnetic fields. The susceptibility was measured at a frequency of 31 Hz (the modulation field was $2\times10^{-4}$ T for measurements along the $C$-axis and $6\times10^{-4}$ T for measurements in the perpendicular direction). The temperature dependences of susceptibility for all the samples were measured in magnetic fields of 0, 1.21, 6.04, 12.08, 18.12, 24.16, 30.25, and 36.24 kOe. The magnetization was studied on a vibrational magnetometer, while the electrical resistance was measured by the four-probe technique in ac. In all the cases, the samples were first cooled to 1.5 K in zero magnetic field, and then the magnetic field was applied, and measurements were made during heating.

## EXPERIMENTAL RESULTS

Figures 1 and 2 show the temperature dependences of ac-susceptibility measured along and across the $C$-axis of the $GdBa_2Cu_3O_{6+\delta}$ single crystals with oxygen contents 6.75 and 6.56. It can be seen that the $\chi_H^{\parallel}(T)$ curves for both samples in a magnetic field applied along the $C$-axis are shifted downwards along the temperature scale. Such a shift can be explained by ordinary suppression of superconductivity by a magnetic field stronger than the upper critical field. Temperature dependences of ac susceptibility in a direction perpendicular to the $C$-axis is of recurrent type. For the sample with oxygen concentration 6.75 (see Fig. 1b) in a field $H=0$, the susceptibility is diamagnetic for $T<T_{\text{onset}}$. As the magnetic field increases, the $\chi_H^{\perp}(T)$ curves are first displaced to the low-temperature region ($H=6$ kOe), then to the high-temperature region ($H=12$ kOe), and again to the region of low temperatures upon a further increase in the magnetic field. For the sample with oxygen content 6.56, the susceptibility in the direction perpendicular to the $C$-axis is paramagnetic for $H=0$ (see Fig. 2b). In strong fields, diamagnetism is observed.

In order to explain the behavior of the temperature dependences of ac susceptibility in a magnetic field, we must take into account the fact that the susceptibility being measured is the sum of the contributions of the magnetic and superconducting subsystems. In order to single out the contribution from the superconducting subsystem, we must subtract from the integral ac-susceptibility being measured the component due to the magnetic subsystem. The magnetic contribution to the integral susceptibility of the superconducting sample is equal to the ac susceptibility of the normal sample if it is also of magnetic origin only and does not change with the oxygen concentration.

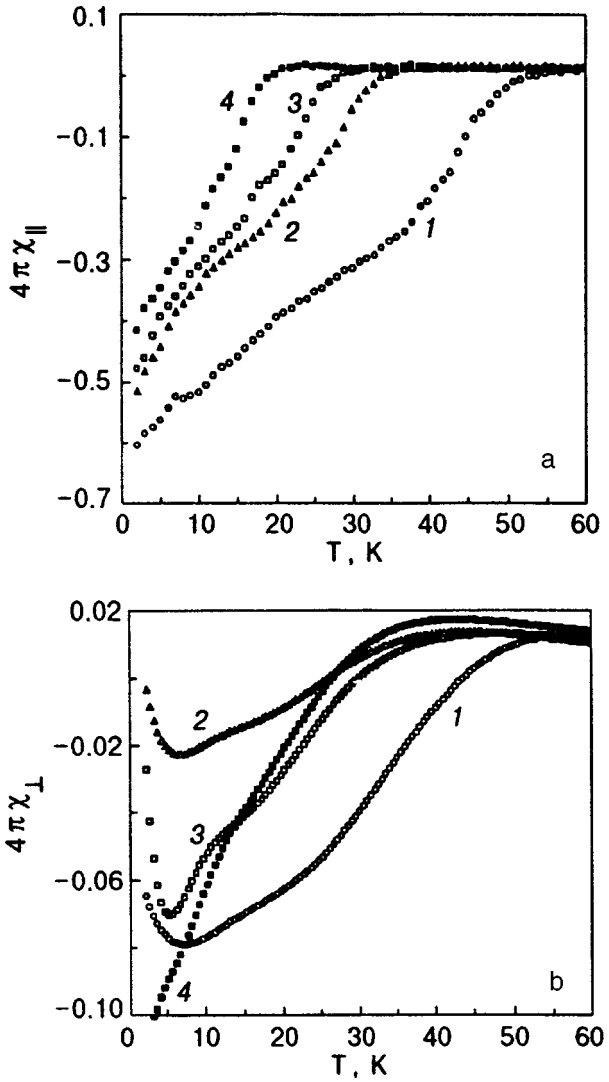


FIG. 1. Temperature dependences of ac susceptibility of a $GdBa_2Cu_3O_{6.75}$ single crystal in constant external magnetic fields $\mathbf{H}\|C$(a) and $\mathbf{H}\perp C$(b): $H=0$ (curve *1*), 6.04 (curve *2*), 12.08 (curve *3*), and 36.24 kOe (curve *4*).

In order to find the origin of the ac susceptibility of a nonsuperconducting sample, we measured the $\chi(T)$ dependences for $GdBa_2Cu_3O_{6.2}$ in fixed external fields along and across the $C$-axis (Fig. 3) and carried out their detailed analysis.[6,7] The analysis is essential in view of singularities on the $\chi_{\parallel}(T)$ and $\chi_{\perp}(T)$ curves in the form of peaks whose position is determined by the magnitude of the magnetic field. Such a behavior of $\chi(T)$ can be due to a change in the conductivity of $GdBa_2Cu_3O_{6.2}$ in a magnetic field, or the conditions of magnetization reversal of the magnetic subsystem (adiabatic nature of ac susceptibility), or purely magnetic phenomena (the Schottky effect). In our case, it is important to eliminate the change in the ac susceptibility associated with a change in conductivity. Only in this case the contribution associated with the superconducting subsystem can be determined by subtracting the susceptibility of normal samples from the susceptibility of the samples in the superconducting state being measured.

The conductivity of $GdBa_2Cu_3O_{6.2}$ in a magnetic field decreases monotonically (the electrical resistance increases)

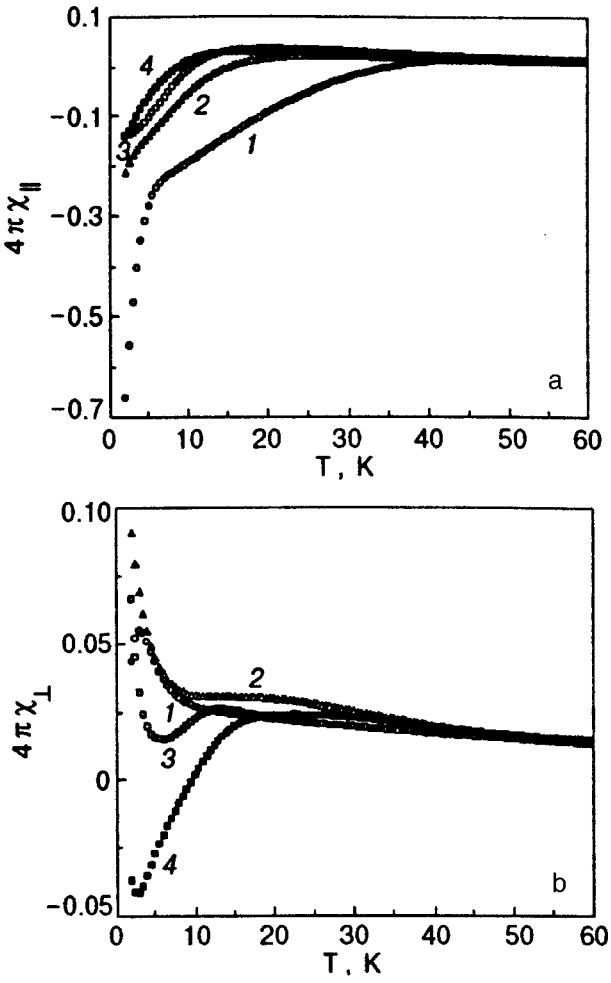


FIG. 2. Temperature dependences of ac susceptibility of a $GdBa_2Cu_3O_{6.56}$ single crystal in constant external magnetic fields $\mathbf{H}\|C$(a) and $\mathbf{H}\perp C$(b): $H=0$ (curve *1*), 6.04 (curve *2*), 12.08 (curve *3*), and 36.24 kOe (curve *4*).

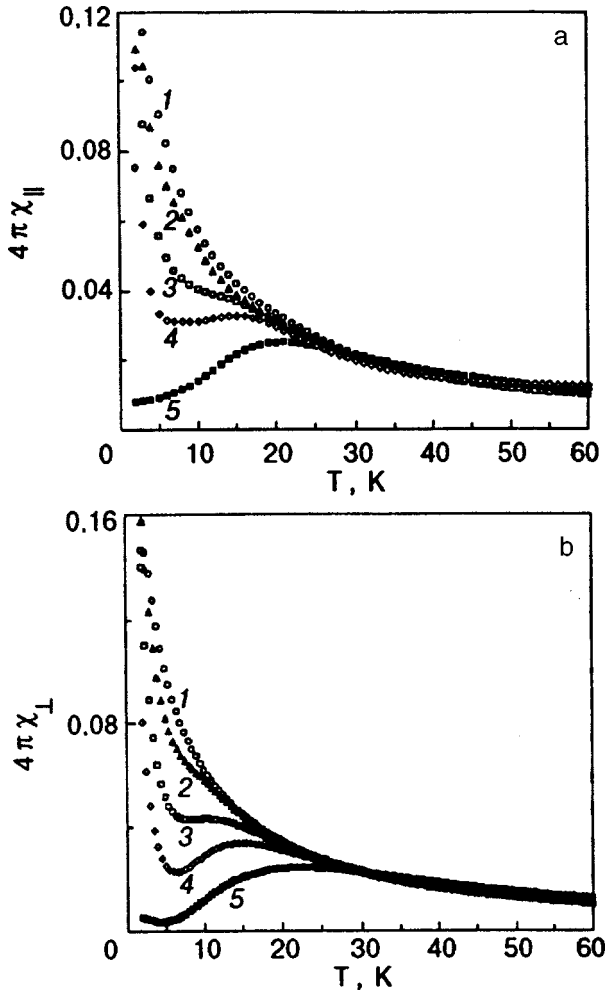


FIG. 3. Temperature dependences of ac susceptibility of a $GdBa_2Cu_3O_{6.2}$ single crystal in constant external magnetic fields $\mathbf{H}\|C(a)$ and $\mathbf{H}\perp C(b)$: $H=0$ (curve *1*), 6.04 (curve *2*), 12.08 (curve *3*), 18.12 (curve *4*), and 36.24 kOe (curve *5*).

with decreasing temperature. The resistance of the sample is of the order of 1 MΩ. Such a magnitude and temperature variation of electrical resistance in magnetic fields lead to the conclusion that the ac susceptibility of the sample in the normal state is of the magnetic origin. The absence of singularities on the temperature and field (at $T=4.2$ K) dependences of magnetization measured on a vibrational magnetometer points to the adiabatic origin of the peaks on the $\chi(T)$ curves (Figs. 3a and 3b). The adiabaticity is due to peculiarities of the magnetic subsystem.[6] On the other hand, the susceptibility of a nonsuperconducting sample is determined only by the Gd subsystem and does not change with the oxygen content in the system.[7] Magnetic anisotropy of the gadolinium subsystem is determined by the exchange anisotropy which is low. For this reason, the susceptibilities measured in the two directions at $T>T_N$ ($T_N$ is the Néel temperature) differ insignificantly. This explains the similarity of figures 3a and 3b. On the other hand, this proves that the qualitative difference in the temperature dependences of the susceptibilities in the two directions for single crystals with $\delta=0.75$ and 0.56 is determined by the superconducting subsystem.

Consequently, we can determine the contributions to the integral susceptibilities of $GdBa_2Cu_3O_{6.75}$ and $GdBa_2Cu_3O_{6.56}$ due to the superconducting subsystems by subtracting the susceptibility of the $GdBa_2Cu_3O_{6.2}$ single crystal from the integral susceptibility. The resultant curves (for the direction perpendicular to the $C$-axis) are shown in Figs. 4 and 5.

It can be seen from Figs. 4 and 5 that anomalies on the temperature dependences of the susceptibility disappear. On the other hand, if we identify $T_c$ with the temperature corresponding to the onset of diamagnetism (which is reasonable since the order parameter fluctuations are suppressed by the varying magnetic field), the shift in $T_c$ induced by the magnetic field will be nonmonotonic for both samples (Fig. 6).

## DISCUSSION

In order to interpret the obtained results, we must proceed from the fact that a magnetic field ($\mathbf{H}\perp$ C) penetrates into layered systems in the form of Josephson vortices. As a result, a structure consisting of alternating superconducting regions and interlayer space filled with vortices is formed. In fields much stronger than the lower critical field $H_{c1}$ we can

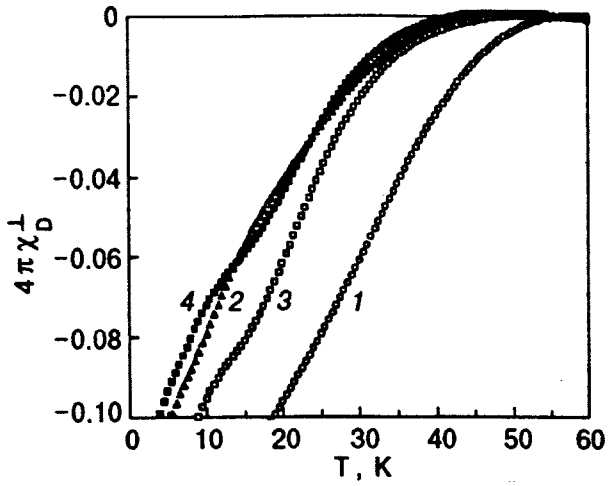


FIG. 4. Temperature dependences of the diamagnetic component of the ac susceptibility of a $GdBa_2Cu_3O_{6.75}$ single crystal in constant external magnetic fields $\mathbf{H}\perp C$: $H=0$ (curve *1*), 6.04 (curve *2*), 12.08 (curve *3*), and 36.24 kOe (curve *4*).

assume that the field applied parallel to the planar superconducting regions of thickness $d$ is constant and equal to the external field to within $a/\lambda_j$ ($a$ is the separation between the centers of Josephson vortices and $\lambda_j$ the Josephson penetration depth). If the inequality $d \ll \xi(T)$ ($\xi(T)$ is the correlation length) holds, we can neglect the variations of the order parameter in the amplitude space. In this case, the properties of resultant phases of the electron wave functions for a Cooper pair acquired during the motion of the electrons from one point in the sample to another upon the reflection at the boundaries of superconducting regions play an exceptionally important role (see, for example, Ref. 4). This exceptional role is associated with an ''antisymmetric'' perturbation exerted by the magnetic field on the electrons of a Cooper pair. Such an 'antisymmetry'' leads in experiments to a number of amazing properties such as a decrease in the superconducting transition temperature. The problem of suppression of superconductivity in a thin film in a longitudinal magnetic field was solved by de Gennes and Tinkham[8,9] (see also Ref. 4). The situation with a layered conductor is more complicated. An increase in the external magnetic field in such systems can lead to a nontrivial dependence of $T_c$ on $H$ associated with processes of penetration of a magnetic field into layered media.

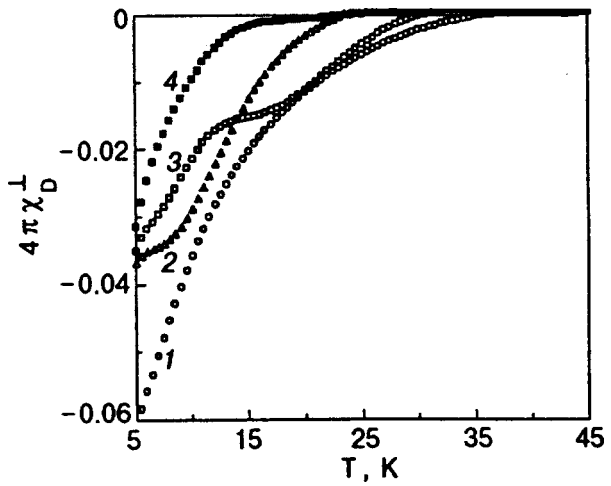


FIG. 5. Temperature dependences of the diamagnetic component of the ac susceptibility of a $GdBa_2Cu_3O_{6.56}$ single crystal in constant external magnetic fields $\mathbf{H}\perp C$: $H=0$ (curve *1*), 6.04 (curve *2*), 12.08 (curve *3*), and 36.24 kOe (curve *4*).

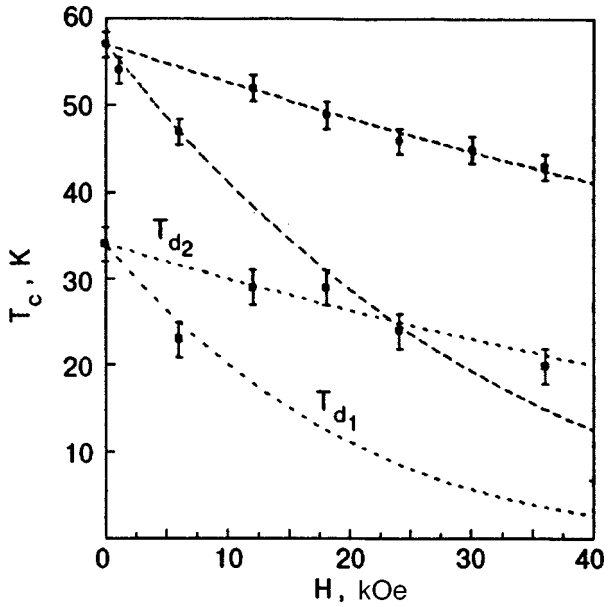


FIG. 6. Superconducting transition temperature as a function of the external magnetic field $\mathbf{H}\perp C$ for $GdBa_2Cu_3O_{6.75}$ (○) and $GdBa_2Cu_3O_{6.56}$ (■). Dashed and dot-and-dash curves correspond to the field dependences $T_d(H)$ calculated on the basis of Eqs. (2) and (4).

The temperature $T_c$ becomes a function of the magnetic field as a result of interaction of a Cooper pair with the magnetic field, which has opposite signs for the electrons of the same pair. Under the assumption that the electrons undergo diffusive reflection at the boundaries of the film (of thickness $d$), de Gennes and Tinkham[4,8,9] found that the superconducting transition temperature obeys the equation

$$kT_c = 1.14\hbar\omega_D e^{-1/\lambda\eta}, \tag{1}$$

where $\omega_D$ is the Debye frequency and $\eta$ the function of the sample parameters and the magnitude of the external field $H$:

$$\eta(H,d)^{1/2} = \frac{2}{d}\int_0^{d/2} dx\ \exp[(\pi H/\Phi_0)(x^2 - d^2/4)]. \tag{2}$$

Here $\Phi_0$ is the flux quantum. In the limiting cases, we have

$$\eta(H,d) = \begin{cases} 1 - \dfrac{\pi}{3}\dfrac{H^2}{\Phi_0}d & \text{for } H \ll \dfrac{\Phi_0}{d^2}, \\ (2\Phi_0/\pi H d^2)^2 & \text{for } H \gg \dfrac{\Phi_0}{d^2} \end{cases}. \tag{3}$$

The analysis of possible mechanisms of high-temperature superconductivity carried out by Ginzburg and Maksimov[10] proved that the normal as well as the superconducting states of HTS systems can be explained to a considerable extent by taking into account the strong electron–phonon interaction. Among other things, such an approach

explains the high values of $T_c$ observed in HTS cuprates on the basis of formula (1) for $\eta=1$. Hence we shall use the results obtained with the help of this theoretical model for describing the effects observed in the present research.

The layered nature of HTS materials strongly affects the superconducting phase transition, which is manifested in a decrease in the superconducting transition temperature in an increasing magnetic field and in its nontrivial behavior as a function of $H$. According to formula (1), the superconducting transition temperature decreases upon an increase in the field $H$ according to the exponential law

$$T_d(H)=T_c(0)\exp\left[\frac{1}{\lambda}\frac{\eta(H,d)-1}{\eta(H,d)}\right], \tag{4}$$

where $T_c(0)$ is the transition temperaure for $H=0$ and the the subscript $d$ on $T$ corresponds to the thickness $d$ of superconducting regions.

In accordance with the ideas developed above, we can use Eq. (4) for estimating the coefficient $\eta(H,d)$ and ultimately the thickness $d$ of superconducting regions. Using the experimentally observed dependences of the superconducting transition temperature on the field $H$ presented in Fig. 6, we find that this coefficient for $T_{d_1}(H)$ (the sample with the oxygen index 6.56) is

$$\eta(H,d)\big|_{H=0.6\ \text{kOe}}=\left[1+\lambda\ \ln\frac{T_c(0)}{T_d}\right]^{-1}\Bigg|_{T_d=23\ \text{K}}=0.892.$$

In the electron–phonon interaction, the frequency boundary for the phonon spectrum of cuprates is $\omega_D=80$ MeV.[10] This allows us to obtain the following value from Eq. (1) for the electron–phonon interaction constant:

$$\lambda=\left(\ln\frac{1.14h\omega_D}{kT_c(0)}\right)^{-1}\Bigg|_{\omega_D=80\ \text{MeV}}=0.304$$

(the experimental value of the superconducting transition temperature $T_c(H=0)=34$ K; see Fig. 6) and to use this value for estimating $\eta(H,d)$.

Simple calculations based on relation (3) for $\eta$ show that the characteristic size $d_1$ of superconducting regions for $H\gg H_{c1}$ amounts to 180 Å.

Let us now consider the $T_{d_2}(H)$ for the sample with the oxygen index 6.56. The estimation of $d_2$ gives the value 89 Å, which is in good agreement with the concepts concerning the penetration of the magnetic field in a layered madium. Indeed, it follows from physical considerations and the results obtained by Bulaevskii and Clem[1] that a first-order transition between lattices with multiple periods must be observed in strong magnetic fields. This actually takes place in our experiments. It follows from relation (3) that the superconducting transition temperature increases with decreasing thickness of superconducting regions (during the rearrangement of the vortex structure).

For the value of λ mentioned above, the values of $d_1$ and $d_2$ for the samples with the oxygen indices 6.56 and 6.75 can be also determined from a comparison of the theoretical [calculated by using formulas (2) and (4)] and experimental field dependences of $T_c$. Using this result, we obtain $d_1=170$ Å and $d_2=84$ Å for the sample $GdBa_2Cu_3O_{6.56}$ while $d_1=145$ K and $d_2=72.5$ Å for the $GdBa_2Cu_3O_{6.75}$ single crystal with the superconducting transition temperature $T_c(0)=57$ K.

A numerical analysis shows that $T_d(H)$ dependence is very weak for small values of $d$. This apparently explains why we could not observe experimentally the transitions between lattices with a finer structure.

It should be noted in conclusion that the problem concerning the role of the layered structure in the formation of properties of superconducting systems has a number of additional aspects. Advances in technology have made it possible to synthesize artificially high-quality multilayered tunnel structures and to simulate some properties of HTS systems experimentally on the macroscopic scale. In fields $H\gg H_{c1}$, such systems must inevitably exhibit the suppression of superconductivity by a strong magnetic field parallel to the lauyers similar to the process considered aove.

The results obtained here also lead to the conclusion that strongly anisotropic superconducting single crystals or layered systems with the tunnel-type conductivity between the layers must exhibit a negative magnetoresistance whose nature is determined by a decrease in the value of $T_c$ for superconducting planes in a magnetic field. Such an effect was observed by Belevtsev and Fomin[11] for granular films.

*E-mail: medvedev@host.dipt.donetsk.ua
**E-mail: lewan@ifpan.edu.pl

[1] L. Bulaevskii and J. R. Clem, Phys. Rev. B **44**, 10234 (1991).
[2] A. K. Asadov, Yu. A. Genenko, G. G. Levchenko *et al.*, Sverkhprovodimost': Fiz., Khim., Tekhn. **5**, 1629 (1992).
[3] A. K. Asadov, Yu. A. Genenko, G. G. Levchenko *et al.*, Physica C **206**, 119 (1993).
[4] P. de Gennes, *Superconductivity of Metals and Alloys*, New York (1966).
[5] V. P. D'yakonov, G. G. Levchenko, V. V. Pashchenko *et al.*, Sverkhprovodimost': Fiz., Khim., Tekhn. **5**, 1884 (1992).
[6] G. G. Levchenko, V. P. D'yakonov, I. M. Fita, and V. V. Markovich, Fiz. Tverd. Tela (St. Petersburg) **38**, 201 (1996) [Phys. Solid State **38**, 111 (1996).
[7] G. G. Levchenko, V. P. D'yakonov, È. E. Zubov *et al.*, Fiz. Tverd. Tela (St. Petersburg) **37**, 395 (1995) [Phys. Solid State **37**, 212 (1995).
[8] P. G. de Gennes and M. Tinkham, Physics **1**, 107 (1964).
[9] P. G. de Gennes, Phys. Kondens. Mater. **3**, 79 (1964).
[10] V. L. Ginzburg and E. G. Maksimov, Sverkhprovodimost': Fiz., Khim., Tekhn. **5**, 1543 (1992).
[11] B. I. Belevtsev and A. V. Fomin, Fiz. Nizk. Temp. **12**, 109 (1986) [*sic*].

Translated by R. S. Wadhwa

# Bound electron pairs in strongly correlated models of high-temperature superconductivity

H. Boyaci and I. O. Kulik*

*Department of Physics, Bilkent University, Bilkent, 06533 Ankara, Turkey***

(Submitted August 7, 1997; revised November 17, 1997)
Fiz. Nizk. Temp. **24**, 316–325 (April 1998)

The ground-state energy of two electrons on a ring is calculated for the one-dimensional Hubbard model with positive and negative on-site interaction and for the contraction model with additive and multiplicative interaction terms. The $hc/2e$ periodicity of the ground-state energy with respect to a flux $\Phi$ threading the loop is derived. The periodicity may serve as an indication of superconductivity. The results are shown to be consistent with the Lieb–Wu solution for $\Phi=0$ limit. In addition, the new states that were missing in the Lieb–Wu solution are derived. © *1998 American Institute of Physics.* [S1063-777X(98)00504-0]

## 1. INTRODUCTION

Among the possible mechanisms of high temperature superconductivity attention was focused in the last years on strongly correlated systems,[1] non Fermi-liquid scenarios,[2,3] magnetic schemes (spin-fluctuation[4,5] and spin-bag[6]) and soft orbital mode interaction mechanisms.[7,8] The generic Hamiltonian underlying these models are the one-, two-, or three-band Hubbard positive- or negative-$U$ Hamiltonians and contraction Hamiltonians with a hopping amplitude which depends upon the sum or product of the near-site occupation number operators. The criterion for superconductivity can be learned in the pairing instability, in the Meissner effect, or in flux quantization. In this paper some of the above models are considered in an assumption that halving of the flux periodicity in the energy versus flux dependence ($hc/e$ to $hc/2e$) may serve as an indication of the superconducting transition.

The purpose of this paper is to show some new states for the one-dimensional Hubbard model, which are missing in the Lieb–Wu[9] solution, and to show that the contraction model may serve as a mechanism for superconductivity. Similar states appear in other strongly correlated models of high-$T_c$ superconductivity. Specifically, we will analyze in this paper three Hamiltonians for strongly correlated fermions:

(1) Hubbard model with repulsive on-site interaction.[5]
(2) Negative-$U$ Hubbard Hamiltonians.[27,28]
(3) Contraction-pairing mechanisms.[7,8,10]

It is known that direct O-O hopping in high-$T_c$ superconductors is important. Since oxygen in oxides like $YBa_2Cu_3O_{6+x}$ has almost filled $p$-shell configuration, holes in a $p^6$ shell may play a similar role for the conduction in oxides in question, as the electrons from nearly empty atomic shells in conventional metals do. Oxygen atoms are specific in the sense that change of the oxygen ionization state ($O^0$ to $O^-$ and $O^{2-}$) results in a dramatic increase of $p_x, p_y$ orbitals in the CuO plane, and therefore in the increase of the magnitude of hopping between near oxygen (as well as near oxygen-copper) sites. A non-$s$-wave orbital configuration[10] is expected to survive with consideration of this occupation-dependent hopping.

## 2. GROUND-STATE ENERGY OF TWO ELECTRONS IN THE HUBBARD MODEL WITH POSITIVE AND NEGATIVE ON-SITE INTERACTION

We consider a loop of $N_a$ lattice sites with a magnetic flux $\Phi$ threading the loop (Fig. 1). The electrons can hop between neighboring lattice sites, and each site can be occupied by at most two electrons with opposite spins. The Hamiltonian for this system has the form

$$H=-t\sum_{j,\sigma}\left(c^+_{j,\sigma}c_{j+1,\sigma}e^{i\alpha}+c^+_{j+1,\sigma}c_{j,\sigma}e^{-i\alpha}\right)+U\sum_j n_{j\uparrow}n_{j\downarrow}, \tag{1}$$

where $c^+_{j,\sigma}$ and $c_{j\sigma}$ are respectively the creation and annihilation operators of an electron with spin projection $\sigma$ at the $j$th lattice site, $t$ is the electron hopping amplitude, $\alpha=(2\pi/N_a)(\Phi/\Phi_0)$ (here $\Phi_0=hc/e$ is the magnetic flux quantum), $n_{j\sigma}$ is the occupation number operator, and $U$ is on-site interaction term. The energy spectrum of $H$ is invariant under the replacement of $t$ by $-t$. Hence, we assume $t=+1$ in appropriate units.

The wave function for two electrons, one with spin up and the other with spin down, is

$$|\Psi\rangle=\sum_{x_1,x_2} f(x_1,x_2)c^+_{x_1\downarrow}c^+_{x_2\uparrow}|0\rangle, \tag{2}$$

where $|0\rangle$ is a vacuum state.

The eigenvalue equation $H|\Psi\rangle=E|\Psi\rangle$ leads to

$$-[(f(x_1+1,x_2)+f(x_1,x_2+1))e^{i\alpha}+(f(x_1-1,x_2)+f(x_1,x_2-1))e^{-i\alpha}]+U\delta(x_1,x_2)f(x_1,x_2)=Ef(x_1,x_2) \tag{3}$$

or, in the momentum space,

 

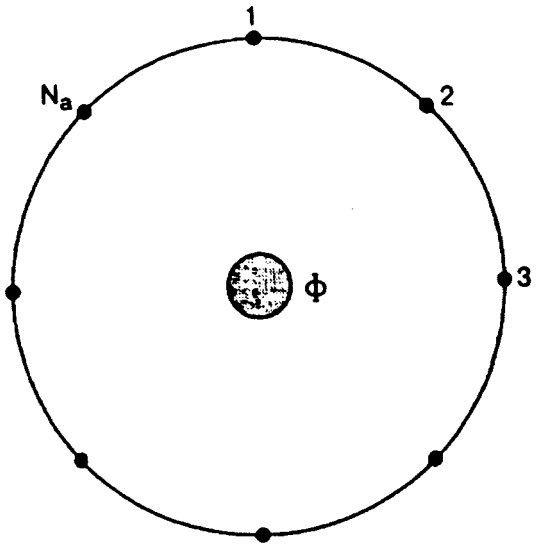


FIG. 1. Configuration of the sample. There are $N_a$ lattice sites on the ring which can be numbered from 1 to $N_a$. The flux $\Phi$ piercing the ring is produced by a solenoid inserted inside the ring.

$$(E+2\cos(K_1+\alpha)+2\cos(K_2+\alpha))f_{K_1,K_2} = \frac{U}{N_a}\sum_K f_{K_1-K,K_2+K}, \tag{4}$$

where $K_{1,2}=(2\pi/N_a)n_{1,2}$ with $n_{1,2}=0,1,2,\ldots,N_a-1$. Here $f_{K_1,K_2}$ is assumed to satisfy the periodicity condition $f_{K_1+2\pi,K_2}=f_{K_1,K_2+2\pi}=f_{K_1,K_2}$. Equation (4) can be rewritten as follows:

$$P_Q\left(1-\frac{U}{N_a}\times\sum_p \frac{1}{E+2\cos(K_1-p+\alpha)+2\cos(K_2+p+\alpha)}\right)=0, \tag{5}$$

where $P_Q=(1/N_a)\Sigma_K f_{K_1-K,K_2+K}$, $Q=K_1+K_2=(2\pi/N_a)n$, and $p=(2\pi/N_a)m$. Hence, either the term inside the parentheses or $P_Q$ should be equal to zero.

**(I)** $P_Q\neq 0$. **The Lieb and Wu solution**

For $P_Q\neq 0$, the term inside the parentheses should be equal to zero, or

$$\frac{1}{U}=S(E), \tag{6}$$

where

$$S(E)=\frac{1}{N_a}\sum_p \frac{1}{E+2\cos(K_1-p+\alpha)+2\cos(K_2+p+\alpha)}. \tag{7}$$

Using the Poisson summation formula,

$$\frac{1}{U}=\sum_{n=-\infty}^{\infty}\int_0^{2\pi}\frac{dp}{2\pi}\frac{\exp(ipN_an)}{E+4\cos(Q/2-p)\cos(Q/2+\alpha)} \tag{8}$$

$S(E)$ becomes

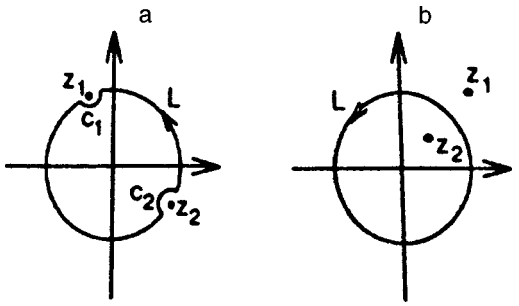


FIG. 2. Poles of the integrand in the complex plane. $E^2<E_0^2$ (a) and $E^2>E_0^2$ (b), where $E_0=-4\cos\beta$ for even $n$ and $E_0=-4\cos\beta\cos(\pi/N_a)$ for odd $n$.

$$S(E)=\sum_{n=-\infty}^{\infty}S_n(E)\equiv S_{n=0}(E)+\sum_{n=1}^{\infty}[S_n(E)+S_n^*(E)]. \tag{9}$$

$S_n(E)$ can be calculated by transforming Eq. (8) to an integral in the complex plane. Setting $z=e^{ip}$, we have

$$S_n(E)=\frac{1}{2\pi i}\times\oint dz\,\frac{z^{N_an}}{z^2(e^{i\alpha}+e^{-i(Q+\alpha)})+Ez+(e^{i(Q+\alpha)}+e^{-i\alpha})}. \tag{10}$$

The poles (Fig. 2) of the integrand are

$$z_{1,2}=-\frac{-E\pm(E^2-E_0^2)^{1/2}}{E_0\exp(-iQ/2)}, \tag{11}$$

where $E_0=4\cos(Q/2+\alpha)$. For $E^2<E_0^2$, both of the poles $z_1$ and $z_2$ are on the unit circle and $S_{n=0}$ vanishes, while for $E^2>E_0^2$ one of them is inside the unit circle and the other one is outside of it, and $S_{n=0}$ does not vanish. For both cases

$$S(E)=\frac{1}{4i\sin x\cos\beta}\frac{\exp(i(Q/2-x)N_a)+1}{\exp(i(Q/2-x)N_a)-1}, \tag{12}$$

where $x$ can be real or complex, depending on whether $E^2$ is smaller or larger than $E_0^2$, and $\beta=Q/2+\alpha$. If we denote new momenta $k_1,k_2$ as

$$k_{1,2}=\frac{Q}{2}+\alpha\pm x, \tag{13}$$

Eq. (6) takes the form

$$\exp[i(k_{1,2}-\alpha)N_a]=\frac{\sin k_{1,2}-\Lambda+iU/4}{\sin k_{1,2}-\Lambda-iU/4}, \tag{14}$$

where

$$\Lambda=\frac{\sin k_1+\sin k_2}{2}. \tag{15}$$

Equation (14) is identical to the Lieb and Wu solution[9] in the $\alpha=0$ limit.

It is possible to express the eigenvalue $E$ of the system as

TABLE I. Minimum energy for different values of $U$.

| | $U>0$ | $U<0$ | |
|---|---|---|---|
| even $n$ | $E=-4\cos x\cos\beta$ with $x$ (real) determined by $\tan(N_a x/2)=U/4\sin x\cos\beta$ | $E=-4\cosh\kappa\cos\beta$ with $\kappa$ determined by $\tanh(N_a\kappa/2)=\lvert U\rvert/4\sinh\kappa\cos\beta$ | |
| | | $U<U_{cr}$ | $U_{cr}<U<0$ |
| odd $n$ | $E=-4\cos\beta\cos(\pi/N_a)$ | $E=-4\cosh\kappa\cos\beta$, where $\kappa$ is determined by $\tanh(N_a\kappa/2)=4\sinh\kappa\cos\beta/\lvert U\rvert$ | $E=-4\cos x\cos\beta$, where $x$ is determined by $\tan(N_a\kappa/2)=4\sinh x\cos\beta/\lvert U\rvert$ |

$$E=-2(\cos k_1+\cos k_2)=-4\cos x\cos\beta, \tag{16}$$

with $x$ determined by

$$\tan\frac{N_a x}{2}=-\sigma\left(\frac{4\sin x\cos\beta}{U}\right)^{\sigma}, \tag{17}$$

where $\sigma=+1$ or $-1$ for odd or even value of $n[n=Q/(2\pi/N_a)]$.

For $U>0$, $E^2$ is always less than $E_0^2$; hence $x$ is always real. For $U<0$ with even $n$, $E^2$ is always larger than $E_0^2$, so that $x$ is complex. But for odd $n$ and small $|U|$ values ($U<0$), $x$ might be real. Let us consider Eq. (17) for negative $U$ and odd $n$ with complex $x=i\kappa$

$$\frac{1}{|U|}=\frac{\tanh(N_a\kappa/2)}{4\sinh\kappa\cos\beta}. \tag{18}$$

To have a solution of this equation, $1/|U|$ should not be larger than the maximum value of its right-hand side. Accordingly, the critical value $|U_{cr}(N_a)|$ can be found. The values of $|U|$ which are smaller than this $|U_{cr}|$ have real $x$; others have complex $x$ in Eq. (17).

**(II)** $P_Q=0$. **The new state**

If $P_Q$ is equal to zero, then either a new eigenvalue of the system is found as

$$E=-2\cos(q+\alpha)-2\cos(Q-q+\alpha), \tag{19}$$

with $K_1=q$ and $K_2=Q-q$, or $f_{K_1K_2}=0$ for any $K_1$ and $K_2$. But all $f$'s cannot be zero; otherwise $|\Psi\rangle=0$. Summation of all $f$'s, so that $P_Q$ is equal to zero while $f$'s are individually not all zero only if for two different values of $q$, $2\cos(q+\alpha)+2\cos(Q-q+\alpha)$ are coinciding.

For positive on-site interaction $U$, this eigenvalue becomes the minimum energy of the system when $n$ is odd. For $U<0$ it does not become the minimum eigenvalue of the system.

The ground-state energy values are summarized in Table I.

The dependence of the ground-state energy on the flux is shown in Fig. 3.

### A. Dependence of the amplitude of energy oscillations on the number of sites

The dependence $E(\Phi)$ is shown schematically in Fig. 4, where $\Delta E_1$ and $\Delta E_2$ are the amplitudes of $hc/e$ and $hc/2e$ oscillations.

For $U<U_{cr}<0$ in the large $N_a$ limit

$$\Delta E_1=\Delta E_2=\Delta E\approx\frac{2\pi^2}{N_a^2}\frac{1}{(U^2+16)^{1/2}}. \tag{20}$$

Here there is a $\Phi_0/2$ periodicity, which resembles the pairing of electrons as in a superconductor, but the amplitude of the energy oscillations decreases with inverse square of the

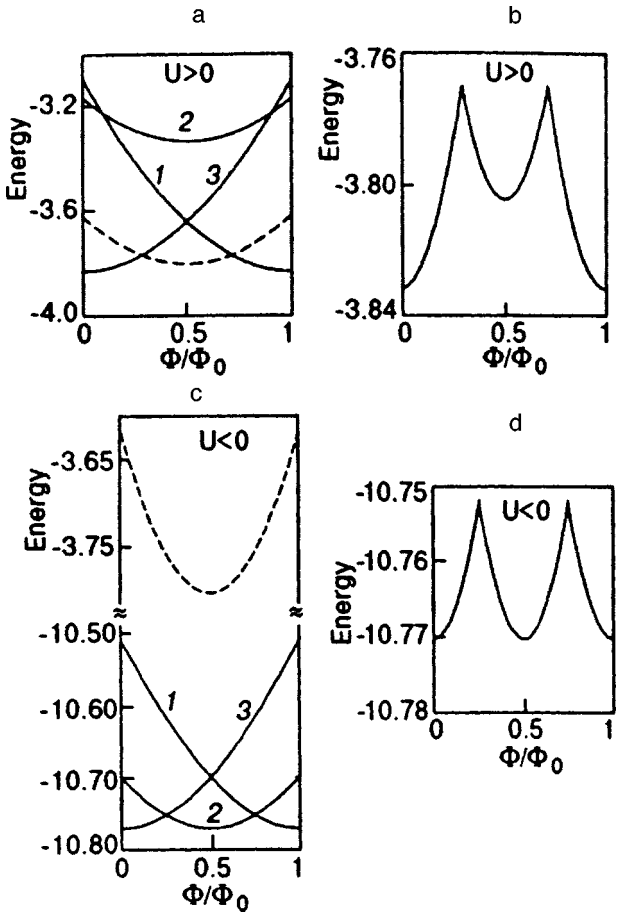


FIG. 3. Energy versus flux for two electrons with $N_a=10$. (a) Solid curves *1–3* correspond to the Lieb–Wu solution and the dashed curve corresponds to the new states found by us. For $U>0$ ($U=10$) this new state becomes the minimum energy of the system. (b) The same as (a) to show the $\Phi_0/2$ periodicity more clearly. It is clearly seen that the Lieb–Wu solution (solid curves *1–3*) does not lead to the $\Phi_0/2$ periodicity alone. (c) $U=-10$. As in (a), the solid curves *1–3* are the lowest-lying eigenvalues found by the Lieb–Wu solution. Similarly, the dashed curve corresponds to the new state found by us. For $U<0$ the new eigenvalue does not become the minimum energy of the system. (d) The same as (c) to show the periodicity more clearly.

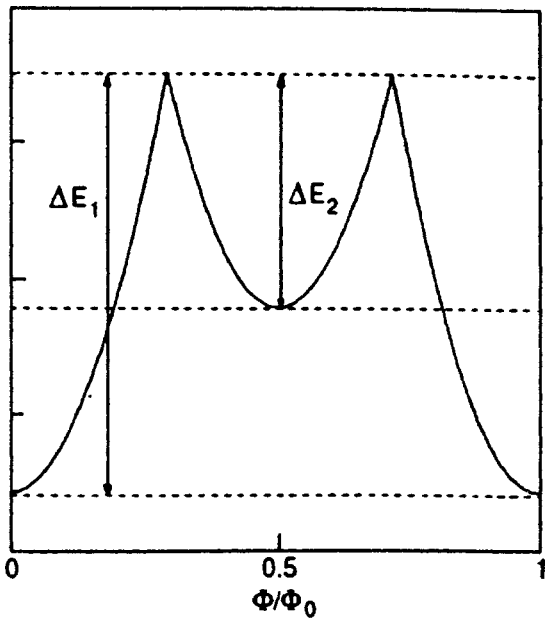


FIG. 4. Energy oscillations for two electrons. $\Delta E_1$—amplitude of $hc/e$ periodicity, $\Delta E_2$—amplitude of $hc/2e$ periodicity.

number of lattice sites (Fig. 5a). If $|U|\to|U_{cr}|$, then the amplitude of oscillation corresponding to $hc/2e$ becomes smaller and at $U=U_{cr}$ it vanishes. Note, however, that for very large values of $N_a$, $|U_{cr}|$ becomes quite small; hence even for very small $|U|$ the behavior of energy with respect to flux is the same. The behavior of ground-state energy is shown explicitly for various values of $U$ and $N_a$ in Figs. 5c–5f. In the very large $N_a$ limit, using Eqs. (16) and (17), we can show that

$$E\approx-\sqrt{U^2+16\cos^2\beta} \tag{21}$$

for even and odd values of $n$. The last expression can be obtained directly from Eq. (7) by changing the summation over $p$ to an integral.

For $U>0$, in the limit $N_a\gg1$

$$\Delta E_1\approx\frac{2\pi^2}{N_a^2}\left(1-\frac{1}{2}\left(\frac{UN_a}{8+UN_a}\right)^2\right)^2, \tag{22}$$

$$\Delta E_2\approx\frac{2\pi^2}{N_a^2}\left(\frac{1}{2}\left(\frac{UN_a}{8+UN_a}\right)^2\right)^2. \tag{23}$$

Hence, for $U\times N_a\to\infty$, $\Delta E_1=\Delta E_2=1/4(2\pi^2/N_a^2)$. Both $\Delta E_1$ and $\Delta E_2$ behave like $1/N_a^2$, and $\Delta E_1/\Delta E_2\to1$ (Fig.

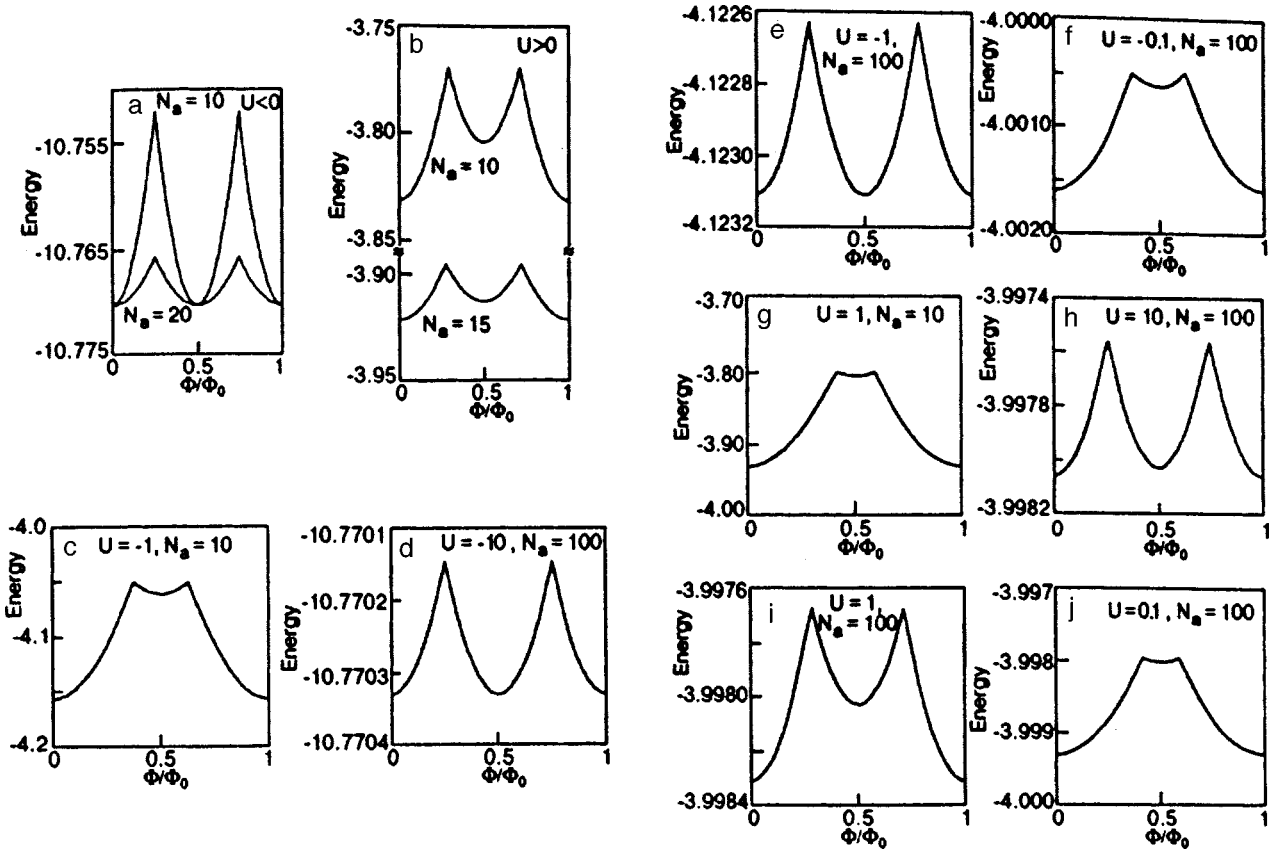


FIG. 5. (a) Minimal energy versus flux for $N_a=10$ and 20 ($U=-10$). Comparison of oscillations for $N_a=10$ and 20 shows the $1/N_a^2$ behavior of the amplitude. (b) Minimal energy versus flux for $N_a=10$ and 15 ($U=10$). As the number of sites increases (larger $N_a$), $\Delta E_1/\Delta E_2$ approaches 1. (c–f) Ground-state energy for different values of $N_a$ and negative $U$. Compared to the oscillations in (a) for $N_a=10$ amplitude $\Delta E_2$ becomes smaller in (c). This occurs because $U$ comes closer to $U_{cr}$, if larger values of $U$ were used, even smaller $\Delta E_2$ values would be obtained. (d), (e), and (f) demonstrates the behavior of the system with $N_a=100$. This time even with $U=-1$, $\Delta E_2$ is still almost equal to $\Delta E_1$, because for larger values of $N_a$, $U_{cr}$ becomes larger and approaches zero. For $U=-0.1$ a decrease in $\Delta E_2$ is observed. (g–j) Ground-state energy for different values of $N_a$ and for positive $U$. For smaller values of $U(U\to0)\Delta E_2$ becomes smaller. But just as in the $U<0$ case, for larger values of $N_a$, even for very small values of $U$, there is still a $\Phi_0/2$ periodicity. It should be noted that in all cases, as $N_a\to\infty$, all oscillations vanish, $\Delta E_{1,2}\to0$.

5b). But for $U\to 0$, $U\times N_a\to 0$; $\Delta E_1=2\pi^2/N_a^2$ and $\Delta E_2=0$. The plots of energy versus flux behavior of the system for positive $U$ are shown explicitly in Figs. 5g–5j.

With the new state found in our work, an $hc/2e$ periodicity of the ground-state energy appears even for positive $U$. This branch vanishes gradually as $U\to 0$. It is not possible to find this periodicity with the Lieb–Wu solution.

### B. Comparison with other theories

The energy oscillations with the $hc/2e$ periodicity were calculated in the strongly correlated electron models, including the Hubbard model, in a number of papers.[11–17] In some papers[18–21] the Hubbard model was examined by using the Lieb and Wu solution.[9] The oscillations with the $hc/2e$ periodicity for negative $U$ can be found by starting directly from the original solution presented by Lieb and Wu, since the new state found in our work does not become the minimum energy state. But for positive $U$, new states should be included to obtain the correct $hc/2e$ periodicity. The Lieb and Wu solution does not lead to the $hc/2e$ periodicity for positive $U$.

1) Why Lieb–Wu is incomplete:
Let us consider the Lieb–Wu equations (with no magnetic flux $\Phi$)

$$\exp(iN_ak_1)=\frac{\sin k_1-\sin k_2+iU/2}{\sin k_1-\sin k_2-iU/2}, \tag{24}$$

$$\exp(iN_ak_2)=\frac{\sin k_2-\sin k_1+iU/2}{\sin k_2-\sin k_1-iU/2}. \tag{25}$$

Dividing the first equation by the second, with $k_1+k_2=Q$ and $k_1-k_2=2\kappa$, we obtain

$$\exp(2iN_a\kappa)=\left(\frac{2\sin\kappa\cos(Q/2+\alpha)+iU/2}{2\sin\kappa\cos(Q/2+\alpha)-iU/2}\right)^2. \tag{26}$$

The energy equation is

$$E=-2(\cos k_1+\cos k_2)=-4\cos(Q/2)\cos\kappa, \tag{27}$$

and the new eigenvalue found by us is

$$E=-4\cos(Q/2)\cos(\pi/N_a). \tag{28}$$

Therefore, $\kappa$ should be equal to $\pi/N_a$ in Eq. (27). According to Eq. (26) it is obvious that this is possible only if $U=0$. The Lieb–Wu solution does not give this result for all $U$ except $U=0$.

In the original paper of Lieb and Wu[9] it is explicitly stated that the momenta $k_j$ should be unequal, which means that both $I_1-I_2$ and $I_1+I_2$ cannot be equal to zero ($I_1$ and $I_2$ are integers in the original paper of Lieb and Wu.[9] This is also the case in our procedures. In terms of our approach, $\kappa=0$ should be excluded from the solution set. But in some papers[14] $k_1$ is assumed to be equal to $k_2$, so that $\kappa=0$ and a $\Phi_0/2$ periodicity is obtained by accident.

## 3. CONTRACTION MODEL

### A. Physical background

In the investigation of unusual electronic properties of metal-oxide compounds it was proposed[7,8,22] that the new features in the electronic band conduction in oxide metals should be included. The first one is the possibility that ''intrinsic-hole'' rather than intrinsic-electron carriers may play a role. The second one is that, provided intrinsic holes are at work, one-particle picture of the electronic transport is not fully adequate, because the interaction between holes (repulsive or attractive) must be included, and because the fact that the hopping of holes in itself cannot be considered as constant in amplitude and is strongly dependent upon site occupation.

Normally, two oxygen atoms have a strong tendency to make covalent bonding, which results in the formation of an oxygen molecule, $O_2$. However, in a proper chemical surrounding, this may not happen if the nearest neighbor atoms are not too close to each other. In this case the other scenario, which is reminiscent of metallic oxygen, applies. We can assume that this is just what happens in the metal-oxide superconductors. In the $CuO_2$ plane of the latter, due to large ionic radii of oxygen, the oxygen orbitals overlap each other almost as strongly as the near site oxygen and copper orbitals do. The $O_2$ molecules therefore are not formed, and the electrons derived from the $p^6$ shell are the conducting electrons. The charge carriers are holes in the $p^6$ shell, which propagate from one oxygen anion to the next nearest one by hopping. Because of the contraction of the $p$ orbital of oxygen as a result of occupation by a hole, hole hopping between nearest-neighbor sites $(i,j)$ is dependent on the opposite-spin hole occupation number. In the second quantization representation it was suggested to consider the hopping matrix element $t_{ij}$ as an operator which depends on the occupation number operators $n_i$ and $n_j$ at the atomic sites $R_i$ and $R_j$. There are three independent matrix elements, $t_0$, $t_1$, and $t_2$ (Refs. 23 and 26), which in the case of two oxygen anions correspond to the following, charge transfer reactions:

$$\begin{aligned} t_0&:\quad \mathrm{O}_i^-+\mathrm{O}_j^{2-}\to\mathrm{O}_i^{2-}+\mathrm{O}_j^-\\ t_1&:\quad \mathrm{O}_i+\mathrm{O}_j^{2-}\to\mathrm{O}_i^{2-}+\mathrm{O}_j,\\ t_2&;\quad \mathrm{O}_i+\mathrm{O}_j^-\to\mathrm{O}_i^-+\mathrm{O}_j, \end{aligned} \tag{29}$$

which result in

$$\begin{aligned} t_{ij}=t_0(1-n_{i,-\sigma})(1-n_{j,-\sigma})+t_1[n_{i,-\sigma}(1-n_{j,-\sigma})\\ +n_{j,-\sigma}(1-n_{i,-\sigma})]+t_2n_{i,-\sigma}n_{j,-\sigma}. \end{aligned} \tag{30}$$

The occupation dependence of the hopping can be represented in another form:

$$t_{ij}=-t+Vn_{i,-\sigma}n_{j,-\sigma}+W(n_{i,-\sigma}+n_{j,-\sigma}), \tag{31}$$

where from Eq. (30) we obtain

$$t=-t_0,\quad V=t_0-2t_1+t_2,\quad W=t_1-t_0. \tag{32}$$

Hence, the $1D$ version of the interacting holes in an anion network can be represented by the following Hamiltonian, which includes the on-site interaction term $U$:

$$H=-\sum_{j\sigma} c_{j\sigma}^{+}c_{j+1,\sigma}\exp(i\alpha)+\text{H.c.}+U\sum_{j} n_{j\uparrow}n_{j\downarrow}$$
$$+\sum_{j,\sigma} c_{j\sigma}^{+}c_{j+1,\sigma}[Vn_{j,-\sigma}n_{j+1,-\sigma}+W(n_{j,-\sigma}$$
$$+n_{j+1,-\sigma})]\exp(i\alpha)+\text{H.c.} \tag{33}$$

The effect of the coupling term W has been considered in great detail in the paper of Hirsch and Marsiglio,[7] as well as by Kulik *et al.*[8,25]

### B. Bound state of two electrons

As before, we use the wave function for two electrons, one with spin up and the other with spin down,

$$|\Psi\rangle=\sum_{x_1,x_2} f(x_1,x_2)c_{x_1\downarrow}^{+}c_{x_2\uparrow}^{+}|0\rangle. \tag{34}$$

In momentum space the eigenvalue equation $H|\Psi\rangle=E|\Psi\rangle$ gives

$$\begin{bmatrix} 1-US_0(E)-WS_1(E) & -WS_0(E) \\ US_1(E)+WS_2(E) & -1+WS_1(E) \end{bmatrix}\times\begin{bmatrix} F_0(Q) \\ F_1(Q) \end{bmatrix}=0, \tag{35}$$

where

$$\frac{1}{N_a}\sum_{K}(\varepsilon_{K_1-K+\alpha}+\varepsilon_{K_2+K+\alpha})^{n}f_{K_1-K,K_2+K}\equiv F_n(Q), \tag{36}$$

$n=0$, 1, and

$$\frac{1}{N_a}\sum_{p}\frac{(\varepsilon_{K_1-p+\alpha}+\varepsilon_{K_2+p+\alpha})^{n}}{E+(\varepsilon_{K_1-p+\alpha}+\varepsilon_{K_2+p+\alpha})}\equiv S_n(E), \tag{37}$$

$n=0$, 1, 2; $\varepsilon_k=2\cos k$. Hence, either the determinant of the first matrix is equal to zero or both terms of the vector are zero.

For two electrons $V$ does not show up. The effect of $V$ in the weak-coupling regime was considered previously.[8]

In the case $F_0=F_1=0$ the energy eigenvalue of the system becomes

$$E=-2\cos(q+\alpha)-2\cos(Q-q+\alpha)$$
$$=-4\cos(Q/2-q)\cos\beta. \tag{38}$$

It is possible to have both $F_0$ and $F_1$ equal to zero, while all $f$'s are not individually equal to zero only if for two different values of $q$, $2\cos(q+\alpha)+2\cos(Q-q+\alpha)$ are coinciding.

For the other case, i.e., when determinant of the first matrix in Eq. (35) is equal to zero, the transcendental equation is found as follows:

$$\frac{(W-1)^2}{U+W(W-2)E}=S_0(E). \tag{39}$$

The plot of $S_0(E)$ is presented in Fig. 6. Equation (39) can be solved numerically, which is done to test our results. If we set $W=0$ in the last equation, we immediately obtain the result of the $1D$ Hubbard model discussed in Sec. 2. With similar calculations as in the previous sections, the minimum energy corresponding to Eq. (39) is found as

$$E=-(\cos k_1+\cos k_2)=-4\cos x\cos\beta, \tag{40}$$

where $x$ is determined by

$$\tan\frac{N_a x}{2}=-\sigma\left(\frac{4(W-1)^2\sin x\cos\beta}{U-4W(W-2)\cos x\cos\beta}\right)^{\sigma}. \tag{41}$$

Here $\sigma=+1$ or $-1$ for odd or even values of $n$. In the hatched region in Fig. 7 for odd values of $n$ the expression

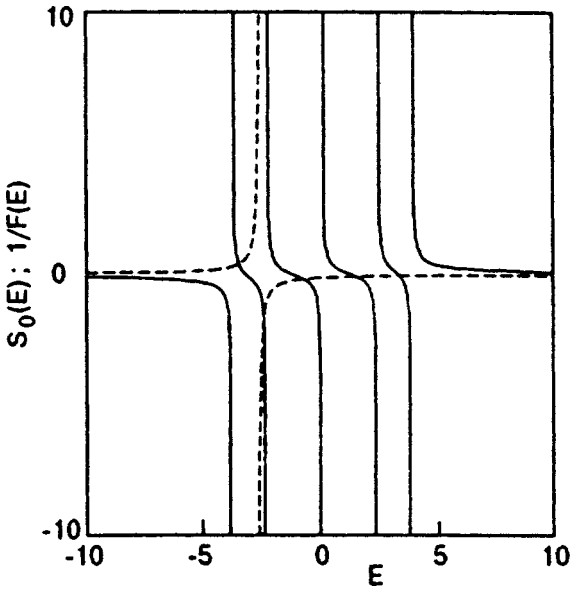


FIG. 6. Plot of the transcendental equation for the contraction model. The intersection points of $S_0(E)$ (solid line) with $1/F(E)$ (dashed line) give the energy eigenvalues. Here $N_a=10$, $\Phi=\Phi_0/2$, $n=9$, $U=-2$, and $W=1.5$.

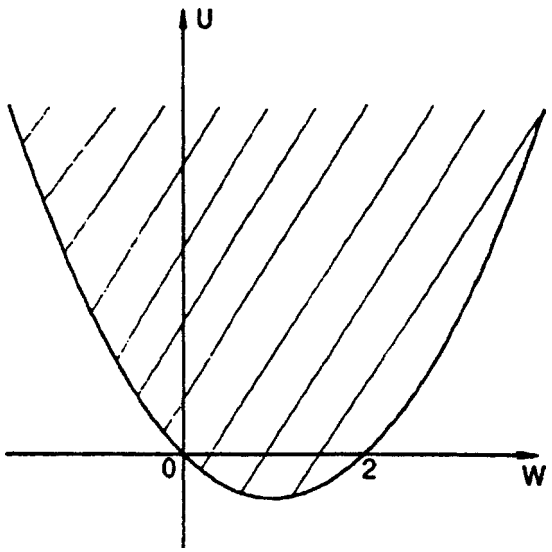


FIG. 7. Phase space for bound states of two electrons. The hatched region corresponds to the free propagating states and the nonhatched region corresponds to the bound states of two electrons within the contraction model. The solid line corresponds to the equation $U=-W(W-2)E_1$, where $E_1=-4\cos\beta$ for even $n$ and $E_1=-4\cos\beta\cos(\pi/N_a)$ for odd $n$.

TABLE II. Minimum energy for different values of $U$.

| | $U>-W(W-2)E_1$ hatched part in Fig. 7 | $U<-W(W-2)E_1$ nonhatched part in Fig. 7 | |
|---|---|---|---|
| even $n$ | $E=-4\cos x\cos\beta$ with $x$ (real) determined by $\tan\left(\frac{N_a x}{2}\right)=\frac{U-4W(W-2)\cos x\cos\beta}{4(W-1)^2\sin x\cos\beta}$ | $E=-4\cosh\kappa\cos\beta$ with $\kappa$ (real) determined by $\tanh\frac{N_a\kappa}{2}=-\frac{U-4W(W-2)\cosh\kappa\cos\beta}{4(W-1)^2\sinh\kappa\cos\beta}$ | |
| | | $U<U_{cr}$ | $U>U_{cr}$ |
| odd $n$ | $E=-4\cos\beta\cos(\pi/N_a)$ | $E=-4\cosh\kappa\cos\beta$, where $\kappa$ is determined by $\tanh\frac{N_a\kappa}{2}=-\frac{4(W-1)^2\sinh\kappa\cos\beta}{U-4W(W-2)\cosh\kappa\cos\beta}$ | $E=-4\cos x\cos\beta$, where $x$ is determined by $\tan\frac{N_a x}{2}=-\frac{4(W-1)^2\sin x\cos\beta}{U-4W(W-2)\cos x\cos\beta}$ |

$$E=-4\cos(\pi/N_a)\cos\beta \tag{42}$$

gives the minimum energy value. The curve in Fig. 7 corresponds to $U=-W(W-2)E_1$, where $E_1=-4\cos\beta$ for even $n$ and $E_1=-4\cos\beta\cos(\pi/N_a)$ for odd $n$. The resulting values of the ground-state energy for different values of $U$ and $W$ are summarized in Table II.

Here $U_{cr}$ is found in a similar way to that of the Hubbard model. The energy-versus-flux dependence for two electrons in the contraction model is shown in Fig. 8.

The amplitudes of the energy oscillations in the $N_a\gg 1$ limit are found as follows:

(i) For the nonhatched region below the curve (the bound states) and $U<U_{cr}$ ($U<U_{cr}<-W(W-2)E_1$):

$$\Delta E_1=\Delta E_2=\Delta E$$

$$\approx\frac{(2\pi^2/N_a^2)(W-1)^4}{\{U^2W^2(W-2)^2+(2W^2-4W+1)[16(W-1)^4+U^2]\}^{1/2}}. \tag{43}$$

Hence there is a $\Phi_0/2$ periodicity. The branch corresponding to the expression in Eq. (42) for odd $n$ does not become the minimum energy; it is shown as a dashed line in Fig. 8a. As $U\to U_{cr}$ from below, the branch which is marked as 2 in Fig. 8c fades away from being the minimum energy. Eventually, at $U=U_{cr}$ there is no more $\Phi_0/2$ periodicity. For very large $N_a(N_a\to\infty)$, $U_{cr}\to 4W(W-2)$. It is interesting that in this very large $N_a$ limit $E_1\to -4$, so that the curve in Fig. 7 corresponds to $U=4W(W-2)\sim U_{cr}$. Hence, for very large $N_a$, any $U$ which satisfies $U<4W(W-2)$ is less than $U_{cr}$; therefore, almost always there is a $\Phi_0/2$ periodicity in the nonhatched region in Fig. 7.

(ii) For the shaded region above the curve in Fig. 7 the expression in Eq. (42) becomes the minimum energy of the system. This branch is shown as the dashed line in Fig. 8a. The corresponding amplitudes are

$$\Delta E_1\approx(2\pi^2/N_a^2)(1-\lambda)^2, \tag{44}$$

$$\Delta E_2\approx(2\pi^2/N_a^2)\lambda^2, \tag{45}$$

where

$$\lambda=\frac{1}{2}\left(\frac{(U-4W(W-2))N_a}{8(W-1)^2+N_a[U-4W(W-2)]}\right)^2. \tag{46}$$

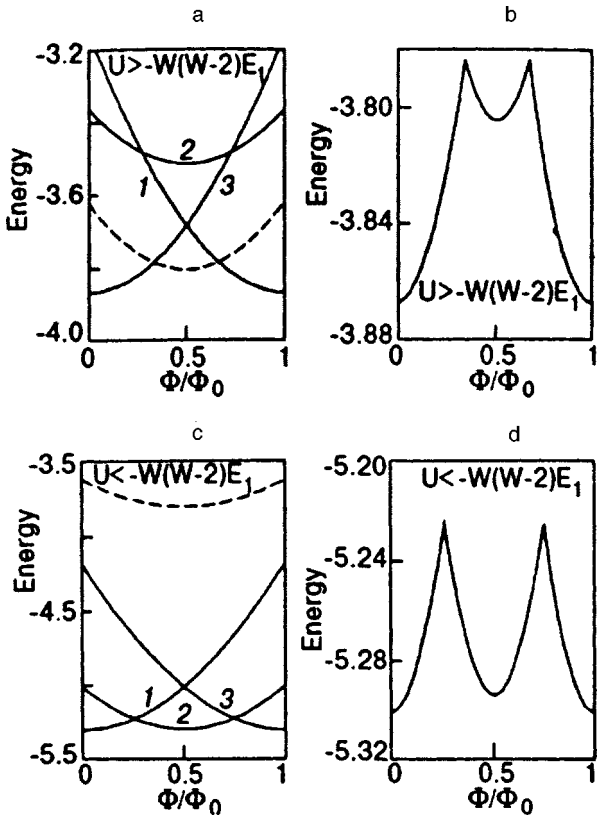


FIG. 8. Energy versus flux for two electrons in the contraction mechanism. Note the resemblance of this figure to Fig. 3. Here instead of $U>0$ there is $U>-W(W-2)E_1$; similarly for $U<0$ there is the $U<-4W(W-2)$ criterion. In (a) the solid curves correspond to the expression (40) and the dashed curve corresponds to the expression (42). Just like for $U>0$ in the Hubbard model, in the contraction model for $U>-W(W-2)E_1$ the dashed curve becomes the minimal energy of the model. (b) The same as (a) to show the behavior of the system more clearly. In (a) and (b) $N_a=10$, $U=-2$, $W=1.5$. In (c) $U<-W(W-2)E_1$, just as in the Hubbard model for $U<0$, the solution corresponding to Eq. (42) does not take place as the minimum energy of the model. The solid curves *1–3* correspond to Eq. (40) and the dashed curve corresponds to Eq. (42). (d) is the same as (c) to show the behavior more clearly. In (c) and (d) $N_a=10$, $U=2$, and $W=-1$.

For $(U-4W(W-2))N_a \to \infty$, $\Delta E_1 = \Delta E_2 = 1/4(2\pi^2/N_a^2)$. But for $(U-4W(W-2))N_a \to 0$, $\Delta E_1 = 2\pi^2/N_a^2$, and $\Delta E_2 = 0$.

All results found here and in the previous section for the Hubbard model are in close correlation. In the Hubbard model and the contraction model two different types of solutions were found. For the Hubbard model a new type of solution gives the $\Phi_0/2$ periodicity for $U>0$, which is absent in the Lieb–Wu solution, while in the contraction model this type of solution gives the $\Phi_0/2$ periodicity for $U>-W(W-2)E_1$. In the Hubbard model for $U<0$ can be larger or smaller than $E_0$, depending on whether $U$ is larger or smaller than a critical value $U_{cr}$. Similarly for the contraction model for $U<-W(W-2)E_1, E$ can be larger or smaller than $E_0$, depending on whether $U$ is larger or smaller than $U_{cr}$. For Hubbard model $U_{cr}$ becomes zero for very large $N_a$, for contraction model it becomes $4W(W-2)$. In all these inequalities one can get Hubbard model type relations setting $W=0$ in contraction model relations.

## 4. CONCLUSIONS

In the one-dimensional Hubbard model and the contraction model for two electrons, the periodicity of ground-state energy with respect to flux is $hc/2e$. Our study shows that the solution for a one-dimensional Hubbard model by Lieb and Wu[9] in 1968 is not complete, at least for two electrons. For positive on-site interaction new states found by us correspond to the ground-state energy. Hence, they play an important role for correct behavior of the ground-state energy of the system. Generalizing the current results to more than two electrons will be the task of a future work. It is very likely that for more than two electrons new states, which cannot be determined by the Lieb and Wu results, will be found. The model for the ground-state energy of contraction has a $hc/2e$ periodicity also. But it is not easy to speak about superconductivity very clearly. For some range of the values of $U$ and $W$ it is likely that this model results in superconductivity. To show that this model serves as a model for superconductivity, other probing methods should be used.

This work was supported in part by the Scientific and Technical Research Council of Turkey TÜBITAK.

*Permanent address: B. Verkin Institute for Low Temperature Physics and Engineering, Nat. Acad. Sci. of Ukraine, 47, Lenin Ave., 310164 Kharkov, Ukraine
**E-mail: kulik@fen.bilkent.edu.tr

[1] E. Dagotto, Rev. Mod. Phys. **66**, 763 (1994).
[2] P. W. Anderson, Science **235**, 1196 (1987).
[3] G. Kotliar, Adv. Phys. **44**, 187 (1995).
[4] D. Pines, Tr. J. Phys. **20**, 535 (1996).
[5] D. J. Scalapino, Phys. Rep. **250**, 329 (1995).
[6] J. R. Schrieffer, X. G. Wen, and S. C. Zhang, Phys. Rev. B **39**, 11663 (1989).
[7] J. E. Hirsch and F. Marsiglio, Phys. Rev. B **39**, 11515 (1989).
[8] I. O. Kulik, Sverhprovodimost': Fiz., Khim., Tekh. **2**, 175 (1989) [Sov. Supercond.: Phys., Chem., Technol. **2**, 201 (1989)].
[9] E. H. Lieb and F. Y. Wu, Phys. Rev. Lett. **20**, 1445 (1968).
[10] I. O. Kulik, Tr. J. Phys. **20**, 627 (1996).
[11] A. Sudbo, C. M. Varma, T. Giamarchi, E. B. Stechel, and R. T. Scalettar, Phys. Rev. Lett. **70**, 978 (1993).
[12] R. M. Fye, M. J. Martins, and D. J. Scalapino, Phys. Rev. B **44**, 6909 (1991).
[13] A. A. Zvyagin, Zh. Éksp. Teor. Fiz. **103**, 307 (1993) [JETP **76**, 167 (1993)].
[14] F. V. Kusmartsev, J. F. Weisz, R. Kishore, and M. Takahashi, Phys. Rev. B **49**, 16234 (1994).
[15] A. Ferretti, I. O. Kulik, and A. Lami, Physica C **185**, 1649 (1991).
[16] J. F. Weisz, R. Kishore, and F. V. Kusmartsev, Phys. Rev. B **49**, 8126 (1994).
[17] A. Ferretti, I. O. Kulik, and A. Lami, Phys. Rev. B **45**, 5486 (1992).
[18] A. A. Zvyagin and I. V. Krive, Zh. Éksp. Teor. Fiz. **102**, 1376 (1992) [Sov. Phys. JETP **75**, 745 (1992)].
[19] A. A. Zvyagin, Fiz. Tverd. Tela **32**, 1546 (1990) [Sov. Phys. Solid State **32**, 905 (1990)].
[20] A. A. Zvyagin, Fiz. Nizk. Temp. **17**, 1436 (1991) [Sov. J. Low Temp. Phys. **17**, 779 (1991)].
[21] Kong-Ju-Block Lee and P. Schlottmann, Phys. Rev. B **38**, 11566 (1988).
[22] J. E. Hirsch, Phys. Lett. A **134**, 451 (1989).
[23] I. O. Kulik, *Contraction Mechanism for Pairing Interaction in Oxides and Hydrides*, in *Progr. in High Temperature Physics*, Vol. 25, R. Nicholsky (Ed.), World Scientific, Singapore (1990).
[24] I. O. Kulik, Fiz. Nizk. Temp. **17**, 1195 (1991) [Sov. J. Low Temp. Phys. **17**, 628 (1991)].
[25] A. Ferretti, I. O. Kulik, and A. Lami, Phys. Rev. B **47**, 12235 (1993).
[26] H. Q. Lin and J. E. Hirsch, Phys. Rev. B **52**, 16155 (1995).
[27] I. O. Kulik and A. G. Pedan, Zh. Éksp. Theor. Phys. **79**, 1469 (1980) [Sov. Phys. JETP **52**, 742 (1980)].
[28] I. O. Kulik, Int. J. Mod. Phys. **B1**, 851 (1988).

This article was published in English in the original Russian journal. It was edited by S. J. Amoretty.

# Peculiarities of vortex state of Bi-2212 single crystals

G. G. Sergeeva

*National Science Center ''Kharkov Institute of Physics and Technology,'' 320108 Kharkov, Ukraine*
(Submitted October 14, 1997; revised December 4, 1997)
Fiz. Nizk. Temp. **24**, 326–329 (April 1998)

A phase diagram of the vortex state of Bi-2212 single crystals in a magnetic field parallel to the $\hat{c}$-axis proposed under the assumption on the two-stage destruction of long-range vortex correlation in such crystals matches with the experimental results obtained by using different methods.[1–7] The intersection of the dimensional crossover line $B_{cr}(T)$ with the line corresponding to violation of long-range vortex correlations in the $(\widehat{ab})$-plane makes it possible to explain the discontinuity at the critical point of the vortex lattice melting curve $T_m(B)$. Possibilities of experimental investigation of low-temperature condensed state for $B>B_{cr}$ and the temperature dependence $B_{cr}(T)$ are considered. © *1998 American Institute of Physics.* [S1063-777X(98)00604-5]

The application of various methods for studying the mixed state of $Bi_2Sr_2Ca_1Cu_2O_x$ (Bi-2212) single crystals led to a considerable advance in constructing the magnetic phase diagram.[1–7] The existence of a vortex lattice which is transformed into a disordered condensed state at $T\leqslant 50$ K upon an increase in the magnetic field to 500 Oe was confirmed in recent experiments on small-angle neutron scattering[1] and spin rotation of muons.[2] As the temperature is elevated to $T>T_m$, where $T_m$ is the melting point, the vortex lattice is transformed into a $3D$ vortex liquid.[1–7] In spite of an astonishing qualitative agreement between the results obtained in Refs. 1 and 2 and the results of resistive, magnetic, and thermal measurements,[3–8] a number of important aspects remain unclear, namely:

(1) discontinuity of the melting curve for a vortex lattice at the critical point[1–7]:
(2) strong dependence of the melting curve on the crystal anisotropy, electron radiation dose,[7] and the magnitude of transport current[6],
(3) the nature of the disordered condensed state in the low-temperature region of the phase diagram in fields weaker than 1000 Oe.[1–3,6,7]

In this communication, we discuss these problems and the model of phase diagram for Bi-2212 in the mixed state matching with the results obtained in Refs. 1–8.

The phase diagram for Bi-2212 in a magnetic field parallel to the $\hat{c}$-axis shown in Fig. 1 is based on the assumption that long-range correlations are destroyed upon an increase in the field or temperature in two stages. The longitudinal and transverse correlation functions should obviously be taken into account in systems for which the number of components in the order parameter is greater than unity (see, for example, Refs. 9 and 10). The two-stage destruction of long-range correlations for anisotropic (quasi-two-dimensional) high-$T_c$ superconductors was considered for the first time by Glazman and Koshelev[11] and was confirmed in recent experiments made by Keener *et al.*[6] It should be noted that the regions of existence of the long-range order in the arrangement of vortices and the long-range superconducting order do not coincide due to nonlocal relations between corresponding fluctuations.

The long-range order in the vortex state is determined by the behavior of the vortex correlation function $C_G$ describing translational correlations for vortex lines in the space of their displacements[12] $u(\rho,z)$, i.e.,

$$C_G(\rho,z)=\langle \exp\, iG[u(\rho,z)-u(0,0)]\rangle, \tag{1}$$

where $G$ is the reciprocal vector of the vortex lattice, $\rho$ the radius vector in the $(\widehat{ab})$ plane, and the $\hat{z}$-axis coincides with the $\hat{c}$-axis. For $z\to\infty$, the asymptotic form of the vortex correlation function is determined by the correlation length $\xi_c^v$ along the $\hat{c}$ axis:

$$C_G(\rho,z\to\infty)=\exp\left[-\frac{1}{2}\,G^2\langle u^2\rangle\right](1+\xi_c^v z^{-1}). \tag{2}$$

For $\rho\to\infty$, the correlation length $\xi_{ab}^v$ in the $(\widehat{ab})$ plane determines the behavior of the correlation function

$$C_G(\rho\to\infty,z)=\exp\left[-\frac{1}{2}\,G^2\langle u^2\rangle\right](1+\xi_{ab}^v \rho^{-1}). \tag{3}$$

The temperature and magnetic-field dependences of vortex correlation lengths are presented in Refs. 10 and 12.

In the case of Bi-2212, the peculiarities of the mixed state and the two-stage nature of destruction of long-range correlations are due to strong anisotropy of electromagnetic interactions and weak pinning of vortex lines in the $(\widehat{ab})$ plane. This leads to the existence of two curves on the $B-T$ plane, where $B$ is the magnetic induction. One of these curves, which is the dimensional crossover curve $B_{cr}(T)$ corresponds to violation of long-range correlations along the $\hat{c}$-axis and is determined from the condition of equality of the correlation length along the $\hat{c}$-axis to the separation $s$ between superconducting copper–oxygen planes:

 

$$\xi_c^v(B,T)=s. \tag{4}$$

The second curve corresponds to the destruction of long-range correlations in the $(\widehat{ab})$ plane and is determined from the condition of equality of the correlation length in the $(\widehat{ab})$ plane to the separation $a=(\Phi_0/B)^{1/2}$ between vortices, where $\Phi_0$ is the magnetic flux quantum:

$$\xi_{ab}^v(B,T)=a. \tag{5}$$

The dimensional crossover curve divides the phase diagram into the two- and three-dimensional parts. An increase in the magnetic field $B>B_{\rm cr}$ in the region $T\leqslant 50$ K leads to dimensional crossover of vortices, and the vortex lattice is transformed into the condensed state of two-dimensional vortices with strong pinning. Violation of long-range correlations along the $\hat{c}$-axis is accompanied by the loss of matching in the arrangement of $2D$-vortices in adjacent copper–oxygen planes $(\widehat{ab})$. The existence of the curve bounding from above the vortex lattice phase at low temperatures is confirmed by various measurements.[1–3,6,7] The assumption concerning the observation of dimensional crossover was discussed in Refs. 1, 7, and 8. The order-of-magnitude estimates give $B_{\rm cr}\approx\Phi_0/(\gamma s)^2=470$ Oe for Bi-2212 ($\gamma^2$ is the ratio of effective masses, $\gamma=140$, $s=15$ Å), which is in accord with the results of measurements.[1–3] We assume that a modification of the Giaever method can be used for determining the nature of the low-temperature state for $B>B_{\rm cr}$. The existence of a dislocation mesh in the $(\widehat{ab})$ plane[13] can lead to strong pinning of $2D$ vortices, observed in magnetic and resistive measurements.[6,7]

The positions of $2D$ vortices at low temperatures on each individual $(\widehat{ab})$ plane are correlated. As the temperature increases to $T>T_{2D}(B)$, long-range vortex correlations in the $(\widehat{ab})$ plane are violated. It is well known that the melting of the lattice of $2D$ vortices differs significantly from the melting of a three-dimensional lattice.[14] For $B>B_{\rm cr}$ and $T>T_{2D}(B)$, no long-range vortex correlations existed in the two-dimensional part of the phase diagram. Such a state known as a two-dimensional vortex liquid differs from the normal state in strong two-dimensional fluctuations. For this reason, the melting curve in magnetic[3,7,15] and resistive[6,16] measurements terminate at the ''critical'' point $T_{\rm cr}$, where $T_m(B)=B_{\rm cr}(T_{\rm cr})$.

In the three-dimensional part of the phase diagram, for $B<B_{\rm cr}$, an increase in temperature leads to the vortex lattice melting (the $T_m(B)$ curve in Fig. 1) and to violation of long-range vortex correlations in the $(\widehat{ab})$ plane: the vortex lattice is transformed into a vortex lines liquid. Like the melting of the crystal lattice, this is a first-order transition accompanied only by the violation of long-range correlations of vortex lines without changing the dimensionality of vortex excitations. This part of the diagram differs insignificantly from the phase diagram for low-temperature superconductors for which ''one-dimensional'' superconductivity was observed at $T<T_c$.[17,18]

The position of the melting curve $T_m(B)$ and the critical point $T_{\rm cr}$ on the phase diagram depends considerably on the extent of anisotropy of the single crystal[3,7] and on the transport current,[6,16] as well as on the time of measurements.[16] In resistive measurements,[6,16] the $T_m(B)$ curve is shifted to the high-temperature region upon a decrease in current and approaches the line corresponding to violation of long-range correlations along the $\hat{c}$-axis. Keener *et al.*[6,16] proposed that the two-stage destruction of long-range vortex correlations is associated with nonequilibrium conditions of melting. This may be due to experimental conditions and can be determined by intrinsic properties inherent in Bi-2212 compounds. During measurements in such a large temperature interval, thermal excitations change the distribution of defects and the dynamics of their movement. It was proved[19] that the action of a magnetic field $H<235$ Oe changes the distribution of defects in Bi ceramic samples so substantially that the initial distribution of defects can be restored only by annealing to 1000 K followed by thermocycling. According to Keener *et al.*,[16] long-term current in the sample causes a shift in the melting curve, reflecting the change in disorder as a result of the movement of defects activated by heating or current.

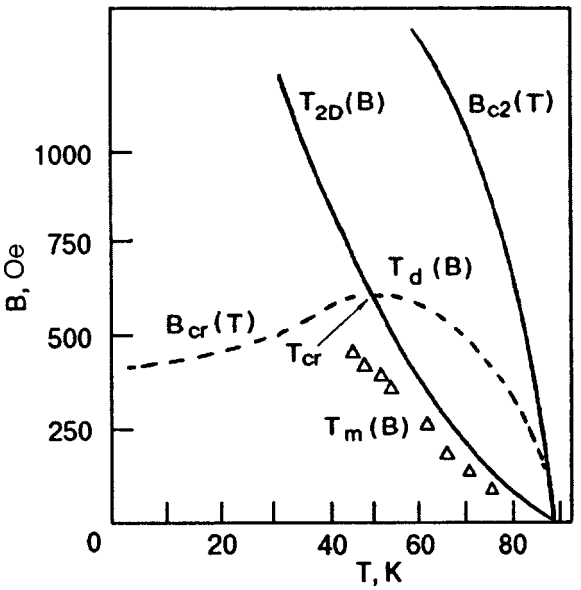


FIG. 1. Schematic phase diagram for Bi-2212 in the mixed state. The solid line marks the upper critical field $B_{c2}$. The lines of destruction of long-range correlations in the $(\widehat{ab})$ plane are curve $T_{2D}(B)$ at $T<T_{\rm cr}$ and the melting curve $T_m(B)$ at $T>T_{\rm cr}(B)$. The dashed curve $B_{\rm cr}(T)$ is the line of destruction of long-range correlations along the $\hat{c}$-axis. The point $T_{\rm cr}$ of intersection of these curves is the discontinuity point on the melting curve. The results of measurements for a sample bombarded by electrons[7] are marked by $\triangle$ (radiation dose $6\cdot 10^{18}$ cm$^{-2}$).

The coincidence of the melting curves obtained from resistive (under a current 20 mA)[6] and magnetic measurements (in fields up to 700 Oe)[11] indicates that the vortex lattice melting in these experiments takes place under identical nonequilibrium conditions. However, considerable changes in melting curves are observed for crystals grown by different methods and for different experimental techniques (see the figure in Ref. 16). Such changes can be explained if we assume that the lines of long-range correlation destruction depend on temperature, and on the concentration of oxygen and Bi, Sr, Ca, and Cu cations. According to Refs. 3, 7,

and 16, the melting temperature $T_m(B)$ increases in the course of sample saturation with oxygen. The crossover line $B_{cr}(T)$ in Fig. 1 consists of three segments. One of them is the low-temperature part, on which only the long-range correlations in the vortex lattice along the $\hat{c}$-axis are violated for $B=B_{cr}(T)$, while correlations in the $(\widehat{ab})$ plane are preserved. The second segment (the line $T_d$ in Fig. 1) is the high-temperature part of the curve corresponding to rupture of bonds between layered in a $3D$ vortex liquid. This means that no long-range vortex correlation are observed at $T>T_d$ and we are dealing with a normal state with strong two-dimensional fluctuations as at $T>T_{2D}(B)$. We assume that the third part existing at moderate temperatures connects the first and second segments of the $B_{cr}(T)$ curve. Recent experiments on low-angle neutron scattering[20,21] indicate that a vortex lattice that is not observed at lower temperatures is formed in fields stronger than 600 Oe at $T>30$ K. This suggests the existence of a maximum on the $B_{cr}(T)$ curve at $T\sim 0.5T_c$. The temperature dependence of the crossover line is probably due to electromagnetic and Josephson bonds between layers, which have different temperature dependences as well as due to the ''size'' effect[10] for $\xi_c^v(B,T)\geqslant l_c$, where $l_c$ is half the transverse size of the sample.

Thus, we have analyzed the phase diagram for Bi-2212 single crystals in a magnetic field parallel to the $\hat{c}$-axis under the assumption of intrinsic two-stage destruction of long-range correlations. The analysis leads to the following conclusions.

(1) The melting curve terminates at the critical point where the dimensional crossover curve $B_{cr}(T)$ intersects the line corresponding to long-range correlation destruction in the $(\widehat{ab})$ plane. The $T_m(B)$ curve is the only line on which long-range correlations are violated without a change in the dimensionality of vortex excitation. We assume that the shape of the $B_{cr}$ curve depends significantly on temperature.
(2) Nonequilibrium conditions of melting lead to the dependence of the melting curve on the methods of measurements and growth of crystals. This is due to a weak pinning of defects (oxygen atoms and vacancies as well as dislocations) and reflects a change in disorder under the action of temperature, current, and magnetic field.
(3) The low-temperature state observed for $B>B_{cr}$ is a condensed state of $2D$ vortices with strong pinning due to the existence of a dislocation mesh in the $(\widehat{ab})$ plane of Bi-2212 single crystals.

In order to verify the last statement and analyze the temperature dependence of $B_{cr}$, one can use a modification of the Giaever method, which makes it possible to determine the dimensionality of vortices.[22] The effect of a two-dimensional dislocation mesh on the pinning of $2D$ vortices can be determined after sample annealing in vacuum for half an hour at 500 °C. The dislocation mesh vanishes upon cooling,[9] and the ordered states of $2D$ vortices must be observed in some $(\widehat{ab})$ planes. Resistive measurements at currents smaller than 0.1 mA should be continued in order to study the origin of nonequilibrium conditions. The coincidence of the $T_m(B)$ and $T_d(B)$ curves would confirm the hypothesis put forth by Keener *et al.*,[6] according to which the two-stage violation of long-range correlations is due to nonequilibrium conditions of measurements. It should be interesting to observe the ''size'' effect predicted by Yeh[10]: as the transverse size $l_c$ of the sample decreases, the $T_d(B)$ curve corresponding to the violation of long-range vortex correlations in the $\hat{c}$-axis must be displaced towards low-temperature region.

[1] R. Cubitt, E. M. Forgan, G. Yang *et al.*, Nature (London) **365**, 407 (1994).
[2] S. L. Lee, M. Warden, H. Keller, and J. W. Schneider, Phys. Rev. Lett. **75**, 922 (1995).
[3] B. Khaykovich, E. Zeldov, D. Majer *et al.*, Phys. Rev. Lett. **76**, 2555 (1996).
[4] W. K. Kwok, J. A. Fendrich, V. M. Vinokur *et al.*, Phys. Rev. Lett. **76**, 4596 (1996).
[5] A. Schilling, Nature (London) **382**, 791 (1996).
[6] C. D. Keener, M. L. Trawick, S. S. Ammirata *et al.*, Phys. Rev. Lett. **78**, 1118 (1997).
[7] B. Khaekovich, E. Zeldov, M. Konczykovski *et al.*, Czech. J. Phys. **46, Suppl. S6**, 3218 (1996).
[8] R. Sasik and D. Stroud, Phys. Rev. B **52**, 3696 (1995).
[9] P. C. Hohenberg, A. Aharony, B. I. Halperin, and E. D. Siggia, Phys. Rev. B **13**, 2986 (1976).
[10] N. S. Yeh, Phys. Rev. B **42**, 4850 (1990).
[11] L. I. Glazman and A. E. Koshelev, Phys. Rev. B **43**, 2835 (1991).
[12] D. R. Nelson and H. S. Seung, Phys. Rev. B **39**, 9153 (1989).
[13] G. Yang, P. Shang, S. D. Sutton *et al.*, Phys. Rev. B **48**, 4054 (1993).
[14] D. S. Fisher, Phys. Rev. B **22**, 1190 (1980).
[15] D. T. Futchs, E. Zeldov, D. Majer *et al.*, Czech. J. Phys. **46, Suppl. S3**, 1583 (1996).
[16] C. D. Keener, M. L. Trawick, S. S. Ammirata, and J. C. Garland, Czech. J. Phys. **46, Suppl. S6**, 3211 (1996).
[17] D. J. Thouless, Phys. Rev. Lett. **34**, 946 (1975).
[18] V. A. Marchenko and A. N. Nikulov, Zh. Éksp. Teor. Fiz. **86**, 1395 (1984) [Sov. Phys. JETP **59**, 815 (1984)].
[19] B. G. Lazarev, Ya. D. Starodubov, G. G. Sergeeva *et al.*, Czech. J. Phys. **46, Suppl. S3**, 1186 (1996).
[20] E. M. Forgan, M. T. Wylie, S. Lloyd *et al.*, Czech. J. Phys. **46, Suppl. S3**, 1571 (1996).
[21] S. M. Aegerter, S. L. Lee, H. Keller *et al.*, Phys. Rev. B **54**, 15661 (1996).
[22] I. Giaver, Phys. Rev. Lett. **5**, 147 (1960).

Translated by R. S. Wadhwa

## LOW-TEMPERATURE MAGNETISM

# Low-temperature resistivity of Zener ferromagnets

V. N. Krivoruchko and A. M. Yakovenko

*A. Galkin Physicotechnical Institute, National Academy of Sciences of the Ukraine, 340114 Donetsk, Ukraine*

(Submitted November 4, 1997)
Fiz. Nizk. Temp. **24**, 330–336 (April 1998)

Low-temperature resistivity $\rho(T)$ of Zener ferromagnets due to the interaction between the conducting and magnetic subsystem is studied. The effective Hamiltonian is obtained by using the representation of Hubbard's operators in terms of local pseudospins and spinless fermions. The contribution to $\rho(T)$ from scattering of charge carriers by spin waves and magnetic inhomogeneities is considered. The latter are simulated by a vector field with random orientation and location of scattering center. The obtained dependence $\rho(T)=\rho_0+\rho_1T^{3/2}+\rho_2T^{5/2}$ is compared with the available experimental and theoretical results. © *1998 American Institute of Physics.* [S1063-777X(98)00704-X]

### INTRODUCTION

Zener[1] introduced the ''double-exchange'' mechanism in order to explain ferromagnetism of compounds with the perovskite structure with ions of the same element but with difference valencies in equivalent positions of the crystal lattice. Kubo and Ohata,[2] who studied the resistivity of a Zener ferromagnet in the low-temperature region $T\ll T_C$ ($T_C$ is the Curie temperature), obtained the dependence $\rho(T)\sim T^{9/2}$. Perovskite-type manganites are regarded as typical representatives of systems with ''double exchange'' [3] (see also Ref. 4). However, none of these systems obeys the temperature dependence of resistivity described by a 9/2-power law in spite of their diversity. For example, a dependence of the type $\rho(T)=A_0-B_0T+C_0T^2$ was obtained for $La_{2/3}Ba_{1/3}MnO_3$ films.[5] The low-temperature behavior of $\rho(T)$ studied by Schiffer *et al.*[6] for $La_{1-x}Ca_xMnO_3$ ($x=0.20$; 0.33; 0.45) is successfully approximated by the dependence $\rho(T)=\rho_0+\rho_1T^{5/2}$. Urushibara *et al.*[7] described the resistivity of $La_{1-x}Sr_xMnO_3$ single crystals with $x=0.2$, 0.3, and 0.4 at $T<200$ K by the function $\rho(T)=\rho(0)+\rho_1T^2$. A detailed analysis of transport and magnetic properties of bulk samples and thin epitaxial films of $La_{0.67}Ca_{0.33}MnO_3$ and $La_{0.67}Sr_{0.33}MnO_3$ was carried out in a recent publication by Snyder.[8] The observed behavior of low-temperature resistivity of these systems is correctly described by the dependence $\rho(T)=\rho_0+\rho_2T^2$. A polynomial of the form $\rho_0+\rho_2T^2+\rho_nT^n$ with $n$ varying in the interval $4<n<5$ made it possible to describe the $\rho(T)$ curve down to the Curie temperature.

The spread in experimental relations for $\rho(T)$ indicates the diversity of elastic and inelastic mechanisms of charge carrier scattering. The contribution of each mechanism can be noticeably enhanced or suppressed by varying the sample preparation technique. However, it is interesting to note that empirical relations for $\rho(T)$[5–8] differ significantly from the theoretical results.[2] Since the concept of ''double exchange'' between the $Mn^{3+}$ and $Mn^{4+}$ ions can be regarded as substantiated for perovskite-type manganites, such a discrepancy can be associated with the mechanisms of formation of low-temperature resistivity of manganites that differ from those considered by Kubo and Ohata,[2] or some of the approximations used for calculating the $\rho(T)$ dependence may not be applicable. In this connection, it is expedient to consider again the theory of low-temperature resistivity of manganites.

Using the slave-fermion representation for Hubbard operators, we consider the magnetic mechanisms of formation of low-temperature resistivity of Zener ferromagnets. The contribution to $\rho(T)$ due to charge carrier scattering by spin waves is described by the dependence $T^{5/2}$, while the terms proportional to $T^{3/2}$ appear in the expression for resistivity if we take into account the scattering of charge carriers by magnetic inhomogeneities. Heterogeneity of the magnetic structure is simulated by the classical vector field with random orientation and location of a scattering center. The obtained $\rho(T)$ dependence is compared with the available experimental and theoretical results.

### 1. EFFECTIVE HAMILTONIAN FOR AN ELECTRON MOVING IN A FERROMAGNETIC MATRIX

We shall first consider the ideal case, i.e., a lattice without magnetic and crystal defects. Suppose that we have a system of spins $\boldsymbol{S}$ localized at crystal lattice sites. Electrons whose number $N_e$ is smaller than the number $N$ of lattice sites move from site to site. In the case when the Coulomb repulsion of electrons at a lattice site is strong, the system can be described by a Hamiltonian of the form

$$H=-\sum_{ij} t_{ij}(1-n_{i\bar{\sigma}})C^+_{i\sigma}C_{j\sigma}(1-n_{j\bar{\sigma}})-K\sum_i S_i\sigma_i - \frac{1}{2}J\sum_{ij} S_iS_j, \quad (1)$$

 

where $t_{ij}$ is the kinetic term describing the motion of electrons between nearest neighbors in the lattice, $K$ the intraatomic exchange integral of interaction between the local spin $S_i$ and the electron spin $\sigma_i$ at the $i$th site (Hund's binding energy), and $J$ the effective exchange interaction of local spins of the lattice. The factor $(1-n_{i\bar{\sigma}})$, where $\bar{\sigma}=-\sigma$ describes the prohibition for an electron with spin $\sigma$ to be at a lattice site containing an electron with the opposite spin. In this way, the condition that electrons move over vacant lattice site is taken into consideration. In Eq. (1), $C_{i\sigma}^{+}$ and $C_{i\sigma}$ are the Fermi operators of creation and annihilation of an electron with spin $\sigma$ at the $i$th lattice site, $\sigma_i=(1/2)\Sigma C_{i\sigma}^{+}\hat{\tau}_{\sigma\sigma'}C_{i\sigma'}$ ($\hat{\tau}$ are Pauli matrices), and $n_{i\sigma}=C_{i\sigma}^{+}C_{i\sigma}$. We shall assume that the initial antiferromagnetic order of the matrix is suppressed by ''double exchange,'' and a metallic phase with the ferromagnetic ordering of local spins exists in the system. The interaction between the electron spin and the spin of a lattice site is also ferromagnetic. The magnetic ordering temperature for manganites is $JS^2\approx 200$ K($\sim 0.02$ eV). According to estimates,[9,10] the conduction band width is $ta^2\approx 1.0$ eV, and the energy of interaction between an electron and a local spin is $KS\approx 1.5$ eV. For the sake of simplicity, however, we shall consider stronger relations between the parameters of the Hamiltonian: $KS\gg ta^2\gg JS^2$.

By virtue of the condition $N>N_e$ and the type of electron movement, the spin at a lattice site is variable. We shall take this fact into account by using the methods developed for investigating strongly correlated electron systems.[11] That is, we shall use the slave-fermion (according to the terminology used by Izyumov[11]) representation for Hubbard operators[12–14] and single out the spin and charge degrees of freedom for electrons by using the following relations between operators:

$$
\begin{aligned}
&C_{i\uparrow}(1-n_{i\downarrow})=h_i^{+}\left(\frac{1}{2}+s_i^z\right), \quad C_{i\downarrow}(1-n_{i\uparrow})=h_i^{+}s_i^{+},\\
&(1-n_{i\downarrow})C_{i\uparrow}^{+}=h_i\left(\frac{1}{2}+s_i^z\right), \quad C_{i\downarrow}^{+}(1-n_{i\uparrow})=h_i s_i^{-},\\
&\sigma_i=s_i h_i h_i^{+}.
\end{aligned}
\tag{2}
$$

Here the operators of spinless fermions (''holes'') $h_i, h_i^{+}$ commute with the operators of pseudospin **s**; as usual, $s^{\pm}=s_x\pm is_y$. The separation of spin and charge degrees of freedom of an electron simplifies the physical aspect of the problem. At the same time, a transition to pseudospins introduces certain difficulties: we must take into account constraints that rule out nonphysical states inevitably introduced by these concepts. This question was analyzed most thoroughly for models of strongly correlated systems (see the review by Izyumov[11]). For example, in the case of the Hubbard model, representation (2) contains only one local constraint which is automatically satisfied in the limit $U\gg t$ ($U$ is the Coulomb repulsion energy for electrons at a lattice site). Besides, conditions (2) do not include a relation between the charge and spin degrees of freedom.[12,14] For models of type (1), these problems have not been discussed. However, there are no additional reasons either for which the role of nonphysical states in model (1) would be more significant than in the Hubbard model. It should also be noted that in Ref. 2 the projection operators $(1-n_{i\sigma})$ were replaced by unity, while we take them into account completely by using representation (2).

Using the slave-fermion representation, we can reduce the initial Hamiltonian (1) for electrons moving in a ferromagnetic matrix to the effective Hamiltonian

$$
\begin{aligned}
H=&\sum_{ij} t_{ij}h_i^{+}h_j\left[\frac{1}{4}+\frac{1}{2}(s_i^z+s_j^z)+s_i^z s_j^z+s_i^{-}s_j^{+}\right]\\
&-K\sum_i h_i h_i^{+}\left[S_i^z s_i^z+\frac{1}{2}(S_i^{+}s_i^{-}+s_i^{+}S_i^{-})\right]\\
&-\frac{1}{2}J\sum_{ij}(S_i^z S_j^z+S_i^{-}S_j^{+})
\end{aligned}
\tag{3}
$$

for spinless ''holes'' moving in the ''two-sublattice'' ferromagnetic matrix with a constant spin $(S+1/2)$ at lattice sites. Following Kubo and Ohata,[2] we shall use the low-temperature expansion of spin variables in Bose operators:

$$
\begin{aligned}
&S_i^{+}=\sqrt{2S}\,a_i, \quad S_i^{-}=\sqrt{2S}\,a_i^{+}, \quad S_i^z=S-a_i^{+}a_i;\\
&s_i^{+}=b_i, \quad s_i^{-}=b_i^{+}, \quad s_i^z=\frac{1}{2}-b_i^{+}b_i.
\end{aligned}
$$

At this stage, The Hamiltonian quadratic in the operators assumes the following form in the Fourier representation:

$$
\begin{aligned}
H_0=&\sum_{\mathbf{k}}(E_{\mathbf{k}}-\mu)h_{\mathbf{k}}^{+}h_{\mathbf{k}}+\sum_{\mathbf{k}}[A_{1\mathbf{k}}a_{\mathbf{k}}^{+}a_{\mathbf{k}}+A_2 b_{\mathbf{k}}^{+}b_{\mathbf{k}}\\
&+B(a_{\mathbf{k}}^{+}b_{\mathbf{k}}+b_{\mathbf{k}}^{+}a_{\mathbf{k}})].
\end{aligned}
\tag{4}
$$

The first term includes the chemical potential $\mu$, and we have used the following notation: $A_{1\mathbf{k}}=K/2+S(J_0-J_K)$, $A_2=SK$, and $B=-K\sqrt{S/2}$; $J_{\mathbf{k}}$ and $E_{\mathbf{k}}$ are Fourier transforms of effective exchange and hopping integral, respectively. It should be emphasized that Hamiltonian (4) preserves the total number of spin deviations. Nevertheless, it is convenient to diagonalize the Hamiltonian and go over to Bose operators of quasiparticles $\alpha_{\mathbf{k}}^{+}, \alpha_{\mathbf{k}}$ and $\beta_{\mathbf{k}}^{+}, \beta_{\mathbf{k}}$. After a $u-v$ transformation of the form $a_{\mathbf{k}}=u_{1\mathbf{k}}a_{\mathbf{k}}+v_{1\mathbf{k}}\beta_{\mathbf{k}}$, $b_{\mathbf{k}}=u_{2\mathbf{k}}\beta_{\mathbf{k}}+v_{2\mathbf{k}}\alpha_{\mathbf{k}}$ with the coefficients

$$
\begin{aligned}
&u_{1\mathbf{k}}=\left(\frac{A_2-\varepsilon_{1\mathbf{k}}}{\varepsilon_{2\mathbf{k}}-\varepsilon_{1\mathbf{k}}}\right)^{1/2}, \quad v_{1\mathbf{k}}=\left(\frac{\varepsilon_{2\mathbf{k}}-A_2}{\varepsilon_{2\mathbf{k}}-\varepsilon_{1\mathbf{k}}}\right)^{1/2}\\
&u_{2\mathbf{k}}=\left(\frac{\varepsilon_{2\mathbf{k}}-A_{1\mathbf{k}}}{\varepsilon_{2\mathbf{k}}-\varepsilon_{1\mathbf{k}}}\right)^{1/2}, \quad v_{2\mathbf{k}}=\left(\frac{A_{1\mathbf{k}}-\varepsilon_{1\mathbf{k}}}{\varepsilon_{2\mathbf{k}}-\varepsilon_{1\mathbf{k}}}\right)^{1/2}
\end{aligned}
$$

we go over to diagonal form of the Bose component of the quadratic Hamiltonian also. The energies of spin-wave (Bose) excitations are given by

$$
\varepsilon_{\mathbf{k}}=\frac{2S}{2S+1}\varepsilon_{\mathbf{k}}, \quad \varepsilon_{2\mathbf{k}}=\left(S+\frac{1}{2}\right)K+\frac{\varepsilon_{\mathbf{k}}}{2S+1},
\tag{5}
$$

where $\varepsilon_{\mathbf{k}}=S(J_0-J_{\mathbf{k}})$. Thus, the interaction between the subsystem of band charge carriers and the local system of spins leads to the emergence of the exchange (optical) branch $\varepsilon_{2\mathbf{k}}$ in addition to the acoustic branch $\varepsilon_{1\mathbf{k}}$ in the spectrum of

spin-wave excitations. Such a situation is typical of magnets in which magnetic ions can be in states with different valencies.

The interaction of spin waves and ''holes'' in the first nonvanishing approximation is described by the Hamiltonian $H_4=H_4'+H_4''$, where

$$H_4'=N^{-1}\sum_{1234}\{\varphi_1 h_1^+\alpha_2^+ h_3\alpha_4+\varphi_2 h_1^+\beta_2^+ h_3\beta_4 + \varphi_3 h_1^+\alpha_2^+ h_3\beta_4+\varphi_4 h_1^+\beta_2^+ h_3\alpha_4\}\Delta(1-2-3-4). \quad (6)$$

Here $\varphi_{1,2,3,4}$ are the amplitudes of scattering of ''holes'' and spin waves at each other, $\mathbf{1}=\mathbf{k}_1$, $\mathbf{2}=\mathbf{k}_2$, and so on. The term $H_4''$ describes scattering of spin waves at one another without the participation of ''holes'' and is important for establishing thermodynamic equilibrium in the spin subsystem. We shall assume that this equilibrium has already set in, and the explicit form of $H_4''$ is not required.

## 2. RESISTIVITY AT LOW TEMPERATURES

Following Kubo and Ohata,[2] (see also Ref. 15), we can obtain the following expression for the temperature dependence resistivity $\rho(T)$:

$$\rho(T)=\left(\frac{1}{3}e^2M^2\right)^{-}\left[N^{-1}\sum_{\mathbf{k}}\left(\frac{\partial E_{\mathbf{k}}}{\partial\mathbf{k}}\right)^2\frac{\partial f_{\mathbf{k}}^0}{\partial E_{\mathbf{k}}}\right]^{-2}N^{-1} \times\sum_{\mathbf{k}}\mathbf{k}I_{\mathrm{coll}}(f_{\mathbf{k}}), \quad (7)$$

where $f_{\mathbf{k}}^0$ is the equilibrium and $f_{\mathbf{k}}$ the nonequilibrium ''hole'' distribution functions (here and below, the Planck constant $\hbar=1$). At low temperatures, the contribution of exchange magnons to the ''hole'' kinetics can be neglected in view of their high activation energy. As a result, we obtain the following expression for the collision integral $I_{\mathrm{coll}}(f_{\mathbf{k}})$:

$$I_{\mathrm{coll}}(f_{\mathbf{k}})=2\pi N^{-2}\sum_{\mathbf{pq}}|\varphi_1|^2\{(1-f_{\mathbf{k}})(1+N_{\mathbf{p}})f_{\mathbf{p}}N_{\mathbf{k+p-q}} - f_{\mathbf{k}}N_{\mathbf{p}}(1-f_{\mathbf{q}})(1+N_{\mathbf{k+p-q}})\}\delta(E_{\mathbf{k}}+\varepsilon_{1\mathbf{p}}-E_{\mathbf{q}} - \varepsilon_{1\mathbf{k+p-q}}).$$

While calculating $I_{\mathrm{coll}}(f_{\mathbf{k}})$, we shall assume that the following conditions are satisfied (in this case, we confine ourselves to the assumptions made by Kubo and Ohata[2]): equilibrium distribution is observed in the magnon system and Fermi-liquid effects are small. The second condition implies that the nonequilibrium ''hole'' distribution function in a weak electric field $\mathbf{E}$ can be presented in the form

$$f_{\mathbf{k}}=f_{\mathbf{k}}^0+f_{\mathbf{k}}^{(1)}=f_{\mathbf{k}}^0-e(\mathbf{E}\cdot\mathbf{v})\tau_{\mathbf{k}}\frac{\partial f_{\mathbf{k}}^0}{\partial E_{\mathbf{k}}}$$

and the effect of weak deviations from equilibrium on the fermion energy $E_{\mathbf{k}}$ can be disregarded. In the above expression, we have used the following notation: $E_{\mathbf{k}}=\mathbf{k}^2/2M$, $\mathbf{v}=\partial E_{\mathbf{k}}/\partial\mathbf{k}$, and $\tau_{\mathbf{k}}$ is the transport relaxation time for ''holes.''

After a number of simple transformations, we obtain the following expression for the sum in the numerator in (7):

$$N^{-1}\sum_{\mathbf{k}}kI_{\mathrm{coll}}(f_{\mathbf{k}})=\frac{2\pi}{N^3}\sum_{\mathbf{kpq}}|\varphi_1|^2N_{\mathbf{p}}N_{\mathbf{k+p-q}}\delta(E_{\mathbf{k}}+\varepsilon_{1\mathbf{p}} - E_{\mathbf{q}}-\varepsilon_{1\mathbf{k+p-q}}) \times\left\{\exp(\beta\varepsilon_{1\mathbf{k+p-q}})\frac{f_k^0}{f_q^0}(\mathbf{k}\cdot\mathbf{q})\frac{\partial f_{\mathbf{q}}^0}{\partial E_{\mathbf{q}}} - \exp(\beta\varepsilon_{1\mathbf{p}})\frac{f_q^0}{f_{\mathbf{k}}^0}(\mathbf{k}\cdot\mathbf{k})\frac{\partial f_{\mathbf{k}}^0}{\partial E_{\mathbf{k}}}\right\}, \quad (8)$$

where $N_{\mathbf{p}}$ and $N_{\mathbf{k+p-q}}$ are the equilibrium distribution functions for acoustic magnons. By virtue of the condition $T\ll T_c$, we can write the scattering amplitude in the form of an expansion in magnon wave vectors. In the first nonvanishing approximation, we can write it in the form $\varphi_1\approx -4SK/(2S+1)$. For the same reason, it is sufficient to confine our analysis to a quadratic energy–momentum relation for spin waves: $\varepsilon_{1\mathbf{k}}=\mathbf{k}^2/2m$. In the first approximation, the derivative $\partial f_{\mathbf{k}}^0/\partial E_{\mathbf{k}}$ can be treated as a $\delta$-function: $\partial f_{\mathbf{k}}^0/\partial E_{\mathbf{k}}\approx-\delta(E_{\mathbf{k}}-E_F)$. Finally, we shall take into account the fact that the ''hole'' mass obeys the relation $M^{-1}\sim ta^2$, while the reciprocal mass of the acoustic magnon $m^{-1}\sim JSa^2$, i.e., $m\gg M$, and the scattering of light electrons at heavy magnons can be regarded as elastic. Expression (8) can be easily made dimensionless, and we obtain the following estimate for $\rho(t)$:

$$\rho(T)-\frac{1}{e^2\mathbf{k}_F}(|\varphi_1|^2mM)\left(\frac{T}{E_F}\right)^{5/2}\left(\frac{m}{M}\right)^{5/2}(a\mathbf{k}_F)^2C_1, \quad (9)$$

where $C_1$ is a numerical constant. Thus, the scattering of ''holes'' by spin waves leads to the dependence $\rho(T)\sim T^{5/2}$.

Let us consider in greater detail the reasons behind the discrepancy between our results and those obtained by Kubo and Ohata.[2] It should be recalled that Kubo and Ohata confined their analysis to the subspace of the lowermost excited states of the system, for which the energy associated with the Hund interaction remains unchanged. This allowed them to eliminate this energy by using a canonical transformation. The resultant Hamiltonian (see formula (2.3) in Ref. 2) contains only the kinetic component describing the motion of effective charge carriers. This Hamiltonian was used by the authors of this publication for determining $\rho(T)$. However, approximation (2.3) from Ref. 2 is insufficient for calculating scattering amplitudes. The latter can be determined by a more consistent elimination of intraatomic exchange at a ''vacant'' site, i.e., higher orders of the canonic expansion are required. In our approach, this is taken into account automatically: the second term of Hamiltonian (3) contains the factor $h_ih_i^+$ which nullifies the Hund energy if a lattice site is occupied by a ''hole.'' This circumstance leads to a change in the amplitude of interaction of the ''hole'' with a spin wave. In the limit of small wave vectors, the amplitude becomes proportional to intraatomic exchange instead of the square of the wave vector.[2] This reduces the exponent in the power dependence $\rho(T)$ from 9/2 to 5/2.

It should also be noted in this connection that the construction of the spin-polaron Hamiltonian of a narrow-band

semiconductor in the monograph by Nagaev[16] cannot be regarded as satisfactory. The arguments given in the derivation of (3.5.14) in Ref. 16 rather reflect the author's point of view and do not result from mathematical transformations. The symmetry requirements suitable for homogeneous systems apparently cannot be extended to systems with a varying magnitude of spin at a lattice site.

### 3. SCATTERING AT MAGNETIC INHOMOGENEITIES

It is important to find the effect of imperfections of the crystal and magnetic lattices on the $\rho(T)$ dependence. Leaving aside a detailed discussion of this problem, let us consider a simple generalization of model (1).

It should be noted that the potential of scattering of electrons at lattice defects contains in the general case a component that does not depend on the orientation of the spin as well as a spin-dependent term. The potential scattering makes a contribution to the temperature-independent (if we disregard interference processes) residual resistivity $\rho_0$ and will not be considered here. The physical reason behind the presence of spin-dependent terms is the spin-orbit interaction. The microscopic expression for spin-orbit scattering has a complex analytical form. We shall use a simple phenomenological expression proposed earlier in Ref. 17, namely, we shall describe the interaction of conduction electrons with magnetic heterogeneities by a Hamilton of the form

$$H_{\text{rand}} = -N^{-1}\sum_{\mathbf{lq}} (\mathbf{R}\cdot\boldsymbol{\sigma}_{\mathbf{q}})\,\eta_{\mathbf{l}} \exp(-i\mathbf{q}\cdot\mathbf{l}). \tag{10}$$

Here $\mathbf{R}$ is the effective field of inhomogeneities distributed randomly over lattice sites and in space, and the factor $\eta_l$ is equal to unity if a site contains a heterogeneity and to zero otherwise. The mean values $\langle R_\alpha\rangle = 0$ in view of the absence of preferred direction of the field $\mathbf{R}$ in space, while the quantities

$$\langle R_\alpha^2\rangle = \int R_0^2 p(R_\alpha, T)\, dR_\alpha, \quad \alpha = x,y,z, \tag{11}$$

differ from zero, where $p(R_\alpha, T)$ is the distribution function for the field $R_\alpha$ at a given temperature, normalized to unity. Relation (11) presumes thermodynamic and configurational averaging; the meaning of configurational averaging is the same as for spin glasses.[18] The local field of magnetic inhomogeneity introduced in this way is very close in its physical meaning to the effective field used in the theory of spin glasses (e.g., in Edwards–Anderson model).[18] This means that formula (10) can also describe the scattering of electrons by nanometer-scale imperfections of the magnetic structure. In this case, $\mathbf{R}$ is the effective magnetic field of magnetic clusters, nuclei of the new phase, and so on.

Carrying out transformation (2) and going over from spin variables to Bose variables, and then to quasiparticle operators, we obtain

$$H_{\text{rand}}^{(1)} = N^{-3/2}\sum_{\mathbf{kpq}} \{\psi_1 \alpha_{\mathbf{k}}^+ h_{\mathbf{p}}^+ h_{\mathbf{q}} + \psi_2 \beta_{\mathbf{k}}^+ h_{\mathbf{p}}^+ h_{\mathbf{q}} + \text{h.c.}\}, \tag{12}$$

where the amplitudes are given by $\psi_1 = 1/2R^+\eta_1\nu_{2\mathbf{k}}$, $\psi_2 = (1/2)R^+\eta_1 u_{2\mathbf{k}}$, $R^\pm = R_x \pm iR_y$. As usual, momentum is not conserved in scattering at heterogeneities. In expression (12), we write only low-order terms leading to temperature corrections to $\rho(T)$.

The collision integral [to be more precise, the right-hand side of (8)] acquires an additional term of the form

$$\frac{2\pi}{N^3}\sum_{\mathbf{kpq}} |\psi_1|^2 N_{\mathbf{p}}\,\delta(E_{\mathbf{k}} + \varepsilon_{1\mathbf{p}} - E_{\mathbf{q}}) \times\left\{\exp(\beta\varepsilon_{1\mathbf{p}})\,\frac{f_{\mathbf{k}}^0}{f_{\mathbf{q}}^0}\,(\mathbf{k}\cdot\mathbf{q})\,\frac{\partial f_{\mathbf{q}}^0}{\partial E_{\mathbf{q}}} - \frac{f_{\mathbf{q}}^0}{f_{\mathbf{k}}^0}\,(\mathbf{k}\cdot\mathbf{k})\,\frac{\partial f_{\mathbf{k}}^0}{\partial E_{\mathbf{k}}}\right\}.$$

We must now carry out summation over impurity coordinates and configuration averaging over the orientations of the field $\mathbf{R}$ at each site. Denoting this averaging by the angle brackets $\langle ...\rangle$, we note that $\langle \eta_{\mathbf{l}}\eta_{\mathbf{l}'}\rangle = \langle \eta_{\mathbf{l}}\rangle\langle \eta_{\mathbf{l}'}\rangle = c^2$, for $l \neq l'$ and $\langle \eta_{\mathbf{l}}\eta_{\mathbf{l}'}\rangle = c$ for $l = l'$, where $c$ is the concentration of inhomogeneities. Repeating the same arguments as in derivation of formula (9) and retaining the terms $\sim c$, we obtain the following estimate for $\rho_{\text{rand}}(T)$, viz., the contribution to resistivity from electron scattering by magnetic inhomogeneities:

$$\rho_{\text{rand}}(T) - \frac{c}{e^2 k_F}\,\frac{\langle R^+R^-\rangle M^2}{2S+1}\left(\frac{T}{E_F}\right)^{3/2}\left(\frac{m}{M}\right)^{3/2}(ak_F)^2 C_2, \tag{13}$$

where $C_2$ is a numerical constant. The value of $\langle R^+R^-\rangle$ in each case is determined by the form of the distribution function $p(R_\alpha)$ in accordance with (11) (we shall not do it here). Thus, $\rho(T)$ acquires terms proportional to $T^{3/2}$ due to scattering of ''holes'' by magnetic inhomogeneities.

### CONCLUSIONS

Let us make some general remarks concerning the applicability of the above model and the obtained results to real systems of perovskite-type manganites.

In the general case, we must expect the existence of two independent mechanisms for formation of resistance in a magnetic conductor, which are associated with elastic and inelastic interactions of charge carriers with the magnetic subsystem. For elastic mechanisms, the conductivity can be described by the band model (taking into account the ''coating'' of electrons with magnons). For inelastic mechanisms, the motion of ''coated'' electrons is jumpwise and is accompanied by the emission and absorption of magnons. These two mechanisms have completely different temperature dependences. In the case of the itinerant description, the resistivity increases with temperature since magnetic fluctuations hamper the motion of electrons. In the case of inelastic processes, resistivity decreases upon an increase in temperature since fluctuations facilitate electron jumps.

In perovskite-type manganites, both mechanisms are apparently equivalent and operate simultaneously. Moreover, an analysis of thermoelectric effects proves[19–21] that manganites contain simultaneously electrons and holes, and the type of conductivity can be changed by varying temperature and/or degree of doping. As a result, the transport properties of various manganite systems can differ considerably.

According to the results obtained in Sec. 1, the amplitudes of interaction between magnons and ''holes'' have no small parameter, i.e., we are dealing with a ''strong coupling.'' This means that a consistent analysis of transport and magnetic properties of the system requires a self-consistent approach taking into account mutual renormalization of ''hole'' and spin-wave states. In the general case, this approach should be based not on the perturbation theory, but on the application, say, of a certain canonical transformation in analogy with the problem of magnetic polaron in strongly correlated electron systems.[11] Such a problem is beyond the scope of this communication. We have used the band model and a standard approach based on the kinetic equation to consider magnetic mechanisms of formation of the low-temperature resistance of Zener ferromagnets. The dependence $T^{5/2}$ was obtained for contributions to $\rho(T)$ associated with intrinsic scattering of charge carriers by spin waves, while the inclusion of scattering by magnetic inhomogeneities led to the emergence of terms in resistivity proportional to $T^{3/2}$. Returning to the experimental situation described in Introduction, we see that expression (9) corresponds to the $\rho(T)$ dependence for the compound $La_{1-x}Ca_xMnO_3$[6] and is close to the low-temperature behavior of $\rho(T)$ observed for other materials.[5,7,8]

The authors are grateful to È. Zubov for fruitful discussions of some aspects of the theory of strongly correlated electron systems.

[1] C. Zener, Phys. Rev. **82**, 403 (1951).
[2] K. Kubo and N. Ohata, J. Phys. Soc. Jpn. **33**, 21 (1972).
[3] S. Krupicka, *Physik der Ferrite und der verwandten magnetischen Oxide*, Academia, Praha (1973).
[4] È. L. Nagaev, Phys. Usp. **166**, 833 (1996).
[5] S. E. Loffland, S. M. Bhagat, H. L. Ju *et al.*, Phys. Rev. B **52**, 15058 (1995).
[6] P. Schiffer, A. P. Ramirez, W. Bao, and S.-W. Cheong, Phys. Rev. Lett. **75**, 3336 (1995).
[7] A. Urushibara, Y. Morimoto, T. Arima *et al.*, Phys. Rev. B **51**, 14103 (1995).
[8] G. J. Snyder, R. Hiskes, S. DiCarolis *et al.*, Phys. Rev. B **52**, 14434 (1996).
[9] T. Arima, Y. Tokura, and J. B. Torrance, Phys. Rev. B **48**, 17006 (1993).
[10] Y. Okimoto, T. Tatsufuji, T. Ishikawa *et al.*, Phys. Rev. Lett. **75**, 109 (1995).
[11] Y. A. Izyumov, Usp. Fiz. Nauk **167**, 465 (1997) [*sic*].
[12] G. G. Haliullin, Pis'ma Zh. Éksp. Teor. Fiz. **52**, 999 (1990) [JETP Lett. **52**, 389 (1990)].
[13] J. L. Richard and V. Yu. Yushankhai, Phys. Rev. B **47**, 1103 (1993).
[14] Y. R. Wong, Phys. Rev. B **51**, 234 (1995).
[15] A. A. Abrikosov, *Fundamentals of the Theory of Metals*, No. Holland, Amsterdam (1988).
[16] È. L. Nagaev, *Physics of Magnetic Semiconductors* [in Russian], Nauka, Moscow (1979).
[17] S. E. Barnes and J. Zitkova-Wilcox, Phys. Rev. B **7**, 2163 (1973).
[18] D. Chowdhury and A. Mookerjee, Phys. Rep. **114**, 1 (1984).
[19] A. Asamitsu, Y. Moritomo, and Y. Tokura, Phys. Rev. B **53**, R2959 (1996).
[20] J. Liebe, E. Kraus, L. Haupt *et al.*, Appl. Phys. Lett. **68**, 2343 (1996).
[21] M. F. Hundley and J. J. Neumeier, Phys. Rev. B **55**, 11511 (1997).

Translated by R. S. Wadhwa

# Heat capacity of reentrant ferrimagnets $Li_{0.5}Fe_{2.5-x}Ga_xO_4$ with $x=0.9$ and 1.2

N. N. Efimova and S. R. Kufterina

*Kharkov State University, 310077, Kharkov, Ukraine*

A. G. Anders, S. V. Startsev, A. M. Gurevich, and V. N. Eropkin

*B. Verkin Institute for Low Temperature Physics and Engineering, National Academy of Sciences of the Ukraine, 310164 Kharkov, Ukraine**

(Submitted August 14, 1997; revised November 11, 1997)
Fiz. Nizk. Temp. **24**, 337–339 (April 1998)

The specific heat $C_m$ of the magnetic subsystem of reentrant ferrimagnets $Li_{0.5}Fe_{2.5-x}Ga_xO_4$ with $x=0.9$ and 1.2 is investigated in the temperature range 1.9–22 K. It is found that, in the low-temperature region of this interval, $C_m$ is a linear function of temperature, while the dependence $C_m \sim T^{3/2}$ is observed for $T>11$ K. Possible mechanisms responsible for such a behavior are discussed. © *1998 American Institute of Physics.* [S1063-777X(98)00804-4]

Linear temperature dependence of the magnetic contribution to the specific heat $C_m(T) \propto T$ is considered as one of the canonical properties of spin glasses (SG).[1,2] Such a dependence has been observed experimentally, with rare exceptions,[3,4] for quite diverse types of SG with long- as well as short-range exchange interaction.[2] For $T<T_f$ (where $T_f$ is the freezing temperature), $C_m \sim T$ not only in SG, but also in reentrant magnets in which a decrease in temperature leads to two succesive phase transitions, one at the Curie temperature $T_C$, and the second at the freezing temperature $T_f<T_C$.[2,5]

In a previous publication,[6] we reported that the $C_m(T)$ dependence in reentrant ferrimagnets $Li_{0.5}Fe_{2.5-x}Ga_xO_4$ with $x=0.9$ and 1.0 follows Bloch's $T^{3/2}$ law at temperatures $T<T_f$. Although theoretical model of formation of reentrant states allows such a dependence in dilute spinels with one type of magnetically active ions,[7] an additional verification had to be made experimentally in view of the following circumstance. Since the $C_m(T)$ dependence is determined by excitations in the magnetic subsystem, their character is directly linked with the general problem of origin of SG type disordered states, including the possibility of identifying SG states of different types with magnetic phases of a substance.[8,9] This is not a trivial problem for Heisenberg reentrant magnets with a short range, as evidenced by the discussion that has been prevailing in the literature for a long time.[4,10,11] From the experimental point of view, the need for supplementary investigations was dictated by the fact that the small number of reliable experimental points obtained in Refs. 5 and 6 allowed us to study the behavior of the heat capacity in low-temperature region $T \leqslant 10$ K (i.e., for $T \leqslant T_f$) only through extrapolation.

In this work, we present the results of experimental studies of the dependences $C(T)$ (Fig. 1) and $C_m(T)$ (Fig. 2) in the temperature range 1.9–22 K for samples of dilute spinels $Li_{0.5}Fe_{2.5-x}Ga_xO_4$ with $x=0.9$ and 1.2 as well as lithium gallate $Li_{0.5}Ga_{2.5}O_4$ (Fig. 1, curve *3*). Measurements were made by using the technique described in Ref. 12. Since the objects of investigation are insulators, we measured the heat capacity $C(T)=C_{ph}+C_m(T)$. According to the detailed discussions in Ref. 5, the phonon contribution $C_{ph}(T)$ can be treated as the heat capacity of nonmagnetic lithium gallate.

It can be seen from Fig. 1 that the lattice contribution $C_{ph}(T)$ to the total heat capacity is quite small in the investigated temperature range, especially at $T<10$ K. Hence the total heat capacity $C(T)$, which is a linear function of temperature for $T \leqslant 11$ K, can be identified with the magnetic contribution $C_m(T)$. As the temperature is increased beyond 11 K, the $C(T)$ dependence varies significantly, the increase in the heat capacity is obviously not related with the increase in $C_{ph}(T)$.

The temperature dependences of the magnetic contributions to the heat capacity of samples with $x=0.9$ and 1.2 are presented in Fig. 2 in $C_m(T)$ vs. $T^{3/2}$ coordinates. It can be seen clearly that the linear dependence $C_m(T)$ observed in the low-temperature region is replaced by the spin-wave dependence $C_m(T) \sim T^{3/2}$ in a narrow temperature interval. Slight departures from the $T^{3/2}$ dependence for samples with $x=1.2$ in the temperature region $\sim 18$ K are associated with the formation of peaks whose origin was discussed earlier by us.[6] It should be noted by the way that the values of $C_m(T)$ obtained in this work coincide with those obtained in Ref. 6 for the temperature range $T>11$ K, where the $T^{3/2}$ dependence is observed.

The obtained results, viz., the classical dependence $C_m(T) \propto T$ for SG systems at $T<T_f$ ($T_f \sim 10$ K) are significant since we are dealing with systems with short-range interactions in which the concentration of nonmagnetic ions corresponds to the initial concentration region of formation of the reentrant states where a large spontaneous magnetization still persists. This region of $x$ vs. $T$ phase diagrams has not been studied adequately for disordered systems.

The linear dependence $C_m(T) \sim T$ is in accord with the traditional concepts concerning the behavior of heat capacity in systems with SG type disorder and may be associated with peculiarities of the spectrum of elementary excitations. It was mentioned in Ref. 13 that, under conditions of conservation of spontaneous magnetic moment, an additional sys-

 

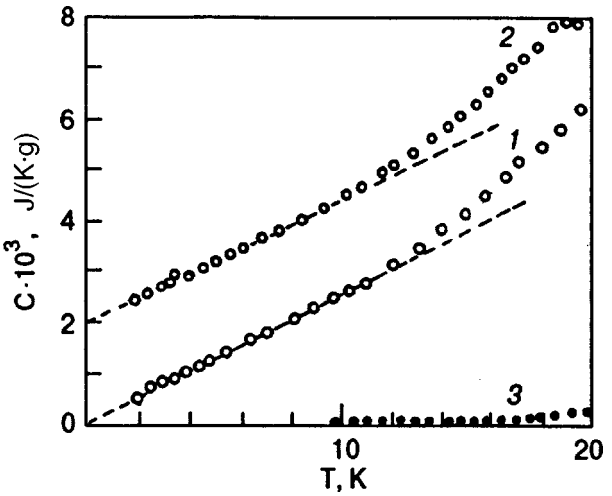


FIG. 1. Temperature dependence of the specific heat of spinels $Li_{0.5}Fe_{1.6}Ga_{0.9}O_4$ (*1*) and $Li_{0.5}Fe_{1.3}Ga_{1.2}O_4$ (*2*), as well as lithium gallate $Li_{0.5}Ga_{2.5}O_4$ (*3*). The origin for curve *2* is displaced by $2\cdot10^3 J\cdot K^{-1}g^{-1}$.

tem of low-lying two-level energy states is formed in the excitation spectrum even for a small concentration of competing exchange bonds (antiferromagnetic bonds in a ferromagnetic matrix). Such a structure of the excitation spectrum determines all low-temperature properties of the magnetic subsystem, including the linear temperature dependence of heat capacity. Thus, on one hand, the results obtained in this work confirm according to phenomenological indications that low-temperature disordered states in these objects belong to SG type states, and on the other hand point towards changes in the elementary magnetic excitation spectrum caused by the presence of competing exchange bonds and frustrations in accordance with the results obtained in Ref. 13.

The results of our investigations also lead to an interesting and, to our knowledge, hitherto unknown fact. It can be seen from Figs. 1 and 2 that the nature of the dependence $C_m(T)$ changes in a comparatively narrow temperature interval around $T\sim11$ K, i.e., the spin-glass region $C_m\propto T$ observed at low temperatures is replaced by the spin-wave region at higher temperatures. In principle, this may happen during a normal thermodynamic phase transition. In such a case, the $x$ vs. $T$ phase diagram of Li–Ga spinels[14] must contain another region of magnetic states. In order to find the nature of the reentrant states and the mechanisms of their formation, the existence of a thermodynamic phase transition and its temperature are quite important factors and require further investigations, which are being carried out at present.

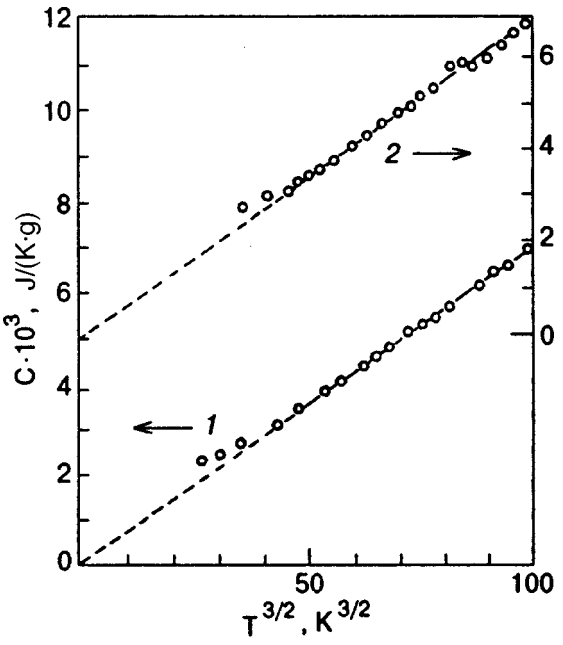


FIG. 2. Temperature dependence of the magnetic contribution to the heat capacity of samples $Li_{0.5}Fe_{1.6}Ga_{0.9}O_4$ (*1*) and $Li_{0.5}Fe_{1.3}Ga_{1.2}O_4$ (*2*).

*E-mail: aanders@ilt.kharkov.ua

[1] I. Ya. Korenblit and E. F. Shender, Usp. Fiz. Nauk **157**, 267 (1989) [ Sov. Phys. Usp. **32**, 139 (1989)].
[2] K. Binder and A. P. Young, Rev. Mod. Phys. **58**, 801 (1986).
[3] J. M. Coey, S. V. Molnar, and R. J. Gambino, Solid State Commun. **24**, 167 (1977).
[4] N. N. Efimova, Yu. A. Popkov, and S. R. Kufterina, Pis'ma Zh. Éksp. Teor. Fiz. **64**, 412 (1996) [JETP Lett. **64**, 450 (1996)].
[5] N. N. Efimova, V. A. Pervakov, V. I. Ovcharenko, and N. Yu. Tyutryumova, Fiz. Tverd. Tela (Leningrad) **35**, 2838 (1993) [Phys. Solid State **35**, 1405 (1993)].
[6] N. N. Efimova, Yu. A. Popkov, S. R. Kufterina *et al.*, Fiz. Nizk. Temp. **20**, 546 (1994) [Low Temp. Phys. **20**, 431 (1994)].
[7] J. Villain, Z. Phys. B **33**, 31 (1979).
[8] P. W. Anderson, *Magnetism of Amorphous Systems* [Russian translation], Metallurgiya, Moscow (1981).
[9] V. S. Dotsenko, Usp. Fiz. Nauk **163**, 1 (1993) [Phys. Usp. **36**, 455 (1993)].
[10] W. M. Saslow and G. Parker, Phys. Rev. Lett. **56**, 1074 (1985).
[11] J. R. Thomson, Hong Guo, and D. H. Ryan, Phys. Rev. B **45**, 3129 (1991).
[12] E. A. Anders, B. Ya. Sukharevskii, and I. A. Volchok, *Thermophysical Properties of Substances and Materials* [in Russian], Iz-vo Standartov, Moscow (1976).
[13] M. V. Feigel'man and A. M. Tsvelik, Zh. Éksp. Teor. Fiz. **76**, 2249 (1979) [Sov. Phys. JETP **49**, 1136 (1979)].
[14] N. N. Efimova, Yu. A. Popkov, and N. V. Tkachenko, Fiz. Nizk. Temp. **16**, 1565 (1990) [Sov. J. Low Temp. Phys. **16**, 881 (1990)].

Translated by R. S. Wadhwa

# Magnetic structure of ferro–antiferromagnet interface. 1. Layered antiferromagnet

A. G. Grechnev

*Kharkov State University, 310077, Kharkov, Ukraine**

A. S. Kovalev

*B. Verkin Institute for Low Temperature Physics and Engineering, National Academy of Sciences of the Ukraine, 310164 Kharkov, Ukraine***

(Submitted October 21, 1997)
Fiz. Nizk. Temp. **24**, 340–344 (April 1998)

The ferro-antiferromagnetic interface is studied by using the classical discrete model. Collinear and noncollinear magnetic configurations of the interface are considered and critical values of parameters are obtained for which a collinear–noncollinear transition takes place.
 [S1063-777X(98)00904-9]

The problem of coexistence of ferromagnetic (FM) and antiferromagnetic (AFM) phases arose while studying the alloys Co/CoO containing AFM grains embedded in an FM matrix. The problem of AFM/FM interface has been studied theoretically by Vlasov and Mitsek.[1] In recent years, multilayered magnetic systems, including systems with alternating FM and AFM layers (Fe/Cr, Co/CoO, etc.), have been studied extensively because of the investigation and practical applications of the giant magnetoresistance phenomenon. Although these materials are characterized by itinerant magnetism, the theoretical description of the interface (IF) is based, as a rule, on simple classical models of magnets in the exchange approximation.[2–4] Cheng and Sy[2] studied spin waves (SW) in multilayer systems containing layers of two different FM, while Stamps and Camley[3] studied SW in AFM films on an FM substrate. Finally, Stamps *et al.*[4] studied FM resonance in two-layered FM/FM and FM/AFM systems, including the system Co/CoO. All these authors considered layers of finite thickness (several interatomic spacings), and the IF structure and SW frequencies were determined to a considerable extent by this thickness.

The aim of our investigations was to study theoretically the magnetic structure of the IF of semi-infinite FM and AFM, as well as the dynamics of surface SW localized in the vicinity of the IF. It was found that the static and dynamic properties of such interfaces depend considerably on the magnetic ordering of the AFM phase and are different for layered AFM (Fig. 1a) and AFM with a normal antiferromagnetic ordering (Fig. 1b). In the present work, we study the possible static configurations of IF between an FM and a layered AFM in the classical model proposed by Stamps *et al.* [4] (in the static case, the obtained results are also valid for IF between two FM).

While studying the static structure of IF and the waves propagating along it, we can treat the problem as one-dimensional, i.e., study the contact between semi-infinite FM and AFM chains. We shall consider the simplest model of uniaxial magnets with an ''easy axis'' type anisotropy in the exchange approximation without taking into account the external magnetic field and magnetic dipole interaction (which is usually quite important for studying surface effects). In this case, the Hamiltonian of the system has the form

$$H=\sum_n \left( -J_{n,n+1}\mathbf{S}_n\mathbf{S}_{n+1}-\frac{1}{2}B_nS_{nz}^2\right), \tag{1}$$

where $\mathbf{S}_n$ is the spin localized at a lattice site, the exchange interaction constant $J_{n,n+1}=J_f$ for $n\geqslant 0$; $J_{n,n+1}=-J_a$ for $n\leqslant -2$; and $J_{-1,0}=J_{fa}$ at the IF ($J_f, J_a>0$); the uniaxial anisotropy constant $B_n=B_f$ for $n\geqslant 0$ and $B_n=B_a$ for $n<0$ ($B_n>0$).

In the case of ferromagnetic interaction through the FM–AFM boundary ($J_{fa}>0$), the ground state with minimum energy corresponds to a configuration with the collinear (anticollinear) spin ordering shown in Fig. 1a. However, more complex static configurations with collinear (anticollinear) spin ordering are also possible. All of them actually describe FM or AFM domain walls (DW) which are parallel to the FM/AFM IF and are situated at various distances from it (the possibility of existence of various states is associated with the discrete nature of the lattice and the existence of Peierls relief for DW). All the above-mentioned states are topologically equivalent to each other and topologically different from the ground state in Fig. 1a.

The DW problem in an infinite FM (or AFM) chain with an easy axis anisotropy was considered in Refs. 5 and 6 where it was shown that the DW ''collapse'' for small exchange interaction: for $J=(3/4)B$, the normal DW with a smooth rotation of the magnetization vector bifurcates into a strictly collinear 180°-DW containing an ''intrinsic mode'' for $J<(3/4)B$ with frequencies $\omega$ in the spectral gap of linear spin waves. We observed an analogous physical situation, albeit with complications caused by interaction of DW and IF: the existence of collinear DW is also possible for small values of exchange interaction. Figure 2a shows configurations with collinear DW lying on the IF ($A$) between layers with numbers $n$ and $n+1$ in the FM half-space ($B_n$) and in the AFM half-space ($C_n$). Figure 2b shows a typical noncollinear configuration (DW in FM half-space) obtained numerically.

 

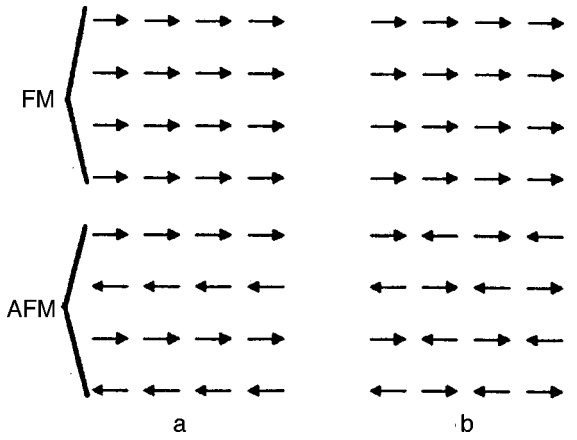


FIG. 1. Interface between FM and AFM in the case of a layered AFM (a) and for its ''staggered'' ordering (b).

In contrast to a homogeneous chain characterized by just one parameter $B/J$, the system considered by us is described by four parameters:

$$\beta_f=\frac{B_f}{J_f},\quad \beta_a=\frac{B_a}{J_a},\quad \rho=\left(\frac{J_a}{J_f}\right)^{1/2}\frac{S_a}{S_f},\quad j=\frac{J_{fa}}{(J_aJ_f)^{1/2}} \tag{2}$$

(the difference between the specific spins $S_a$ and $S_f$ may be taken into consideration through renormalization of the corresponding exchange integrals). The quantity $\rho$ describes the difference between various magnets, while the parameter $j$ characterizes the IF as a magnetic defect.

In order to define the transformation of collinear structures into noncollinear ones, we must find the relation between the critical values of parameters $\beta,\rho$, and $j$ which is a surface in the space of these parameters. The cross-sections

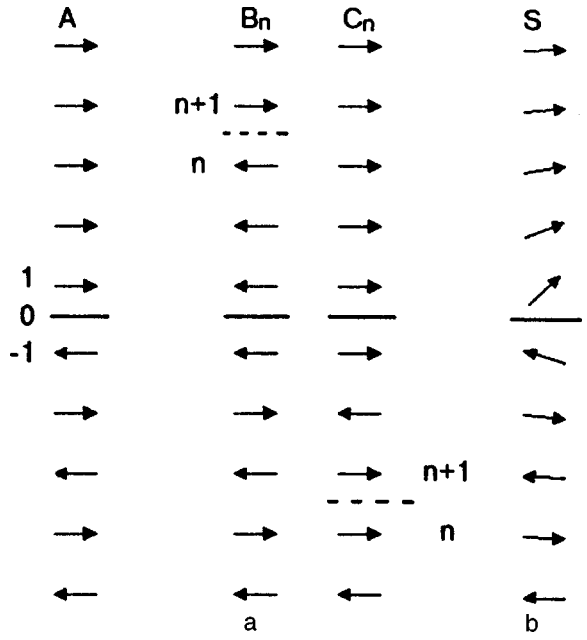


FIG. 2. Collinear configurations of DW in the presence of an interface (a) and a noncollinear FM/AFM DW in the ferromagnetic half-space near this interface (b).

of this surface, describing the dependences $\beta=\beta(j)$ and $\rho=\rho(j)$, appear to be most typical and informative.

The study of magnetization distribution in noncollinear structures involves computer calculations (see Fig. 2b), while collinear structures and their transition to noncollinear structures can be studied analytically without any difficulty. The energies $B_n$ and $C_n$ of collinear structures do not depend on the number $n$, and in terms of notation (2), the energies of all inhomogeneous states, which are measured from the ground state energy, have the form

$$E_A=2E_0j,\quad E_B=2E_0/\rho,\quad E_C=2E_0\rho, \tag{3}$$

where the characteristic energy $E_0=(J_aJ_f)^{1/2}S_aS_f$ has been introduced. Thus, the parameters $j$ and $\rho$ characterize the DW lying on the IF between media or in the magnetic half-space (FM or AFM).

Bifurcation values of parameters for which a collinear structure (CS) is transformed into a noncollinear structure (NCS) are determined in the standard way (see, for example, Ref. 5). It is well known that a transition in a such system is accompanied by spontaneous symmetry breaking, when one of its eigenfrequencies vanishes. If we use equations of magnetization dynamics (discrete Landau–Lifshitz equations) in polar coordinates associated with the anisotropy axis,[7] i.e.,

$$\sin\,\theta_n\frac{d\varphi_n}{dt}=-\frac{1}{\hbar S_n}\frac{\partial H}{\partial\theta_n}, \tag{4}$$

where $S_n(\sin\theta_n\cos\varphi_n,\sin\theta_n\sin\varphi_n,\cos\theta_n)=\mathbf{S}_n$, the quantity $\omega=d\varphi_n/dt$ in CS defines the frequency of precession, which vanishes at the CS–NCS transition point.

The dependence $\omega(\beta)$ for the frequency of an intrinsic mode of the collinear structure of the DW in a homogeneous chain is determined analytically in Ref. 5, and $\omega=0$ at the point of transition to a NCS ($\beta=B/J=4/3$). In NCS, the dependence $\omega(\beta)$ can be found numerically.

In our case, the CS–NCS boundaries (with $\omega=0$) are also defined by the condition of existence of nontrivial solutions of the linearized static equations

$$\left.\frac{\partial H}{\partial\theta_n}\right|_{\theta_n\to 0}\to 0. \tag{5}$$

In the bulk of each magnet, these equations are reduced to the following relations:

$$\theta_n(2+\beta_{f,a})-\theta_{n+1}-\theta_{n-1}=0, \tag{6}$$

while for boundary spin layers we have

$$\theta_0(1+\beta_f-\rho j)-\theta_1-\rho j\theta_{-1}=0, \tag{7}$$

$$\theta_{-1}(1+\beta_a-j/\rho)-\theta_{-2}-j/\rho\theta_0=0.$$

The general solution of the difference equations (6) has the form

$$\theta_n=aP^n+bP^{-n}, \tag{8}$$

where

$$P_{f,a}=P(\beta_{f,a})=1+\frac{\beta_{f,a}}{2}-\sqrt{\beta_{f,a}+\beta_{f,a}^2/4}. \tag{9}$$

For structures of the type $A,B_0 \equiv B$ and $C_{-2} \equiv C$ in which the DW center lies on the IF between the media ($A$) or is separated from it by an atomic layer in the FM ($B$) or AFM half-space ($C$), we must put $a=0$ for FM ($n \geqslant 0$) and $b=0$ for AFM ($n \leqslant 1$). After the substitution of solution (8) into the boundary conditions (7), the equality of the determinant of the obtained system of linear homogeneous equations for $a$ and $b$ to zero gives a relation between the parameters $j,\rho,\beta_a$, and $\beta_f$ for which a transition from collinear structures $A,B$, and $C$ to the corresponding noncollinear structures takes place:

$$\frac{1}{j}=\frac{\rho}{F_f}+\frac{1}{\rho F_a}, \qquad (A) \qquad (10)$$

$$\frac{1}{j}=-\frac{1}{\rho F_a}=\rho\frac{\beta_f-P_f}{1+(\beta_f-1)(\beta_f-P_f)}, \qquad (B) \qquad (11)$$

$$\frac{1}{j}=-\frac{\rho}{F_f}+\frac{1}{\rho}\frac{\beta_a-P_a}{1+(\beta_a-1)(\beta_a-P_a)}, \qquad (C) \qquad (12)$$

where

$$F_{f,a}=1+\beta_{f,a}-P_{f,a}=\frac{\beta_{f,a}}{2}+\sqrt{\beta_{f,a}+\beta_{f,a}^2/4}. \qquad (13)$$

For configurations $B_n$ with $n \geqslant 1$ and $C_n$ with $n \leqslant -3$, we must retain both terms in solution (8) for spin layers lying between the IF of the magnets and the center of the collinear DW. In this case, the relation between critical values of parameters becomes more complicated:

$$\left[\frac{1}{\rho F_a}+\frac{1}{j}\right][F_f(2-F_f)+P_f^{2n+1}2\beta_f]+\frac{\rho}{F_f}[F_f(2-F_f) -P_f^{2n}2\beta]=0, \quad (B_n) \qquad (14)$$

$$\left[\frac{\rho}{F_f}+\frac{1}{j}\right][F_a(2-F_a)+P_a^{-2(N+2)+1}2\beta_a]+\frac{1}{\rho F_a} \times[F_a(2-F_a)-P_a^{-2(n+2)}2\beta_a]=0. \quad (C_n) \qquad (15)$$

In order to analyze dependences (10)–(15) for critical values of the parameters, it is convenient to fix a pair of these values and study the relations between the remaining two parameters. First of all, let us analyze the dependence $\beta(j)$. It was mentioned above that the parameter $j$ characterizes the IF between two media as a magnetic defect, and hence the dependence $\beta(j)$ describes the effect of this interface on the DW structure. For the sake of simplicity, we put $\beta_a=\beta_f$ and $\rho=1$, i.e., we shall assume that the two half-spaces are identical. The dependence $\beta(j)$ for transitions from a collinear to a noncollinear structure in this case is presented in Fig. 3. If the separation between the DW and the IF is large (structure of the $B_n$ type with a large number $n$), the effect of the interface is insignificant, and we arrive at the result $\beta \approx 4/3$ obtained in Refs. 5 and 6. The dependence $\beta(j)$ remains weak for the structures $B_n$ with numbers $n \geqslant 1$ (see curve $B1$ in Fig. 3). However, the effect of the interface on the rearrangement of DW is significant for structures $A,B$, and $C$ in which the DW lies near the FM/AFM interface (the boundaries of transition to the noncollinear

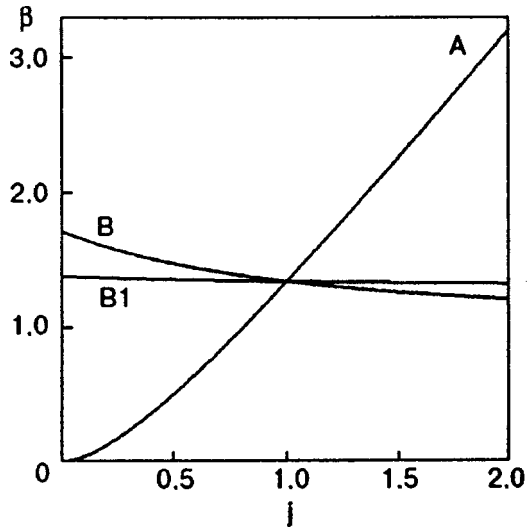


FIG. 3. Dependence $\beta(j)$ for critical values of parameters upon a transition of a collinear DW into a canted DW for $\beta_a=\beta_f$ and $\rho=1$ ($J_a=J_f$).

structure for a DW of the type $A$ and $B$ are shown in Fig. 3 by the curves $A$ and $B$). All the curves in Fig. 3 pass through the point $j=1,\beta=4/3$ since with our choice of the parameters ($\beta_f=\beta_a$ and $\rho=1$) the value of $j=1$ corresponds to a homogeneous (in the static case) chain for which a transition to a noncollinear DW occurs for the anisotropy value $\beta=4/3$. Moreover, according to formulas (3), the sign of the difference in the energies of $A$- and $B_n$-structures changes at the point $j=1$ (for $\rho=1$). For $j<1$, the energy of the $A$-structure is lower than that of $B_n$-type structures, i.e., the interface in the given case ''attracts'' a collinear DW (although the energies of $B_n$-structures do not depend on the number $n$, i.e., on the separation between DW and IF). In the opposite case $j>1$, the IF ''repels'' domain walls, and their

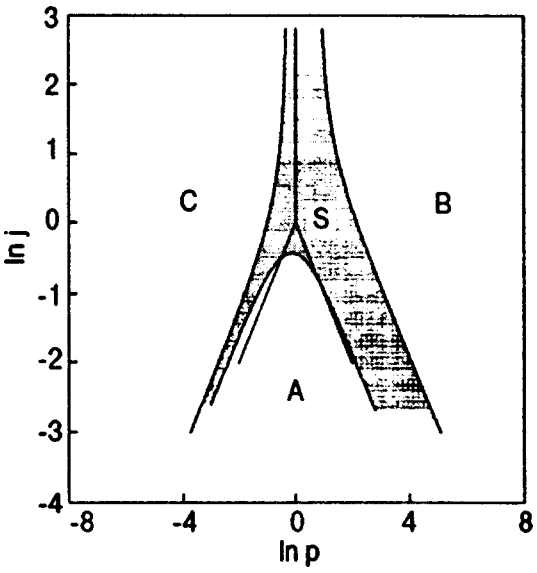


FIG. 4. Diagram $j(\rho)$ of a bifurcation transition of collinear structures $A,B$, and $C$ to noncollinear structures (hatched region) for the values of the parameters $\beta_f=0.6$ and $\beta_a=0.9$.

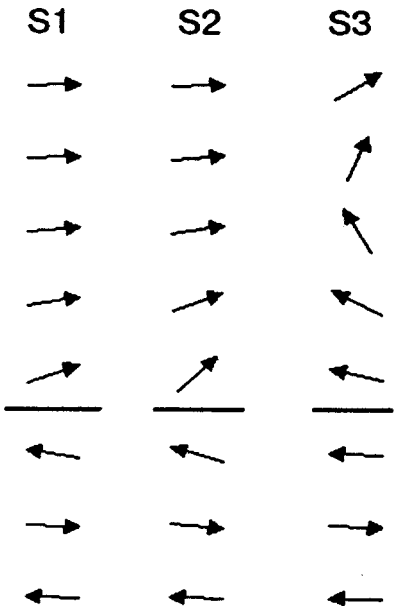


FIG. 5. Noncollinear configurations of DW for $\beta_f=0.6, \beta_a=0.9$, and $\rho=1.2$ and various values of $j$: 0.64 ($S1$), 0.655 ($S2$), and 0.66 ($S3$).

location at a finite distance from the interface is stable only relatively and is associated with the presence of the Peierls relief.

In order to describe the effect of the difference in magnetic properties of two magnetic subspaces on the type of a DW transition from a CS to a NCS, it is convenient to fix the values of $\beta_f$ and $\beta_a$ (associated with ''magnetic lengths'' $l_{f,a}=1/\sqrt{\beta_{f,a}}$ in FM and AFM) and to construct the critical dependences $j(\rho)$. The parameter $\rho$ characterizes the difference in magnetic properties of contacting media. In Fig. 4, the critical dependences $j(\rho)$ for CS/NCS transitions are presented on the logarithmic scale for the values $\beta_f=0.6$ and $\beta_a=0.9$. For such anisotropy constants, the collinear structures $B_n$ with $n\geqslant 1$ and $C_n$ with $n\leqslant -3$ are unstable, and hence Fig. 4 shows the boundaries of the stability region for collinear DW only for $A$-, $B$-, and $C$-structures. The regions $A$,$B$, and $C$ correspond to stable collinear domain walls, while the hatched region $S$ corresponds to noncollinear DW. In region $S$, there exist several types of canted DW with various distances from the IF, which can be determined by using numerical methods. Figure 5 shows the evolution of a collinear DW in the region $S$ upon an increase in $j$ above the critical value for a fixed parameter $\rho=1.2$. It can be seen that the noncollinear DW moves from its position on the IF between media ($S1$) over several atomic spacings from it ($S3$) even upon an insignificant increase in the parameter $j$ above its critical value.

Solid curves in Fig. 4 indicate the values of parameters for which the energies of collinear structures $A$, $B$, and $C$ become identical. It follows from expressions (3) and definitions (2) that this occurs for the energies of FM and AFM collinear DW on the curve with $j>1$, $\rho=1$, the energies of collinear DW in the FM subspace and on the IF become equal on the curve with $j<1$, $j=1/\rho$, while in the case of an AFM domain wall this takes place on the straight line $j<1, j=\rho$. The boundaries of transition to noncollinear DW in Fig. 4 in the limit of large and small values of $\rho$ and $j$ are parallel to these straight lines. For example, expression (10) for $\rho\to\infty$ has the asymptotic form $j\approx\rho F_a$. In the initial physical variables, this asymptotic form corresponds to the following relation between the parameters: $J_{fa}\approx J_a(S_a/S_f)F_a$ for $J_f\to\infty$, i.e., the bifurcation of a collinear DW at the FM/AFM interface in the case of the contact between an antiferromagnet and a ''rigidly frozen'' ferromagnet. The asymptotic forms of bifurcation dependences $\rho\to$const, $j\to\infty$ correspond to an infinitely strong exchange interaction at the FM/AFM interface.

Pay attention to the fact that for a certain choice of the parameters of magnetic media (as in the case presented in Fig. 4), a situation is possible when a collinear DW on the IF ($A$-structure) is relatively stable and is not transformed to a canted structure even in the regions where its energy is higher than the energies of collinear $C$- and $B$-structures (the CS/NCS transition curve intersects the straight lines $j=\rho$ and $j=1/\rho$ in Fig. 4).

*E-mail: grechnev@ilt.kharkov.ua
**E-mail: kovalev@ilt.kharkov.ua

[1] K. B. Vlasov and A. I. Mitsek, Fiz. Met. Metalloved. **14**, 487 (1962).
[2] F. Cheng and H. K. Sy, J. Phys.: Condens. Matter **7**, 6591 (1995).
[3] R. L. Stamps and R. E. Camley, Phys. Rev. B **54**, 15200 (1996).
[4] R. L. Stamps, R. E. Camley, and R. J. Hicken, Phys. Rev. B **54**, 4159 (1996).
[5] A. N. Goncharuk, A. A. Stepanov, and D. A. Yablonskii, Fiz. Tverd. Tela (Leningrad) **31**, 132 (1989).
[6] B. Rumpf, Phys. Lett. A **221**, 197 (1996).
[7] A. M. Kosevich, B. A. Ivanov, and A. S. Kovalev, *Nonlinear Magnetization Waves. Dynamic and Topological Solitons* [in Russian], Naukova Dumka, Kiev (1983).

Translated by R. S. Wadhwa

# Spectra of coupled magnetoelastic waves and peculiarities of phase transitions in easy-plane ferromagnets under mechanical boundary conditions

Yu. N. Mitsai, Yu. A. Fridman, O. V. Kozhemyako, and B. L. Eingorn

*M. Frunze State University, 333036 Simferopol, Ukraine*[*]

(Submitted February 26, 1997; revised October 22, 1997)
Fiz. Nizk. Temp. **24**, 345–352 (April 1998)

Possible types of phase transitions as well as the spectra of coupled magnetoelastic waves are studied in an easy-plane ferromagnet with a rigidly fixed face. It is shown that the presence of such mechanical boundary conditions leads to a change in the type of phase transition. The dynamic properties of the system become most interesting at the point of absolute instability of the system rather than at the phase transition point. © *1998 American Institute of Physics.* [S1063-777X(98)01004-4]

## INTRODUCTION

Experimental studies of magnetoelastic (ME) properties involve various methods of fixing the sample in the experimental setup, which impose certain mechanical boundary conditions. The latter determine the structure of spontaneous deformations in a magnetically ordered crystal.

The magnitude and structure of spontaneous deformations affect thermodynamic as well as kinetic characteristics of a magnet.

The importance of the analysis of mechanical boundary conditions has been noted by a number of authors (see, for example, Refs. 1 and 2), but this question has not been studied extensively so far.

In this paper, we analyze the effect of mechanical boundary conditions in the case when this effect is manifested most clearly.[3,4] We study the spectra of ME waves in the vicinity of a spin-reorientation phase transition in an easy-plane ferromagnet in a magnetic field perpendicular to the easy plane.

## FREE ENERGY OF AN EASY-PLANE FERROMAGNET UNDER MECHANICAL BOUNDARY CONDITIONS

Let us consider the simplest situation in which the effects under investigation are manifested most clearly, i.e., the low-temperature region ($T \ll T_C$, where $T_C$ is the Curie temperature). Without loss of generality we assume for simplicity that the spin $S$ of a magnetic ion is equal to unity.

As a model system, we consider an easy-plane ferromagnet ($X0Y$ is the basal plane) in a uniform magnetic field $H$ parallel to the axis $0Z$.

The Hamiltonian of such a system in the rotation-invariant theory of ME interaction[3] can be written in the form

$$\mathscr{H} = -H\sum_n S_n^z + \frac{\beta}{2}\sum_n (R_{zi}^{-1}S_n^i)^2 - \frac{1}{2}\sum_{n,n'} I(n-n')\mathbf{S}_n\mathbf{S}_{n'} + \nu\sum_n (R_{if}^{-1}S_n^f)(R_{jg}^{-1}S_n^g)\varepsilon_{ij}(n) + \int dr\left\{\frac{\lambda+\eta}{2}(\varepsilon_{xx}^2+\varepsilon_{yy}^2+\varepsilon_{zz}^2) + 2\eta(\varepsilon_{xy}^2+\varepsilon_{xz}^2+\varepsilon_{yz}^2) + \lambda(\varepsilon_{xx}\varepsilon_{yy}+\varepsilon_{xx}\varepsilon_{zz}+\varepsilon_{yy}\varepsilon_{zz})\right\}. \quad (1)$$

In this equation, the following notation is used: $I(n-n')$ is the exchange integral, $\beta>0$ the anisotropy constant, $\nu$ the ME coupling constant, $S_n^i$ the spin operator at the $n$th site, $\lambda$ and $\eta$ are the elastic moduli of the crystal, $\hat{R}$ is the operator of local rotations, which can be represented in the form $R_{ij} = (\partial x_i/\partial\xi_k)(I+\varepsilon)_{kj}^{-1/2}$, where $\hat{I}$ is the unit operator, $\varepsilon_{ij} = u_{ij} + (1/2)(u_{ik}-\omega_{ik})(u_{ki}+\omega_{kj})$ and the finite strain tensor, and $u_{ij} = (1/2)(\partial u_i/\partial x_j + \partial u_j/\partial x_i)$ and $\omega_{ij} = (1/2)(\partial u_i/\partial x_j - \partial u_j/\partial x_i)$ are the symmetric and antisymmetric components of the distortion tensor $\partial u_i/\partial x_j$, respectively. The first three terms in (1) describe the magnetic subsystem, the fourth term the magnetoelastic coupling, and the fifth term the elastic coupling. Further, we assume that the sample under investigation is fixed rigidly in the $Z0X$ plane (see Fig. 1), which corresponds to the following mechanical boundary conditions:

$$\varepsilon_{xx} = \varepsilon_{zz} = \varepsilon_{xz} = \varepsilon_{yx} = 0;$$
$$\varepsilon_{yz} = u_{yz} = -\omega_{yz}; \quad (2)$$
$$\varepsilon_{yy} = u_{yy} + \frac{1}{2}u_{yy}^2 + 2u_{yz}^2.$$

Subsequent calculations will be carried out in the formalism of Hubbard operators.[5,6] In terms of Hubbard operators, we can exactly take into account the energy of one-ion anisotropy and the energy of ME coupling.

Hubbard operators are constructed on the basis of wave functions, which are the solution of the one-ion problem:

$$\mathscr{H}_0(n)\psi_n(M) = E_M\psi_n(M) \quad (3)$$

and have the form $X_n^{MM'} = |\psi_n(M')\rangle\langle\psi_n(M)|$. These operators describe the transition of a magnetic ion from the state $M$ to the state $M'$ ($M = -1,0,1$).

The one-ion Hamiltonian $\mathscr{H}_0(n)$ has the form

 

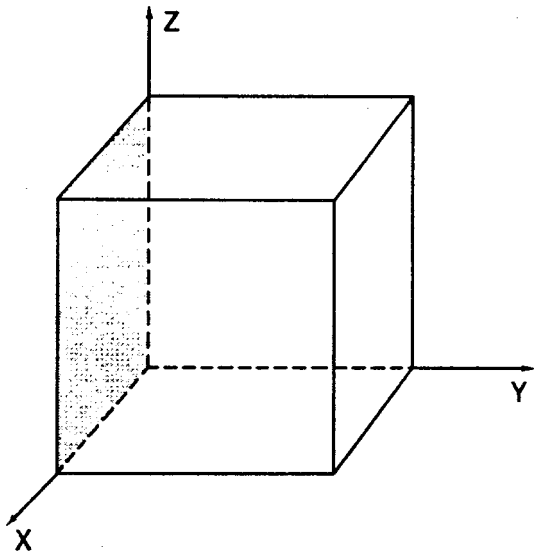


FIG. 1. Fixation of the sample.

$$\mathscr{H}_0(n)=-(H\cos\theta+I_0\langle S\rangle)S_n^z-\frac{i}{2}H(S_n^+-S_n^-)\sin\theta+\frac{\beta}{2}(S_n^z)^2\cos^2\theta-\frac{\beta}{8}\{(S_n^+)^2+(S_n^-)^2-S_n^+S_n^--S_n^-S_n^+\}\sin^2\theta+i\frac{\beta}{8}\{S_n^+S_n^z+S_n^zS_n^+-S_n^zS_n^--S_n^-S_n^z\}\sin 2\theta,$$

where $I_0$ is the zeroth Fourier component of the exchange integral and $\theta$ the angle between the directions of magnetic field and magnetic moment.

This angle can differ from zero for two reasons (see Fig. 2). First, shear deformations decline the anisotropy axis from the direction existing in an undeformed crystal. Second, as the magnetic field decreases, the magnetic moment deviates from the direction of $H$ towards the easy plane. The emergence of a nonzero angle $\theta$ in the standard theory of spin-reorientation phase transitions is interpreted as a phase transition, and $\theta$ plays the role of the order parameter.

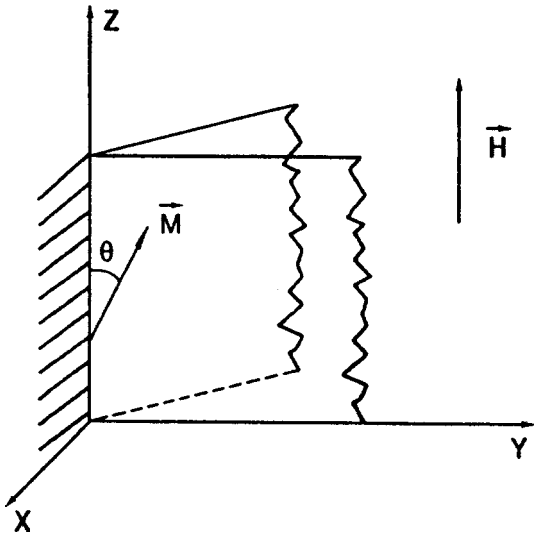


FIG. 2. Orientation of magnetic moment as a function of spontaneous deformations of the crystal and magnetic field.

Henceforth, we assume that $\theta\ll 1$, i.e., we are in the vicinity of the transition from the angular ($\theta\neq 0$) to the ferromagnetic (FM) ($\theta=0$) phase.

The solution of Eq. (3) leads to the following results. The energy levels of a magnetic ion can be determined to within $\theta^4$, but we shall give here the results accurate to $\theta^2$ since exact expressions are very cumbersome:

$$E_1=\frac{\beta}{2}-\bar{H}+\frac{I_0\langle S\rangle}{2}\frac{\beta/2-H}{\beta/2-\bar{H}}\theta^2,$$

$$E_0=\frac{\beta}{2}\frac{I_0^2\langle S\rangle^2}{\bar{H}^2-\beta^2/4}\theta^2; \tag{4}$$

$$E_{-1}=\frac{\beta}{2}+\bar{H}-\frac{I_0\langle S\rangle}{2}\frac{\beta/2+H}{\beta/2+\bar{H}}\theta^2,$$

where $\bar{H}=H+I_0\langle S\rangle$. We shall write a modified one-ion problem taking into account the contribution of spontaneous deformations to the one-ion Hamiltonian in the form

$$\tilde{\mathscr{H}}_0(n)\tilde{\psi}_n(M)=\tilde{E}_M\tilde{\psi}_n(M), \tag{5}$$

where $\tilde{\mathscr{H}}_0(n)=\mathscr{H}_0(n)+\mathscr{H}_{\rm me}(n)+\mathscr{H}_{\rm ame}(n)$, $\mathscr{H}_{\rm me}(n)$ the fourth term in Hamiltonian (1), and $\mathscr{H}_{\rm ame}(n)=(1/2)\beta(R_{zi}^{-1}S_n^i)^2-(1/2)\beta(S_n^z)^2$. The last term describes the deviation of the anisotropy axis from the direction existing in an undeformed crystal.

Finally, taking into account spontaneous deformations, we obtain following expressions for energy levels of a magnetic ion:

$$\tilde{E}_1=\frac{\beta}{2}-\bar{H}+\frac{1}{2}\left(\nu u_{yy}^{(0)}+\beta u_{yz}^{(0)^2}+\frac{\bar{H}\beta/2}{\beta/2-\bar{H}}u_{yz}^{(0)^2}\right)+\varepsilon_1^{(1)}+\varepsilon_2^{(1)}+\varepsilon_3^{(1)}+\varepsilon_4^{(1)};$$

$$\tilde{E}_0=\nu u_{yy}^{(0)}-\frac{\bar{H}^2\beta/2}{\beta^2/4-\bar{H}^2}u_{yz}^{(0)^2}+\varepsilon_1^{(0)}+\varepsilon_2^{(0)}+\varepsilon_3^{(0)}+\varepsilon_4^{(0)};$$

$$\tilde{E}_{-1}=\frac{\beta}{2}+\bar{H}+\frac{1}{2}\left(\nu u_{yy}^{(0)}+\beta u_{yz}^{(0)^2}+\frac{\bar{H}\beta/2}{\beta/2+\bar{H}}u_{yz}^{(0)^2}\right)+\varepsilon_1^{(-1)}+\varepsilon_2^{(-1)}+\varepsilon_3^{(-1)}+\varepsilon_4^{(-1)}, \tag{6}$$

where $u_{ij}^{(0)}$ are spontaneous deformation and $\varepsilon_i^{(M)}$ the corrections to energy levels in powers of the angle $\theta$.

The expressions for these quantities are very cumbersome, and hence we shall write only some of them by way of an example, where the energy levels defined by formulas (4) appear in them as additive terms:

$$\varepsilon_1^{(1)}=\theta\frac{I_0\langle S\rangle}{\bar{H}-\beta/2}u_{yz}^{(0)}\left\{\nu-\frac{\beta}{2}+\frac{\beta}{4}(u_{yz}^{(0)}+u_{yy}^{(0)})\right\}; \tag{7}$$

$$\varepsilon_2^{(1)}=\theta^2\left\{\frac{(H-\beta/2)I_0\langle S\rangle-H\beta/2}{2H-\beta}-\frac{\beta}{4}u_{yz}^{(0)^2}\right\}.$$

Since we are studying the low-temperature limit, we confine our analysis only to the inclusion of the lowermost energy level. It can be seen from expressions (6) that the lowermost level in the given case is $\tilde{E}_1$. The subsequent calculations will be made in the approximation $I_0\langle S\rangle$, $\eta\gg\beta,\nu,H$.

Spontaneous deformations and the angle of deviation of magnetization from the direction of the magnetic field can be determined from the condition of minimum of the free energy density:

$$F=F_{\rm el}-T\ \ln\ Z, \tag{8}$$

where

$$F_{\rm el}=\frac{\lambda+\eta}{2}\ \varepsilon_{yy}^{(0)^2}+2\ \eta\varepsilon_{yz}^{(0)^2}$$

is the elastic energy density and

$$Z=\sum_M\ \exp(-\tilde{E}_M/T)$$

is the partition function. Since $\tilde{E}_1$ is the lowermost energy level, we have $Z\approx\exp(-\tilde{E}_1/T)$, and Eq. (8) assumes the form

$$F=\frac{\lambda+\eta}{2}\ \varepsilon_{yy}^{(0)^2}+2\ \eta\varepsilon_{yz}^{(0)^2}+\tilde{E}_1. \tag{9}$$

Substituting (6) into (9) and minimizing the latter expression in $u_{yy}^{(0)}$ and $u_{yz}^{(0)}$, we obtain a system of equations in spontaneous deformations. These equations have the following solutions:

$$u_{yy}^{(0)}=-\frac{\nu}{2\eta}-\theta^2\ \frac{\beta(\beta/2-\nu)}{16\eta^2}+\frac{\theta^3}{8}\ \frac{\beta^2(\beta/2-\nu)}{16\eta^3}$$
$$-\frac{\theta^4}{4}\ \frac{\beta^2(\beta/2-\nu)}{32\eta^3};$$
$$u_{yz}^{(0)}=\theta\ \frac{\beta/2-\nu}{4\eta}-\theta^2\ \frac{\beta(\beta/2-\nu)}{32\eta^2}+\theta^3\ \frac{\beta(\beta/2-\nu)}{32\eta^2}$$
$$-\frac{\theta^4}{4}\ \frac{\beta\nu^2(\beta/2-\nu)}{32\eta^4}. \tag{10}$$

Substituting the explicit form of spontaneous deformations into (9), we obtain the free energy density as a function of the order parameter:

$$F=-\frac{\nu^2}{8\eta}+\frac{c}{2}\ \theta^2+\frac{b}{3}\ \theta^3+\frac{a}{2}\ \theta^4, \tag{11}$$

where

$$c=H-\frac{\beta}{2}+\frac{\beta/2-\nu}{4\eta}\left\{\nu-\frac{\beta}{2}-\frac{\nu\beta}{4\eta}+\frac{\beta(\beta/2-\nu)}{8\eta}\right\},$$
$$b=\frac{3}{64}\ \frac{\beta(\beta/2-\nu)}{\eta^2}\left\{\frac{\beta}{2}-\nu+\frac{\nu\beta}{4\eta}-\frac{\beta(\beta/2-\nu)}{4\eta}\right\},$$

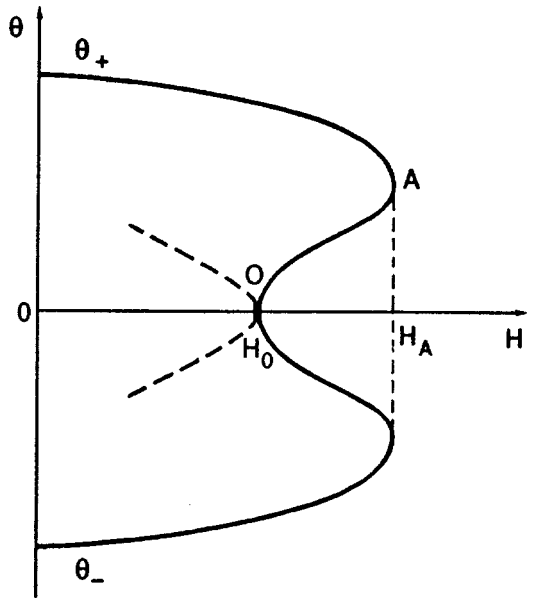


FIG. 3. Solutions of the equation of state. Dashed curve corresponds to the second-order phase transition for $b=0$.

$$a=\frac{\beta(\beta/2-\nu)}{16\eta^2}\left\{\nu-\frac{\beta}{2}-\frac{\nu\beta}{4\eta}+\frac{\beta(\beta/2-\nu)}{4\eta}\right\}$$
$$+\frac{\beta^2(\beta/2-\nu)}{128\eta^3}\left\{3\nu-\beta+\frac{\beta(\beta/2-\nu)}{8\eta}\right\}+\frac{\beta}{3}. \tag{12}$$

It can be seen from (11) that the free energy density differs from the standard form in the presence of the term proportional to $\theta^3$. This term is due to the inclusion of rotation invariance as well as the presence of nondiagonal spontaneous deformations which are due to the mechanical boundary conditions under investigation. A comparison of expression (11) with the corresponding expression for a completely free sample or a sample pressed from all sides[2] readily shows that they differ basically in the presence of this term. Izyumov and Syromyatnikov[10] proved that the presence of the cubic term in expansion (11) makes this transition a first order phase transition.

Minimizing (11) in the order parameter $\theta$, we obtain the equation of state of the system, i.e., $\theta(c+b\,\theta+a\,\theta^2)=0$, which has two nonzero solutions:

$$\theta_{\pm}=-\frac{b}{2a}\pm\left[\left(\frac{b}{2a}\right)^2-\frac{c}{a}\right]^{1/2}. \tag{13}$$

These solutions are real-valued in the case of a positive discriminant, i.e., for $c\leqslant b^2/4a$. Solutions (13) as functions of magnetic field are presented in Fig. 3. The multiple values of the order parameter $\theta$ in the field range between the points $O$ and $A$ correspond to instability of states on a segment of the type $OA$ on the $\theta(H)$ curve. For

$$c>c_A=b^2/4a \tag{14}$$

a nonzero value of the order parameter cannot exist, and hence the field $H_A$ (determined from (14)) specifies the boundary of absolute instability of the disordered phase. On

the other hand, the field $H_0$ (determined from the condition $c=0$) corresponds to the absolute instability boundary of the ordered phase.

It can easily be seen that the fields $H_A$ and $H_0$ are connected through the simple relation

$$H_A-H_0=b^2/4a; \quad \theta_A=-b/2a. \tag{15}$$

where

$$H_0=\frac{\beta}{2}-\frac{\beta/2-\nu}{4\eta}\left\{\nu-\frac{\beta}{2}-\frac{\nu\beta}{4\eta}+\frac{\beta(\beta/2-\nu)}{8\eta}\right\},$$

and the quantities $a$ and $b$ are defined in (12).

It should be noted that $H_0$ corresponds to the field of a second-order phase transition in the absence of the cubic term in expansion (11).

On the other hand, the phase transition occurs for $H_0<H_C<H_A$. The value of this field and the corresponding value of the order parameter $\theta_C$ can be determined from the joint solution of the equation of state and the equality of free energies in the ordered and disordered phases:

$$\frac{c}{2}\,\theta^2+\frac{b}{3}\,\theta^3+\frac{a}{2}\,\theta^4=0.$$

The magnitude of the transition field and the jump in the order parameter at the transition point are determined from the expression

$$H_C=H_0+\frac{2b^2}{9a}; \quad \theta_C=-\frac{2b}{3a}. \tag{16}$$

Substituting the values of the coefficients $a$ and $b$ into these expressions, we obtain an estimate for a jump of the order parameter $\theta_C\sim\beta^2/\eta^2$. This estimate shows that the magnitude of the jump is small for $\beta\ll\eta$, and hence we are dealing with a first order phase transition close to a second-order transition.

## SPECTRA OF MAGNETOELASTIC WAVES OF AN EASY-PLANE FERROMAGNET UNDER MECHANICAL BOUNDARY CONDITIONS

Let us now analyze the spectra of coupled ME waves in the vicinity of the first-order PT.

It is well known that the elementary excitation spectra of the system are determined by the poles of the Green's function.[8] We define the total Green's function as follows:

$$G^{\alpha\alpha'}(n,\tau,n',\tau')=-\langle\hat{T}\tilde{Y}_n^{\alpha}(\tau)\tilde{Y}_{n'}^{-\alpha'}(\tau')\rangle,$$

where $\hat{T}$ is Wick's operator, $\tilde{Y}_n^{\alpha}(\tau)=e^{\mathscr{H}\tau}Y_n^{\alpha}e^{-\mathscr{H}\tau}$ the Hubbard operator in the Heisenberg representation, and $\mathscr{H}=\mathscr{H}_{\rm tr}+\mathscr{H}_{\rm int}$. The Hamiltonian $\mathscr{H}_{\rm int}$ is the exchange component of Hamiltonian (1) which has the following form in the representations of Hubbard operators:

$$\mathscr{H}_{\rm int}=-\frac{1}{2}\sum_{\substack{M,M'\\n,n'}} I_{nn'}^{MM'}H_n^M H_{n'}^{M'}-\frac{1}{2}\sum_{\substack{M,\alpha\\n,n'}} I_{nn'}^{M\alpha}H_n^M X_{n'}^{\alpha}$$

$$-\frac{1}{2}\sum_{\substack{\alpha,\beta\\n,n'}} I_{nn'}^{\alpha\beta}X_n^{\alpha}X_{n'}^{\beta};$$

$$I_{nn'}^{MM'}=I(n-n')\Gamma_{\parallel}(M)\Gamma_{\parallel}(M');$$

$$I_{nn'}^{M\alpha}=I(n-n')\Gamma_{\parallel}(M)\gamma_{\parallel}(\alpha); \tag{17}$$

$$I_{nn'}^{\alpha\beta}=I(n-n')\left\{\gamma_{\parallel}(\alpha)\gamma_{\parallel}(-\beta)+\frac{1}{2}[\gamma_{\perp}(\alpha)\gamma_{\perp}^{*}(-\beta)+\gamma_{\perp}^{*}(-\alpha)\gamma_{\perp}(\beta)]\right\}.$$

The quantities $\Gamma_{\parallel}(M)$ and $\gamma_{\parallel}(\alpha)$, $\gamma_{\perp}(\alpha)$ determine the relation between the spin operators and the Hubbard operators, which in the general case has the form[5,6]

$$S^{+}=\sum_{\alpha}\gamma_{\perp}(\alpha)X^{\alpha}; \quad S^{-}=(S^{+})^{+};$$

$$S^{z}=\sum_{M}\Gamma_{\parallel}(M)H^{M}+\sum_{\alpha}\gamma_{\parallel}(\alpha)X^{\alpha}.$$

In our case, the quantities $\Gamma_{\parallel}(M)$ and $\gamma_{\parallel}(\alpha)$, $\gamma_{\perp}(\alpha)$ have the following form (to within linear terms in $\theta$):

$$\Gamma_{\parallel}(1)=1, \quad \Gamma_{\parallel}(0)=0, \quad \Gamma_{\parallel}(-1)=-1,$$

$$\gamma_{\parallel}(\alpha_1)=-\gamma_{\parallel}(\alpha_2)=i\,\frac{\theta}{\sqrt{2}}\,\frac{H-\beta/2}{\overline{H-\beta/2}};$$

$$\gamma_{\parallel}(\alpha_3)=\gamma_{\parallel}(\alpha_4)=0;$$

$$\gamma_{\parallel}(\alpha_6)=-\gamma_{\parallel}(\alpha_5)=i\,\frac{\theta}{\sqrt{2}}\,\frac{H+\beta/2}{\overline{H+\beta/2}};$$

$$\gamma_{\perp}(\alpha_1)=\gamma_{\perp}(\alpha_4)=\gamma_{\perp}(\alpha_6)=0;$$

$$\gamma_{\perp}(\alpha_2)=\gamma_{\perp}(\alpha_5)=\sqrt{2};$$

$$\gamma_{\perp}(\alpha_3)=-i\theta\,\frac{\beta I_0\langle S\rangle}{\overline{H^2-\beta^2/4}}.$$

The quantities $\alpha_i$ are the root vectors determining the algebra of Hubbard operators. These vectors can be found from the relations[5,9]

$$[H_n^M,X_{n'}^{pq}]=\delta_{nn'}(\delta_{pM}-\delta_{Mq})X_{n'}^{pq}=\delta_{nn'}\alpha(p,q)X_{n'}^{\alpha(p,q)}. \tag{18}$$

The subsequent calculations will be carried out in the mean field approximation; hence we shall require in the further analysis only the ''transverse'' component of Hamiltonian (17), which has the form[9]

$$\mathscr{H}_{\rm int}^{\perp}=-\frac{1}{2}\sum_{\substack{\alpha,\beta\\n,n'}}\frac{I(n-n')}{2}A_i^{-\alpha}B_i^{\beta}X_n^{\alpha}X_{n'}^{\beta},$$

where

$$A_1^{\alpha}=\begin{pmatrix}2\gamma_{\parallel}(\alpha)\\ \Gamma_{\parallel}(M)\end{pmatrix}; \quad A_2^{\alpha}=\begin{pmatrix}\gamma_{\perp}^{*}(\alpha)\\ 0\end{pmatrix}; \quad A_3^{\alpha}=\begin{pmatrix}\gamma_{\perp}(-\alpha)\\ 0\end{pmatrix};$$

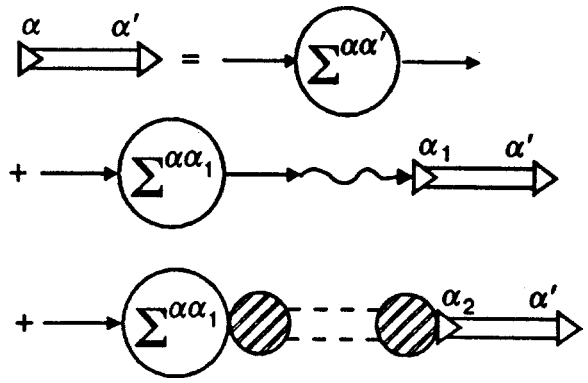


FIG. 4. Equation for Green's function $G^{\alpha\alpha'}(k,\omega_n)$.

$$B_1^\alpha=\begin{pmatrix}\gamma_\parallel(\alpha)\\ \Gamma_\parallel(M)\end{pmatrix};\quad B_2^\alpha=\begin{pmatrix}\gamma_\perp(\alpha)\\ 0\end{pmatrix};\quad B_3^\alpha=\begin{pmatrix}\gamma_\perp^*(\alpha)\\ 0\end{pmatrix}.$$

The Hamiltonian $\mathscr{H}_{\rm tr}$ of transformations, which describes the conversion of magnons into phonons and vice versa, can be written in the form[6]:

$$\mathscr{H}_{\rm tr}=\sum_n\left\{\sum_M P_M H_n^M+\sum_\alpha P_\alpha X_n^\alpha\right\},$$

where

$$P_{M(\alpha)}=\frac{1}{\sqrt{N}}\sum_{k,\lambda}(b_{k,\lambda}+b_{-k,\lambda}^+)T_n^{M(\alpha)}(k,\lambda).$$

Here $N$ is the number of sites in the crystal lattice, $b_{-k,\lambda}^+(b_{k,\lambda})$ are the creation (annihilation) operators for phonons with the polarization $\lambda$, and $T_n^{M(\alpha)}(k,\lambda)$ are the transformation amplitudes.

We shall carry out subsequent calculations assuming that the wave vector of phonon propagation is directed along the axis $0X(\mathbf{k}\|0X)$. In such a geometry, $e_\tau^y$, $e_l^x$, and $e_t^z$ are nonzero components of the unit vector of phonon polarization.

The equation for the Green's function $G^{\alpha\alpha'}(k,\omega_n)$ presented in Fig. 4 is similar to the Larkin equation.[8] The solid line corresponds to $G^{\alpha\alpha'}(k,\omega_n)$; $\Sigma^{\alpha\alpha'}(k,\omega_n)$ is the component irreducible in the Larkin sense, the hatched circle corresponds to the amplitude of transformations, while the double dashed line is the Green's function for a free $\lambda$-polarized phonon with the energy–momentum relation $\omega_\lambda(k)=c_\lambda k$ ($c_\lambda$ is the velocity of sound):

$$D_\lambda(k,\omega_n)=2\omega_\lambda(k)/[\omega_n^2-\omega_\lambda^2(k)].$$

These quite complex equations can be solved owing to the split dependence on the root vector $\alpha$. In our geometry, the dispersion equation splits into three equations:

$$\omega_1(k)=\omega_l(k);\quad \omega_2(k)=\omega_\tau(k);\tag{19}$$

$$\det\left|\delta_{ij}+\frac{I(k)}{2}G_0^\alpha(\omega_n)b(\alpha)B_j^\alpha A_i^\alpha+K_t(k,\omega_n)B_j^\alpha A_i^\beta\right|=0.$$

It can be seen from (19) that the longitudinally polarized ($l$) and one transversely polarized ($\tau$) acoustic modes do not interact with the magnetic subsystem, and their energy–momentum relation has the conventional form.

The last equation in (19) defines the energy–momentum relation for coupled ME waves emerging due to the interaction of magnons with $t$-polarized phonons. In the mean field approximation, the irreducible component in Larkin's sense has the form

$$\Sigma^{\alpha\alpha'}(k,\omega_n)=\delta_{\alpha\alpha'}b(\alpha)G_0^\alpha(\omega_n),$$

where $b(\alpha)=\langle(\alpha H)\rangle$; $G_0^\alpha(\omega_n)=[i\omega_n+(\alpha\tilde{\mathbf{E}})]^{-1}$ is the zeroth Green's function.

Taking into account what has been said above as well as the explicit form of $K_t(k,\omega_n)$, i.e.,

$$K_t(k,\omega_n)=\frac{D_t(k,\omega_n)}{1-Q_{tt}D_t(k,\omega_n)}T^{-\alpha}(k,t)G_0^\alpha(\omega_n)b(\alpha)\times T^\beta(-k,t)G_0^\beta(\omega_n)b(\beta),$$

where $Q_{tt}=T^\alpha(-k,t)G_0^\alpha(\omega_n)b(\alpha)T^{-\alpha}(k,t)$, we can write the dispersion equation in the form

$$\begin{aligned}&1+\frac{I(k)}{\tilde{E}_{10}}+\frac{\omega_t^2(k)A_0}{2\eta\tilde{E}_{10}}\\&\times\frac{I(k)}{\omega^2-\omega_t^2(k)\left[1+\dfrac{A_0^2+2A_0A\theta^2}{2\eta\tilde{E}_{10}}-\dfrac{B^2\theta^2}{\eta\tilde{E}_{1-1}}\right]}\\&+\frac{\omega_t^2(k)A_0A\theta^2}{\eta\tilde{E}_{10}}\\&\times\frac{I(k)}{\omega^2-\omega_t^2(k)\left[1+\dfrac{A_0^2+2A_0A\theta^2}{2\eta\tilde{E}_{10}}-\dfrac{B^2\theta^2}{\eta\tilde{E}_{1-1}}\right]}\\&-\theta^2\frac{I^2(k)}{\tilde{E}_{10}^2}\left(\frac{H-\beta/2}{H-\beta/2}\right)^2\\&\times\left\{1+\frac{\tilde{E}_{10}}{I(k)+\tilde{E}_{10}}\frac{\omega_t^2(k)A_0^2}{2\eta\tilde{E}_{10}}\right.\\&\left.\times\frac{I(k)}{\omega^2-\omega_t^2(k)\left[1+\dfrac{A_0^2+2A_0A\theta^2}{2\eta\tilde{E}_{10}}-\dfrac{B^2\theta^2}{\eta\tilde{E}_{1-1}}\right]}\right\}=0.\end{aligned}\tag{20}$$

While deriving Eq. (20), we assumed that the magnitude of the ME gap is much smaller than the lowermost energy level, i.e.,

$$\omega\ll\tilde{E}_{ij}\quad(\tilde{E}_{ij}=\tilde{E}_i-\tilde{E}_j;\quad i,j=1,0,-1).$$

In addition, we have introduced the following notation:

$$A_0=\nu-\beta/2;$$

$$A=-(\nu-\beta/2)\left\{\frac{\overline{H}I_0^2\langle S\rangle^2+\frac{\beta}{4}(H+\overline{H})^2}{2\overline{H}(\overline{H}+\beta/2)^2}\right.$$
$$+\frac{I_0^2\langle S\rangle^2}{4\eta(\overline{H}-\beta/2)}\frac{\beta/2-\nu}{\eta(\overline{H}-\beta/2)}\left[\frac{\beta}{\overline{H}+\beta/2}\right.$$
$$\left.\left.+\nu\left(1+\frac{\nu}{4\eta}\right)\right]\right\};$$
$$B=(\nu-\beta/2)\left\{\frac{\overline{H}H-\overline{H}^2}{\overline{H}^2-\beta^2/4}-\frac{\beta}{4\eta}\frac{I_0\langle S\rangle}{\overline{H}-\beta/2}\right\}.$$

The solution of Eq. (20) has the following form (to within the terms of the order of $\theta^2$):

$$\omega^2(k)=\omega_t^2(k)\left\{\alpha k^2+H-\frac{\beta}{2}-\frac{\nu^2}{4\eta}-\frac{A_0^2}{2\eta}\right.$$
$$-\frac{A_0A\tilde{E}_{1-1}-B^2(\tilde{E}_{10}+I_0)}{\eta\tilde{E}_{1-1}}\theta^2$$
$$\left.+\left(\frac{H-\beta/2}{\overline{H}-\beta/2}\right)^2\frac{I_0^2}{\tilde{E}_{10}}\left(1+\frac{A_0^2}{2\eta(\tilde{E}_{10}+I_0)}\right)\theta^2\right\}$$
$$\times\left\{\alpha k^2+H-\frac{\beta}{2}-\frac{\nu^2}{4\eta}\right.$$
$$\left.+\left(\frac{H-\beta/2}{\overline{H}-\beta/2}\right)^2\frac{I_0^2}{\tilde{E}_{10}}\theta^2\right\}^{-1},$$

where $\alpha=I_0R_0^2$, $R_0$ being the radius of interaction.

Let us analyze the solution of the dispersion equation in the two cases:

(1) at the point of the first-order PT (for $H=H_C$);

(2) at the point of absolute instability of the disordered phase (for $H=H_A$).

According to the solution of the dispersion equation. the quasiphonon spectrum remains linear at the point of the first-order PT: $\omega^2\approx\omega_t^2(k)[1-0(\nu^2/\eta)]$, while the quasimagnon spectrum has the energy gap due to the ME interaction: $\varepsilon(k)=\alpha k^2+(a/2)\theta_C^2$. Such a behavior of the spectra of ME waves indicates that the soft mode is absent at the point of the first-order PT ($H=H_C$).

A different situation arises at the point of absolute instability of the disordered phase (for $H=H_A$). For these fields, in the long-wave limit

$$\left(\alpha k^2\ll a\theta_A^2+\frac{\beta/2-\nu}{4\eta}\left(\frac{\beta}{2}-\nu+\frac{\nu\beta}{4\eta}-\frac{\beta(\beta/2-\nu)}{8\eta}\right)\right)$$

the quasimagnon spectrum has the ME gap $\varepsilon(k)=\alpha k^2+d_0$, where

$$d_0=a\theta_A^2+\frac{\beta/2-\nu}{4\eta}\left(\frac{\beta}{2}-\nu+\frac{\nu\beta}{4\eta}-\frac{\beta(\beta/2-\nu)}{8\eta}\right),$$

while the quasiphonon spectrum has the form $\omega^2=\omega_t^2(k)\times(\alpha k^2+H-H_A)(\alpha k^2+H-H_A+d_0)^{-1}$ and is softened at the point of absolute instability of the disordered phase (in the long-wave limit): $\omega^2=\omega_t^2(k)\alpha k^2/d_0$.

## CONCLUSIONS

The presence of mechanical boundary conditions strongly affects the critical behavior of the system as well as its dynamic properties.

Above all, this effect is manifested in the change in the functional dependence of the free energy density on the order parameter $\theta$. The emergence of the cubic term makes the phase transition a first-order phase transition.

As expected, the soft mode of elementary excitations is absent at the point of the first-order PT. The softening of the quasiphonon mode takes place at the point of absolute instability of the disordered phase.

The authors thank N. M. Lavrinenko for valuable critical remarks and fruitful discussions.

*E-mail: man@expl.cris.crimea.ua

[1] V. G. Bar'yakhtar, I. M. Vitebskii, N. M. Lavrinenko, and V. L. Sobolev, Zh. Éksp. Teor. Fiz. **90**, 1111 (1986) [Sov. Phys. JETP **63**, 647 (1986)].
[2] I. M. Vitebskii, N. M. Lavrinenko, A. N. Maiorova *et al.*, Preprint IMK 93- 8, Kharkov (1993).
[3] V. G. Bar'yakhtar and E. A. Turov, in *Electron Structure and Electronic Properties of Metals and Alloys* [in Russian], Naukova Dumka, Kiev (1988), 39 pp.
[4] E. A. Turov and V. G. Shavrov, Usp. Fiz. Nauk **140**, 429 (1983) [Sov. Phys. Usp. **26**, 593 (1983)].
[5] R. O. Zaitsev, Zh. Éksp. Teor. Fiz. **68**, 207 (1975) [Sov. Phys. JETP **41**, 100 (1975)].
[6] Yu. N. Mitsai and Yu. A. Fridman, Teor. Mat. Fiz. **81**, 263 (1989).
[7] A. Z. Patashinskii and V. L. Pokrovskii, *Fluctuational Theory of Phase Transitions*, 1st ed., Pergamon, Oxford (1979).
[8] Yu. A. Izyumov, F. A. Kassan-Ogly, and Yu. N. Skryabin, *Field Methods in the Theory of Ferromagnetism* [in Russian], Nauka, Moscow (1974).
[9] V. V. Val'kov, T. A. Val'kova, and S. G. Ovchinnikov, Zh. Éksp. Teor. Fiz. **88**, 550 (1985) [Sov. Phys. JETP **61**, 323 (1985)].
[10] Yu. A. Izyumov and V. N. Syromyatnikov, *Phase Transitions and Symmetry of Crystals* [in Russian], Nauka, Moscow (1984).
[11] I. E. Dikshtein, E. A. Turov, and V. G. Shavrov, in *Dynamic and Kinetic Properties of Magnets* [in Russian], Nauka, Moscow (1986).

Translated by R. S. Wadhwa

# Contribution of longitudinal oscillations of magnetization to spin dynamics of spontaneous reorientation

N. K. Danshin and Yu. I. Nepochatykh

*A. Galkin Physicotechnical Institute, National Academy of Sciences of the Ukraine, 340114 Donetsk, Ukraine**

(Submitted October 8, 1997; revised November 26, 1997)
Fiz. Nizk. Temp. **24**, 353–359 (April 1998)

Comparative analysis of the results of measurements of soft magnetic resonant modes in weak ferromagnets with different temperatures of spontaneous reorientation is carried out. It is shown that the longitudinal oscillations of magnetization make a contribution to the energy gap even in zero magnetic field (in the case of spontaneous reorientation) and increases with increasing temperature alone. © *1998 American Institute of Physics.* [S1063-777X(98)01104-9]

## 1. INTRODUCTION

In most cases, the spin dynamics of orientational magnetic transitions observed in experiments can be described correctly by taking into account only the precession of magnetization and disregarding its longitudinal oscillations. This allows one to interpret correctly magnetic resonance experiments at temperatures considerably lower than the temperatures $T_N$ of spin ordering. However, longitudinal oscillations of magnetization[1] should also be taken into account at higher temperatures apart from precession.

Analyzing soft magnetic resonant modes in several rare-earth orthoferrites (REOF) $RFeO_3$ (R = Yb, Tm, and Er)[2,3] and in $Fe_3BO_6$,[4] we established that the contributions of reorientation due to precession and longitudinal oscillations of magnetization to spin dynamics always coexist and are additive and competing. The ratio of partial magnitudes of these quantities depends on the parameter $\tau_{SR}=T_{SR}/T_N$ which was called relative spontaneous reorientation ($T_{SR}$ is the averaged temperature of spontaneous reorientation and $T_N$ the temperature of spin ordering for iron). This parameter is individual for each orthoferrite since the values of temperature $T_{SR}$ for them can differ by more than an order of magnitude for virtually the same values of temperature $T_N \simeq 700$ K. This allowed us to carry out appropriate experiments in the range of $\tau_{SR}=0.1-1$ by choosing antiferomagnets with the composition indicated above. This research is devoted to substantiation of the conclusion that heating leads to continuous redistribution of contributions to spin dynamics of spontaneous reorientation from precession to longitudinal oscillations of magnetization.

## 2. FORMULATION OF THE PROBLEM AND PRELIMINARY INFORMATION

The study of soft magnetic resonance modes in rare-earth orthoferrites revealed that considerable energy gaps $\nu_0$ are observed at the points of completion for spin reorientation. Figure 1*a* shows the structure of the spontaneous reorientation between the symmetric phases $\Gamma_2$ and $\Gamma_4$ through the angular phase $\Gamma_{24}$, which is most typical in these compounds. The values of temperature $T_1(T_2)$ correspond to the point of termination (onset) of the reorientation through the second-order phase transition (PT-2). The interval $\Delta T=T_1-T_2$ can amount to from a few to tens kelvins for different REOF and, like the averaged reorientation temperature $T_{SR}=(T_1+T_2)/2$, is an individual characteristic of a given REOF.

The three ground states $\Gamma_2, \Gamma_{24}$ and $\Gamma_4$ depicted in Fig. 1 *a* correspond to two-sublattice weakly ferromagnetic subsystem of ordered spins in iron. Here $\mathbf{G}=\mathbf{M_1}-\mathbf{M_2}$ and $\mathbf{F}=\mathbf{M_1}+\mathbf{M_2}$ are antiferro- and ferromagnetism vectors respectively, while $\mathbf{M}_1$ and $\mathbf{M}_2$ are the magnetizations of sublattices. As the temperature changes, a number of spontaneous PT-2 are realized in succession. For example, a decrease in $T$ in $ErFeO_3$ leads to a sequence of transitions $\Gamma_4$–$\Gamma_{24}, \Gamma_{24}$–$\Gamma_2$, and $\Gamma_2$–$\Gamma_{12}$. In the absence of spontaneous transitions, the phase $\Gamma_4$ always sets in at $T<T_N$ (e.g., in $YFeO_3$). The application of an infinitely weak field $\mathbf{H}\|\mathbf{c}$ at $T<T_2$ or $\mathbf{H}\|\mathbf{a}$ at $T>T_1$ immediately transforms the collinear phases $\Gamma_2$ and $\Gamma_4$ into the angular phase $\Gamma_{24}$. As the field increases, reorientation always occurs from the angular phase to a collinear phase determined by the orientation of $\mathbf{H}$. For $\mathbf{H}\|\mathbf{a}$, the transition $\Gamma_{24}$–$\Gamma_2$ takes place. Such a detailed reference to the well-known facts (see, for example, Ref. 5) concerning the structure of the reorientation $\Gamma_2$–$\Gamma_4$ is made in order to emphasize that the transitions $\Gamma_{24}$–$\Gamma_2$ and $\Gamma_{24}$–$\Gamma_4$, which are absolutely identical in the static case, differ basically when we consider spin dynamics.[1] The difference lies in the following. The theory[1] has been constructed for transitions in the iron subsystem occurring under the action of the applied field. The most important conclusion of the theory is that in the main approximation, the numerical value of the experimentally observed frequency gap at the point of completion of spin reorientation obeys the relation $\nu_0 \sim(\chi_\parallel/\chi_\perp)^{1/2}H_{\rm tr}$ ($\chi_\parallel$ and $\chi_\perp$ are the longitudinal and transverse susceptibilities and $H_{\rm tr}$ is the transition field at the relevant temperature). Thus, the gap can increase both with longitudinal susceptibility and with the applied field. Figure 1*b* shows that simultaneous increase in $\chi_\parallel$ and $H_{\rm tr}$ is observed only for the transitions $\Gamma_{24}$–$\Gamma_2$. Conversely, for $\Gamma_{24}$–$\Gamma_4$ an increase in the field is accompanied by a decrease in $\chi_\parallel$. The latter circumstance naturally does not imply that an

 

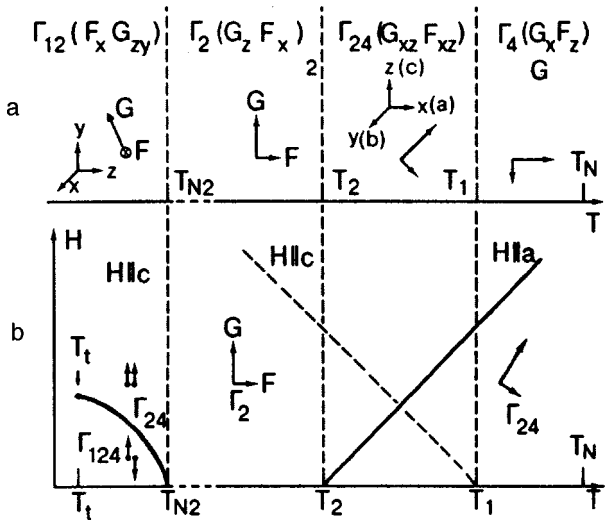


FIG. 1. (a) Basic states for spontaneous transitions in the ordered iron spin subsystem in rare-earth orthoferrites ($\Gamma_2$,$\Gamma_{24}$,$\Gamma_4$,$\Gamma_{12}$). $T_N$,$T_1$,$T_2$, and $T_{N2}$ are the points of spontaneous second- order phase transitions from the paramagnetic phase of iron to the ordered phase $\Gamma_4$, spin reorientation transitions $\Gamma_{24}$–$\Gamma_4$,$\Gamma_{24}$–$\Gamma_2$, and $\Gamma_{12}$–$\Gamma_2$, respectively (the latter transition occurs only in $ErFeO_3$). (b) Low-field fragment of the $H-T$ phase diagram for rare-earth orthoferrites in the vicinity of orientational transitions $\Gamma_{24}$–$\Gamma_2$ (in the field $\mathbf{H}\|\mathbf{a}$), $\Gamma_{24}$–$\Gamma_4$ (in the field $\mathbf{H}\|\mathbf{c}$) in the iron subsystem, and the metamagnetic transition $\Gamma_{124}$–$\Gamma_{24}$ (in the field $\mathbf{H}\|\mathbf{c}$ in the erbium subsystem in $ErFeO_3$). $T_t$ is the tricritical point. Notation of phases and the structure of transition in the temperature range $T_{N2}$–$T_N$ is shown for $\mathbf{H}\|\mathbf{a}$.

increase in $H_{\rm tr}$ is always compensated by a decrease in $\chi_\parallel$, and the effect predicted by the theory[1] (increase in the gap width upon an increase in the external field) is suppressed. In the general case, the longitudinal susceptibility and field can affect the gap widths differently. For definiteness, we shall henceforth take into account the model situation in which an increase in the transition field corresponds to an increase in longitudinal susceptibility, i.e., the situation typical of the $\Gamma_{24}$–$\Gamma_2$ transition in the field $\mathbf{H}\|\mathbf{a}$. Accordingly, we shall be interested only in the energy gap $\nu_{02}$ in the vicinity of the temperature $T=T_2$. The theory[1] was developed and tested for the first time just for such a transition in $YFeO_3$. In this material, no spontaneous reorientation takes place, and hence only the $\Gamma_{24}$–$\Gamma_2$ transition can occur in the field. The $H$–$T$ phase diagram of $YFeO_3$ in the field $\mathbf{H}\|\mathbf{a}$ is such[6] that this transition can be induced in the experimentally admissible temperature range only by fields of 70–80 kOe. This means that it is impossible to eliminate the effect of the field on the energy gap in $YFeO_3$. If, however, a reorientation of the same type occurs spontaneously, the induced reorientation can be caused by an infinitely weak field, and all the effects associated with manifestations of longitudinal oscillations (if they exist) can be rightfully associated mainly with $\chi_\parallel$. A spontaneous Morin transition $\Gamma_1$–$\Gamma_4$ occurs at $T\simeq 40$ K in $DyFeO_3$ in which the effects of longitudinal oscillations of magnetization were observed.[7] However, the $H$–$T$ phase diagram of this orthoferrite is such that the transition $\Gamma_{24}$–$\Gamma_2$ we are interested in can occur near the Morin temperature only in the field $\geqslant 40$ kOe. However, in the temperature range $T>78$ K in which the experiments[7] were carried out, this transition can be induced only in a field not weaker than 60 kOe. For such values of $T$ and $H$, the contribution of longitudinal oscillations to the energy gap is quite large, but it is due to both cofactors in the expression for the gap. Although the theory[1] was developed for transitions induced by an applied field, we can conclude from general considerations that the contribution of longitudinal oscillations of magnetization to the spin reorientation dynamics can also be expected for spontaneous transitions if the latter occur at sufficiently high temperatures. Let us substantiate this assumption proceeding from the results of our experiments on REOF with different values of the parameter $\tau_{SR}$.

## 3. DISCUSSION OF EXPERIMENTAL RESULTS

It should be noted at the very outset that the energy gap observed in REOF with relatively low values of $\tau_{SR}$ in the case of spontaneous transitions can be successfully explained when only the precession of magnetization is taken into account. In most cases, we managed to explain quantitatively the reorientation dynamics as the result of interaction of different oscillatory subsystems of REOF (ordered spins of iron, paramagnetic rare-earth ions, elastic, and dipole (electromagnetic) subsystems) on the basis of a modified theory.[8] These results were used as the starting point in the search for effects associated with manifestations of longitudinal oscillations in the spin reorientation dynamics. The experimental technique and corresponding methodical approaches required for this purpose were described in detail in Refs. 2–4. Since the theory[1] disregards the above mechanisms of gap formation (due to the interaction of various oscillatory subsystems), it leads to the conclusion that the gap width tends to zero as $H\to 0$. Since this contradicts the reality and wide gaps are observed in all REOF even for $H=0$, the effects associated with manifestation of longitudinal oscillations should be sought in the form of increments of these ''initial'' gaps after the application of the field. For this reason, the general methodical approach in experiments was as follows. At first, we reconstructed the energy gap $\nu_0$ for the corresponding spontaneous transition. Then the temperature–field dependence of this gap was measured in a comparatively weak field (up to 10–12 kOe) oriented strictly along the crystallographic axis. The sought effect was estimated from the magnitude of the derivatives $\partial\nu_0/\partial T$ and $\partial\nu_0/\partial H$. The latter derivative must be positive (according to Refs. 1,7), but the derivative $\partial\nu_{02}/\partial T$ is also always positive for the $\Gamma_{24}$–$\Gamma_2$ transition. If the above-mentioned temperature–field dependence of the gap is such that $\partial\nu_{02}/\partial T$, $\partial\nu_{02}/\partial H\neq 0$ for $T\to T_2$ and $H\to 0$, respectively, we can state that longitudinal oscillations make a contribution to the spin dynamics of the field-induced as well as spontaneous transition. Since the transition field in this case can be quite small, the prevailing contribution to the effect will be determined for a certain magnitude of the field by the longitudinal susceptibility alone. Naturally, this conclusion does not follow from the theory,[1,7] and the results obtained while testing this model for $YFeO_3$ and $DyFeO_3$[7] appear rather as the strong field effect. For this reason, a detailed comparison of the actually observed spin dynamics with the theory is hardly correct. In

TABLE I. Characteristics of spin dynamics of orientational transitions in REOF and $Fe_3BO_6$ measured experimentally by us.

| Parameters | Substance | | | | | | |
|---|---|---|---|---|---|---|---|
| | $YbFeO_3$ | $TmFeO_3$ | $ErFeO_3$ (1) | $NdFeO_3$ | $SmFeO_3$ | $Fe_3BO_6$ | $ErFeO_3$ (2) |
| Type of transition | $\Gamma_{24}-\Gamma_2$ | $\Gamma_{24}-\Gamma_2$ | $\Gamma_{24}-\Gamma_2$ | $\Gamma_{24}-\Gamma_2$ | $\Gamma_{24}-\Gamma_2$ | $\Gamma_{24}-\Gamma_2$ | $\Gamma_{124}-\Gamma_{24}$ |
| $T_{SR}=(T_1+T_2)/2$, K | 7.4 | 88 | 95 | 123 | 463 | 415 | 3.9 |
| Energy gap for spontaneous transition at the point $T=T_2$, GHz | 37.5 | 20 | 26.5 | 56 | 35 | 17.5 | 26.1 |
| $\tau_{SR}=T_{SR}/T_N$ | 0.01 | 0.14 | 0.15 | 0.17 | 0.7 | 0.8 | 1.0 |
| $\partial\nu_{02}/\partial T$ for $T\to T_2$, GHz/K | 0 | 0 | 0 | 0* | 0.3* | 0.5 | 60 |
| $\partial\nu_{02}/\partial H$ for $H\to 0$, GHz/kOe | 0 | 0 | 0 | 0* | – | 0.7 | 4 |

*Remarks:* (a) Asterisks mark expected values. (b) The following substitutions should be made for $ErFeO_3$ (2): $T_{SR}$, $T_N$, and $T_2$ should be replaced by $T_{N2}$ and $\nu_{02}$ by $\nu_{0N2}$.

this research, we shall use only the main conclusion of the theory (and experimental test), i.e., the fact that an increase in the gap with the field is an indication of a contribution of longitudinal oscillations of magnetization to the reorientation dynamics. According to experiments,[4,9] this contribution can increase upon a decrease as well as an increase in temperature. We shall confine our analysis to the latter case.

Let us analyze all the experiments in the ascending order of parameter $\tau_{SR}$. For this purpose, it is convenient to present the main results and information on REOF and $Fe_3BO_6$ obtained in our experiments in the form of a table.

It can be seen from Table I that orthoferrites characterized by relatively low temperatures of spontaneous reorientation $\Gamma_{24}-\Gamma_2(\tau_{SR}<0.15)$ have the gradient $\partial\nu_{02}/\partial T=0$. Moreover, the results of measurements[2,4] show that in ytterbium, thulium, and erbium orthoferrites this gradient is equal to zero not only for $H=0$, but also in a nonzero field.

The field dependences of energy gap width presented in Fig. 2 show that the gradient $\partial\nu_{02}/\partial H$ in these REOF is also equal to zero not only in zero field, but also in fields up to 6–10 kOe. The general result of measurements can be formulated as follows: the gap width $\nu_{02}$ inherent in the spontaneous $\Gamma_{24}-\Gamma_2$ transition in $YbFeO_3$, $TmFeO_3$, and $ErFeO_3$ remains unchanged upon the application of a comparatively weak field. This means that the energy gaps in these orthoferrites at the points corresponding to this spontaneous transition are formed mainly due to precession mechanisms. For $\tau_{SR}<0.15$, the contribution of longitudinal oscillations of magnetization to the gap width is negligibly small against this background and is not manifested in experiments to within the attained accuracy of measurements (see Refs. 2,3).

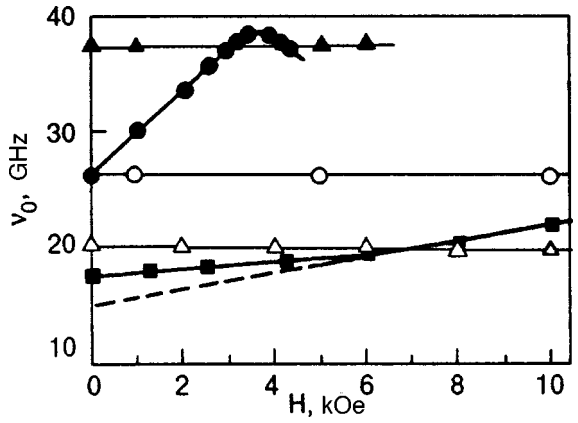


FIG. 2. Field dependences of energy gap widths in different orthoferrites: on the curve corresponding to the transition $\Gamma_{24}-\Gamma_2$ induced by the field $\mathbf{H}\|\mathbf{a}$ in $TmFeO_3$(△), $ErFeO_3$(○), $YbFeO_3$ (dark triangles), and $Fe_3BO_6$(■), and on the curve corresponding to the metamagnetic transition $\Gamma_{124}-\Gamma_{24}$ induced by the field $\mathbf{H}\|\mathbf{c}$ in the erbium subsystem in $ErFeO_3$(●). The dashed line is the linear extrapolation of the field dependence of the gap width in $Fe_3BO_6$ in the field region $H>8$ kOe.

The magnetic resonance measurements for $NdFeO_3$ show[10] that the range of angular phase and the energy gap width in this orthoferrite are very sensitive to the quality of the initial raw material for the samples. For this reason, the experiment meeting our requirements would be characterized by a large error. However, no measurements were made for $NdFeO_3$ since it was clear beforehand that such measurements would not give any new qualitative results other than those obtained from experiments with $ErFeO_3$. Indeed, $\tau_{SR}=0.17$ for $NdFeO_3$, i.e., this parameter is very close for neodymium and erbium orthoferrites. Hence an increase in the gap width with the field and temperature in $NdFeO_3$ could hardly be observed.

The compound $SmFeO_3$ with a record-high value of $\tau_{SR}=0.7$ among REOF attracts considerable attention of the researchers. However, the attempts to make magnetic resonance measurements in this compound were not successful in view of a low intensity and a large absorption line width,[11] which is apparently due to strong attenuation introduced by the rare-earth subsystem at a large value of $T_{SR}$ inherent in this REOF. For this reason, it was essential to find a suitable magnet that does not belong to the well-known set of REOF and has a high value of $\tau_{SR}$. Such a magnet was $Fe_3BO_6$ isomorphic to REOF, which is a weak orthorhombic ferromagnet for $T<T_{SR}=508$ K. This compound exhibits at $T=T_{SR}=415$ K the spontaneous reorientation $\Gamma_2-\Gamma_4$ typical of REOF, but occurring jumpwise and not through the angular phase. The $H-T$ phase diagram corresponding to it differs from that for REOF only in that $T_1=T_2$ in $Fe_3BO_6$.[4] However, the structures of transitions induced by the applied field are absolutely identical to those realized in REOF. In this case also we shall be interested only in reorientation in the field $\mathbf{H}\|\mathbf{a}$. It can be seen from Fig. 2 that the energy gap width in $Fe_3BO_6$ increases with the field. The gradient

$\partial\nu_{02}/\partial H \neq 0$ in this case even for $H=0$ and amounts to 0.7 GHz/kOe. The gap width also increases with temperature, its gradient being $\partial\nu_{02}/\partial T \neq 0$ even at the point of spontaneous transition: $\partial\nu_{02}/\partial T \approx 0.5$ GHz/K at $T=T_{SR}$. This means that the ''initial'' gap inherent in spontaneous transitions is formed not only due to precession mechanisms,[8] but also due to longitudinal oscillations of magnetization.[1] This is a direct consequence of a high value of the parameter $\tau_{SR}$ which attains the value 0.8 for $Fe_3BO_6$. It should be stipulated that the above value of $\partial\nu_{02}/\partial H$ was determined by the linear extrapolation of the field dependence of the gap width in the range of the strongest field. This gives $\sim$15 GHz for the initial gap, while the experimentally obtained field dependence of the gap width (see Fig. 2) gives $\sim$17.5 GHz. A detailed substantiation of the need to use this approach is given in Ref. 4.

In all the cases considered above, field-induced transitions occur for an exchange energy which is much higher (by $\sim$3 orders of magnitude) than the anisotropy energy. For this reason, the ratio $\chi_\parallel/\chi_\perp$ in this case cannot in principle be greater than unity and that too at $T=T_N$ only. It was found that the inverse relation between exchange and anisotropy can be realized in $ErFeO_3$. Such a possibility appears in view of antiferromagnetic ordering in erbium at $T=T_{N2}\simeq 4$ K. At this point, a spontaneous combined order–order transition occurs in the iron subsystem (conventional smooth reorientation of **G**, but now in the $zy$ plane), and disorder–order transition in the erbium subsystem (antiferromagnetic ordering of spins in erbium along the $z$-axis). The rare-earth subsystem acquires the properties of a metamagnet due to a high one-ion anisotropy of erbium, which is much stronger than the energy of $f$–$f$ interaction. The field $\mathbf{H}\|\mathbf{c}$ induces a metamagnetic transition in this subsystem, which involves the collapse of the magnetic moments of erbium.[12] Figure 1*b* shows schematically a fragment of the $H$–$T$ phase diagram corresponding to the transition to the temperature region in which it takes place as a PT- 2. In $ErFeO_3$, this corresponds to the temperature interval $T=T_t-T_{N2}=2.7$–4 K($T_t$ is the tricritical point). In our earlier measurements made on spherical samples,[3,12] the interval of the applied field $H$ in this temperature range was 0–4.1 kOe. A detailed description of high-frequency experiments with this metamagnetic transition can be found in Ref. 3. Here we only recall that an exceptionally high longitudinal susceptibility and a vanishingly low transverse susceptibility are typical properties of metamagnets. For this reason, even a formal application of the theory[1] should lead to the corresponding increase in the gap width. Indeed, according to Fig. 2, the energy gap width at the metamagnetic transition curve increases almost by a factor of 1.5 in a comparatively weak field. Direct measurements of the high-frequency susceptibility give the ratio $\chi_\parallel/\chi_\perp=7$. The temperature dependences of $\chi_\parallel/\chi_\perp$ and of the gap width $\nu_{0N2}$ also correlate even in details. This is the most convincing evidence of the fact that the increment of the gap width in a field shown in Fig. 2 is associated with longitudinal oscillations of magnetic sublattices of erbium. In the present research, we are interested in the field and temperature gradients of the gap width in the vicinity of a spontaneous transition. For $T\to T_{N2}$ and $H\to 0$, these gradients have the following values: $\partial\nu_{02}/\partial T=60$ GHz/kOe, $\partial\nu_{0N2}/\partial H=4$ GHz/kOe. However, it cannot be stated in this case that the existence of such large gradients of the gap width near $T=T_{N2}, H=0$ indicate an adequate contribution of longitudinal oscillations to the ''initial'' gap width $\nu_{0N2}$ at this point. In all probability, the above gradients emerge only in the field. It should be noted that the structure of the transition typical of the spontaneous reorientation $\Gamma_{24}-\Gamma_2$ (see Fig. 1*b*) does not change upon the application of the field $\mathbf{H}\|\mathbf{a}$, while the field $\mathbf{H}\|\mathbf{c}$ transforms the spontaneous transition $\Gamma_2$–$\Gamma_{12}$ into the transition $\Gamma_{124}$–$\Gamma_{24}$. This means that the latter can be realized only in the field (otherwise it could not be a metamagnetic transition!). Antiferromagnetically ordered erbium in this case becomes ferrimagnet with the difference in the magnetizations of sublattices in the form of the $z$-component of ferromagnetism of Er. In all probability, the maximum gradients of the gap width in field and temperature at $T=T_{N2}$ and $H=0$ are associated just with the change in the structure of the initial phases. As regards the contribution of longitudinal oscillations to the gap width in the case of a spontaneous transition, it must correspond to the value $\chi_\parallel/\chi_\perp=1$ at the point $T_{SR}=T_{N2}$ according to the arguments presented in Introduction. The measurements of high-frequency susceptibility[3] give the value $\chi_\parallel/\chi_\perp\simeq 3$ at this point.

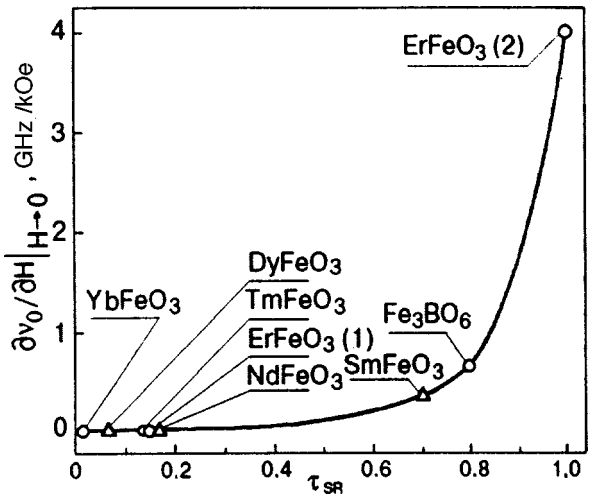


FIG. 3. Values of $\partial\nu_0/\partial H$ at the points of spontaneous transitions in different compounds for corresponding dimensionless temperatures $\tau_{SR}=(T_1+T_2)/2T_N$: measured (○) and expected (△) values. Suffixes (1) and (2) to $ErFeO_3$ indicate that in the former case we are dealing with the $\Gamma_{24}$–$\Gamma_2$ transition in the iron subsystem, while in the latter case we have $\Gamma_{124}$–$\Gamma_{24}$ transition in the erbium subsystem.

Figure 3 shows the resultant two-dimensional diagram characterizing the evolution of $\partial\nu_0/\partial H$ for $H=0$ with a change in the parameter $\tau_{SR}$. Obviously, this diagram can be supplemented with the third coordinate characterizing the field dependence of $\partial\nu_0/\partial H$. For this purpose, we must carry out high-field measurements of the gap width in the REOF presented above according to the technique used in Refs. 1,7 for $YFeO_3$ and $DyFeO_3$. Among the compounds represented in this diagram, such measurements were made only for $Fe_3BO_6$.[9] The smooth curve connecting ''experimental'' point in Fig. 3 can give an idea about the values of $\partial\nu_0/\partial H$

for $H=0$, which can be expected for some other REOF proceeding from the known values (e.g., for $DyFeO_3$, $NdFeO_3$, $SmFeO_3$). In all probability, the situation with $DyFeO_3$ and $NdFeO_3$ will be the same as in ytterbium, thulium, and erbium orthoferrites, i.e., $\partial\nu_0/\partial H=0$. On the other hand, the contribution of longitudinal oscillations to the spontaneous reorientation dynamics in $SmFeO_3$ must be noticeable (with $\partial\nu_{02}/\partial H=0.3$ GHz/kOe). This is natural since the $\Gamma_{24}$–$\Gamma_2$ transition in this case occurs for comparatively large value of $\chi_\parallel/\chi_\perp$. It follows from the temperature dependence of $\chi_\parallel/\chi_\perp$ obtained by Balbashev et al.[7] and the value of $\tau_{SR}=0.8$ for $SmFeO_3$ that the susceptibility ratio is $\sim 0.7$. Unfortunately, the entire set of REOF contains no appropriate compounds for filling the gap between $NdFeO_3$ and $SmFeO_3$ on the given diagram. This gap could be filled in principle by appropriate isomorphic compounds. However, the most obvious and probably attainable way of obtaining an appropriate continuous set is the method of mutual substitution of rare-earth ions in REOF with the soft mode of the same origin, but with noticeably differing temperatures of spontaneous reorientation (e.g., $Tm^{3+}$ and $Sm^{3+}$). But even the diagram presented here allows us to state with a certain degree of confidence that it is reasonable to seek the contribution of longitudinal oscillations to the spin dynamics of spontaneous reorientation at the modern level of accuracy of measurements and the quality of raw materials for $\tau_{SR}>0.5$. On the other hand, the corresponding effects must be observed for all above-mentioned ''low-temperature'' orthoferrites undergoing transition induced by quite strong fields. Such effects were actually observed in $DyFeO_3$,[7] but the same effects can be expected with confidence for ytterbium, thulium, erbium, and neodymium orthoferrites also. The $H$–$T$ phase diagram of the corresponding compound can be used to estimate the magnitude of the required external field. For example, this field for the $\Gamma_{24}$–$\Gamma_2$ transition in $ErFeO_3$ must be not weaker than 60–70 kOe (see the $H$–$T$ phase diagram in Ref. 13). Only in such fields the value of $\tau_{SR}=T_{IR}/T_N=0.5$ can be expected ($T_{IR}$ is the temperature of induced transition). Finally, Table I and the figures do not imply that higher values of the energy gap width in the case of a spontaneous transition corresponds to a larger contribution of longitudinal oscillations to the spin reorientation dynamics. No correlation between the values of these quantities can be traced in the results presented here. This means that the ''initial'' value of the gap and its increment in the field are due to different mechanisms. They make additive contributions to spin dynamics. The competition of these contributions in a certain transition region of $T$ and $H$ can lead to the situation when one of these contributions becomes insignificant against the background of the other contribution which becomes dominant. In our opinion, the features of such a competition were observed earlier for $YFeO_3$ and $DyFeO_3$.[6] As the temperature decreases to $T<100$ K, the experimental values of $\chi_\parallel/\chi_\perp$ and the gap width become virtually independent of $T$, while the calculations based on the theory[1] predict their further decrease. In all probability, precession mechanisms play a decisive role in the gap formation at these temperatures,[8] and the contribution of longitudinal oscillations is insignificant against this background. This is in accord with the results of measurements presented here for ytterbium, thulium, and erbium orthoferrites for which the gap width is also independent of temperature in the region $T<100$ K.

## 4. CONCLUSIONS

(1) The spin dynamics of orientational transitions in real experimental conditions is formed under the effect of precession as well as longitudinal oscillations of magnetization. The ratio of corresponding contributions to energy gap widths for spontaneous transitions is mainly determined by static properties of a given compound and can be characterized by the dimensionless temperature parameter, viz., the ratio of the spontaneous transition temperature to the temperature of ordering of the spin subsystem.

(2) Commensurate contributions of precession and longitudinal oscillations of magnetization to the energy gap widths at the points of spontaneous transitions should be expected for values of this parameter $\sim 0.5$. In strong magnetic fields, however, longitudinal oscillations can play significant role generally for an infinitely small value of this parameter.

(3) An analysis of the entire body of experimental data presented here as well as in Refs. 1–10 leads to the urgent need in creating a new, more comprehensive and universal theory describing the spin dynamics of orientational transitions. The contributions from precession and longitudinal oscillations of magnetization to spin dynamics must dominate at the boundaries of the temperature region of spin ordering, i.e., at $T\to 0$ and $T\to T_N$, respectively. For most of the experimentally observed soft modes and energy gaps in magnetic resonance spectra, we have to accept the unusual statement that they cannot be identified as modes of purely precession or of purely relaxation origin and by no means of purely spin origin. Moreover, soft magnetic resonant modes (in their classical meaning) apparently can never be observed in experiments; the more so, they cannot be observed evenin principle in view of fundamental limitations (e.g., due to spontaneously broken symmetry).[14] Since coupled oscillations of various subsystems of a magnet always take place in actual practice at the points of reorientation,[8] energy gaps do not vanish even if we disregard longitudinal oscillations.

This research was supported by the Foundation of Fundamental Studies at the Ministry of Science of the Ukraine.

*E-mail: danshin@host.dipt.donetsk.ua

[1] A. M. Balbashev, A. G. Berezin, Yu. M. Gufan, *et al.*, Zh. Éksp. Teor. Fiz. **93**, 302 (1987) [Sov. Phys. JETP **66**, 174 (1987)].
[2] N. K. Danshin and G. G. Kramarchuk, Fiz. Nizk. Temp. **19**, 888 (1993) [Low Temp. Phys. **19**, 632 (1993)].
[3] N. K. Danshin, Fiz. Nizk. Temp. **20**, 353 (1994) [Low Temp. Phys. **20**, 422 (1993)].
[4] N. K. Danshin, Yu. I. Nepochatykh, and V. F. Shkar', Zh. Éksp. Teor. Fiz. **109**, 639 (1996) [JETP **82**, 341 (1996)].
[5] K. P. Belov, A. K. Zvezdin, A. M. Kadomtseva, and R. Z. Levitin, *Ori-*

*entational Transitions in Rare-Earth Magnets* [in Russian], Nauka, Moscow (1977).
[6] A. E. Egoyan and A. A. Mukhin, Fiz. Tverd. Tela **36**, 1715 (1994) [Phys. Solid State **36**, 938 (1994)].
[7] A. M. Balbashev, Yu. M. Gufan, N. Yu. Marchuk, and E. G. Rudashevskii, Zh. Éksp. Teor. Fiz. **94**, 305 (1988) [Sov. Phys. JETP **67**, 821 (1988)].
[8] V. D. Buchel'nilov, N. K. Danshin, L. T. Tsymbal, and V. G. Shavrov, Phys. Usp. **166**, 585 (1996) [*sic*].
[9] V. E. Arutyunyan, K. N. Kocharyan, R. M. Martirosyan, *et al.*, Zh. Éksp. Teor. Fiz. **98**, 712 (1990) [Sov. Phys. JETP **71**, 398 (1990)].
[10] S. N. Barilo, A. P. Ges', A. M. Guretskii *et al.*, Fiz. Tverd. Tela (St. Petersburg) **33**, 621 (1991) [Sov. Phys. Solid State **33**, (1991)].
[11] S. N. Barilo, A. P. Ges', N. K. Danshin *et al.*, Zh. Éksp. Teor. Fiz. **96**, 1921 (1990) [Sov. Phys. JETP **69**, 1083 (1990)].
[12] N. K. Danshin, V. N. Derkachenko, N. M. Kovtun, and M. A. Sdvizhkov, Fiz. Tverd. Tela (Leningrad) **28**, 2609 (1986) [Sov. Phys. Solid State **28**, 1461 (1986)].
[13] K. P. Belov, A. M. Kadomtseva, N. M. Kovtun *et al.*, Phys. Status Solidi A **36**, 415 (1976).
[14] E. A. Turov and V. G. Shavrov, Usp. Fiz. Nauk **140**, 429 (1983) [Sov. Phys. Usp. **26**, 593 (1983)].

Translated by R. S. Wadhwa

## LOW-DIMENSIONAL AND DISORDERED SYSTEMS

# Thermal conductivity and electrical resistivity of the layered compound $Nb_{1-x}Sn_xSe_2$

V. I. Beletskii, O. A. Gavrenko, B. A. Merisov, M. A. Obolenskii, A. V. Sologubenko, G. Ya. Khadjai, and Kh. B. Chashka

*Kharkov State University, 310077 Kharkov, Ukraine**

(Submitted November 3, 1997)
Fiz. Nizk. Temp. **24**, 360–366 (April 1998)

The thermal conductivity $\lambda(x=0,0.15,0.3,0.6;T=2-200\ \mathrm{K})$ and electrical resistivity $\rho(0\leqslant x\leqslant 0.5;T=6-300\ \mathrm{K})$ of layered crystals $Nb_{1-x}Sn_xSe_2$ are measured in the **ab** plane. The metal–semiconductor transition is observed at $x\approx 0.5$. The magnitude of the resistivity anomaly observed at 33 K and associated with a transition to the charge density wave phase increases with increasing $x$ for $x>0.15$. The thermal conductivity of the metallic samples ($x<0.5$) increases with temperature at $T>90$K, which is in accord with the nonlinearity of the $\rho(T)$ dependence. The absence of such an increase in $\lambda(T)$ for a semiconducting sample indicates that this singularity is connected with the electronic subsystem. The observed nonmonotonicity of the $\rho(x)$ dependence may be associated with the existence of a sharp peak in the electron density of states near the Fermi level. Approximation of the $\lambda(T)$ dependence reveals the existence of a phonon scattering mechanism with a relaxation rate proportional to the square of the frequency. © *1998 American Institute of Physics.* [S1063-777X(98)01204-3]

### 1. INTRODUCTION

The transport properties of layered superconductors are of interest due to the fact that in several cases, the high anisotropy of the properties of the electron subsystem associated with the singularities of the crystal structure leads to the emergence of a state with a charge density wave (CDW) competing with the superconducting state. Niobium diselenide, which is a layered superconductor of this kind, allows the investigation of CDW and superconducting transition in easily attainable temperature regions. As Nb is replaced by Sn, the compound $Nb_{1-x}Sn_xSe_2$ undergoes a metal–semiconductor concentration transition at $x\approx 0.5$ while the basic structure of the $NbSe_2$ type is preserved.

The present paper aims are studying the effect of replacement of niobium by tin on heat and charge transport processes in the compound $Nb_{1-x}Sn_xSe_2$ over a wide temperature interval.

### 2. SAMPLES AND EXPERIMENTAL TECHNIQUE

Single crystals of $NbSe_2$ were grown by the method of direct gas transport in an atmosphere of Se in a gradient furnace at 750°C and a mean gradient of 5 K/cm. The growth time was about 240 hours. The composition of the obtained crystals was analyzed by the x-ray electronic technique on the set-up KRATOS-800. The crystals grown in this way had sizes of the order of $3\times 2\times 0.1$mm. The thermal conductivity $\lambda$ was determined in the plane of the layers by the method of uniaxial steady-state thermal flow. The temperature difference was measured by using a chromel–Au+0.07%Fe thermocouple. The resistivity $\rho$ was also measured in the layer plane by the standard four-probe technique.

### 3. DISCUSSION OF RESULTS

#### 3.1. Electrical Resistivity

Figure 1 shows the temperature dependence of the electrical resistivity of $Nb_{1-x}Sn_xSe_2$ samples ($x=0-0.5$). The temperature dependence $\rho(T)$ is of metallic type for $x\leqslant 0.45$ and typically semiconducting type for $x=0.5$, the magnitude of resistivity of $Nb_{0.5}Sn_{0.5}Se_2$ being three orders of magnitude higher than for compounds with a lower concentration of Sn. This points towards a concentration-induced metal–insulator transition in the interval $0.45<x<0.5$. The dependences $\rho(T)$ display weakly manifested anomalies in the vicinity of $T_d=33$ K associated with the CDW-transition. These anomalies are manifested more clearly on the temperature dependences of the derivatives $d\rho/dT$ presented in Fig. 2. It is well known[1] that CDW can be suppressed in layered superconductors by intercalation or doping. However, CDW-effect for electrical resistance is enhanced in $Nb_{1-x}Sn_xSe_2$ for $x>0.15$. Figure 3 shows the concentration dependence of the jump in the derivative of the resistivity $\rho_l'/\rho_h'$, where $\rho_l'$ is the resistivity derivative at the initial segment of the CDW transition, and $\rho_h'$ is the resistivity derivative at the final segment (the choice of $\rho_l'$ and $\rho_h'$ for the sample $Nb_{0.7}Sn_{0.3}Se_2$ is illustrated in Fig. 2). It can be seen from Fig 3 that this jump has the highest value for $x\approx 0.4$, i.e., near the concentration corresponding to metal–insulator transition, the dependence $\rho_{200}/\rho_{10\,\mathrm{K}}$ correlating with the dependence $\rho_l'/\rho_h'$ (see Fig 3). It can be concluded

 

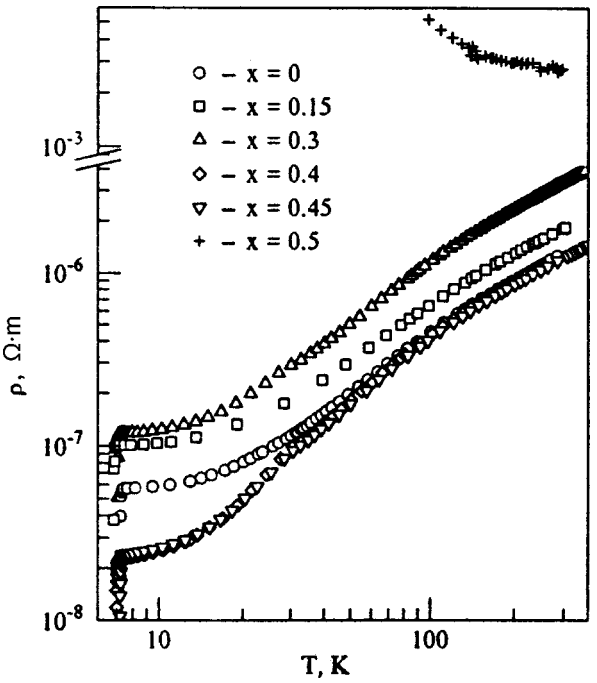


FIG. 1. Temperature dependence of the resistivity of $Nb_{1-x}Sn_xSe_2$.

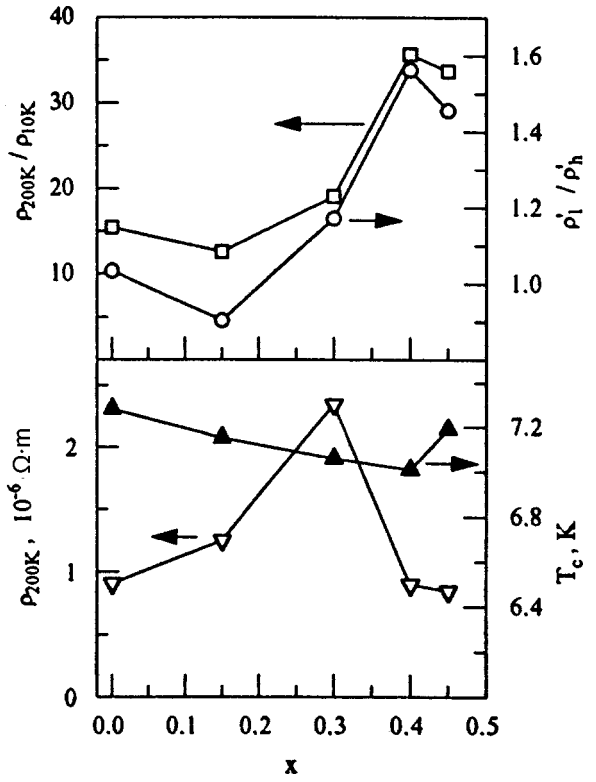


FIG. 3. Dependences $\rho_{200\,K}/\rho_{10\,K}$, $\rho_l'/\rho_h'$, $\rho_{200\,K}$ and $T_c$ on tin concentration in $Nb_{1-x}Sn_xSe_2$.

from Fig. 3 that the compound with $x=0.15$ is the most ''defective,'' and the compound with $x=0.4$ is the least ''defective'' from the point of view of resistivity and the magnitude of the CDW-effect.

It can be seen from Fig. 2 that the $\rho'(T)$ dependences are qualitatively similar for different Sn concentrations. The solid curve shown in Fig 2 is the temperature derivative of the function $f_{s-d}(T)=A(T/\Theta)^3J_3(\Theta/T)$, where $\Theta$ is the Debye temperature ($\Theta=222$ K),[2] and $J_n(x)\int_0^x e^z(e^z-1)^{-2}z^n dz$ is the Debye integral. This curve is in qualitative agreement with the experimental dependence except in the vicinity of the CDW-transition and the high- temperature region $T>100$ K. The function $f_{s-d}(T)$ describes the temperature dependence of the resistivity of a metal containing $s$- and $d$-band electrons for the case when phonon-induced $s-d$ transitions dominate.[3] An approximation of the experimental results by the function

$$\rho_{id}(T)=\rho_0+A(T/\Theta)^3J_3(\Theta/T) \quad (1)$$

shows that at temperatures below $T_d$, i.e., in the range of existence of charge density waves, the value of the parameter A is much larger, and of $\rho_0$ smaller, than the corresponding values for $T>T_d$. Table I shows the values of the parameters A and $\rho_0$ before ($T_c<T<20$ K) and after ($T>40$ K) the CDW-transition. Thus, although the overall variation of $\rho(T)$ in the CDW transition region is small,[2] contributions from individual mechanisms of electron scattering undergo significant variations.

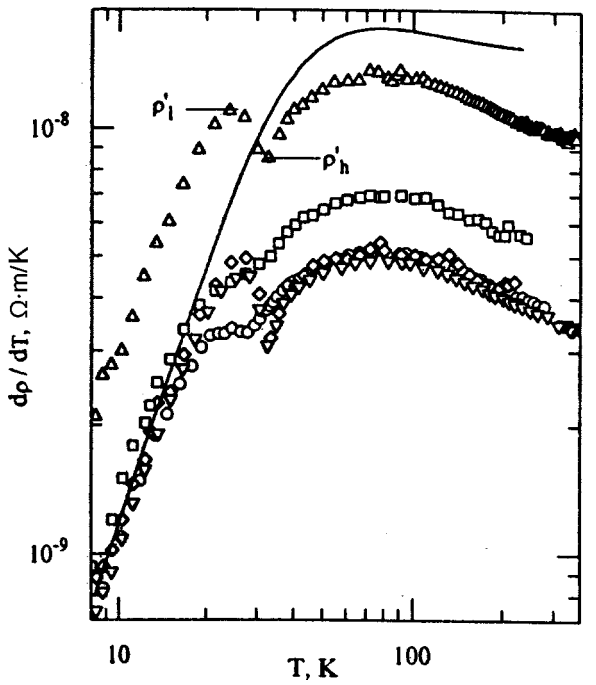


FIG. 2. Temperature dependence of the derivative $d\rho/dT$ for $Nb_{1-x}Sn_xSe_2$. The notation is the same as in Fig. 1. The solid curve shows the temperature derivative of the function $f_{s-d}(T)$ (see formula (1)).

TABLE I. Approximation parameters for resistivity of $Nb_{1-x}Sn_xSe_2$.

| | $x$ | | | | |
|---|---|---|---|---|---|
| Parameter, Ω·m | 0.00 | 0.15 | 0.30 | 0.40 | 0.45 |
| $\rho_0(T<20\text{ K}),\ 10^{-8}$ | 5.56 | 9.49 | 11.35 | 2.13 | 2.26 |
| $\rho_0(T>40\text{ K}),\ 10^{-8}$ | 8.95 | 13.50 | 21.50 | 6.85 | 6.50 |
| $A(T<20\text{ K}),\ 10^{-6}$ | 5.85 | 7.90 | 17.00 | 6.85 | 6.06 |
| $A(T>40\text{ K}),\ 10^{-6}$ | 2.12 | 2.88 | 5.49 | 2.15 | 2.04 |

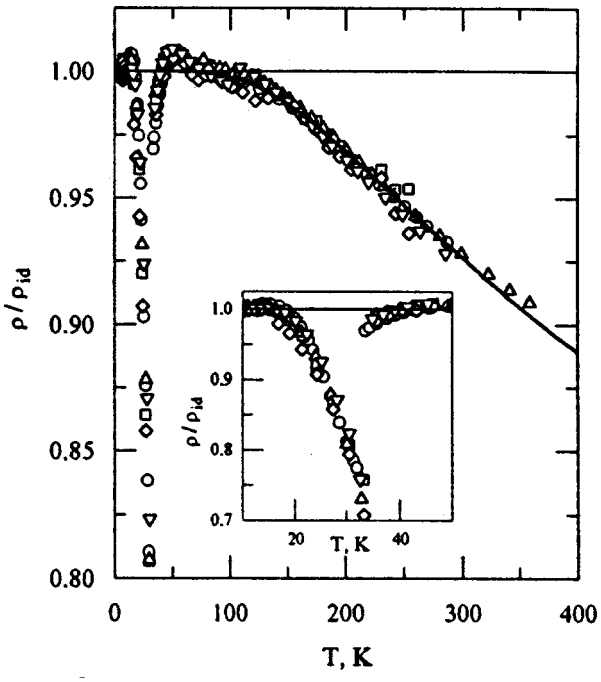


FIG. 4. Departure of the experimental values of resistivity $\rho$ from the function $\rho_{id}(T)=\rho_0+A(T/\Theta)^3 J_3(\Theta/T)$ for $Nb_{1-x}Sn_xSe_2$ (the notation is the same as in Fig. 1). Solid curves correspond to approximation by the function $[1+0.48\exp(-540/T)]^{-1}$. The inset shows the temperature dependence of $\rho/\rho_{id}$ in the vicinity of the CDW transition.

The absolute value of resistivity is maximum for $x=0.3$ (see Fig. 3). For $T>T_d$, the dependences $\rho(T)$ are quite close for pure $NbSe_2$ and for compounds with tin concentrations close to the metal–insulator transition ($x=0.4$ and $x=0.45$) (Fig. 1).

At temperatures above 100 K, the experimental dependences $\rho(T)$ deviate from the approximate expression given by (1) towards decreasing resistivity. Such an effect of resistivity ''saturation'' is also observed in other compounds with a d-band.[4,5] The deviation of the experimental values of resistivity from the approximate relation (1) is represented in Fig. 4 in the form of the ratio $\rho/\rho_{id}$. It can be seen that these deviations practically fall on a single curve for all samples, which is approximated quite well for $T>T_d$ by the expression $[1+\beta\exp(-E/T)]^{-1}$ ($\beta=0.48$, $E=540$ K). A similar expression was also used for describing the high-temperature dependences $\rho(T)$ for transition metal alloys[6] and associated with the additional contribution to the conductivity of electron states in one of the bands the energy at whose bottom exceeds the Fermi energy $E_F$ by an amount $E$. Considering the complex structure of the energy bands of $NbSe_2$,[7] and the fact that Nb states make the dominating contribution to the electronic properties of $NbSe_2$, the interpretation offered by Claisse et al.[6] can also be applied to the present case.

Peculiarities of the transport properties observed for the system $Nb_{1-x}Sn_xSe_2$ can be interpreted unambiguously by taking into consideration the existence of a sharp peak on the density of $d$-states near the Fermi energy.[7] In the rigid-band model, an increase in the value of $x$ changes the band occupancy, and $E_F$ crosses the peak of the density of $d$-states at a tin concentration $x\approx 0.3$, which corresponds to the maximum value for the constant A (the expression[3] for the constant $A$ contains the ratio $N_d/N_s$, where $N_d$ and $N_s$ represent the density of $d$- and $s$-electrons, respectively, at the Fermi level).

Figure 3 shows the dependence of the superconducting transition temperature $T_c$ on $x$, the width of the transition being about 0.2 K for all samples. Note that the dependence $T_c(x)$ is weak although, like resistivity, the superconducting transition temperature is also sensitive to the density of states at the Fermi level. It is possible that in this case, we can use the results obtained by Hopfield[8] who showed that for transition metals, the electron-phonon interaction constant with which the value of $T_c$ is associated depends not on the total density of states $N(E_F)$, but on the partial density of all electron states at the Fermi level with the exception of the $d$-state (the contribution from $p$-type states dominates in the case of transition metals). Consequently, a weak dependence of the density of $s$- and $p$-states on $x$ in $Nb_{1-x}Sn_xSe_2$ leads to a weak variation of $T_c$.

It can also be assumed that, since niobium diselenide belongs to superconductors with a strong coupling[9,10] for which McMillan's relation

$$T_c=\frac{\Theta}{1.45}\exp\left[-\frac{1.04(1+\lambda)}{\lambda-\mu^*(1+0.62\lambda)}\right], \tag{2}$$

holds, $\lambda$ being the electron–phonon coupling constant and $\mu^*$ the effective parameter of Coulomb interaction, the weak variation of $T_c$ upon an increase in tin concentration can be due to renormalization of the electron–phonon coupling constant associated with the introduction of a heavy impurity (the ratio of atomic masses of Sn and Nb is $\sim 1.27$).

### 3.2. Thermal Conductivity

Figure 5 shows the experimental results on the thermal conductivity of the compounds $Nb_{1-x}Sn_xSe_2$ with $x=0,0.15,0.3$, and 0.6. No sharp variation was observed in the temperature dependence of the thermal conductivity in the vicinity of the superconducting transition, which is in accord with the results obtained by Roeske et al.[11] The thermal conductivity of samples with metal conductivity ($x<0.5$) increases with temperature above 100 K, i.e., at the same temperatures where noticeable departures from the dependence (1) are observed. Similar peculiarities were also observed for other metallic compounds with a $d$-band, e.g., $V_3Si$,[5], $TiSe_2$,[12] and $TaSe_2$.[13] However, no such increase is observed in the semiconducting sample $Nb_{0.4}Sn_{0.6}Se_2$ whose room-temperature resistivity is of the order of 0.1 $\Omega\cdot$m. The fact that the semiconducting compound does not display an increase in the value of $\lambda(T)$ indicates unambiguously that this peculiarity is directly related with the electron subsystem.

In order to determine the main mechanism of thermal resistivity in $Nb_{1-x}Sn_xSe_2$, we approximated the experimental data under the assumption that the total thermal conductivity $\lambda$ can be treated as the sum of electron ($\lambda_e$) and phonon ($\lambda_{ph}$) components. In the region of elastic scattering of electrons, the electronic component of thermal conductivity in the normal state is defined by the Wiedemann-Franz law

$$\lambda_e^n=L_0T/\rho, \tag{3}$$

TABLE II. Approximation parameters for thermal conductivity of $Nb_{1-x}Sn_xSe_2$.

| | $x$ | | |
|---|---|---|---|
| Parameter | 0.00 | 0.30 | 0.60 |
| $K_1$, $10^{-42}$ s$^3$ | 1.25 | 4.05 | 14.3 |
| $K_2$, $10^{-30}$ K$^{-1}\cdot$s$^2$ | – | – | 1.34 |
| $K_3$, $10^{-17}$ s | 5.15 | 7.7 | 12.8 |
| $d$, mm | 110 | 75 | 190 |
| $b$ | – | – | 6 |
| $l_{\min}$, $10^{-9}$ m | – | – | 2.2 |
| $K_4$, $10^{-4}$ | 0.3 | 200 | – |

where $L_0=2.45\times10^{-8}\mathrm{W}\cdot\Omega/\mathrm{m}$. The phonon component of thermal conductivity was approximated by using the formula[14]

$$\lambda_{\mathrm{ph}}=\frac{k_b}{2\pi^2 v}\left(\frac{k_b}{\hbar}\right)^3 T^3\int_0^{\Theta/T}\frac{y^4e^y}{(e^y-1)^2\tau^{-1}(y,T)}\,dy, \qquad (4)$$

where $y=\hbar\omega/k_bT$ ($\omega$ is the phonon frequency), $v$ the average velocity of sound, and $\tau(y,T)$ the total phonon relaxation time. The parameters $\Theta$ and $v$ were not determined separately for each sample, but since the elastic properties of $NbSe_2$ and $SnSe_2$ do not differ significantly,[15,16] identical values $\Theta=222$ K$^2$ and $v=1.75\times10^3$m/s[17] were used for approximating the thermal conductivity of all $Nb_{1-x}Sn_xSe_2$ samples.

The contribution of electrons in heat transport and phonon scattering is negligibly small in the semiconducting sample $Nb_{0.4}Sn_{0.6}Se_2$. It was found that the temperature dependence of the thermal conductivity of $Nb_{0.4}Sn_{0.6}Se_2$ is best approximated (the error in the temperature interval 2– 300 K is $\sim1.8\%$) by using the following expression for $\tau^{-1}$:

$$\tau^{-1}=\tau_b^{-1}+K_1\omega^4+K_2T\omega^3\,\exp\left(-\frac{\Theta}{bT}\right)+K_3\omega^2. \qquad (5)$$

The first term on the right-hand side $\tau_b^{-1}=v/d$ corresponds to the scattering of phonons at the sample boundaries ($d$ is the corresponding mean free path), the second term corresponds to Rayleigh scattering at point defects, and the third to phonon-phonon umklapp processes. A fourth term proportional to $\omega^2$ had to be introduced for describing the low-temperature segment of the dependence $\lambda(T)$. An analogous contribution to the phonon scattering was also reported in other works devoted to the thermal conductivity of layered dichalcogenides.[9,18] Khadjai et al[19] attributed the contribution to the relaxation rate proportional to $\omega^2$ to phonon scattering by crystal lattice distortion fields produced by point defects in layered crystals.

In order to approximate the experimental data in the high-temperature region, the minimum possible mean free path $v\tau$ of phonons had to be restricted to the minimum length $l_{\min}$. The existence of the smallest possible high-temperature thermal conductivity defined by $l_{\min}$ was analyzed by Cahill et al.[20] for materials with a strong phonon scattering.

The values of approximation parameters $K_1, K_2, K_3, b, d$ and $l_{\min}$ are presented in Table II.

An estimation of the electron contribution to the thermal conductivity of $Nb_{1-x}Sn_xSe_2$ samples with a metal-type conductivity ($x<0.5$) in the normal state carried out by using formula (3) showed that $\lambda_e^n$ amounts to 10–30% of the total thermal conductivity. A precise splitting of the thermal conductivity into components $\lambda_e$ and $\lambda_{\mathrm{ph}}$ was carried out for samples of $NbSe_2$ and $Nb_{0.7}Sn_{0.3}Se_2$ at temperatures below 10 K, where elastic scattering of electrons at defects dominates ($\rho\approx\rho_0$) (see Fig. 1). The validity of Wiedemann–Franz law for $NbSe_2$ at $T<10$ K was confirmed in the experimental work of Roeske et al.[11] The electronic thermal conductivity in the superconducting state was approximated by formula $\lambda_e^s=\lambda_e^n f(T/T_c)$, the function $f(T/T_c)$ being defined in Ref. 21. The scattering of phonons by electrons was taken into account by introducing the term $K_4\omega g[\Delta(T),T,\omega]$, where $K_4$ is a constant, and the function $g[\Delta(T),T,\omega]$ is also defined in Ref. 21, and $\Delta(T)$ is the band gap. The value $\Delta(0)=1.76k_b\cdot T_c$ from the BCS theory was used in the approximation, and the temperature dependence $\Delta(T)/\Delta(0)$ was tabulated in Ref. 22.

Below 10 K, the phonon–phonon scattering does not make any contribution to the thermal resistivity, and hence the corresponding term in (5) was omitted during approximation. The values of parameters $K_1, K_3, K_4$, and $d$ for $NbSe_2$ and $Nb_{0.7}Sn_{0.3}Se_2$ are presented in Table II. It was found that the experimental results cannot be approximated quite well in the temperature range $T<T_c$ by assuming that all phonons are scattered by electrons. It is well known[23] that the acoustic vibrations polarized across the layers in layered materials are virtually not scattered by electrons. Hence we carried out computations under the assumption that phonons belonging to one of the three acoustic branches are not scattered by electrons , i.e., the corresponding coefficient $K_4\equiv0$ for them (the remaining coefficients were the same for all vibrational branches). Such an assumption made it possible to approximate with a good degree of precision (to within 1.5%) the experimental thermal conductivity data both in normal and superconducting states (solid curves in Fig. 5). The use of independent sets of approximation coefficients for each of the three acoustic phonon branches[24] would enormously increase the number of fitting parameters as well as the uncertainty associated with them.

Note that the behavior of the thermal conductivity in the vicinity of $T_c$ can also be approximated satisfactorily under the assumption that phonons belonging to all three acoustic branches are scattered identically by electrons, but by using the value $\Delta(0)/k_bT_c=1.1$ instead of the value 1.76 from the BCS theory. However, it was shown experimentally[25] that the band gap in $NbSe_2$ is close to the theoretical value, and hence we assume that the former assumption is more realistic.

Analyzing the obtained values of the approximation parameters (Table II), we observe that the coefficient $d$ is close to the thickness of the corresponding sample. For samples with $x>0$, the values of the parameters $K_1$ and $K_3$ are larger than for pure $NbSe_2$ because of a larger number of defects in the samples upon replacement of Nb by Sn. The value of $K_4$ determined by the electron–phonon interaction is much higher for $Nb_{0.7}Sn_{0.3}Se_2$ than for $NbSe_2$, which is in accord

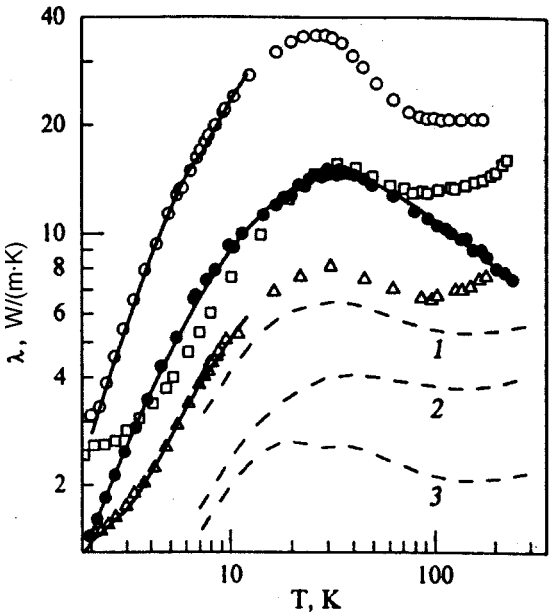


FIG. 5. Temperature dependence of the thermal conductivity of $Nb_{1-x}Sn_xSe_2$ (● correspond to $x=0.6$, rest of the notation is the same as in Fig. 1). Solid curves correspond to approximation (see text). The dashed curves estimate the electronic contribution calculated according to the Wiedemann- Franz law $\lambda_e = L_0 T/\rho$ (curve *1* corresponds to $NbSe_2$, curve *2* to $Nb_{0.85}Sn_{0.15}Se_2$, and curve *3* to $Nb_{0.7}Sn_{0.3}Se_2$.

with the values of the parameter $A$ for resistivity (Table I). The assumption that the electron density of states at the Fermi level is maximum for the compound $Nb_{0.7}Sn_{0.3}Se_2$ explains the increase in the value of $K_4$ as well as $A$. The phonon–electron scattering coefficient is defined as follows[24]:

$$K_4 = \frac{(m^*)^2 C_D^2}{2\pi D_0 v \hbar^3}, \tag{6}$$

where $m^*$ is the effective electron mass, $C_D$ is the deformation potential, and $D_0$ the density. Obviously, the proximity of the Fermi level to the sharp density of states peak for $Nb_{0.7}Sn_{0.3}Se_2$ leads to an increase in the value of both $m^*$ and $C_D$. Since these quantities are quadratic in formula (6), the value of the parameter $K_4$ increases much more sharply than parameter $A$ upon a transition from $NbSe_2$ to $Nb_{0.7}Sn_{0.3}Se_2$.

## CONCLUSION

A transition to the charge density wave state in the compound $Nb_{1-x}Sn_xSe_2$ samples leads to a decrease in the residual resistivity (scattering of phonons by defects) and an increase in the electron–phonon scattering. An increase in the tin concentration beyond $x=0.15$ enhances the effect of CDW-transition on the resistivity. The strongest electron–phonon scattering is observed for the compound with $x=0.3$. For samples with metal-type conductivity, mutually correlating deviations of thermal conductivity and electrical resistivity are observed at temperatures above 100 K. The observed peculiarities in the electrical resistivity, electronic thermal conductivity and phonon scattering by electrons for $Nb_{1-x}Sn_xSe_2$ samples are apparently associated with the fact that replacement of Nb by Sn changes the occupancy of the *d*-band whose density of states has a sharp peak in the vicinity of the Fermi level.

To approximate the thermal conductivity of $Nb_{1-x}Sn_xSe_2$ with an accuracy close to the experimental one, we must introduce into the total phonon relaxation time a term proportional to the square of frequency. At high temperatures, the phonon mean free path is restricted to a certain minimum value.

The behavior of thermal conductivity in the superconducting transition region points towards a weak interaction between electrons and a part of the phonon spectrum, most probably the vibrations polarized at right angles to the layers.

*E-mail: george.ya.khadjai@univer.kharkov.ua

[1] M. Ikebe, K. Katagiri, K. Noto, and K. Muto, Physica B **99**, 209 (1980).
[2] J. M. E. Harper, T. H. Geballe, and F. J. DiSalvo, Phys. Rev. B **15**, 2943 (1977).
[3] L. Colquitt, Jr., J. Appl. Phys. **36**, 2454 (1965).
[4] M. Nunez-Regueiro, Solid State Commun. **60**, 797 (1986).
[5] A. F. Khoder, M. Couach, M. Locatelli *et al.*, J. Phys. **42**, 383 (1981).
[6] F. Claisse, M. Cormier, and C. Frigout, High Temp.-High Press. **4**, 395 (1972).
[7] L. F. Mattheiss, Phys. Rev. Lett. **30**, 784 (1973).
[8] J. J. Hopfield, Phys. Rev. **186**, 443 (1969).
[9] D. Prober, R. Schwall, and M. Beasly, Phys. Rev. B **21**, 2717 (1981).
[10] Kh. B. Chashka, M. A. Obolenskii, V. I. Beletskii, and V. N. Beilinson, Fiz. Nizk. Temp. **12**, 865 (1986) [Sov. J. Low Temp. Phys. **12**, 491 (1986)].
[11] F. Roeske, H. R. Shanks, and D. K. Finnemore, Phys. Rev. B **16**, 3929 (1977).
[12] M. Nunez-Regueiro, C. Ayache, and M. Locatelli, Physica B & C **108**, 1035 (1981).
[13] M. Nunez-Regueiro, J. Lopez Castello, and C. Ayache, Lect. Notes Phys. **217**, 137 (1985).
[14] R. Berman, *Thermal Conduction*, Oxford Univ. Press, Oxford (1976).
[15] J.-Y. Harbec, B. M. Powell, and S. Jandl, Phys. Rev. B **28**, 7009 (1983).
[16] N. Wakabayashi, H. G. Smith, and R. Shanks, Phys. Lett. **50A**, 367 (1974).
[17] R. Lagnier, C. Ayache, J.-Y. Harbec *et al.*, Solid State Commun. **48**, 65 (1983).
[18] E. K. Sichel, B. Serin, and J. F. Revelli, J. Low Temp. Phys. **16**, 229 (1974).
[19] G. Ya. Khadjai, B. A. Merisov, and A. V. Sologubenko, Phys. Status Solidi B **200**, 413 (1997).
[20] D. J. Cahill, S. K. Watson, and R. O. Pohl, Phys. Rev. B **46**, 6131 (1992).
[21] J. Bardeen, G. Rickayzen, and L. Tewordt, Phys. Rev. **113**, 982 (1959).
[22] B. Muhlschlegel, Z. Phys. **155**, 313 (1959).
[23] M. Kaveh, M. F. Cherry, and M. Weger, J. Phys. **C14**, L789 (1981).
[24] J. Ziman, *Electrons and Phonons*, Oxford (1960).
[25] L. N. Bulaevskii, Usp. Fiz. Nauk **116**, 449 (1975) [Sov. Phys. Usp. **18**, 514 (1975)].

Translated by R. S. Wadhwa

# Orientation effect in sound absorption by layered conductors

O. V. Kirichenko, D. Krstovska, and V. G. Peschansky

*B. Verkin Institute for Low Temperature Physics and Engineering, National Academy of Sciences of the Ukraine, 310164 Kharkov, Ukraine**

(Submitted October 28, 1997)
Fiz. Nizk. Temp. **24**, 367–370 (April 1998)

It is shown that the damping decrement for acoustic waves in a layered conductor with a quasi-two-dimensional electron energy spectrum depends considerably on the orientation of the magnetic field relative to the layers in a wide range of magnetic fields if charge carriers can drift along the sound wave vector. The positions of extrema on the angular dependence of the sound damping decrement contain detailed information on the Fermi surface. © *1998 American Institute of Physics.* [S1063-777X(98)01304-8]

Layered conductors having a strong anisotropy of metal-type electrical conductivity and placed in a magnetic field **H** exhibit a number of effects typical of quasi-two-dimensional conductors,[1–9] such as acoustic transparency stimulated by the magnetic field and the orientation effect, i.e., the presence of sharp peaks and narrow valleys on the dependences of kinetic characteristics on the angle $\theta$ between the normal **n** to the layers and the vector of a strong magnetic field when the radius of curvature $r$ of a conduction electron is much smaller than not only its mean free path $l$, but also the electromagnetic or acoustic wavelength $1/k$. It will be shown below that the orientation effect is possible in a wider range of magnetic fields including the case when $kr \gg 1$ if charge carriers can drift in the magnetic field along the sound wave vector $k$. The energy of charge carriers in quasi-two-dimensional conductors

$$\varepsilon(\mathbf{p}) = \sum_{n=0}^{\infty} \varepsilon_n(p_x, p_y)\cos(anp_z/h) \tag{1}$$

depends weakly on the momentum component $p_z = \mathbf{p}\cdot\mathbf{n}$, and their drift along the magnetic field is negligibly small, while charge carriers in two-dimensional conductors, for which all the components with a nonzero $n$ in formula (1) are equal to zero, do not drift at all. The coefficients of the cosines in formula (1) decrease strongly with increasing $n$ so that the maximum value of the function $\varepsilon_1(p_x, p_y)$ on the Fermi surface $\varepsilon(\mathbf{p}) = \varepsilon_F$ is equal to $\eta\varepsilon_F \ll \varepsilon_F$. The drift velocity of charge carriers along **k** is proportional to $\eta$, and the orientation effect can occur only in perfect single crystals in which the drift over the mean free time $\tau$ is much larger than the sound wave length.

Let an acoustic wave propagate in the plane of the layers along the $x$-axis. It follows from the equation

$$\frac{d\mathbf{p}}{dt} = \frac{e}{c}[\mathbf{v}\times\mathbf{H}] \tag{2}$$

of motion of a charge in a magnetic field that for $\mathbf{H} = (H\sin\theta, 0, H\cos\theta)$, the following equation holds for the velocity components averaged over the period of motion $T = 2\pi m^* c/eH$:

$$\overline{v_x} = \tan\theta\,\overline{v_z}; \quad \overline{v_\alpha} = \frac{1}{T}\int_0^T v_\alpha(t_H)dt_H. \tag{3}$$

The displacement of an electron over a period of motion along the wave vector is given by

$$\begin{aligned}\overline{v_x}T &= -\tan\theta\sum_{n=1}^{\infty}\left(\frac{an}{h}\right)\int_0^T dt\varepsilon_n(t,p_H)\sin\left(\frac{anp_z}{h}\right)\\ &= -\tan\theta\sum_{n=1}^{\infty}\left(\frac{an}{h}\right)\int_0^T dt\varepsilon_n(t,p_H)\sin\left\{\frac{anp_H}{h\cos\theta}\right.\\ &\quad \left. -\frac{anp_x(t,p_H)\tan\theta}{h}\right\}.\end{aligned} \tag{4}$$

If we take into account the fact that $p_x$ and $p_y$, and hence $\varepsilon_n$, depend weakly on the integral of motion $p_H = p_x\sin\theta + p_z\cos\theta$ in a magnetic field, the electron drift velocity along **k** in the main approximation in the small parameter of quasi-two-dimensionality $\eta$ of the electron energy spectrum assumes the form

$$\overline{v_x} = -\tan\theta\ \mathrm{Im}\sum_{n=1}^{\infty}\left(\frac{an}{h}\right)\exp\left\{\frac{ianp_H}{h\cos\theta}\right\}I_n(\tan\theta), \tag{5}$$

where

$$I_n(\tan\theta) = T^{-1}\int_0^T dt\varepsilon_n(t)\exp\left\{-ianp_x(t,p_H)\frac{\tan\theta}{h}\right\}. \tag{6}$$

It can easily be seen that the principal term in formula (5), which is proportional to $I_1(\tan\theta)$, vanishes at certain values of $\tan\theta$, and the angle $\theta$ has many values $\theta_c$ near the zeros of the function $I_1(\tan\varphi)$, for which the drift velocity $\overline{v_x}$ of charge carriers along the sound wave vector coincides with the velocity $s$ of propagation of an acoustic wave, and their interaction with the wave is most effective. Consequently, we can expect the presence of narrow peaks on the curve describing the dependence of the damping decrement of sound waves

$$\Gamma = Q/\rho\omega^2 u^2 s \tag{7}$$

 

on the orientation of the magnetic field relative to the layers.

Here $e$ and $m^*$ are the charge and cyclotron effective mass of a conduction electron, $t_H$ the time of its motion in the magnetic field, $c$ the velocity of light, $a$ the separation between layers, $h$ Planck's constant, $\rho$ the density of the crystal, $u$ the displacement of ions, and $s$ the velocity of propagation of the acoustic wave with frequency $\omega$, which will be regarded as monochromatic in the subsequent analysis. The dissipative function $Q$ can easily be found if we know the solution of the Boltzmann kinetic equation for the charge carrier distribution function $f(\mathbf{p},\mathbf{r},t)$:

$$\frac{\partial f}{\partial t}+\frac{\mathbf{v}\partial f}{\partial \mathbf{r}}+\left[e\left(\tilde{\mathbf{E}}+\frac{[\mathbf{v}\times\mathbf{H}]}{c}\right)-\frac{\partial\delta\varepsilon}{\partial\mathbf{r}}\right]\frac{\partial f}{\partial\mathbf{p}}=W_{\mathrm{coll}}(f\ ). \quad (8)$$

The collision integral $W_{\mathrm{col}}(f\ )$ vanishes if we substitute into it the equilibrium Fermi distribution function $f_0(\varepsilon-\mathbf{p}\times\dot{\mathbf{u}})$ for charge carriers in the concomitant reference system moving with the velocity $\dot{\mathbf{u}}=\partial\mathbf{u}/\partial t$ of ion displacements.

The electric field in the same reference system, i.e.,

$$\tilde{\mathbf{E}}=\mathbf{E}+\frac{(\tilde{\mathbf{u}}\times\mathbf{H})}{c}+\frac{m\ddot{\mathbf{u}}}{e} \quad (9)$$

can be determined by solving the Maxwell equations

$$\mathrm{curl\ curl}\ \mathbf{E}=\frac{4\pi i\omega}{c^2}\,\mathbf{j}. \quad (10)$$

In the linear approximation in the small strain tensor $u_{ij}=\partial u_i/\partial x_j$ for the crystal lattice, the solution of the kinetic equation for the nonequilibrium distribution function $f=f_0(\varepsilon-\mathbf{p}\dot{\mathbf{u}})-\psi(\mathbf{p},\mathbf{r})\exp(-iwt)\partial f_0/\partial\varepsilon$ for charge carriers in the $\tau$- approximation for the collision integral $W_{\mathrm{coll}}(f\ )=(f_0-f\ )/\tau$ assumes the form

$$\psi=[\exp(\nu T+i\mathbf{k}\cdot\overline{\mathbf{v}}T)-1]^{-1}\int_t^{t+T}dt'[g(t')+h(t')]\exp\{i\mathbf{k}\cdot[\mathbf{r}(t')-\mathbf{r}(t)]+\nu(t'-t)\}, \quad (11)$$

where $\nu=1/\tau-i\omega$, $q(t)=-i\omega\Lambda_{ji}(t)k_iu_j$, $h(t)=e\mathbf{v}(t)\cdot\tilde{\mathbf{E}}$, and the components of the deformation potential tensor $\Lambda_{ij}(\mathbf{p})$ describe the energy renormalization of conduction electrons under the action of crystal deformation

$$\delta\varepsilon=\Lambda_{ij}(\mathbf{p})u_{ij} \quad (12)$$

taking into account the conservation of the number of charge carriers. Here and below, the subscript ''$H$'' on $t_H$ is omitted. Using the solution of the kinetic equation (11), we can calculate the dissipative function by using the formula

$$Q=\frac{2eH}{c(2\pi h)^3}\int d\varepsilon\,\delta(\varepsilon-\varepsilon_F)\int dp_H\times\int_0^T dt\,\psi\hat{W}_{\mathrm{coll}}(\psi)\equiv\langle\psi\hat{W}_{\mathrm{coll}}(\psi)\rangle. \quad (13)$$

For $kr\gg1$, the integrand in formula (11) is a rapidly oscillating alternating function $t'$, and we can use the stationary phase method for calculating the dissipative function

$$Q=\left\langle\frac{|\psi|^2}{\tau}\right\rangle=\left\langle\frac{\int_t^{t+T}dt'g(t')\int_t^{t+T}dt''g^*(t'')\exp\{i\mathbf{k}\cdot[\mathbf{r}(t')-\mathbf{r}(t'')]\}}{2\tau[\cosh(T/\tau)-\cos(k\overline{v_x}-\omega)T]}\right\rangle. \quad (14)$$

In the numerator of this expression we have omitted small corrections in the parameters $T/\tau\ll1$ and $\omega T\ll1$. Assuming that the cross section of the Fermi surface by the plane $p_H=\mathrm{const}$ contains not more than two points of the stationary phase, at which charge carriers move in phase with the wave, i.e., $v_x(t_1)=v_x(t_2)=s$, we obtain the following expression for $Q$:

$$Q=\frac{2eH}{c(2\pi h)^3}\times\int_0^{2\pi h\cos\theta/a}dp_H\,\frac{(T/\tau)2\pi/kv_x'(t_1)}{(T/\tau)^2+4\sin^2(k\overline{v_x}-\omega)T/2}\times\{|g_1|^2[1+\sin(k\Delta x)]+|h_1|^2[1-\sin(k\Delta x)]-ig_1(h_1-h_1^*)\cos(k\Delta x)\}, \quad (15)$$

where $g_1=g(t_1)$, $h_1=h(t_1)$, the asterisk marks complex conjugate values, and

$$\Delta x=x(t_2)-x(t_1)=\frac{[p_y(t_1)-p_y(t_2)]c}{eH\cos\theta}+\tan\theta\int_{t_1}^{t_2}v_2(t,p_H)dt. \quad (16)$$

If the displacement of the electron along $\mathbf{k}$ over the period $T$ is much smaller than the acoustic wave length, i.e., $kr\eta\tan\theta\ll1$, the value of $k\Delta x$ weakly depends on $p_H$, and the expression in the braces in formula (14) can be taken outside the integral. However, the denominator depends significantly on $p_H$ for $kl\eta\tan\theta\gg1$ since $\overline{v_x}$ oscillates upon variation of $p_H$. After simple calculations, for $1\ll kl\eta\tan\theta\ll l/r$ we obtain

$$Q=\frac{L(\alpha)eHh\tau\cos\theta}{akvc(2\pi h)^3}\{|g_1|^2[1+\sin(k\Delta x)]+|h_1|^2[-1\sin(k\Delta x)]-ig_1(h_1-h_1^*)\cos(k\Delta x)\}, \quad (17)$$

where $\alpha=k\overline{v_x}\tau$, and

$$L(\alpha)=(2/\pi)\int_0^{\pi/2}d\phi\,\frac{1}{1+\alpha^2\sin^2\phi}. \quad (18)$$

In formulas (15) and (17), we have omitted insignificant corrections in the small parameter equal to the ratio of the velocity of sound to the Fermi velocity $v$ of conduction electrons in the plane of the layers. If we use the approximation of the quadratic momentum dependence of the function $\varepsilon_0(p_x,p_y)$, the quantity $\alpha$ assumes the form

$$\alpha=kl\eta\tan\theta\,J_0\,\frac{aD_p}{2h}\tan\theta, \quad (19)$$

where $J_0$ is the Bessel function having an infinite number of zeros on the real axis, and $D_p$ is the diameter of the Fermi surface along the axis $p_y$.

Maxwell's equations (10) make it possible to find the relation between the function $h$ and the ion displacement $u$. Using the solution of the kinetic equation (11), we can easily find the expression for the current density $j_i(x)=\langle ev_i\psi\rangle$, which has the following form in the Fourier representation:

$$j_i(x)=\int dk\ \exp(ikx)[\sigma_{ij}(k)\tilde{E}_j(k)+a_{ij}(k)k\omega u_j(k)]. \tag{20}$$

Here $\tilde{E}_j(k)$ and $u_j(k)$ are Fourier transforms of electric field and ion displacement, while the acoustoelectron coefficients are given by the formulas

$$\sigma_{ij}(k)=e^2\left\langle v_i(t)\int_{-\infty}^{t}dt'F(t,t',k)v_j(t')\right\rangle, \tag{21}$$

$$a_{ij}(k)=e\left\langle v_i(t)\int_{\infty}^{t}dt'F(t,t',k)\Lambda_{jx}(t')\right\rangle, \tag{22}$$

where $F(t,t',k)=\exp\{\nu(t'-t)+ik[x(t')-x(t)]\}$. In the case of a longitudinal acoustic wave, in the main approximation in the small parameter $\eta$ we have

$$h(t)=uev_y(t)\ \frac{i\omega H\ \cos\ \theta/c+\xi k\omega\tilde{a}_{yx}}{1-\xi\tilde{\sigma}_{yy}}. \tag{23}$$

The acoustoelectron coefficients $\tilde{\sigma}_{yy}=\sigma_{yy}-\sigma_{yx}\sigma_{xy}/\sigma_{xx}$ and $a_{yx}=a_{yx}-a_{xx}\sigma_{yx}/\sigma_{xx}$ can be calculated easily for $kr\gg 1$ on the basis of the stationary phase method. For infinitely small values of $\eta$, we have

$$\tilde{\sigma}_{yy}=\frac{\sigma_0}{kD}\,[1-\sin(kD)]L(\alpha), \tag{24}$$

$$\tilde{a}_{yx}=-i\ \frac{\sigma_0\Lambda}{kDev}\cos(kD)L(\alpha), \tag{25}$$

where $\Lambda=\Lambda_{xx}(t_1)$, and $D=cD_p/eH\ \cos\ \theta$.

For $kD=2\pi(n+1/4)$, where $n$ is any integer, we must take into account corrections proportional to $\eta$ in the above formulas for acoustoelectron coefficients. Using formulas (23)–(25) and relations (7) and (17), we obtain the following expression for the damping decrement of a longitudinal acoustic wave:

$$\Gamma=(\omega/v)\ \frac{r/l+\alpha^2(1+\alpha^2)^{-1}\ \sin^2(kD)}{1-\sin(kD)+(r/l)^2}. \tag{26}$$

In the case when $\sin kD$ differs significantly from unity, the acoustic transparency of a layered conductor decreases by a factor of $kl\eta\ \tan\ \theta$ in the presence of charge carrier drift along the wave vector (we omit insignificant factors of the order of unity in formula (26)). For a fixed value of magnetic field and for the values of $\theta=\theta_c$, when the value of $\alpha$ vanishes, the damping decrement of the sound wave as a function of $\tan\ \theta$ assumes the minimum value, while for $\sin kD=-1$ and for the same orientations of the magnetic field relative to the layers of the conductor the latter becomes absolutely transparent. For $\tan\ \theta\gg 1$, the minima in the angular dependence of $\Gamma$ are repeated periodically with the same period as for $kr\ll 1$. From the magnitude

$$\Delta(\tan\ \theta)=2\pi h/aD_p$$

of these periods, we can determine the diameter $D_p$ of the Fermi surface to a sufficiently high degree of accuracy.

We are grateful to the Ministry of Science of the Ukraine for financial support of this research (Grant 2.4/192).

*E-mail: peschansky@ilt.kharkov.ua

[1] V. G. Peschansky, J. A. Roldan Lopez, and Toyi Gnado Yao, J. Phys. (Paris) **1**, 1469 (1991).
[2] V. G. Peschansky, S. N. Savel'eva, and H. Kheir Bek, Fiz. Tverd. Tela (St. Petersburg) **34**, 1640 (1992) [Sov. Phys. Solid State **34**, 871 (1992)].
[3] V. G. Peschansky, H. Kheir Bek, and S. N. Savel'eva, Fiz. Nizk. Temp. **18**, 1012 (1992) [Sov. J. Low Temp. Phys. **18**, 711 (1992)].
[4] O. V. Kirichenko and V. G. Peschansky, J. Phys. (Paris) **4**, 823 (1994).
[5] O. V. Kirichenko and V. G. Peschansky, Fiz. Nizk. Temp. **20**, 574 (1994) [Low Temp. Phys. **20**, 453 (1994)].
[6] V. G. Peschansky, G. Espeho, and Tesgera Bedassa, Fiz. Nizk. Temp. **21**, 971 (1995) [Low Temp. Phys. **21**, 768 (1995)].
[7] V. M. Gokhfeld, O. V. Kirichenko, and V. G. Peschansky, Zh. Éksp. Teor. Fiz. **108**, 2147 (1995) [JETP **81**, 1171 (1995)].
[8] O. Galbova, G. Ivanovski, O. V. Kirichenko, and V. G. Peschansky, Fiz. Nizk. Temp. **22**, 425 (1996) [Low Temp. Phys. **22**, 331 (1996).
[9] O. Galbova, G. Ivanovski, O. V. Kirichenko, and V. G. Peschansky, Fiz. Nizk. Temp. **23**, 173 (1997) [Low Temp. Phys. **23**, 127 (1997).
[10] A. I. Akhiezer, Sov. Phys. JETP **8**, 1338 (1938).

Translated by R. S. Wadhwa

# High-frequency impedance of organic metals in a strong magnetic field

V. M. Gokhfel'd

*A. Galkin Physicotechnical Institute, 340114 Donetsk, Ukraine*

V. G. Peschansky and D. A. Toryanik

*B. Verkin Institute for Low Temperature Physics and Engineering, National Academy of Sciences of the Ukraine, 310164 Kharkov, Ukraine**

(Submitted October 28, 1997)
Fiz. Nizk. Temp. **24**, 371–374 (April 1998)

Propagation of electromagnetic waves is studied theoretically in layered organic conductors with metal-type conductivity, whose Fermi surface (apart from a slightly corrugated cylinder) *a priori* contains two sheets in the form of weakly corrugated planes. It is shown that the presence of such a group of charge carriers significantly affects the magnitude of wave attenuation.
 [S1063-777X(98)01404-2]

The unusual behavior of the magnetoresistance of a family of ion-radical salts with charge transfer based on tetrathiafulvalene of the type $(BEDT\text{-}TTF)_2MHg(SCN)_4$ indicates[1–9] that the Fermi surface of layered organic conductors is quite complicated. One of the types of topological structures of the electron energy spectrum of these materials which explains the experimentally observed field dependence of the resistivity is a Fermi surface containing two quasi-one-dimensional sheets in addition to a weakly corrugated cylinder. These sheets are weakly corrugated planes on which the velocity of charge carriers has a preferred direction in the layer plane.[10,11] A combination of quasi-two-dimensional and quasi-one-dimensional cavities in the Fermi surface of such conductors may be manifested significantly in high-frequency phenomena. By way of an example, let us consider the propagation of electromagnetic waves along layers in a conductor whose charge carriers obey an energy–momentum relation of the type

$$\varepsilon(\mathbf{p})=\frac{p_x^2+p_y^2}{2m}+A\cos\frac{ap_z}{h},\varepsilon_1(\mathbf{p})=\pm p\mathbf{N}v, \tag{1}$$

where $a$ is the separation between layers, $h$ is the Planck's constant, the unit vector $\mathbf{N}$ lies in the plane of the layers and forms an angle $\varphi$ with the direction of wave propagation ($x$-axis).

The conduction electron velocity $v_z$ along the normal $\mathbf{n}$ to the layers depends weakly on the momentum component $p_z=\mathbf{p}\cdot\mathbf{n}$, so that $Aa/h=v_0\eta\ll v_0$, where $v_0$ is the velocity of electrons with Fermi energy $\varepsilon_F=mv_0^2/2$ belonging to the weakly corrugated cylinder and $v$ is the Fermi velocity of charge carriers belonging to a plane sheet on the Fermi surface). In a very strong magnetic field $\mathbf{H}=(0,H\cos\theta, H\sin\theta)$, when the radius of curvature $r$ of the trajectory of charge carriers with a quasi-two-dimensional energy spectrum is much smaller than the skin-depth $\delta$, their contribution to the high frequency current is not sensitive to the state of the surface $x_s=0$ of the conductor since the fraction of electrons colliding with surface boundary and interacting effectively with the electromagnetic field is of the order of $r/\delta$. Electrons with a one-dimensional energy spectrum do not respond to the magnetic field and, as in the case $H=0$, carry information about the field in the skin layer into the bulk of the sample in the form of Reuter–Sondheimer waves[12] with a velocity $v_x=v\cos\varphi$. If the charge carriers are reflected almost specularly at the surface of the conductor, the relation between the Fourier transforms of the electric field and the current density

$$\mathbf{E}(k)=2\int_0^\infty dx\mathbf{E}(x)\cos(kx),$$

$$\mathbf{j}(k)=2\int_0^\infty dx\mathbf{j}(x)\cos(kx) \tag{2}$$

can be treated as local:

$$j_i(k)=\{\sigma_{ij}(k)+\sigma_{ij}^{(1)}(k)\}E_j(k). \tag{3}$$

The contribution to the rf conductivity components of charge carriers with a quasi-two-dimensional energy spectrum has the form

$$\sigma_{ij}(k)=\frac{2e^3H}{c(2\pi H)^3}\int dp_H\int_0^T dtv_i(t,p_H)\times\int_{-\infty}^t dt'v_j(t',p_h)\exp\{\nu(t'-t)\}\times\cos k\{x(t',p_H)-x(t,p_H)\}\equiv\langle e^2v_i\hat{R}v_j\rangle, \tag{4}$$

while the contribution to the electrical conductivity

$$\sigma_{ij}^{(1)}(k)=\sigma_1(k)N_iN_j,\quad \sigma_1(k)=\frac{\omega_1^2\nu_1}{(\mathbf{k}\cdot\mathbf{v})^2+\nu_1^2}, \tag{5}$$

from charge carriers with an energy–momentum relation $\varepsilon_1(p)=\pm\mathbf{p}\cdot\mathbf{N}v$ is obviously independent of the magnetic field.

Here, $e$ is the electron charge, $\nu_1=1/\tau_1-i\omega$, $\tau_1$ and $\omega_1$ are the mean free time and frequency of plasma oscillations of conduction electrons with a one-dimensional energy spec-

 

trum, $T=2\pi mc/eH\cos\theta$ is the time period during which the charge carriers belonging to a quasi-two-dimensional Fermi surface cavity move along a closed orbit, $\nu=1/\tau-i\omega$, and $\tau$ is the mean free time of charge carriers. The component of the electron momentum along the magnetic field $p_H=p_y\sin\theta+p_z\cos\theta$ is an integral of motion in view of the equality

$$dp/dt=(e/c)(\partial\varepsilon(\mathbf{p})\partial\mathbf{p}\times\mathbf{H}). \tag{6}$$

We assume that the electromagnetic wave is monochromatic and has a frequency $\omega$, while $t$ and $t'$ in formula (4) are the times during which the charge moves in a magnetic field. Integration in formula (4) is carried out over all states of charge carriers with Fermi energy $\varepsilon_F$.

Using Maxwell's equation in Fourier representation

$$[k^2-\omega^2/c^2]E_\alpha(k)-4\pi i\omega j_\alpha(k)/c^2=-2E'_\alpha(0),$$

$$\alpha=(y,z) \tag{7}$$

we can easily determine the Fourier transforms of varying electric field, and then use inverse Fourier transformation to determine the electric field distribution in the conductor also.

The skin depth can be determined easily with the help of the dispersion equation

$$\det\{\delta_{\alpha\beta}-\xi\tilde{\sigma}_{\alpha\beta}(k)\}=0;\alpha,\beta=(y,z), \tag{8}$$

where $\xi=4\pi i\omega/(k^2c^2-\omega^2)$, and

$$\tilde{\sigma}_{\alpha\beta}(k)=\sigma_{\alpha\beta}(k)+\sigma^{(1)}_{\alpha\beta}(k)-[\sigma_{\alpha x}(k)+\sigma^{(1)}_{\alpha x}(k)][\sigma_{x\beta}(k)+\sigma^{(1)}_{x\beta}(k)]/[\sigma_{xx}(k)+\sigma^{(1)}_{xx}(k)]. \tag{9}$$

Using the energy-momentum relation (1) for charge carriers and formulas (4), (5) and (9), we obtain the following expression for the matrix components $\tilde{\sigma}_{\alpha\beta}(k)$ in the main approximation in small parameters $\eta$, $kr$ and $\gamma=T/\tau\ll1$:

$$\tilde{\sigma}_{yy}(k)=\frac{\gamma\sigma_0\sigma_{xy}+\sigma_1(k)(\sigma_0\gamma^2\cos^2\varphi+\sigma_{zz}\tan^2\theta\cos^2\varphi+\gamma\sigma_{xy}\sin^2\varphi)}{\sigma_1(k)\cos^2\varphi+\gamma\sigma_{xy}},$$

$$\tilde{\sigma}_{yz}(k)=\tilde{\sigma}_{zy}(k)=\sigma_{zz}\frac{\sigma_1(k)\operatorname{tg}\theta\cos^2\varphi}{\sigma_1(k)\cos^2\varphi+\gamma\sigma_{xy}},$$

$$\tilde{\sigma}_{zz}(k)=\sigma_{zz}, \tag{10}$$

where $\sigma_0$ is the contribution for $H=0$ from charge carriers to the conductivity along the layers in which the Fermi surface cavity has the form of a corrugated cylinder.

It can be easily seen that in the absence of a drift of charge carriers along the direction of propagation of electromagnetic waves, i.e., for $\varphi=\pi/2$, the attenuation length of the electric field $E_y$ in an extremely strong magnetic field is the same as in the absence of the latter, i.e., $\delta_0\{2\pi\omega(\sigma_0+\sigma_1)\}^{-1/2}$. The attenuation length of the electric field $E_z$ depends significantly on the magnetic field orientation relative to the layers, i.e., on the angle $\theta$ between the normal to the layers and vector **H**, and may attain a value of the order of $\delta_0/\eta^2$ for certain values of the angle $\theta$ when the electrical conductivity across the layers decreases sharply.[13]

However, the attenuation length of electromagnetic waves varies significantly if charge particles can drift in the direction of wave propagation. In order to simplify calculations, we shall assume that the vectors $N$ and $k$ are parallel to each other, i.e., $\varphi=0$. In this case, the dispersion equation assumes the form

$$1-\xi\frac{(\gamma^2\sigma_0+\sigma_{zz}\cos^{-2}\theta)\sigma_1(k)}{\gamma\sigma_{xy}+\sigma_1(k)}+\xi^2\frac{\gamma^2\sigma_0\sigma_{zz}\{\sigma_0+\sigma_1(k)\}}{\gamma\sigma_{xy}+\sigma_1(k)}=0. \tag{11}$$

If the depth of penetration of an electromagnetic wave into a conductor considerably exceeds the mean free path of charge carriers ($l=v\tau_1$) and the dependence of $\sigma_1$ on $k$ can be disregarded to a high degree of accuracy, it can be concluded from the solution of Eq. (11) that the propagation of two weakly attenuating waves is possible. For $\eta\ll\gamma\ll1$, these waves attenuate over distances $\delta_1=\delta_0/\eta$ and $\delta_2=\delta_0/\gamma$, while for $\gamma\ll\eta\ll1$ the attenuation length $\delta_1=\delta_0/\gamma\cos\theta$ increases for one of the waves as the magnetic field deviates from the normal to the layers and, conversely, the attenuation length of the second wave decreases with $\theta$, i.e., $\delta_2=\delta_0\cos\theta/\eta$. In the expressions for $\delta_1$ and $\delta_2$, we disregard insignificant numerical factors of the order of unity.

Under conditions of anomalous skin-effect, when the mean free path of charge carriers is the largest parameter of the problem having the dimension of length, one of the waves attenuates over the mean free path of charge carriers in moderately strong magnetic fields for $\eta\delta_0/l\ll|\gamma|\ll1$ and $\delta_0/\eta^2\ll l$, while the other wave attenuates over the depth $\delta\cong(\delta_0 l)^{1/2}/\eta$. In quite strong magnetic fields, when $\eta\delta_0/l\geqslant|\gamma|$, the attenuation length of one of the waves decreases with increasing magnetic field, while that of the other increases:

$$\delta_1\cong l|\gamma|\cos\theta/\eta;\delta_2\cong\delta_0\eta/|\gamma|\cos\theta. \tag{12}$$

The obtained results can be generalized easily to the case of a weakly corrugated plane as one of the Fermi surface cavities. In this case, only numerical factors of the order of unity in the above formulas need to be refined according to the specific form of the electron energy spectrum, while the effect of the quasi-one-dimensional Fermi surface cavity on the high frequency properties remains the same in organic conductors of the type $(\text{BEDT-TTF})_2\text{MHg(SCN)}_4$.

The authors are obliged to the Ministry of Science for financial support of this research (Grant No. 2.4/192).

*E-mail: peschansky@ilt.kharkov.ua

[1] T. Sasaki and N. Toyota, Solid State Commun. **75**, 93 (1990).
[2] T. Osada, R. Jagi, A. Kawasumi *et al.*, Phys. Rev. B **41**, 5428 (1990).
[3] M. V. Kartsovnik, A. E. Kovalev, V. N. Laukhin *et al.*, Pis'ma Zh. Éksp. Teor. Fiz. **55**, 337 (1992) [JETP Lett. **55**, 339 (1992)].
[4] N. D. Kushch, L. I. Buravov, M. V. Kartsovnik *et al.*, Synth. Mat. **46**, 271 (1992).
[5] M. V. Kartsovnik, A. E. Kovalev, V. N. Laukhin, and S. I. Pesotskii, J. Phys. (Paris) **2**, 223 (1992).
[6] A. E. Kovalev, M. V. Kartsovnik, and N. D. Kushch, Solid State Commun. **87**, 705 (1993).
[7] A. E. Kovalev, M. V. Kartsovnik, R. P. Shibaeva *et al.*, Solid State Commun. **89**, 575 (1994).
[8] M. V. Kartsovnik, A. E. Kovalev, R. P. Shibaeva *et al.*, Physica B **201**, 459 (1994).
[9] M. V. Kartsovnik, A. E. Kovalev, V. N. Laukhin *et al.*, Synth. Met. **70**, 811 (1995).
[10] R. Rossenau, M. L. Doublet, E. Canadell *et al.*, J. Phys. (Paris) **6**, 1527 (1996).
[11] T. Sasaki, H. Ozawa, H. Mori *et al.*, J. Phys. Soc. Jpn. **65**, 213 (1996).
[12] G. E. H. Reuter and E. H. Sondheimer, Proc. Roy. Soc. London **195**, 336 (1948).
[13] V. G. Peschansky, H. Kheir Bek, and S. N. Savel'eva, Fiz. Nizk. Temp. **18**, 1012 (1992) [Sov. J. Low Temp. Phys. **18**, 711 (1992)].

Translated by R. S. Wadhwa

## PHYSICAL PROPERTIES OF CRYOCRYSTALS

# Study of matrix isolation of nitrogen atoms in solid $N_2$

Yu. A. Dmitriev and R. A. Zhitnikov

*A. F. Ioffe Physicotechnical Institute, 194021 St. Petersburg, Russia**
(Submitted August 6, 1997; revised December 10, 1997)
Fiz. Nizk. Temp. **24**, 375–382 (April 1998)

The process of matrix isolation of nitrogen atoms in solid $N_2$ is studied by the method of condensation from the gaseous phase. In order to vary the flow rates of nitrogen atoms and molecules at the sample surface over a wide range, $N_2$–He mixtures of various compositions have been passed through the gas discharge zone. It is found that the EPR line width for N atoms in $N_2$ increases upon a decrease in the nitrogen flow rate from the discharge zone to a cold substrate. It is shown that this increase is due to an increase in the concentration of atomic nitrogen in the matrix leading to an enhancement of the dipole–dipole interaction between atoms. It is established that a decrease in the intensity of recombination of atoms in the course of diffusion at the sample surface due to a decrease in the surface density of these atoms plays a decisive role in the growth of the concentration of matrix-isolated atoms in the experiments. It is found that for a constant flow rate of atoms from the discharge, their concentration in the matrix increases and attains saturation upon an increase in the discharge intensity. The dependence of concentration on the discharge intensity is attributed to a change in the degree of dissociation of molecular nitrogen in the discharge. © *1998 American Institute of Physics.* [S1063-777X(98)01504-7]

### 1. INTRODUCTION

In experiments on matrix isolation of atoms (including N atoms in solid $N_2$) by the method of condensation from the gaseous phase, the rate of flow of matrix particles (molecules or atoms) to a substrate is usually much larger than for a flow of matrix-isolated atoms. Under these conditions, surface diffusion and recombination of atoms at the matrix surface do not play a significant role since adsorbed atoms are rapidly covered by layers of condensed matrix particles, are fixed and have no time to migrate over the surface. In order to create matrix isolation conditions, under which the flow rate of matrix particles ($N_2$ molecules) to the substrate is comparable with or even smaller than the flow rate of matrix-isolated N atoms, we passed a $N_2$–He gas mixture instead of pure nitrogen through the gas-discharge zone to the substrate. For a considerable dilution of nitrogen with helium, the degree of dissociation of nitrogen molecules increases significantly and attains 100% for very low concentrations of $N_2$ in He. Since helium evaporates and is evacuated from the setup, the flow rate of matrix $N_2$ molecules can become smaller than the flow rate of matrix-isolated N atoms. By varying the concentration of $N_2$ in He, we can change the degree of dissociation of nitrogen, i.e., vary the ratio of flow rates of atoms and matrix particles to the matrix substrate, which allows us to study the effect of surface diffusion and recombination of atoms on the process of their matrix isolation. We assume that the concentration of nitrogen atoms adsorbed at the surface of the $N_2$ matrix is so large that the time of their surface diffusion before the recombination ($t_{\mathrm{rec}}$) is much shorter than the desorption time $t_{\mathrm{des}}$, and desorption can be neglected. In our experiments, we used the EPR method for studying the process of matrix isolation under the conditions when the $N_2$–He gaseous mixtures with various nitrogen concentrations ares used. The experiments were made on the setup described earlier.[1]

### 2. EXPERIMENTAL RESULTS

The EPR spectrum of nitrogen atoms trapped in pure (containing no He) molecular $N_2$ has the form of a triplet due to hyperfine interaction of the electron state $^4S_{3/2}$ with a nucleus having the spin $I=1$ and is characterized by the following parameters. The hyperfine structure constant (HSC) for these atoms is $A=11.85(6)$ MHz, the relative matrix shift of the HSC is $\Delta A/A_f=13.4(6)\%$, where $A_{fr}=10.45$ MHz is the HSC for a free nitrogen atom, the $g$-factor is $g=2.00201(12)$, and the line width measured between the points of extrema of the derivative is $\Delta H=0.49(3)$ G. In order to eliminate the effect of the electron dipole–dipole interaction between N atoms on the line width, we ensured a low concentration of atoms in the sample. For this purpose, we deposited the gas passed though a low-intensity pulsed discharge with a period $\theta=500$ $\mu$s and a pulse duration $\tau=36$ $\mu$s. The substrate temperature $T$ varied from 1.5 to 4.2 K during the sample deposition and did not affect the line width. The estimation of the intensities of anisotropic (dipole–dipole) and isotropic (contact) interactions of the electron spin of an atom with nuclear magnetic

 

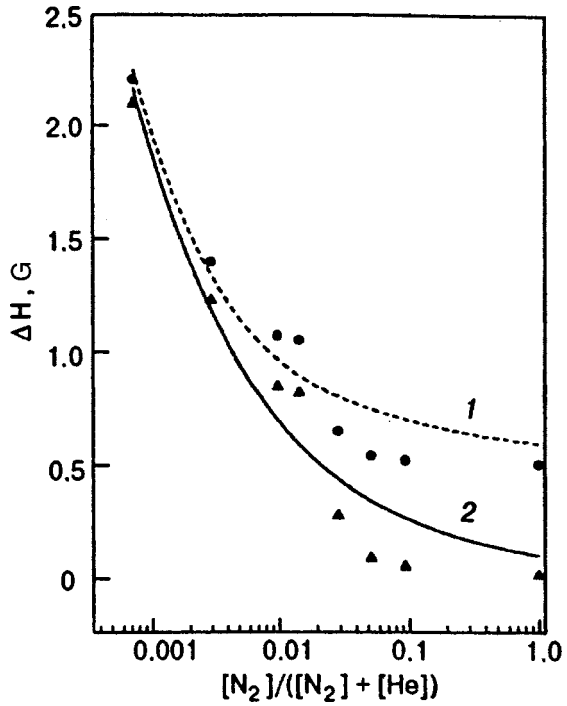


FIG. 1. Dependence of the EPR line width for N atoms in the $N_2$ matrix on the concentration of molecular nitrogen in the $N_2$–He gas mixture in the discharge: measured line width (●, curve *1*), Lorentzian component of line width (dark triangles; curve *2* describes the approximation of the dependence for the Lorentz component by a power function).

moments of molecules located at crystal lattice sites gives the EPR line width $\Delta H = 0.61$ G close to that recorded in our experiments ($\sim 0.5$ G).

For subsequent experiments, we prepared $N_2$–He gas mixtures with concentrations of molecular nitrogen in helium varying within the interval $[N_2]:[He+N_2] = 0.07-100\%$. These mixtures were passed through the zone of a pulsed discharge whose parameters were constant: $\theta = 380$ $\mu$s and $\tau = 70$ $\mu$s. The products of the gas discharge were deposited on a substrate kept at a low temperature, and then the EPR spectra of the obtained samples were studied. The temperature of liquid helium estimated from the vapor pressure in the helium bath being evacuated was $T_{He} \simeq 2$ K, while the temperature of the substrate during sample deposition was $T_{surf} \simeq 2.5$ K according to estimates. It was found that the HSC and the $g$-factor in the recorded EPR spectra of nitrogen atoms coincide with the corresponding values for N in pure $N_2$. This means that as a result of deposition of the mixture $N:N_2$:He, atoms are trapped in the formed nitrogen crystallites. In contrast to the HSC and $g$-factor, the EPR linewidth for nitrogen atoms proved to be very sensitive to the composition of gaseous mixture passed through the discharge zone onto the substrate. Figure 1 shows the dependence of the line width $\Delta H$ on the molecular nitrogen concentration in the gas mixture, i.e., on the ratio $c_{N_2} = [N_2]/([N_2]+[He])$. It was found that the line width increases upon a decrease in the nitrogen concentration in the mixture. It was proposed that such a broadening is due to an increase in the concentration of nitrogen atoms in the sample due to a change in the atomic flow rate from the discharge zone to the matrix surface. The dipole–dipole interaction between the electron moments of N atoms in the matrix must make a contribution to the width of their EPR lines, which increases with the concentration of these atoms. A comparison with the theoretical curves shows that the shape of a line changes from the Gaussian (discharge in pure nitrogen) to Lorentzian (even for the concentration $c_{N_2} \sim 1\%$). This can be explained as follows. It is well known[2] that the shape of the line is Gaussian when the paramagnetic centers broadening the line are arranged regularly and Lorentzian when they are distributed chaotically. For a low concentration of atoms, EPR lines are broadened due to ultrahyperfine interaction with the nuclear magnetic moments of matrix molecules, i.e., broadening centers are distributed regularly, and hence the lines are Gaussian. For a high concentration of N atoms, the line broadening occurs mainly due to their electron dipole spin–spin interaction. In this case, the line is Lorentzian if the concentration $c$ of atoms does not exceed $0.01c_0$, where $c_0 = 1/r_0^3$, and $r_0$ is the separation between nearest sites in the matrix crystal lattice[2] since in this case atoms are arranged chaotically. For a higher concentration, we approach a regular distribution, and the contribution of the Gaussian component increases again.[2] It will be clear from the subsequent analysis that the maximum atomic concentration in our samples was of the order of $0.001c_0$. Thus, the observed change in the shape of the line confirms the interpretation of line broadening by an increase in the concentration of N atoms in the $N_2$ matrix. The observed decrease in the spin–lattice relaxation time $T_1$ upon a decrease in the concentration of molecular nitrogen in the gas mixture from which the sample was prepared can serve as an additional confirmation of the proposed explanation for line broadening. Thus, for $c_{N_2} = 1$, the time $T_1 = 6.9 \times 10^{-5}$ s, while $T_1 = 8.3 \times 10^{-7}$ s for $c_{N_2} = 0.01$. The time $T_1$ is inversely proportional to the squared concentration of paramagnetic centers.[2] Consequently, the atomic concentration in the sample increases by a factor of nine upon a decrease in the molecular nitrogen concentration by a factor of 100, i.e., approximately in inverse proportion to the square root of the molecular nitrogen concentration in the gas mixture. It will be proved below that exactly this dependence is also observed for the line width.

We assume that in our case the increase in the degree of dissociation of molecular nitrogen, i.e., the ratio $[N]/([N]+[N_2])$, in the discharge upon a decrease in the value of $c_{N_2}$ can be one of the reasons behind EPR line broadening. This is due to the fact that the recombination of nitrogen atoms in the discharge zone slows down as a result of dilution with helium. In order to verify this assumption, we carried out experiments in which the degree of dissociation of molecules was changed by varying the discharge intensity at a constant $c_{N_2} = 0.01$. The duration of $\tau$ and the period $\theta$ of discharge pulses changed at a constant amplitude and $c_{N_2}$. Figure 2 shows the dependence of the EPR line width for nitrogen atoms on the discharge intensity measured in the units of $\eta = \tau/(\tau+\theta)$, which is proportional to the generator power supplied to the discharge. The value $\eta = 1$ corresponds to a continuous discharge, i.e., maximum degree of dissociation of nitrogen, and hence the maximum concen-

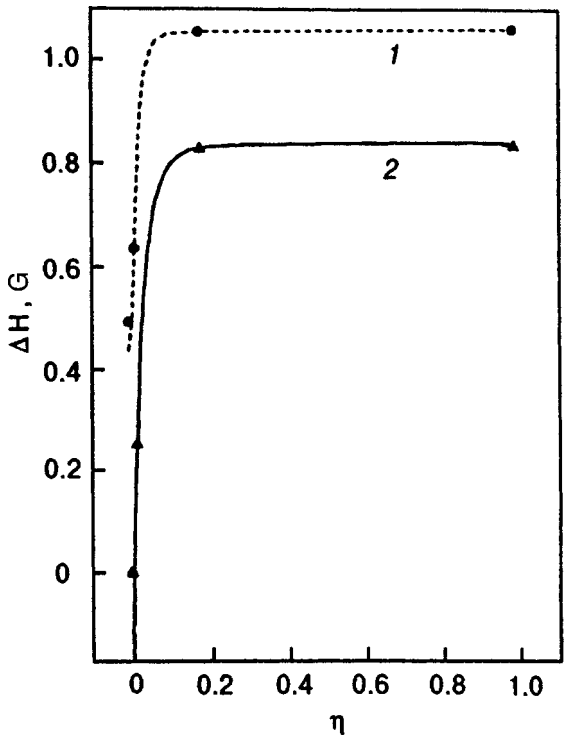


FIG. 2. Dependence of the EPR line width for N atoms in the $N_2$ matrix on the discharge intensity: measured line width (curve *1*), Lorentzian component of line width (curve *2*). On the abscissa axis, we lay out the quantity $\eta=\tau/(\tau+\theta)$, where $\tau$ is the duration of discharge pulses and $\theta$ the pulse repetition period.

tration of nitrogen atoms in the matrix. The value $\eta=0$ corresponds to the extremely low discharge power for which the concentration of atoms in the sample is so low that the effect of the electron spin–spin interaction of atoms causing broadening is negligibly small, i.e., broadening occurs only due to nuclear moments of the matrix crystal lattice. It can be seen from the figure that the line width is an increasing function of the discharge intensity attaining saturation, and hence this dependence can be explained qualitatively by a change in the degree of dissociation of molecules in the discharge. Since the EPR line in our experiments is broadened due to two interactions one of which leads to the Gaussian shape of the line and the other to the Lorentzian shape, the shape of the resultant line can be described by the convolution of the Gaussian and Lorentzian distributions. Knowing the experimental line width $\Delta H$ and the Gaussian contribution $(\Delta H)_G=0.49$ G, we can find[2] the Lorentzian line width $(\Delta H)_L$ reflecting the concentration of atoms in the sample. Figure 2 also shows the points corresponding to the values $(\Delta H)_L=[\Delta H^2-(\Delta H)_G^2]/\Delta H$. Since the width of the Lorentzian component is proportional to the concentration of paramagnetic atoms in the sample,[2] this curve also describes the dependence of the concentration of trapped atoms on the discharge intensity. In addition, the curve in Fig. 2 indicates that dissociation of molecules for the discharge parameters typical of our experiments ($\theta=380$ $\mu$s and $\tau=70$ $\mu$s) for which the dependence of the line width on the concentration of nitrogen molecules in the gas mixture was obtained (see Fig. 1) is complete even for $c_{N_2}=0.01$. Consequently, although the mechanism considered above contributes to line broadening, it cannot be responsible for an increase in $\Delta H$ when the value of $c_{N_2}$ decreases from values of the order of one percent.

### 3. SURFACE DIFFUSION AND RECOMBINATION OF NITROGEN ATOMS

In order to explain the form of the dependence presented in Fig. 1, we must consider the trapping of nitrogen atoms in the $N_2$ matrix. We shall estimate the concentration of atoms in the sample as a function of the flow rate to the surface taking into account their surface recombination. Let us simplify the problem assuming that desorption of atoms can be neglected in this case. We shall consider the following mechanism of trapping of atoms in the matrix: (1) adsorption of atoms at the matrix surface; (2) diffusion of adsorbed atoms over the surface, during which a fraction of atoms collide and recombine, while the remaining atoms are trapped at the steps of growth islets and subsequently either undergo recombination, or are trapped in the matrix. Proceeding from this model, we shall calculate the concentration of N atoms trapped in the $N_2$ matrix. Let $I_{at}$ be the flow rate of atoms from the discharge tube to the sample surface, $k_{at}$ the rate of their trapping at the growth steps, and the quantity $1/k_{at}$ reciprocal to this rate is the lifetime $t_{at}$ of a free atom at the surface relative to its trapping on a step. Let $1/k_{mol}$ be the lifetime of a free molecule at the surface, i.e., the characteristic time of its trapping at a growth step. We shall wrote two simple balance equations for the number $n_{at}$ of atoms moving freely over the surface and the number $n_{mol}$ of free molecules on the sample surface in the case of complete dissociation of molecules in the discharge and the absence of molecular flow to the surface. We denote by $a$ the recombination rate constant for atoms at the surface. Then we can write

$$I_{at}-k_{at}n_{at}-an_{at}^2=0; \tag{1}$$

$$\frac{1}{2}(I_{at}-k_{at}n_{at})=k_{mol}n_{mol}. \tag{2}$$

The coefficient 1/2 appears in Eq. (2) since we are dealing with diatomic molecules.

In accordance with the adopted model, N atoms are trapped at steps which form the boundary of the growth of the second layer of densely packed spheres (face centered cubic lattice of molecular nitrogen at helium temperatures), and then an atom diffuses to the corner of a growth step, where it has six nearest neighbors. In this case, the concentration of atoms in the sample is described by the following equation:

$$C_{at}=\frac{k_{at}n_{at}(1-C_{at})^6p_m^6}{[I_{at}+k_{at}n_{at}(1-C_{at})^6p_m^6]/2+I_{mat}}. \tag{3}$$

This relation is valid for a more general case, when dissociation in the discharge is incomplete, and an additional molecular flow is supplied to the sample surface at a rate $I_{mat}$. In Eq. (3), the following notation in used: $C_{at}$ is the concentration of atoms in the sample, defined as the ratio of the

number of matrix-isolated atoms to the total number of particles (molecules and matrix-isolated atoms) in the sample, and $p_m$ the probability that a particle incident on a growth step is a molecule formed as a result of recombination at the surface, or a molecule from the discharge, i.e.,

$$p_m=\frac{k_{\rm mol}n_{\rm mol}+I_{\rm mat}}{k_{\rm mol}n_{\rm mol}+k_{\rm at}n_{\rm at}+I_{\rm mat}},$$

where the numerator contains the rate of molecular flow to growth steps and the denominator contains the total flow rate of particles (including atoms and molecules) to these steps. The numerator of the fraction in expression (3) is the number of atoms trapped in the matrix per unit time, which is equal to the flow rate $k_{\rm at}n_{\rm at}$ of atoms to the growth sites, multiplied by the probability of the absence of recombination at the step corner for an atom occupying this site. This probability is defined as the product of the probability of the absence of a trapped atom among the six neighbors of the step and the probability that the next six neighbors are molecules. The denominator in (3) is the number of lattice sites occupied by molecules and atoms per unit time.

The values of $n_{\rm at}$ can be determined from Eq. (1), and the expression for $p_m$ assumes the form

$$p_m=\frac{I'_{\rm at}-\sqrt{1+2I'_{\rm at}}+1+2I_{\rm mat}}{I'_{\rm at}+\sqrt{1+2I'_{\rm at}}-1+2I'_{\rm mat}},$$

where $I'_{\rm at}=2I_{\rm at}a/k_{\rm at}^2$, $I'_{\rm mat}=2I_{\rm mat}a/k_{\rm at}^2$ or, if we introduce the notation $2a/k_{\rm at}^2=at_{\rm at}^2/0{,}5=1/q$, we can write

$$I'_{\rm at}=\frac{I_{\rm at}}{q},\quad I'_{\rm mat}=\frac{I_{\rm mat}}{q}.$$

Since the maximum value of $C_{\rm at}$ cannot exceed $\sim 0.1$ (atoms at the neighboring nodes of the lattice matrix recombine), we can put $(1-C_{\rm at})^6\approx 1-6C_{\rm at}$ in Eq. (3). This leads to a quadratic equation for $C_{\rm at}$, whose solution has the form

$$C_{\rm at}=\frac{1}{12}\left[(13+A)-\sqrt{(13+A)^2-48}\right], \tag{4}$$

where

$$A=\frac{I'_{\rm at}+2I'_{\rm mat}}{\sqrt{1+2I'_{\rm at}}}\left(\frac{I'_{\rm at}+\sqrt{1+2I'_{\rm at}}-1+2I'_{\rm mat}}{I'_{\rm at}-\sqrt{1+2I'_{\rm at}}+1+2I'_{\rm mat}}\right)^6.$$

It was noted above that the width of the Lorentzian component of the EPR line for nitrogen atoms is proportional to the atomic concentration in the sample. Consequently, knowing the experimental value of $(\Delta H)_L$, we can determine the concentration of atoms in the sample: $(\Delta H)_L\approx 10^{-9}\rho_{\rm at}$, where $\rho_{\rm at}$ is the density of atoms.[2] The density of nitrogen molecules in solid molecular $N_2$ is $\rho_{N_2}=2.77\times 10^{22}$ cm$^{-3}$. Hence we obtain the following expression for the atomic concentration: $C_{\rm at}\approx 4\times 10^{-4}(\Delta H)_L$. The maximum value of $(\Delta H)_L$ obtained by us here is 2.1 G, which corresponds to the atomic nitrogen concentration $C_{\rm at}\sim 10^{-3}$. This means that the value of $A$ determining $C_{\rm at}$ in formula (4) is much greater than unity in the range of atomic concentrations used in our experiments. This gives the following expression for $C_{\rm at}$:

$$C_{\rm at}\approx 2/A \tag{5}$$

or, for zero flow rate of the matrix gas and complete dissociation of molecules in the discharge,

$$C_{\rm at}\approx\frac{2\sqrt{2}}{\sqrt{I'_{\rm at}}}=\frac{2k_{\rm at}}{\sqrt{1_{\rm at}a}}, \tag{6}$$

i.e., the concentration of atoms in the sample is inversely proportional to the square root of the flow rate of atoms from the discharge to the surface. Consequently, for complete dissociation of molecular nitrogen in the discharge and a constant flow rate of the gas mixture to the substrate, we obtain the following dependence of the line width on the concentration of the $N_2$ impurity in the $N_2$–He mixture:

$$(\Delta H)_L-1/\sqrt{c_{N_2}}. \tag{7}$$

An expression of the type (6) for the atomic concentration in the sample, in which $a$ and $I_{\rm at}$ appear to the power $-1/2$, while $k_{\rm at}$ appears to the first power indicates that a decrease in the number of free atoms at the surface is mainly due to their surface recombination rather than due to trapping at the growth steps. Indeed, putting $k_{\rm at}\simeq 0$ in formula (1), we obtain $n_{\rm at}\approx\sqrt{I_{\rm at}/a}$ for the number of atoms at the surface. In this case, the flow rate of atoms to growth steps is equal to $k_{\rm at}\sqrt{I_{\rm at}/a}$. Considering that $n_{\rm mol}\approx I_{\rm at}/2$, we obtain the following expression for the atomic concentration in the sample with a low $C_{\rm at}$:

$$C_{\rm at}\approx\frac{k_{\rm at}\sqrt{I_{\rm at}/a}}{I_{\rm at}/2}=\frac{2}{\sqrt{I_{\rm at}a/k_{\rm at}^2}}=\frac{2\sqrt{2}}{\sqrt{I'_{\rm at}}},$$

i.e., we arrive at relation (6).

The solid curve in Fig. 1 describes the approximation of the experimental dependence of $(\Delta H)_L$ as a function of $c_{N_2}$ (symbols in the figure) by the power function $(\Delta H)_L^2=X_1(c_{N_2})^{X_2}$. The exponent was found to be indeed close to $\sim 0.5$ (see (7)): $X_2=-0.44$. It is interesting to note that this conclusion is confirmed by the data on the spin–lattice relaxation time for a lower dilution of molecular nitrogen with helium also. For example, it was shown in Sec. 2 that a decrease in $c_{N_2}$ by a factor of 100 reduces $T_1$ by a factor of 9, which corresponds to an increase in the atomic concentration by an order of magnitude. Using formula (6) and experimental values of line width, we can determine the value of $I'_{\rm at}$ for the molecular nitrogen concentration $c_{N_2}=1\%$ in the mixture, which was used in our experiments involving variation of discharge intensity. This gives $I'_{\rm at}(1\%)=5.5\times 10^7$. In such experiments (see Fig. 2), an increase in the atomic flow rate to the substrate due to an increase in the discharge intensity leads to an increase in the atomic concentration in the sample. This contradicts the dependence presented by formula (6) describing the results of experiments in which the atomic flow rate from the discharge increases due to an increase in the concentration of molecular nitrogen in helium. Such a discrepancy can be explained as follows. In experiments with a discharge with varying intensity, we are dealing with incomplete dissociation of molecular nitrogen in the discharge. Using formula (4), we take the flow rate of undis-

sociated $N_2$ for the matrix gas flow rate $I_{mat}$. Obviously, the quantity $I'_{at}+2I'_{mat}=B$ in this case is constant (for an invariable $C_{N_2}$ and the gas flow through the discharge), i.e., independent on the discharge intensity. This means that $B(1\%)=5.5\times10^7$ for $c_{N_2}=1\%$ and for any intensity of the discharge. We can write the expression for the quantity $A$ appearing in formula (4) in the form

$$A=\frac{B}{\sqrt{1+2I'_{at}}}\left(\frac{B+\sqrt{1+2I'_{at}}-1}{B-\sqrt{1+2I'_{at}}+1}\right)^6,$$

or, taking into account the inequalities $B\gg1$, $B\gg\sqrt{I'_{at}}$, $A\approx B/\sqrt{2I'_{at}}$. Substituting this value into formula (5), we obtain

$$C_{at}\approx\frac{2\sqrt{2}}{B}\sqrt{I'_{at}}. \tag{8}$$

Thus, the dependence of the concentration of atoms in the sample on their flow rate to the surface in the case when the flow rate varies due to a change in the discharge intensity (see Fig. 2) is indeed opposite to that given by formula (6) describing the results of experiments with a change in the concentration of molecular nitrogen in helium (see Fig. 1). Unfortunately, it is impossible to verify expression (8) quantitatively from experimental points in Fig. 2 without knowing the law governing the growth in the degree of dissociation upon an increase in the discharge intensity, and hence we have to remain content with the qualitative coincidence.

## 4. SUITABILITY OF THE MATRIX INSULATION MODEL AND SOME NUMERICAL ESTIMATES

The results presented in Secs. 2 and 3 lead to the conclusion that the concentration of trapped atoms in our experiments with low flow rates of molecular components to the deposition surface is mainly determined by their surface recombination occurring as a result of diffusion of atoms over the surface.

The dimensionless quantity $I'_{at}$ determined from the experimental width of EPR lines (formula (6) and Fig. 1) is the flow rate of atoms to the substrate, normalized to the ratio

$$q=0{,}5/at_{at}^2\,. \tag{9}$$

Since the flow rate of atoms to the surface in the case of complete dissociation of nitrogen in the discharge can be estimated from the flow rate of the gas recorded in experiments, we can obtain the experimental value of this ratio.

While determining $q$, we used the data on the $N_2$ concentration in the mixture $N_2$–He, which is equal to $10^{-3}$. For example, $I'_{at}(0.1\%)=10^7$, and the flow rate of atoms to the substrate is $I_{at}=5\times10^{13}\ s^{-1}$. Consequently, $q_{exp}=5\times10^6\ s^{-1}$. Let us now estimate the values of the quantities appearing in the expression (9) for $q$. Since we are considering processes at the surface, the problem is two-dimensional. While evaluating $a$, it is expedient to assume that the recombination cross section is equal to the doubled internuclear spacing $2l_{N_2}$ in a nitrogen molecule. Moving over the surface, an atom jumps from one potential well to another with the hopping rate $\nu$. Denoting the lattice parameter by $l_{lat}$, we obtain the following expression for the average velocity of an atom moving over the surface: $V_{dif}=\nu l_{lat}$. Consequently, for the constant $a$ [equation (1)] we have $a\approx2l_{N_2}l_{lat}\nu/S_{sub}$, where $S_{sub}$ is the area of the substrate. The order of magnitude of the lifetime $t_{at}$ of a free atom on the surface relative its capture at a growth step is determined by the time of its diffusion over the surface, required for displacement over a distance of the order of the microcrystal size $L_{cr}$. In the random walk model, the displacement of an atom from a given point over a certain time interval is proportional to the square root of the number of jumps during this time, and hence $L_{cr}\approx l_{lat}\sqrt{t_{at}\nu}$, whence $t_{at}\approx(1/\nu)(L_{cr}/l_{lat})^2$. Substituting the obtained expressions for $a$ and $t_{at}$ into formula (9) and assuming that $q=q_{exp}=5\times10^6\ s^{-1}$, we can estimate the time $\tau_{jump}$ between two consecutive jumps, which is a quantity reciprocal to the hopping rate $\nu$:

$$\frac{1}{\nu}\approx\frac{10^{-7}S_{sub}l_{lat}^3}{2l_{N_2}L_{cr}^4}. \tag{10}$$

On the other hand, the time $\tau_{jump}$ can be expressed in terms of the activation energy of surface diffusion $E_{surf}$:

$$\tau_{jump}=\tau_0\ \exp\left(\frac{E_{surf}}{kT}\right), \tag{11}$$

where $\tau_0\sim10^{-13}$ s. We can estimate this activation energy by using relations (10) and (11). These expressions contain the quantities $S_{sub}=1\ cm^2$, $l_{lat}=4.0$ Å, $l_{N_2}=1.1$ Å, $T=2.5$ K, and the crystallite size is of the order of 0.1 $\mu$m. Indeed, Ref. 3 contains the values of $L_{cr}$ for various cryocrystals including solid Ar for which the mean value of $L_{cr}$ at the condensation temperature 6.0 K is 60 nm. At a given temperature, the size of crystallites is mainly determined by the heat of sublimation $Q_{sub}$ whose values for Ar and $N_2$ are close: $Q_{sub}^{N_2}=250$ J/g and $Q_{sub}^{Ar}=200$ J/g.[4] The size of crystallites of the order of 0.1 $\mu$m in solid hydrogen films obtained by slow deposition (with a rate of the order of 1 mmole/h and smaller) was noted by Tam *et al.*[5] As a result, from relations (10) and (11) we obtain $E_{surf}(N–N_2)_{est1}\approx66$ K. However, another mechanism of atomic loss is also possible, i.e., the recombination of atoms trapped by the surface of a cryocrystal but yet not thermalized, which migrate over the surface, losing gradually their excess kinetic energy. The value $E_{surf}(N–N_2)_{est1}\approx66$ K was obtained by us under the assumption that the diffusion of nitrogen atoms over the surface of the $N_2$ matrix is of the activation type. If the value obtained in this way were considerably smaller than the estimate that should be expected proceeding from the available experimental or theoretical data, this would indicate that diffusion of nonthermalized atoms makes a significant contribution to recombination.

Let us evaluate $E_{surf}(N–N_2)$ by using another method based on the available data. For example, the experimental value of surface diffusion activation energy for hydrogen molecules on the surface of solid $H_2$ is known to be 23 K.[6] The activation energy of surface diffusion of a particle is proportional to its energy of absorption at the surface of a

cryocrystal, which is proportional (in the first approximation) to the product of polarizabilities of a matrix particle and the particle being adsorbed. Such a treatment allows us to obtain a rough estimate of the surface diffusion activation energy for N on $N_2$ proceeding from the experimental value of $E_{surf}(H_2-H_2)=23$ K and polarizabilities $\alpha(N)=7.5a_0^3$; $\alpha(H_2)=5.178a_0^3$; $\alpha(N_2)=11.74a_0^3$, where $a_0$ is the Bohr radius. This gives the following estimate: $E_{surf}(N-N_2)_{est2}\approx 76$ K. In all probability, this estimate is slightly lower since we must take into account not only the change in polarizability, but also a considerable increase in the mass of the adsorbed particle as well as the matrix molecules as we go over from hydrogen to nitrogen, which must obviously lead to a higher value of $E_{surf}(N-N_2)_{est2}$. Thus, we can assume that a significant fraction of nitrogen molecules is formed as a result of surface recombination of atoms that have not thermalized as yet.

## 5. ON LIMITING CONCENTRATIONS OF MATRIX ISOLATED ATOMS

Among other things, intense studies of matrix isolation of free radicals aim at accumulating high concentrations of radicals required for analyzing fundamental processes in systems with a high density of unpaired spins as well as for developing new kinds of fuel.[7–10] The available theories used for estimating the maximum possible concentrations of matrix-isolated atoms, including static theories based on the calculation of the number of ways of arrangement of particles forming the matrix as well as dynamic theories in which the value of limiting concentration of radicals was determined by the beginning of chain recombination in the sample, do not take into account the recombination in the course of diffusion of atoms over the sample surface. At the same time, the results of the present research show that this channel of the decrease in the concentration of matrix-isolated atoms is very significant. Formula (4) makes it possible to construct the dependence of concentration on the quantity $l'_{at}$, i.e., the atomic flow rate to the sample surface, normalized to the ratio $q=0.5/at_{at}^2$. Figure 3 shows this dependence calculated for conditions under which no additional matrix gas is supplied. It can be seen from the figure that for a constant $q$ there exists a value of the flow rate at which the atomic concentration attains its maximum value equal approximately to 4.5%. The reason behind the possible existence of such a peak lies in gradual transition (upon a decrease in the flow rate of atoms to the surface) from the recombination of atoms moving freely over the surface to their recombination predominantly after their trapping at growth steps. In order to attain this maximum, we must reduce the atomic flow rate to the sample surface by a factor of $3\times 10^4$ as compared to the minimum value attained in our experiments. If we do it only by reducing the concentration of molecular nitrogen in helium, this concentration must be smaller than $10^{-5}$%, which is difficult to attain since such a condition presumes extremely high purity of gases. We could try to reduce the gas flow rate through the discharge as well as the concentration of $N_2$ impurity in He. Obviously, an increase in the concentration of trapped atoms may also be caused by a decrease in the substrate temperature, which ''freezes'' the mobility of thermalized atoms, and a decrease in the temperature of the gas (N:He) supplied to the substrate since the diffusion length of nonthermalized atoms decreases in this case. An analysis of formula (4) also shows that the supply of additional matrix gas to the substrate does not lead to an increase in the maximum possible concentration of atoms in the sample.

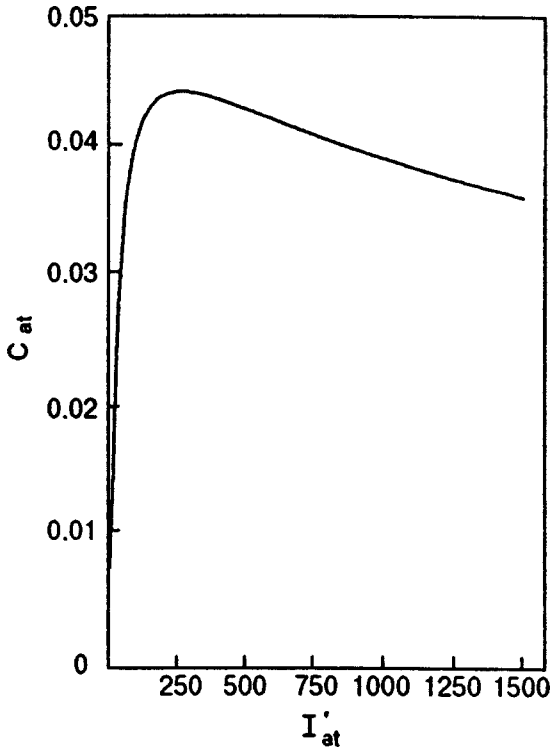


FIG. 3. Calculated dependence of the concentration of nitrogen atoms in the $N_2$ matrix on the normalized flow rate to the substrate in the case of complete dissociation of nitrogen in the discharge. Here $I'_{at}=2I_{at}a/k_{at}^2$ is the dimensionless quantity proportional to the flow rate $I_{at}$ of atoms to the substrate.

The analysis presented in this section shows that surface recombination should be taken into account in the theoretical estimation of the limiting concentration of atoms trapped in the matrix.

## 6. CONCLUSIONS

In this research, we measured the EPR line width for nitrogen atoms trapped from a gas discharge in solid $N_2$ for various values of the atomic flow rate to the sample surface. It was found that the concentration of atoms in the sample is inversely proportional to the square root of the flow rate of atoms to the surface for constant discharge parameters; in the case of a constant flow rate, the concentration increases and attains saturation upon an increase in the discharge intensity. The dependence of the concentration of matrix isolated atoms on the flow rate of atoms to the surface was explained by the loss of atoms due to surface recombination, while the dependence on the discharge intensity was explained by a change in the degree of dissociation of molecular nitrogen in the discharge. It was proved that surface recombination re-

stricts the limiting concentration of N in $N_2$ (to $\sim 4\%$) in the case of deposition of gas discharge products on a cold surface.

One of the authors (Yu. A. Dmitriev) expresses his gratitude to A. E. Kilyup for attention to this research and support.

*E-mail: dmitr@inep.as.ru

[1] R. A. Zhitnikov and Yu. A. Dmitriev, J. Phys.: Condens. Matter **6**, 2727 (1994).
[2] Ya. S. Lebedev and V. I. Muromtsev, *EPR and Relaxation of Stabilized Radicals* [in Russian], Khimiya, Moscow (1972).
[3] R. Hafer, *Cryovacuum Technology* [Russian trans.], Energoatomizdat, Moscow (1983).
[4] M. P. Mal'kov, *Handbook on Physical and Engineering Foundations of Cryogenics* [in Russian], Energoatomizdat, Moscow (1985).
[5] S. Tam, M. Macler, and M. E. Fajardo, J. Chem. Phys. **106**, 8955 (1997).
[6] U. Albrecht, R. Conradt, S. Heninghaus, and P. Leiderer, Fiz. Nizk. Temp. **22**, 158 (1996) [Low Temp. Phys. **22**, 117 (1996)].
[7] E. B. Gordon, A. A. Pel'menev, O. F. Pugachev, and V. V. Khmelenko, Dokl. Akad. Nauk SSSR **280**, 1174 (1985) [Sov. Phys. Dokl. **30**, 712 (1985)].
[8] G. W. Collins, J. R. Maienschein, E. R. Mapoles *et al.*, Phys. Rev. B **48**, 12620 (1993).
[9] A. T. Pritt, Jr., N. Presser, and R. R. Herm, J. Propul. Power **9**, 714 (1993).
[10] M. E. Fajardo, S. Tam, T. L. Thompson, and M. Cordonier, Chem. Phys. **189**, 351 (1994).

Translated by R. S. Wadhwa

## LATTICE DYNAMICS

# Low frequency vibrational spectrum of $CsDy(MoO_4)_2$

V. I. Kut'ko

*B. Verkin Institute for Low Temperature Physics and Engineering, National Academy of Sciences of the Ukraine, 310164 Kharkov, Ukraine**

(Submitted October 10, 1997; revised November 11, 1997)
Fiz. Nizk. Temp. **24**, 383–389 (April 1998)

Transmission spectrum of $CsDy(MoO_4)_2$ single crystals is measured in polarized light in the longwave IR region (10–100 $cm^{-1}$) at low temperatures 6–40 K. The change in the vibrational spectrum during first-order structural phase transition ($T_c \sim 38$ K) is detected experimentally. The vibrational spectrum of $CsDy(MoO_4)_2$ is analyzed in the model of ''quasi-chipped off'' vibrational modes. © *1998 American Institute of Physics.*
[S1063-777X(98)01604-1]

### INTRODUCTION

We investigated a compound belonging to the series of rhombic double alkaline-rare earth molybdates undergoing low-temperature structural phase transitions of the type of cooperative Jahn–Teller effect (CJTE).[1,2] This compound also displays a structural phase transition accompanied by a considerable rearrangement of the electronic spectrum of $Dy^{3+}$ ions.[3] A distinguishing feature of this phase transition is that it is of jump type and is accompanied by hysteresis as $T_c$ is passed from above or below, hence it was identified as a first-order phase transition. Later, it was observed during specific heat measurements[4] that a structural phase transition in $CsDy(MoO_4)_2$ is accompanied by an enthalpy jump $\Delta H = 0.64 + 0.2$ kJ/mol. Other parameters determining the structural variations in this compound during phase transition were also found to vary significantly. The energy of the ground state of $f$-electrons in $Dy^{3+}$ ions decreases by $\sim 80$ $cm^{-1}$.[5] Raman and IR spectral measurements reveal that the optical phonon frequencies also vary abruptly.[6]

Studies of the temperature dependence of the unit cell parameters have shown that the lattice parameter $a$ of $CsDy(MoO_4)_2$ undergoes a significant variation $\sim 0.67\%$ in the structural phase transition region.[7]

Such an abrupt variation of parameters in the structure of the compound being investigated is not characteristic of phase transitions of cooperative Jahn–Teller effect type, which were treated as second-order phase transitions with a slight rearrangement of energy spectrum of rare-earth ions in earlier investigations of vanadates as well as in molybdates.[8] The effect of the external magnetic field on the temperature of structural phase transition in $CsDy(MoO_4)_2$ was also found to be unusual. It was shown by El'chaninova et al.[9] that the phase transition temperature remains practically unchanged in fields up to $\sim 7$ T which is not characteristic of CJTE type phase transitions. An analysis shows[10] that the contribution to the latent heat of transition from the enthalpy variation in the electron subsystem of $Dy^{3+}$ is insignificant. It is also worth noting that a first-order structural phase transition ($T_c \sim 135$ K) was also observed in the isostructural diamagnet $CsBi(MoO_4)_2$, whose external manifestations are the same as in $CsDy(MoO_4)_2$.[11]

All the above-mentioned facts indicate that, judging by the physical properties, the phase transition in $CsDy(MoO_4)_2$ differs from the CJTE type phase transitions studied earlier in compounds containing rare-earth ions. Hence it cannot be stated with certainty whether the phase transition in $CsDy(MoO_4)_2$ is indeed a CJTE type transitions.

The dynamic theory of structural phase transitions associated with the CJTE is based on an analysis of temperature dependences of the low-frequency electron–phonon mode energies. In the case of ferrodistortional ordering, the analysis is usually confined to the interaction between an electron branch and an acoustic branch. The frequency of the latter is equal to zero at the structural phase transition temperature. In the real situation, the number of active modes is much larger. Other spectral branches are considered either with a view to explain the physical singularities that cannot be explained on the basis of a single-mode behavior during a ferro- or antiferrodistortional type ordering. Hence the experimental information about the low-frequency phonon spectrum of these systems is quite important.

In order to find the peculiarities of the crystal lattice dynamics, as well as the nature of structural phase transition, we carried out experimental studies of the low-frequency absorption spectrum of $CsDy(MoO_4)_2$ crystals by using the longwave IR spectroscopic technique.

### EXPERIMENTAL TECHNIQUE

The compound $CsDy(MoO_4)_2$ crystallizes in rhombic space group $D_{2h}^3$ with parameters $a = 9.51$ Å, $b = 7.97$ Å and $c = 5.05$ Å of the unit cell containing two formula units of the compound.[12] The structure consists of $[Dy(MoO_4)_2]_{\infty\infty}^-$ and $[Cs]_{\infty\infty}^+$ layers alternating along the parameter $a$. Within each

 

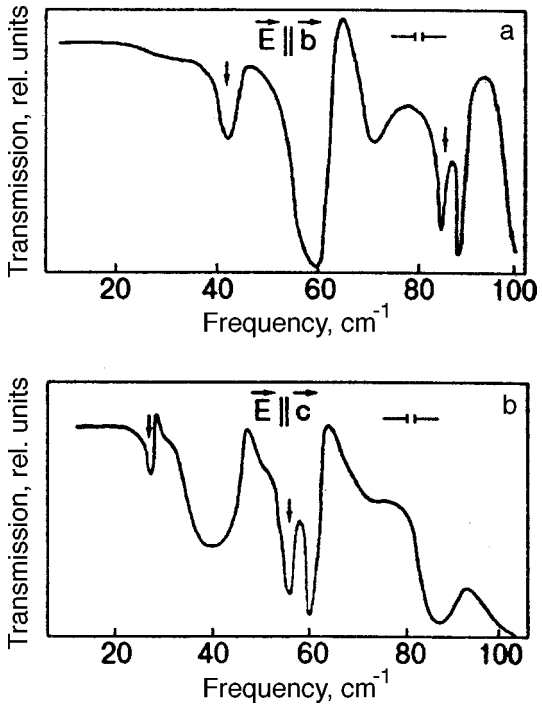


FIG. 1. The form of the transmission spectrum for a $CsDy(MoO_4)_2$ crystal in the frequency range 10–100 $cm^{-1}$ at 6 K for two polarizations of incident light: $\mathbf{E}\|\mathbf{b}$(a) and $\mathbf{E}\|\mathbf{c}$(b). The arrows indicate the bands formed at a temperature below the structural phase transition point.

$[Dy(MoO_4)_2]^{-}_{\infty\infty}$ layer, the $Dy^{3+}$ ions form a chain structure along the **b**-axis. The $Dy^{3+}$ ions are located in distorted oxygen octahedra and have a very low local symmetry $D_2$. Hence the lowest multiplet $^6H_{15/2}$ of the $Dy^{3+}$ ion is split into eight Kramers doublets by the crystal field.

Crystals of $CsDy(MoO_4)_2$ were grown by spontaneous crystallization technique from solution in the melt. Such crystals have a faintly yellow color and characteristic dimensions $10\times10\times1$ mm, and are easily split into layers in the (100) plane.

Measurements were made on an IR spectrometer with a cooled InSb photoresistance, as well as a cooled germanium bolometer. Measurements were made in the frequency range 10–100 $cm^{-1}$. The samples were of the size $5\times10\times1$ mm. Upon an increase in sample temperature beyond the structural phase transition point, the transmission decreased considerably, and hence temperature measurements were made selectively. A polarization microscope was used for orienting the samples along the crystallographic axes.

## EXPERIMENTAL RESULTS

Figure 1 shows the frequency dependence of the IR radiation transmission at low temperatures ($\sim$6 K). It can be seen from the figure that the spectrum contains five absorption bands for a polarization $\mathbf{E}\|\mathbf{b}$ of the radiation and five absorption bands for a polarization $\mathbf{E}\|\mathbf{c}$. A characteristic feature of the measured spectra is two bands with doublet structure at frequencies 56.2 and 59.9 $cm^{-1}$ for polarization $\mathbf{E}\|\mathbf{c}$, and frequencies 84.5 and 88 $cm^{-1}$ for polarization $\mathbf{E}\|\mathbf{b}$.

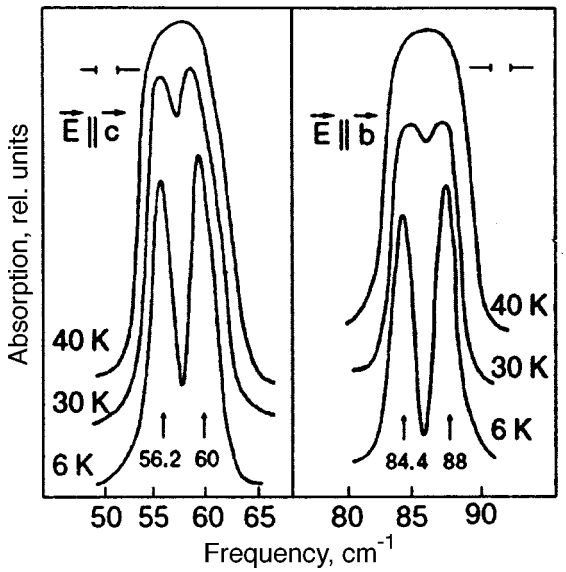


FIG. 2. Absorption bands of a $CsDy(MoO_4)_2$ crystal having doublet structure at different temperatures.

The doublet structure gradually disappears as the temperature is raised to $\sim$40 K (see Fig. 2). In order to confirm that this structure is associated with the phase transition and not with the initial high-temperature phase, we measured the absorption spectrum of the crystal $CsTb(MoO_4)_2$ which has the same structure as $CsDy(MoO_4)_2$ but which does not display a structural phase transition. The doublet structure of the bands was not observed in this case (Fig. 3), and hence it can be uniquely verified that the doublet structure emerging in the $\sim$57 $cm^{-1}$ band for $\mathbf{E}\|\mathbf{c}$ polarization and in the

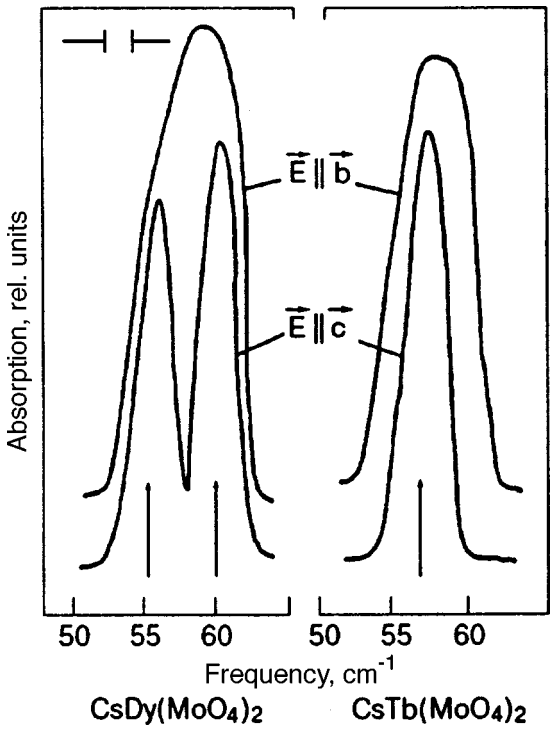


FIG. 3. Absorption bands of $CsDy(MoO_4)_2$ and $CsTb(MoO_4)_2$ crystals at low temperatures.

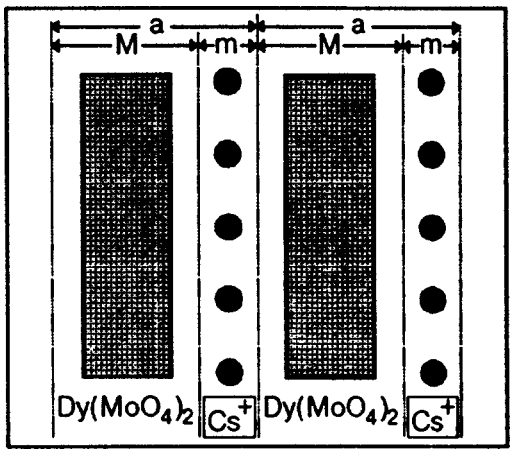


FIG. 4. Schematic diagram for the structure of $CsDy(MoO_4)_2$, in which layers have different masses and are charged oppositely (the layers are bounded by dashed lines).

$\sim 87\ cm^{-1}$ band for $\mathbf{E}\|\mathbf{b}$ polarization is associated with the structural phase transition in $CsDy(MoO_4)_2$. The transmission of IR radiation decreases considerably upon an increase in temperature, hence the spectra were recorded for spectral gaps comparable with the absorption band half- width. This rules out the possibility of a proper analysis of the shape and intensity of the absorption bands. For the same reason, we did not determine the phase transition temperature.

Apart from the above-mentioned bands, the transmission spectrum also displays the following absorption bands for the polarization $\mathbf{E}\|\mathbf{b}$: a high-intensity band at frequency $\approx 59\ cm^{-1}$, which is actually the depolarized component of the band at $\approx 57\ cm^{-1}(\mathbf{E}\|\mathbf{c})$, a weak band at frequency $\approx 41\ cm^{-1}$, as well as a band at frequency $\approx 70\ cm^{-1}$. The band at frequency $\approx 41\ cm^{-1}$ for polarization $\mathbf{E}\|\mathbf{c}$ is quite intense and broad. Another high- intensity absorption band observed in the region $\approx 87\ cm^{-1}$ is actually the depolarized component of the band split in the polarization $\mathbf{E}\|\mathbf{b}$.

## DISCUSSION OF EXPERIMENTAL RESULTS

The crystal $CsDy(MoO_4)_2$ studied by us has a layered structure. The ion interaction forces inside the $[Dy(MoO_4)_2]^-_{\infty\infty}$ layers are stronger than the binding forces between these layers and the $Cs^+$ sublattice which also forms a layer. This is due to the fact that $Cs^+$ ions are monovalent.

The crystal $CsDy(MoO_4)_2$ can be presented in the form of a packet of alternating layers with opposite charges and different masses: the $[Dy(MoO_4)_2]^-_{\infty\infty}$ layer has a mass $M$ and the layer $Cs^+_{\infty\infty}$ has a mass $m<M$ (Fig. 4). These layers alternate along the $a$ axis which corresponds to the largest parameter of the unit cell. Such a system is multilayered with a lattice period along one of the crystallographic directions exceeding the characteristic range of ionic interaction,[13] which leads to a decrease in the effect of long-range order of regular ion arrangement in the crystal on the phonon spectrum and vibrational characteristics.

It was shown by Feodosyev et al.[14] that, under the effect of local anisotropy of interaction between ions, ''quasi-chipping off'' of one or several vibrational modes whose polarization vector is oriented along one of crystallographic directions can take place in such lattices. Such a ''quasi-chipping off'' is similar to the quasi-chipping of phonon branches in a layered crystal, which are polarized at right angles to its layers.[15]

We assume that quasi-chipped off modes in the given crystal are two coupled phonon modes corresponding to synphase and antiphase shear displacements of two layers relative to each other, the first layer being formed by $Cs^+$ ions and the second by $[Dy(MoO_4)_2]^-$ ions.

If we completely disregard the interaction between these branches and the remaining vibrational modes, these oscillations can be described by the following system of equations:

$$m\omega^2 Y_{Cs} = \alpha\{2Y_{Cs} - [Y^{(+1)}_{Dy(MoO_4)_2} + Y^{(-1)}_{Dy(MoO_4)_2}]\}$$

$$m\omega^2 Y_{Dy(MoO_4)_2} = \alpha\{2Y_{Dy(MoO_4)_2} - [Y^{(+1)}_{Cs} + Y^{(-1)}_{Cs}]\}, \quad (1)$$

where $\alpha$ is the effective force constant corresponding to the retrieving force acting during a displacement of a layer of ions parallel to the remaining layers, and $Y_{Cs}$ and $Y_{Dy(MoO_4)_2}$ are the displacement of Cs and $Dy(MoO_4)_2$ layers, respectively.

The system of equations (1) is similar to the system of equations describing vibrations of a linear chain with two ions in a unit cell, but in our case the polarization of oscillations is transverse since oscillations propagate at right angles to the layers.

In this model we have two vibrational branches (optical and acoustical). The values of limiting frequencies for these branches are

$$\omega_0 = [2\alpha(1/m + 1/M)]^{1/2} \quad \text{for } k = 0, \quad (2)$$

$$\omega_0 = [2\alpha/m]^{1/2} \quad \text{for } k = \pi/a, \quad (3)$$

for the optical branch and

$$\omega_a = [2\alpha k^2 (a/2)^2/(M=m)]^{1/2} \quad \text{for } k = 0, \quad (4)$$

$$\omega_a = (2\alpha/M)^{1/2} \quad \text{for } k = \pi/a, \quad (5)$$

for the acoustical branch, where $\omega = 2\pi\nu$ is the cyclic frequency and $k$ the quasi-wave vector.

Using the experimental values of frequencies $\nu_1 \simeq 58.1\ cm^{-1}$ for $\mathbf{E}\|\mathbf{c}$ and $\nu_2 \simeq 86.1\ cm^{-1}$ for $\mathbf{E}\|\mathbf{b}$ at $T \simeq 40$ K, we can determine the elastic shear moduli from formula (2) for different polarizations ($\mathbf{E}\|\mathbf{c}$ and $\mathbf{E}\|\mathbf{b}$). Using formulas (3) and (5), we can find the frequencies of optical and acoustic branches at the boundary of the Brillouin zone. The same model was employed to find the velocities of transverse sound, which were compared with the data obtained by ultrasonic methods.[16] All numerical calculations were made for the high-temperature phase since the velocity of sound was determined at room temperature. The limiting frequencies of vibrational branches as well as the velocities of sound are given in Table I.

Using the values of $\alpha$ obtained above and the formula for dispersion of the optical and acoustic branches from the one-dimensional model, i.e.,

$$\omega^2 = \alpha(1/m + 1/M) + \alpha[(1/m + 1/M)^2$$

TABLE I. Values of shear constants $\alpha$, limiting frequencies $\omega_0$ and $\omega_a$ of optical and acoustic branches, as well as theoretical and experimental values of the velocity of sound.[13].

| | | Energy, $cm^{-1}$ | | | Velocity of sound | |
|---|---|---|---|---|---|---|
| | | | $k=\pi/a$ | | $v$, m/s | |
| Polarization | $\alpha$, N/m | $k=0$ | $\omega_0$ | $\omega_a$ | theory | experiment |
| **E**‖**b** | 22.8 | 86.1 | 76.2 | 40 | $3.17\times10^3$ | $(2.71\pm0.1)\times10^3$ |
| **E**‖**c** | 10.4 | 58.1 | 51.5 | 27 | $2.15\times10^3$ | $(1.74\pm0.1)\times10^3$ |

*Remark:* IR radiation with polarizations **E**‖**b** and **E**‖**c** induces displacements corresponding to acoustic waves with displacement vector polarizations **u**‖**b** and **u**‖**c**.

$$-4\sin^2(ka/2)/mM]^{1/2}, \tag{6}$$

we can calculate the dispersion of acoustic and optical branches over the entire Brillouin zone.

It can be seen from the Table that the calculated values of the velocity of sound are in satisfactory agreement with the result of ultrasonic measurements.[16] In our opinion, small discrepancy in the values is due to the following circumstances: at temperatures above the structural phase transition, the first excited electron state of $Dy^{3+}$ ions ($\approx 30\ cm^{-1}$) lies in the region of acoustic spectrum,[5] which leads to their interaction leading to the formation of a quasi-gap ($\Delta \approx 6\ cm^{-1}$ according to estimates), and ultimately to a decrease in the velocity of sound.[17] It cannot be ruled out, however, that this decrease can be due to anharmonism of interlayer vibrations.

The splitting of absorption bands $\nu_1 = 58.1\ cm^{-1}$ in the polarization **E**‖**c** and $\nu_2 = 86.1\ cm^{-1}$ in the polarization **E**‖**b** at a temperature below the structural phase transition point indicates that the proposed model satisfactory describes the mechanism of formation of the low-frequency vibrational spectrum of the $CsDy(MoO_4)_2$ crystal.

The formation of a superstructure in a direction perpendicular to the layers $[Cs]^+_{\infty\infty}$ and $[Dy(MoO_4)_2]^-_{\infty\infty}$ leads to the splitting of the absorption bands $\nu_1$ and $\nu_2$ in the corresponding polarizations due to the convolution of the Brillouin zone. According to the diagram presented in Fig. 5, the spectrum also acquires bands with the frequencies $40\ cm^{-1}$ for the polarization **E**‖**b** and $27\ cm^{-1}$ for the polarization **E**‖**c**. In Fig. 1, these bands are marked by arrows and are manifested as weak bands in the absorption spectrum. The emergence of these bands in the spectrum and a good agreement between the values of their frequencies and the calculated values (see Table I) prove the correctness of the chosen model. The calculated values of frequencies at the boundary of the Brillouin zone at the point $\pi/a$ on acoustic branches are in accord with experimental data, while the experimentally obtained values of corresponding splittings on optical branches are slightly smaller than the values calculated by using the proposed model. This can be due to the fact that the frequencies of optical branches are close to the frequencies of interlayer vibrations of the layer $[Dy(MoO_4)_2]^-_{\infty\infty}$, and hence the vibrations of the cesium sublattice are more localized than in the proposed model.

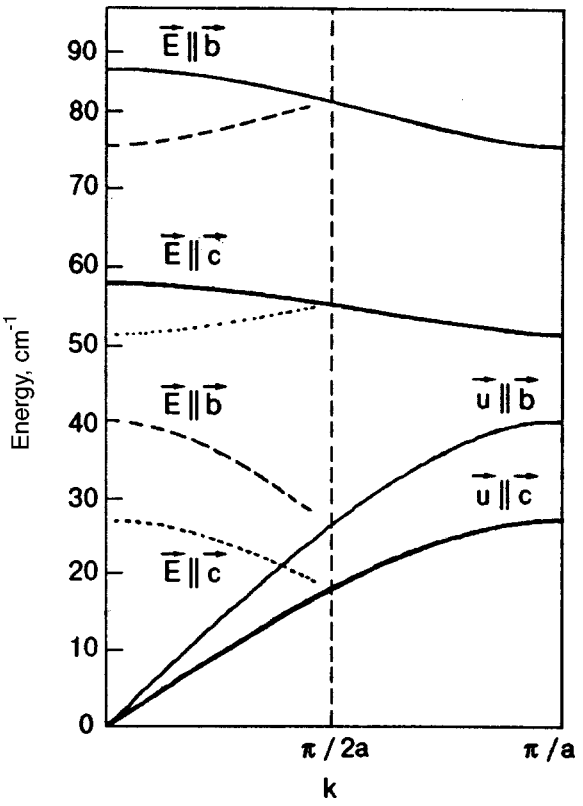


FIG. 5. Dispersion curves of the low-frequency spectrum of a $CsDy(MoO_4)_2$ crystal, calculated by formula (6) of the proposed model.

Thus, a comparison of low-frequency absorption spectra at temperatures lower and higher than the phase-transition point enabled us to establish the main peculiarity in their formation.

Let us estimate the energy of uniform deformation in the structural phase transition region in $CsDy(MoO_4)_2$ ($T_c \simeq 38$ K) as well as the energy of transformation in the course of this phase transition.

According to El'chaninova and Zvyagin,[5] the lowermost electron state of $Dy^{3+}$ ions in $CsDy(MoO_4)_2$ at $T_c$ is lowered abruptly by $\Delta\nu \simeq 80\ cm^{-1}$. In this case, the energy of the electron subsystem of $Dy^{3+}$ ions changes by $\Delta E \simeq 1$ kJ/mol. This variation of energy is associated with a change the enthalpy in the structural phase transition region, which was determined experimentally by Anders et al.[4] and amounts to $\Delta H = (0.64+0.02)$kJ/mol and with the energy of elastic deformation of the crystal lattice.

According to x-ray diffraction data,[7] the parameter $a$ in $CsDy(MoO_4)_2$ at $T_c$ undergoes a jump by 0.68%, corresponding to an increase in the value of $a$ by $\sim 0.064$ Å, while other parameters virtually remain unchanged. This leads to a uniform deformation of the crystal along this direction. We can estimate the elastic energy of this deformation by using the force constant obtained on the basis of the above model.

The data obtained by Zvyagina et al.[16] on the velocity of longitudinal sound for **k**‖**a** and **u**‖**a** (where **u** is the displacement vector of ions) for this compound can be used to evaluate the elastic modulus $\alpha$ on interlayer bonds considering that longitudinal acoustic waves are vibrations of $[Dy(MoO_4)_2]^-_{\infty\infty}$ layers as a single entity along the direction

of the $a$-axis in the crystal, i.e., across the layers. According to estimates, $\alpha = 24$ N/m. Using this value and the value of the jump in the order parameter $a$ in the structural phase transition region, we can estimate the elastic energy of uniform deformation of the crystal: $\Delta U = 0.3$ kJ/mol. Thus, $\Delta U + \Delta H \simeq 0.94$ kJ/mol, which approximately corresponds to the change in the energy corresponding to the lowermost electron state of $Dy^{3+}$ ions ($\Delta E \simeq 1$ kJ/mol). Proceeding from what has been said above, we can state confidently that the structural phase transition in $CsDy(MoO_4)_2$ occurs without a change in the free energy of the crystal lattice and is determined only by a change in the energy of the electron subsystem of $Dy^{3+}$ ions, i.e., is a cooperative Jahn–Teller effect.

Since the phase transition in $CsDy(MoO_4)_2$ due to CJTE is accompanied by the emergence of a uniform equilibrium spontaneous deformation of the crystal, the Hamiltonian of the system must contain, apart from the electron–phonon interaction, the electron–deformation interaction also. The constant of coupling with the uniform deformation of the lattice can be regarded as the limiting value of the constant of coupling of electrons with the acoustic mode for the wave vector $\mathbf{k} = 0$. According to the form of uniform deformation in our case, this mode is the longitudinal acoustic mode with $\mathbf{k} \| \mathbf{a}$ and $\mathbf{u} \| \mathbf{a}$.

Thus, the electron–deformation interaction plays the leading role in the dynamics of structural phase transition in $CsDy(MoO_4)_2$, although we cannot rule out the electron–phonon interaction also, which is responsible for the formation of a superstructure in the crystal. In our opinion, this superstructure is formed along the $a$-direction in the crystal; for this reason, the interaction with acoustic or optical modes having the wave vector $\mathbf{k} \| \mathbf{a}$ near the Brillouin zone boundary must apparently play a noticeable role in the electron–phonon interaction in $CsDy(MoO_4)_2$ also. The fact that the energy of the first excited electron state of $Dy^{3+}$ in the high-symmetry phase is close to the energy of corresponding acoustic modes at the boundary of the Brillouin zone is obviously important in this case. The closeness of the energy of the first excited electron state of $Dy^{3+}$ ions ($\nu \approx 30$ cm$^{-1}$) to the energy of transverse acoustic modes with $\mathbf{k} \| \mathbf{a}$ at the Brillouin zone boundary generates their dynamic relation which is apparently responsible for the doubling of the unit cell parameter below the phase transition temperature in this compound and for the emergence of a nonuniform deformation. According to our estimates, the nonuniform deformation from the energy point of view is considerably smaller than the uniform deformation. This statement is in accord with the temperature dependence of the doublet structure of absorption bands. With increasing temperature, the structure of the doublet is blurred below the phase-transition temperature in $CsDy(MoO_4)_2$ ($T_c \approx 38$ K) (see Fig. 2).

## CONCLUSIONS

The analysis of the low-frequency edge of the phonon spectrum for $CsDy(MoO_4)_2$ has made it possible to establish the main feature of its formation. Low-frequency optical and acoustic modes are due to shear vibrations of layer packets as a single entity along the corresponding crystallographic axes. The proposed model describes the low-frequency vibrational spectrum.

The numerical estimates of energy transformations in the course of the structural phase transition in $CsDy(MoO_4)_2$ lead to the conclusion that this transition is apparently a cooperative Jahn–Teller effect.

In the material under investigation, the electron–deformation interaction of the electron subsystem of $Dy^{3+}$ ions with the crystal lattice dominates over the electron–phonon interaction.

The structural phase transition of CJTE type in $CsDy(MoO_4)_2$ is accompanied by the doubling of the unit cell parameter in the direction perpendicular to the plane of layer packets.

The author is grateful to N. F. Kharchenko, N. M. Nesterenko, V. I. Fomin, E. S. Syrkin, and S. B. Feodos'ev for fruitful discussions of the results of this work.

This research was carried out under the financial support of the INTAS foundation (Grant No. 94-935).

*E-mail: kutko@ilt.kharkov.ua

[1] A. I. Zvyagin, T. S. Stetsenko, V. G. Yurko, and R. A. Vaishnoras, Pis'ma Zh. Éksp. Teor. Fiz. **17**, 190 (1973) [JETP Lett. **17**, 135 (1973).
[2] I. V. Skorobogatova and A. I. Zvyagin, Fiz. Nizk. Temp. **4**, 800 (1978) [Sov. J. Low Temp. Phys. **4**, 381 (1978)].
[3] A. I. Zvyagin, S. D. El'chaninova, T. S. Stetsenko, et al., Fiz. Nizk. Temp. **1**, 79 (1975) [Sov. J. Low Temp. Phys. **1**, 39 (1975)].
[4] È. E. Anders, A. I. Zvyagin, and L. S. Shestachenko, Fiz. Nik. Temp. **6**, 1356 (1980) [Sov. J. Low Temp. Phys. **6**, 661 (1980)].
[5] S. D. El'chaninova and A. I. Zvyagin, Fiz. Nizk. Temp. **9**, 1200 (1983) [Sov. J. Low Temp. Phys. **9**, 619 (1983)].
[6] N. M. Nesterenko, V. I. Fomin, V. I. Kut'ko, and A. I. Zvyagin, Preprint No. 26-82, Kharkov (1982).
[7] S. D. El'chaninova, A. I, Zvyagin, and Z. A. Kozei, Fiz. Nizk. Temp. **8**, 303 (1982) [Sov. J. Low Temp. Phys. **8**, 152 (1982)].
[8] G. A. Gehring and K. A. Gehring, Rep. Prog. Phys. **38**, 1 (1975).
[9] S. D. El'chaninova, A. I, Zvyagin, and Yu. G. Litvinenko, Fiz. Tverd. Tela (Leningrad) **22**, 3171 (1980) [Sov. Phys. Solid State **22**, 1856 (1980)].
[10] È. E. Anders, A. I. Zvyagin, S. V. Startsev, and L. S. Shestachenko, Fiz. Nik. Temp. **9**, 1218 (1983) [Sov. J. Low Temp. Phys. **9**, 629 (1983)].
[11] L. N. Pelikh and A. I. Zvyagin, Fiz. Tverd. Tela (Leningrad) **20**, 1912 (1978) [Sov. Phys. Solid State **20**, 1106 (1978)].
[12] V. A. Vinokurov and P. V. Klevtsov, Kristallografiya **17**, 127 (1972).
[13] S. V. Startsev, È. E. Anders, A. I. Zvyagin *et al.*, Kristallografiya **37**, 772 (1992).
[14] S. B. Feodosyev, I. A. Gospodarev, A. M. Kosevich, and E. S. Syrkin, Phys. Low-Dimens. Semicond. Struct. **10/11**, 209 (1995).
[15] A. M. Kosevich, E. S. Syrkin, and S. B. Feodosyev, Phys. Low-Dimens. Semicond. Struct. **3**, 47 (1994).
[16] G. A. Zvyagina, S. V. Zherlitsyn, V. D. Fill, and A. A. Gurskas, Ferroelectrics **110**, 35 (1990).
[17] V. I. Kut'ko, Yu. N. Kharchenko, N. M. Nesterenko, and A. A. Gurskas, Fiz. Nizk. Temp. **22**, 785 (1996) [Low Temp. Phys. **22**, 603 (1996)].

Translated by R. S. Wadhwa